UNIVERSITÀ DEGLI STUDI DI PADOVA

UNIVERSITÀ DEGLI STUDI DI PADOVA

Dipartimento di Ingegneria Elettrica

SCUOLA DI DOTTORATO DI RICERCA IN INGEGNERIA INDUSTRIALE

Indirizzo Ingegneria Elettrotecnica

CICLO XXIV

Studies on the impact of the ITER Pulsed Power Supply System on the Pulsed Power Electrical Network

Direttore della Scuola : Ch.mo Prof. Paolo Bariani

Coordinatore d'indirizzo: Ch.mo Prof. Giovanni Attilio Martinelli

Supervisore: Ch.mo Prof. Piergiorgio Sonato

Co-supervisore: Dott. Ing. Elena Gaio

Dottorando : Claudio Finotti

31 Gennaio 2012

Table of contents

Summary 3
Summario 7
1 The fusion research framework 11
1.1 The energetic problem 11
1.2 The fusion background 11
1.3 ITER experiment 13
1.3.1 The ITER magnet system 14
1.3.2 The Neutral Beam Injector of ITER 15
2 The ITER Power Supply System 17
2.1 The ac/dc converter base unit 18
2.2 The reactive power compensation system 19
References 21

Analytical models for stability analysis in high power ac/dc converters applied to the ITER case 23
3 The Simplified Power Supply System (SPSS) 25
4 Quasi-Static Model used to investigate the power and voltage stabilities of the ac/dc converter system 29
4.1 Power stability analysis 31
4.2 Voltage stability analysis 32
5 The Dynamic Model 35
5.1 The building of the Dynamic Model of each subsystem 35
5.2 The Phase Locked Loop 38
5.2.1 The analytical model equations of the PLL in dq frame 38
5.3 The analytical model equations of the mean value calculation 39
5.4 The analytical model equations of the Tuned Filters Subsystems 40
5.4.1 The Dynamic Model of the Tuned Filters subsystem 42
5.5 The TCR subsystem 42
5.5.1 TCR dynamic modeling 43
5.5.2 Calculation of the reactive power consumed from the ac/dc conversion system and of the reference input applied to the TCR system 49
5.5.3 The Dynamic Model of the TCR system (included the PLL) 52
5.6 The ac/dc conversion subsystem 53
5.6.1 The ac/dc converter in 6 pulse operation 53
5.6.2 The ac/dc converter base unit in 12 pulse operation 63
5.6.3 The ac/dc converter base unit in circulating mode 71
5.7 The state space matrix of the Dynamic Model of the SSPS 79
5.8 The stability analysis of the Dynamic Model of the SPSS 83
5.8.1 The participation of the state variables in the instable mode 87
5.8.2 Example of setting of the parameters of the controller 88
5.8.3 Verification of the Dynamic Model of SPSS with ac/dc converter opearating in 12 pulses and circulating operating modes. 89
6 Conclusions 93
References 95

Study of Active-Front-End design for the Acceleration Grid Power Supply of ITER Neutral Beam Injector 97
Acronyms 99
7 Reference Design of the Accelerator Grid Power Supply System 101
7.1 Calculation of the main design parameters 102
7.1.1 Step down transformer and ac/dc conversion system 102
7.1.2 Rating of the dc link capacitor banks 103
8 Active Front-End ac/dc Converter and respective control scheme for NBI AGPS 105
8.1 Choice of the topology of AFE Converter for AGPS 105
8.2 Control scheme of 3L NPC converter 108
8.3 Current controller of PWM VSC 108
8.3.1 Pulsed Width Modulation Strategies 115
8.4 The reference angle detector 117
8.5 The dc-link voltage controller 118
8.6 The differential voltage controller 119
8.7 The input filter of AFE - VSC 120
8.7.1 Synchronous Active Front-End 122
9 Design of the ac/dc section of AGPS based on Active Front-End approach 131
9.1 Choice of the transformer secondary voltage and of the L filter 132
9.2 Choice of the switching frequency 134
9.3 Description of the model and control parameters optimization for AFE converter 137
9.3.1 Power circuit model 138
9.3.2 Current control and CB PWM with 1/6 ZSS strategy model 140
9.3.3 The reference angle detector 142
9.3.4 The dc-link total voltage controller 143
9.3.5 The dc-link differential voltage control 145
9.3.6 The carrier waveforms generation model 146
9.4 Thermal analysis on the switches to determine the number of parallel NPC VSC in Synchronous AFE configuration 147
9.4.1 The PSIM circuit model used to carry out the thermal analysis on the switches 147
9.4.2 Thermal analysis on the switches of the NPC VSCs 151
9.5 The harmonic content on the grid phase current 157
9.6 Fault analysis 159
10 Thyristor versus Active Front-End ac/dc conversion systems 163
10.1 Ac/dc conversion models with the acceleration grids load 163
10.2 Comparison among the dynamic responses between the two ac/dc conversion topologies 167
10.3 Reactive Power Consumption and Current Harmonic Content 169
10.3.1 Reactive power consumption and current harmonic content with ac/dc thyristor conversion system 169
10.3.2 Reactive power consumption and current harmonic content with ac/dc AFE conversion system 171
11 Conclusion 175
References 177
12 Acknoledgements 179

Summary

ITER experiment will be built at Cadarache (France) and its main goal will be to prove the viability of fusion as an energy source.
In a fusion reactor, the plasma (an ionized gas of Deuterium and Tritium) has to be heated up to temperatures of millions of Celsius degrees in order to sustain the fusion reaction. No materials are able to withstand these temperatures; therefore the plasma is kept away from the walls of the reactor vacuum vessel by means of appropriate magnetic fields, produced by the currents flowing in the superconducting coils, which interact with the charged particles of the plasma.
Besides the ohmic heating, two additional sources are foreseen in ITER, based on radiofrequency electromagnetic waves and neutral beam injection. Two Neutral Beam Injectors (NBIs) will heat the plasma; each of them is based on five 200 kV stages in series accelerating negative ions of deuterium or hydrogen, which are neutralized and injected in ITER plasma. The high energy (1 MeV) and beam power (16.7 MW) make this design very complex, close to the state of the art of the components.
The ac/dc conversion system necessary to supply the superconducting coils of the magnet system and the auxiliary systems (as the NBIs) may consume a total active and reactive power respectively up to 500 MW and 900 Mvar.
In the past years many studies have been carried out on the ITER power supply system and its impact on the electrical network (called Pulsed Power Electrical Network PPEN).
Several methods have been considered to improve the power factor, based both on Q reduction and compensation techniques. As for the first, sequential and asymmetric controls, with internal bypass or external freewheeling have been evaluated. Concerning the compensation approach, the current reference design is based on Static Var Compensation System with nominal power of 750 Mvar based on Thyristor Controlled Reactor (TCR) + Tuned Filter (as fixed capacitor). Nevertheless, studies are still in progress aimed to further improvements.

This PhD thesis aims to investigate two topics related to the impact on the PPEN of the ITER power supply system with a novel approach.

The former concerns the study of the stability of the PPEN and mainly aims to investigate interaction phenomena among the ac/dc conversion and Q compensation and filtering systems, due in particular to the relatively high power ratings and operating scenarios with significant power transients during the plasma pulses.
It is not an easy task: the overall system is very complex, the numerical simulation of its operation via programs capable of reproducing the instantaneous current and voltage profiles requires very long calculation time and most of all it does not provide any sensitivity data concerning the stability of the whole power system.
Therefore I have followed an analytical approach. The study took the starting points from the methods developed for the HVDC applications, which however can not be directly applied to the ITER case; therefore I have developed specific analytical models.
The former model is a Quasi Static Model, which aims to evaluate the strength of the electrical network feeding the ITER power supply system by sensitivity analysis. I have derived the equations of the model by the power flow equations as a function of some relevant parameters in order to carry out sensitivity analysis. This model allows the calculation of some indexes as the Critical Short Circuit Ratio (CSCR) and Voltage Sensitivity Factor (VSF). No critical conditions have been found.

The latter is a Dynamic Model; it is based on the state space formulation and it aims to investigate the dynamic stability of the whole system, including also the control system. Nevertheless the ac/dc conversion and the TCR systems are non-linear and discrete, thus difficult to be modelled; therefore, taking the starting point from the methods described in literature, I have approximated the discrete phenomena by continuous transfer functions, and I have worked out the linearization around an equilibrium point such that the small signal analysis approach can be used. I have adopted a modular approach, developing an analytical Dynamic Model for each subsystem (Tuned Filters, TCR and ac/dc conversion system).
Then I have built numerical models of the subsystems with a program (PSIM) capable to reproduce the instantaneous waveforms for the validation of the analytical Dynamic Models (run in Matlab Simulink program, state space tool) in frequency and time domain by a comparison between the simulation results. Finally I have built the Dynamic Model of the whole system and validated by comparison with the PSIM one.
From the results of the frequency analysis, the dynamic model is accurate for frequency range less than 50 Hz, but it may be used to obtain some insight about the system stability also for frequency range up to 100 Hz.
Some unstable operating conditions have been discovered, and the cause has been identified due to resonance between the tuned filters and the grid.
It is highlighted that this model may be easily implemented with more detail to the whole ITER power supply system and it can be a very useful and fast tool to aid the design of the power supply system and set the parameters of the control system.

As the second topic of my PhD thesis, I have studied the feasibility of adopting a more advanced technology based on the Active Front End approach for the design of the main ac/dc conversion system (called AGPS) of the NBI power supply (56 MW, 88 MVar) to improve its impact in ITER PPEN in terms of current harmonic and reactive power minimization.
After giving a short description of the AGPS reference design, based on thyristor technology, the conceptual design of the AFE alternative topology that I have developed for the input ac/dc rectifier is illustrated; its feasibility, and the advantages and drawbacks with respect to the thyristor solution are evaluated and discussed.
The results obtained by the analysis show that the AFE solution is feasible and it significantly improves the impact of the AGPS on the Pulsed Power Electrical Network of ITER with respect to thyristor one. The modifications of the present design parameters to allow the full compliance with the requirements of the technical specifications with the implementation of the AFE solution are also proposed and discussed.

This thesis is organized as follows.
In the Chapter 1 a brief introduction to the fusion research framework is given.
The ITER power supply system is described in the chapter 2.

The first part of the PhD thesis related to the development of the analytical model starts in the chapter 3, with the description of the simplified equivalent scheme of the ITER Power Supply. The Quasi-Static and Dynamic Models are described in chapter 4 and 5 respectively, and in the chapter 6 are given the conclusions related to this part.

The second part of the PhD thesis related to Study of Active-Front-End design for the Acceleration Grid Power Supply of ITER Neutral Beam Injector start in the chapter 7,

describing the reference design of the AGPS based on thyristor solution. Then an overview of the AFE converter topologies and control systems is given and their application to AGPS is discussed in the chapter 8. In chapter 9 the conceptual design of the AGPS based on AFE approach is described in detail. In the chapter 10 the AFE and thyristor solution are compared in terms of impact on the PPEN (reactive power and ac current harmonic)

Summario

L'esperimento ITER sarà costruito a Cadarache (Francia) e il suo obiettivo principale sarà quello di dimostrare la fattibilità tecnologica di produzione di grandi quantità d'energia attraverso la fusione in un plasma di deuterio e trizio
In un reattore a fusione, il plasma (un gas ionizzato di deuterio e trizio) deve essere riscaldato fino a temperature di milioni di gradi Celsius al fine di sostenere la reazione di fusione. Non vi sono materiali in grado di resistere a tali temperature, per cui il plasma è tenuto lontano dalle pareti della camera da vuoto del reattore per mezzo di opportuni campi magnetici, prodotto dalle correnti nelle bobine superconduttrici, che interagiscono con gli ioni del plasma.
Oltre al riscaldamento ohmico, altri due sistemi di riscaldamento sono previsti nel progetto di ITER, basati sulle onde elettromagnetiche a radiofrequenza e iniezione di neutri. Due iniettori di fasci di neutri (Neutral Beam Injectors NBIs) saranno utilizzati per scaldare il plasma; ciascuno è composto da un sistema di griglie che formano cinque stadi di accelerazione da 200 kV ciascuno, che accelerano gli ioni negativi di deuterio o idrogeno, che vengono poi neutralizzati e iniettati nel plasma di ITER. L'alta energia (1 MeV) e la potenza del fascio (16,7 MW) rendono questo progetto molto complesso, vicino alla stato dell'arte dei componenti.
Il sistema di conversione ac/dc necessario per alimentare le bobine superconduttrici del sistema di magneti e dei sistemi ausiliari (come i NBIs) può consumare complessivamente una potenza attiva e reattiva rispettivamente fino a 500 MW e 900 Mvar.
Negli ultimi anni molti studi sono stati effettuati sul sistema di alimentazione ITER e sul suo impatto sulla rete elettrica (chiamata Pulsed Power Electrica Networ PPEN).
Diverse tecniche sono state considerate per migliorare il fattore di potenza dei sistemi di conversione ac/dc a tiristori di ITER. Per quanto riguarda la riduzione dell'assorbimento sono state studiate tecniche quali il controllo sequenziale ed asimmetrico, con bypass interno o con freewheeling esterno. Per quanto riguarda invece la compensazione, l'attuale progetto di riferimento è basato sulla tecnologia Static Var Compensator (SVC) con potenza nominale di 750 Mvar, composto da Thyristor Controlled Reactor (TCR) + Filtri per le armonche di corrente (che hanno la funzione di fornire potenza reattiva). Tuttavia, gli studi sono ancora in corso con l'obiettivo di ulteriori miglioramenti.

Questa tesi di dottorato studia due aspetti legati all'impatto sulla rete PPEN del sistema di alimentazione di ITER, con un approccio diverso rispetto a quelli già effettuati.

Il primo riguarda lo studio della stabilità della rete elettrica PPEN e principalmente si propone di studiare i fenomeni di interazione tra i sistemi di conversione ac/dc e di compensazione della reattiva, dovuti in particolare all'elevato consumo di potenza durante gli scenari di funzionamento di ITER.
Non è un compito facile: il sistema di alimenatzione di ITER è molto complesso, le simulazioni numeriche del suo funzionamento attraverso programmi in grado di riprodurre i profili istantanei di tensione e corrente richiede tempi di calcolo molto lunghi e soprattutto non forniscono alcuna sensibilità riguardo la stabilità del sistema. Ho quindi applicato un approccio analitico e, considerando i metodi sviluppati per le applicazioni HVDC che però non possono essere direttamente applicati al caso ITER, ho sviluppato specifici modelli analitici.
Il primo modello è il "Quasi-Static Model", che ha lo scopo di valutare l'adeguatezza della rete elettrica del sistema di alimentazione di ITER attraverso un'analisi di

sensibilità. Ho ricavato le equazioni del modello dalle equazioni ai flussi di potenza in funzione di alcuni parametri rilevanti per l'analisi di sensibilità. Con questo modello ho potuto calcolare alcuni indici come il rapporto critico cortocircuito (Critical Short Circuit Ratio) e il fattore di sensibilità di tensione (Voltage Sensitivity Factor). Nessuna condizione criticha è stata trovata.

Il secondo è un modello dinamico (chiamato Dynamic Model), ed è basato sulla formulazione alle variabili di stato e si propone di indagare la stabilità dinamica di tutto il sistema, tra cui anche il sistema di controllo. Tuttavia il sistema di conversione ac/dc e i TCR sono componenti non lineari e discreti, e sono difficili da modellare; considerando i metodi descritti in bibliografia, ho approssimato i fenomeni discreti con funzioni di trasferimento continue, e ho eseguito la linearizzazione attorno ad un punto di equilibrio, utilizzando così l'approccio ai piccoli segnali. Ho adottato un approccio modulare, sviluppando cioè un modello dinamico per ogni sottosistema (i filtri delle armoniche di corrente, i TCR e il sistema di conversione ac/dc). Poi ho costruito modelli numerici dei sottosistemi, con un programma (PSIM) in grado di riprodurre le forme d'onda istantanee per la validazione dei modelli dinamici (implementato con il programma Matlab Simulink, state space tool) attraverso il confronto dei risultati nel dominio della frequenza e del tempo. Infine ho costruito il modello dinamico di tutto il sistema e validato con il modello equivalente in PSIM.
Dai risultati delle analisi in frequenza, il modello dinamico è accurato per frequenze inferiori a 50 Hz, ma può essere utilizzato per ottenere qualche informazione circa la stabilità del sistema anche per frequenze fino a 100 Hz.
Alcune condizioni di funzionamento instabili sono state individuate e sono dovute alla risonanza tra i filtri e la griglia.
Questo modello può essere facilmente implementato con maggiori dettagli per l'intero sistema di alimentazione ITER e può essere uno strumento molto utile e veloce per aiutare la progettazione del sistema di alimentazione e impostare i parametri del sistema di controllo.

Come secondo argomento della mia tesi di dottorato, ho studiato la fattibilità tecnologica di utilizzare una tecnologia più avanzata basata su un approccio di rettificazione attiva (Active Front End AFE) per la progettazione del principale sistema di conversione ac/dc (chiamato Acceleration Grid Power Supply AGPS) del sistema di alimentazione del NBI (56 MW , 88 MVAr) per migliorare il suo impatto in sulla rete PPEN in termini di minimizzazione della potenza reattiva e delle armoniche di corrente.
In questa parte della tesi, dopo una breve descrizione del progetto di riferimento dell'AGPS basato sulla tecnologia a tiristori, ho descritto il progetto concettuale del sistema di rettificazione dell'AGPS basato sulla soluzione alternativa AFE che ho sviluppato; la sua fattibilità ed i vantaggi e gli svantaggi rispetto alla soluzione tiristori sono stati valutati e discussi.
I risultati ottenuti dalle analisi mostrano che la soluzione AFE è fattibile e migliora significativamente l'impatto della AGPS sulla rete PPEN di ITER rispetto a quella a tiristori. Inoltre sono state proposte e discusse alcune modifiche di alcuni parametri del progetto di riferimento per consentire la piena conformità con i requisiti delle specifiche tecniche con l'implementazione della soluzione AFE.

Questa tesi è organizzata come segue.

Nel capitolo 1, una breve introduzione descrive la ricerca sulla fusione. Il sistema di alimentazione di ITER è descritto nel capitolo 2.

La prima parte della tesi di dottorato relativa allo sviluppo dei modelli analitici inizia nel capitolo 3, con la descrizione dello schema equivalente semplificato del sistema di alimentazione ITER. I modelli quasi-statico e dinamico sono descritti rispettivamente nei capitoli 4 e 5, e nel capitolo 6 sono presenti le conclusioni relative a questa parte.

La seconda parte della tesi di dottorato relativa allo studio di una soluzione di rettifficazione attiva applicata al sistema d'alimentazione dell griglie (AGPS) dell'iniettore di fasci di neutri inizia nel capitolo 7, che descrive il progetto di riferimento della AGPS basato sulla soluzione tiristori. Poi sono descritte diverse soluzioni AFE e dei sistemi di controllo trovati in bibliografia, e la loro applicazione alla AGPS è discussa nel capitolo 8. Nel capitolo 9 il progetto concettuale della AGPS basato sull'approccio AFE è descritto in dettaglio. Nel capitolo 10 la soluzioni AFE e tiristori sono confrontati in termini di impatto sulla rete PPEN (potenza reattiva e armoniche di corrente)

1 The fusion research framework

1.1 The energetic problem

Nowadays the need of energy is mainly satisfied for 80% by fossil fuels (oil, coal, natural gas, see Figure 1-1) and it is expect to grow in the next years [1].

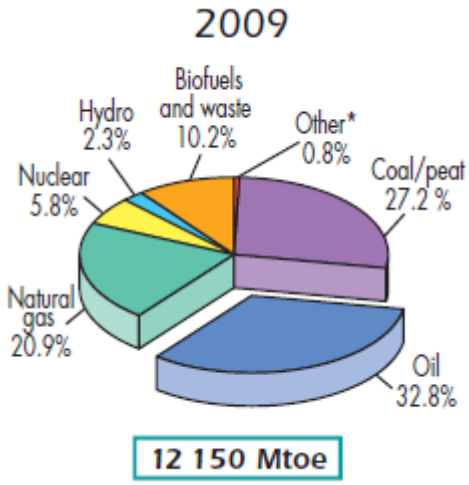

Figure 1-1 Fuel shares of the world total primary energy supply of 2009

Nevertheless the reserves of fossil fuels are not infinite and for the principle of the supply and demand the price will rise. Moreover them utilization for energy production have relevant impact on the environment due to the emissions of greenhouse gas and other air pollutants. Therefore new safe and sustainable energy source are being researched. The nuclear fusion technology is one of them.

1.2 The fusion background

The most viable fusion reaction for a future fusion power plant considers as reacting elements Deuterium and Tritium, which are isotopes of Hydrogen [2],[3]:

$$D + T \rightarrow {}^{4}He\ (3.5\ MeV) + n\ (14.1\ MeV) \qquad \text{(eq. 1-1)}$$

If Deuterium and Tritium are heated at very high temperatures, in the order of 20 keV (which corresponds to about $200 \cdot 10^6$ K), the kinetic energy of the nuclei overcomes the Coulomb repulsion, then the nuclei likely collide and react, producing a nucleus of Helium, a neutron and energy.
A significant amount of fusion reactions may be achieved only by heating the plasma (an ionized gas of Deuterium and Tritium) up to temperatures of millions of Celsius degrees and it must be confined and insulated in order to maintain high temperatures. No materials are able to withstand these temperatures; therefore the plasma is kept away from the walls of the reactor vacuum vessel by means of appropriate magnetic fields which interact with the charged particles of the plasma and this approach is called "magnetic confinement fusion".
The most promising configuration of magnetic confinement is the tokamak [4], which consist of a toroidal machine where the plasma acts as the secondary winding of a transformer while the primary winding is made of the poloidal field coils: a change of

current in the primary winding induces a current in the plasma (inductive phenomena); moreover a high toroidal field is imposed to confine the plasma (Figure 1-2).

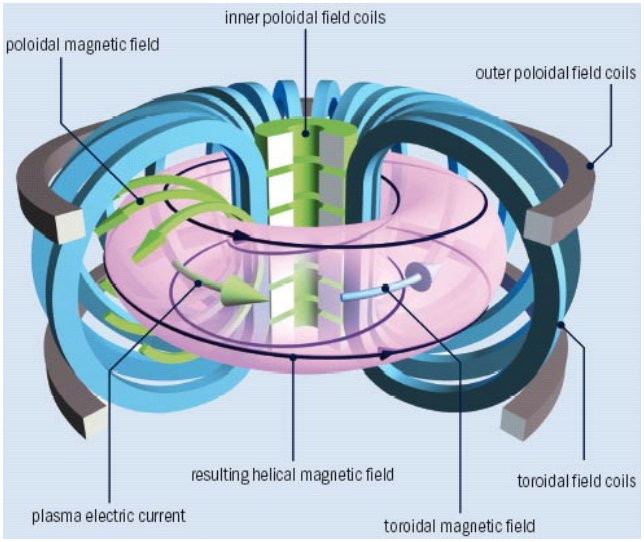

Figure 1-2 Schematic view of the main field coils and of plasma current in a tokamak

The plasma current generates a further magnetic field which contributes to confine the plasma and it also provides some heating because of electrical resistance of the plasma. Nevertheless the heating due just the Joule losses on to the resistance of the plasma is not sufficient to achieve a plasma temperature of millions of Celsius degrees and a transformer cannot generate a current continuously, therefore Heating and Current Drive systems are necessary to rise the temperature and sustain the current of plasma. The Heating and Current Drive (H&CD) systems may be an appropriate combination of Neutral Beam Injectors (NBI) and Radio Frequency (RF) H&CD antennas operating at the electron cyclotron (EC) and ion cyclotron (IC) frequency.

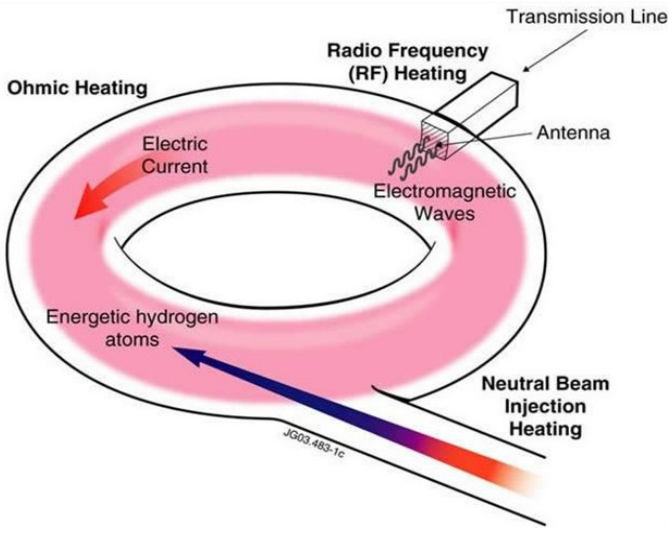

Figure 1-3 The Heating and Current Drive (H&CD) systems

When the Helium nuclei transfer their energy to the plasma, they are extracted together to the plasma impurity by the divertor situated along the bottom of the Vacuum Vessel.
A blanket covers the interior surfaces of the vacuum vessel providing shielding to the vessel and to the field coils from the heat and neutron fluxes of the fusion reaction.

Moreover the blanket slows down the neutron, and their kinetic energy is transformed into heat energy and collected by the coolants, which in a future fusion power plant will be used for electrical power production. If the blanket contains liquid Lithium, it may be used as a breeding blanket, allowing the producing Tritium on-site as a result of a nuclear reaction among Lithium and neutron.
It is highlighted that fusion power plant is safer than the fission one, because in case of loss of the control in a fusion reactor the plasma gets cold very fast and the reaction stop, while the runaway in a fission reactor can be very dangerous. Moreover, at the same output power condition, in a fusion reactor the production of radioactive wastes are less and their radioactive decay time is lower.
Respect to the fossil fuels fusion power plant has the following advantages:

- the fuels abundant in the earth
- no emission of greenhouse and other air pollutants.

1.3 ITER experiment

The long-term objective of the magnetic confinement fusion R&D is a prototype reactor for power station, which will allow an energy production without emission of greenhouse gas and other air pollutants, safe and long-term availability of the fuels.
The strategy to achieve this long term objective includes the development of an international experimental reactor ITER [5], which aims to demonstrate the scientific and technological feasibility of fusion energy and it is being built at Cadarache, in France.
The ITER fusion reactor is designed to produce 500 MW of thermal power, with a ratio Q between output fusion power and input power to the tokamak higher than 10. Hereby the machine is expected to demonstrate the principle of getting more energy out of the fusion process than is used to sustain it, a target not yet achieved in the present experimental fusion reactors. Nevertheless, ITER will be again an experimental device, unable to inject electricity into the grid.
The main parameters of the ITER experimental reactor are listed in the Table 1-1.

Table 1-1 Main parameters of the ITER experimental reactor

Parameter	**Value**
Total fusion power	500 MW
Q = fusion power/auxiliary heating power	≥10 (inductive)
Average neutron wall loading	0.57 MW/m^2
Plasma inductive burn time	≥400 s
Plasma major radius	6.2 m
Plasma minor radius	2.0 m
Plasma current	15 MA
Toroidal field @ 6.2 m radius	5.3 T
Plasma volume	837 m^3
Plasma surface	678 m^2
Installed auxiliary heating/current drive output power	73 MW

The principal aims for ITER are:

- to achieve extended burn in inductively-driven plasmas with ratio Q between the fusion power and the injected power by auxiliary heating system ≥ 10 at nominal fusion power output of about 500 MW for a range of operating scenarios and with a duration sufficient (≥ 400 s) to achieve stationary conditions;
- to aim at demonstrating steady state operation using non-inductive current drive with a ratio Q of at least 5.

ITER will also develop and test technologies and processes needed for future fusion plants: superconducting magnets, components able to withstand high neutron fluxes and remote manipulation.
In the following paragraphs two among the main systems of ITER are briefly described: the magnet system used to confine the plasma and the Neutral Beam Injector which is one of the main Heating and Current Drive systems.

1.3.1 The ITER magnet system

The magnet system of ITER [6],
[7] mainly consists of 18 Toroidal Field (TF) coils, a Central Solenoid (CS), 6 Poloidal Field (PF) coils and 18 Correction Coils (CCs) (see Figure 1-4). The power of the magnetic fields required to confine the plasma in the ITER vacuum vessel is extreme. For maximum efficiency and to limit energy consumption, ITER uses superconducting magnets, which are cooled with supercritical Helium in the range of 4 Kelvin (-269°C).

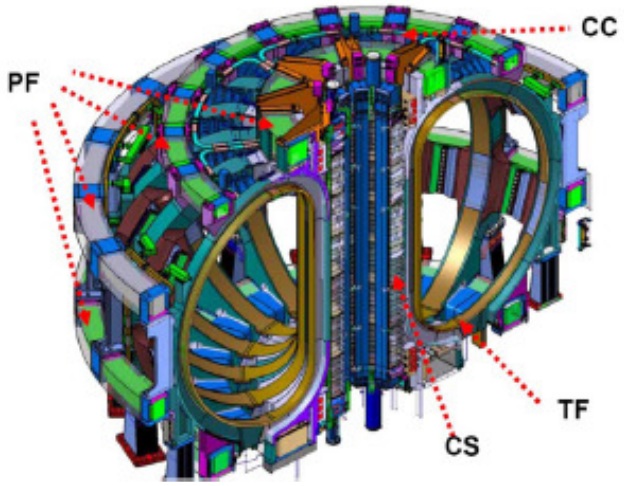

Figure 1-4 Schematic view of the main field coils of ITER magnet system

The 18 toroidal field coils generate a constant toroidal field on axis of 5.3 T to confine the plasma during an ITER pulse. The ITER toroidal field coils will be made of Niobium-Tin (Nb3Sn) Cable-In-Conduit superconductors and designed to have a total magnetic energy of 41 GJ and a maximum magnetic field of 11.8 T.
The central solenoid provides the inductive flux to ramp up plasma current and contribute to plasma shaping. The Central Solenoid will be composed of six independent winding packs that use a Niobium-Tin (Nb3Sn) Cable-in-Conduit superconducting conductor, held together by a vertical precompression structure.
The poloidal field coils provide the position equilibrium of plasma current (i.e. the fields to confine the plasma pressure) and the plasma vertical stability. The poloidal field coil system consists of six horizontal coils placed outside the toroidal magnet structure. They will be made by Niobium-Titanium (NbTi) alloy.
The correction coils allow the correction of error field due to position errors as well as from busbars and feeders. Figure 1-5 shows the layout of the correction coils in ITER. The correction coil system it is located outside the toroidal field coils; it consists of three sets of Niobium-Titanium (NbTi) superconducting coils (top, side and bottom), each consisting of six coils distributed poloidally.
The main electrical data of the coils of ITER magnet system are given in the table:

Table 1-2 Main electrical data of the coils of ITER magnet system

	Poloidal Field	Central Solenoid	Toroidal Field	Correction Coils
Number of coils	6	6	18	18
Number of turn per coil or per winding pack	115-459	549	134	20-32
Stored magnetic energy [GJ]	4	7	41	-
Maximum operating current [kA]	45	45	68	10
Nominal peak field [T]	6	13.0	11.8	5

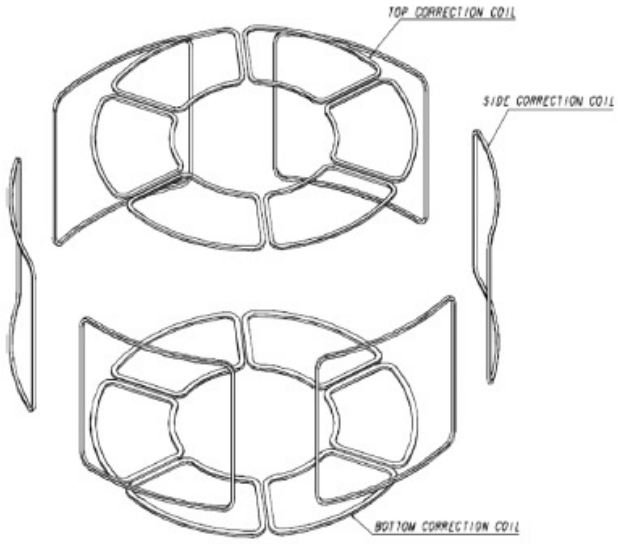

Figure 1-5 Schematic view of the layout of the correction coils in ITER

1.3.2 The Neutral Beam Injector of ITER

The Neutral Beam Injection H&CD is a complex process.
In ITER NBI (Figure 1-6), negative ions of Deuterium or Hydrogen are produced by the Ion Source and accelerated to the required energy; then they are neutralized through the process of charge exchange with a gas of hydrogen or deuterium and residual ions are removed. The neutrals are injected into the plasma and they go along straight lines, because they are not affected by magnetic field. Finally the neutrals are deposited in the central region of the plasma and they transfer their energy to it by collision.

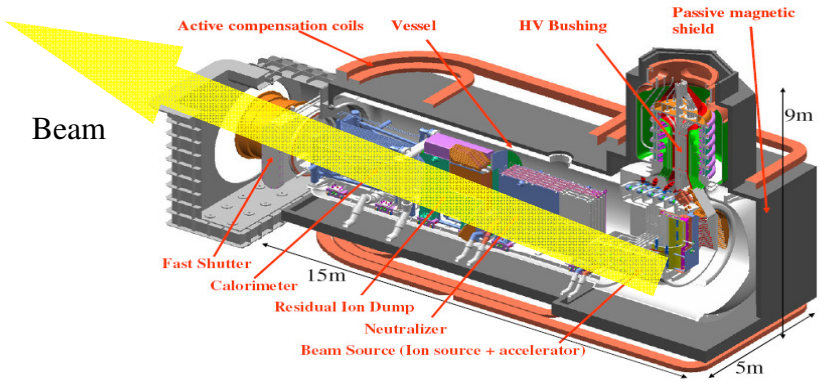

Figure 1-6 Schematic view of ITER neutral beam

At least two NBIs will be installed in ITER and each one will provide a beam power of 16.5 MW and a prototype in full scale will be built at Consorzio RFX (Padova, Italy) [9].
To avoid undue beam deflections inside the NBI, the stray magnetic fields along the ion beam path should be minimized by active compensation coils. Moreover, the beam optics is determined by the shape of the grid surfaces and of the grid holes and it is optimized if the accelerating voltage and the ion beam current follow a certain equation, called perveance matching law:

$$I_{beam} = \frac{k}{\sqrt{m_i}} \cdot V_{acc}^{1.5} \qquad \text{(eq. 1-2)}$$

where I_{beam} is the ion beam current which crosses the grids, V_{acc} is the accelerating voltage, m_i is the mass of the ions and k is a constant which is determined by the accelerator geometry.

1.3.2.1 The electrostatic accelerator and breakdown phenomena

The ITER NBI electrostatic accelerator is based on a Multi Aperture Multi Gap (MAMuG) configuration. Five accelerating grids at different increasing potentials are used, the last grid being referred to the NBI ground reference (the vacuum vessel). In Deuterium operation, the rated voltage across each couple of grids is 200 kV, to reach a total accelerating voltage of -1 MV and the beam current of 40 Amps. The maximum pulse length is 3600 seconds.
For reasons related to the optimization of beam optics the acceleration grids operate at voltages close to those of discharge; therefore during normal operation breakdowns among the acceleration grids may be frequent and unpredictable, even with just few seconds between one and the next. This phenomenon has to be considered normal operation condition and the NBI system has to be able to withstand the stresses related to it.

2 The ITER Power Supply System

The ITER experiment is supplied by the High Voltage grid at 400 kV with a short circuit power of about 12 GVA; the reactive power demand is required to be limited to around 200 MVar [10],[11]. The ac/dc conversion systems are equally distributed among three independent 66 kV and 22 kV distribution systems, called Pulse Power Electrical Network (PPEN) (see Figure 2-1), supplied by three identical three winding step-down transformers (Table 2-1). The largest power supplies (mainly the superconducting coil ac/dc converters with nominal power > 20 MVA and the power supplies of the acceleration grids of the Neutral Beam Injectors) are connected to 66 kV busbars; for each one the total installed power of the ac/dc converters and of the reactive power compensation system (TCR + Tuned Filters) are about 500 MVA and 250 Mvar respectively. In the next paragraphs brief descriptions of the base unit of the main ac/dc converters and of the reactive power compensation system are given. The power supplies of the acceleration grids of the Neutral Beam Injectors are dealt in the chapter...

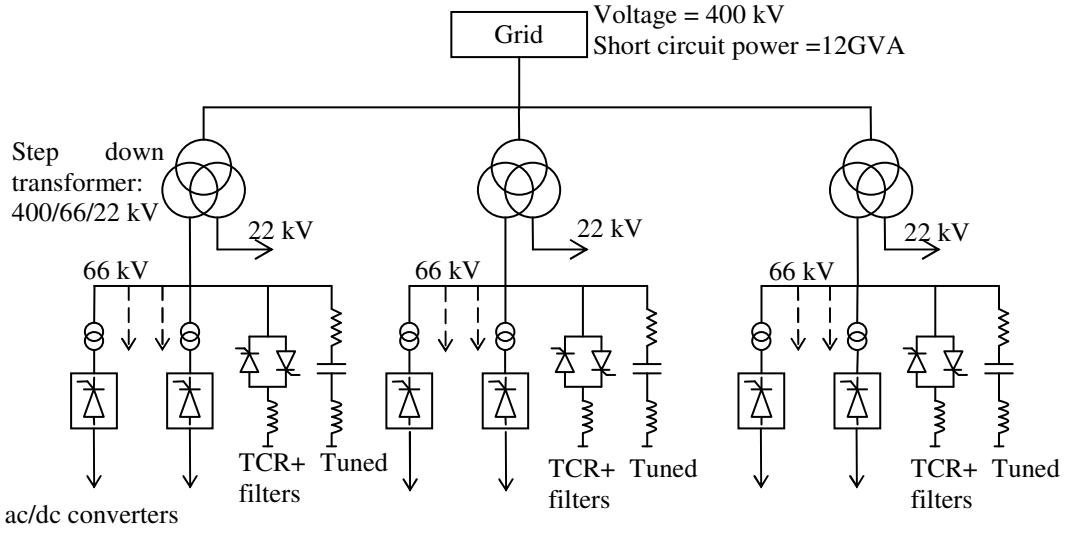

Figure 2-1 Schematic representation of the ITER Pulsed Power Electrical Network

Table 2-1 Main parameters of the step down transformer 400 kV / 66 kV

Item	Symbol	Value	Unit
Rated power of the primary winding	S_{400}	300	MVA
Rated power of the secondary winding	S_{66}	250	MVA
Rated power of the tertiary winding	S_{22}	150	MVA
Rated Frequency	f	50	Hz
Nominal primary voltage	U_{1N}	400	kV
Nominal secondary voltage	U_{2N}	66	kV
Nominal tertiary voltage	U_{3N}	22	kV
Short circuit voltage primary-secondary (at 300 MVA)	$v_{SC\%}$	12	%
Short circuit voltage primary-tertiary (at 300 MVA)	$v_{SC\%}$	27	%
Short circuit voltage secondary-tertiary (at 300 MVA)	$v_{SC\%}$	15	%

2.1 The ac/dc converter base unit

The superconducting coils are supplied by ac/dc converters based on thyristor technology. For each type of coil different requirements of currents, voltages and dynamic response are specified (Table 2-2); nevertheless, a modular approach has been chosen for the design and a base unit has been defined. Their requirements are satisfied by using appropriate series/parallel connections of the base units. The ac/dc converter base unit is shown in Figure 2-2.

It consists of two subunits connected in parallel in twelve pulses configuration, each one composed of two back to back thyristor bridges. The base unit rating adopted is ±1.35 kV, ± 45/55/22.5 kA. During the ITER operation the ac/dc converter are voltage and current controlled.

The voltage control allows supplying to the coil the right voltage required from the ITER operating scenarios, while the current control is necessary to control the current sharing between the subunits in parallel.

In particular there are three different operations of the current control:

- 12 pulses operation: the two subunits operate in parallel configuration and the current controller aims to balance the current between them (load current $I_{Load} > I_{6p} \times I_r$).
- 6 pulses operation: only one subunit operates in order to avoid misfiring of the thyristors during the transition between the 12 pulses operation and circulating mode; current control is disabled in this phase ($I_{cir} \times I_r < I_{Load} < I_{6p} \times I_r$)..
- Circulating mode: the dc output current of one subunit is the sum of the coil current and the current flowing in the anti-parallel thyristors, in this way, even at low coil current (near zero) the dc output currents of the subunits are high enough to avoid the current blocking in any bridge ($I_{Load} < I_{cir} \times I_r$ and the goal of the current control is to keep the circulating current equal to $I_{cir} \times I_r$)..

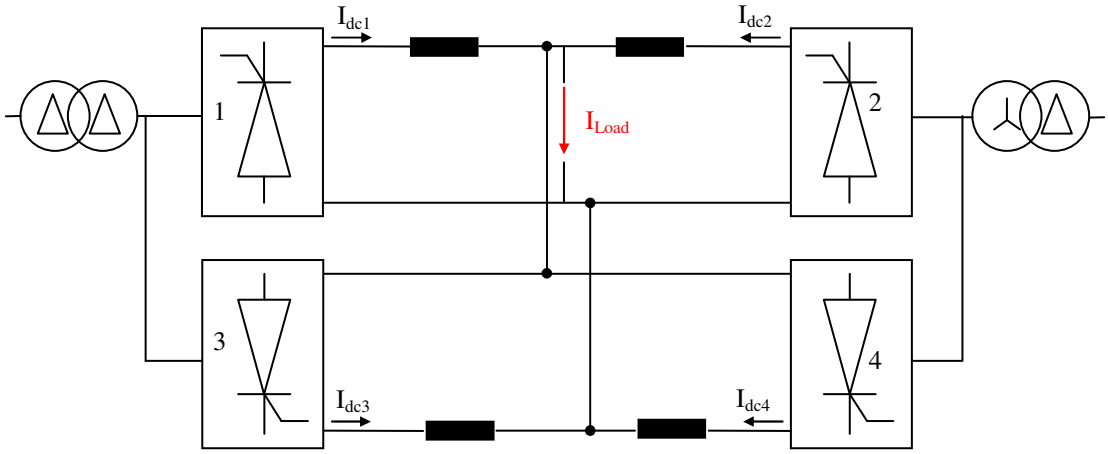

Figure 2-2 ac/dc converter base unit supplying the coils of the ITER main magnet systems

Table 2-2 Main parameters of the ac/dc converter base unit of the several superconducting coils

Converter type	Poloidal Field (PF)	Central Solenoid (CS)	Toroidal Field (TF)	Correction Coils Upper/Lower (CCU/CCL)	Correction Coils Side (CCS)
DC side data					
Rated DC current (A) Ir	55000	45000	68000	10000	10000
DC no load voltage (V)	1366	1366	351	90.5	455

Transformer data					
Rated power S_N [MVA]	39(×2)	32(×2)	13(×2)	0.5(×2)	2.4(×2)
Primary rms voltage U_{1N} [kV]	66	66	66	22	22
Secondary rms voltage U_{2N} [V]	1012	1012	260	67	337
Winding resistance r_W (‰)	2.3	2.3	2.3	2.3	2.3
No load current (%)	0.3	0.3	0.3	0.3	0.3
Iron losses (%)	0.053	0.053	0.053	0.053	0.053
Short-circuit reactance x_{SC} (%)	17.5	17.5	35	17.5	17.5
Current control data					
Current 12 pulse to 6pulse mode I_{6p} (% of rated current)	30	30	30	30	30
Current 6 pulse to circulating current mode I_{cir} (% of rated current)	15	15	15	15	15

2.2 The reactive power compensation system

The reactive power demand from the grid is controlled by a Static Var Compensator (SVC) system based on Thyristor Controlled Reactor (TCR) in combination with tuned filters which have to reduce the current harmonic content injected into the grid and to provide reactive-capacitive power. The whole system is called Reactive Power Compensation and Harmonic Filtering (RPC&HF) system (Figure 2-3).

The TCR system is controlled to minimize the reactive power demand from the grid; it operates in feed-forward mode, i.e. the reference signal to control the firing angle α_L of the TCR system is calculated using the measurement of the reactive power of the ac/dc conversion system corrected on the basis of the measurement of the busbar voltage. The phase inductance (delta-connection) of the TCR is 112.174 mH, and the main parameters of the tuned filters (star connection) are listed in the Table 2-3.

Table 2-3 Main parameters of the tuned filters

Filter order	resonant frequency	Capacity	Inductance	Quality Factor	Resistance	Q at 50Hz, 66 kV	P at 50 Hz, 66 kV
h	[Hz]	[μF]	[mH]		[Ω]	[Mvar]	[kW]
3	149	9.71	118.2	50	2.2066	15	114
5	247	41.92	9.9	25	0.6136	60	504
7	346	35.78	5.9	17	0.7703	50	442
11	539	43.63	2	13	0.536	60	446
13	637	36.74	1.7	10	0.6732	51	396
23	1129	11.05	1.8	8	1.5178	15	80
TOTAL						251	1982

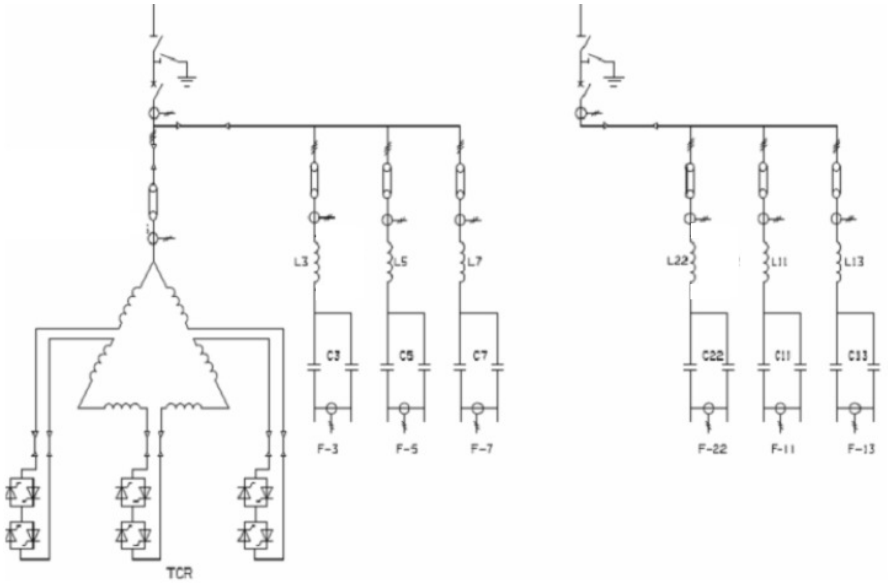

Figure 2-3 Diagram of the ITER RPC&HF System on one 66kV busbar.

References

[1] IEA key world energy statistics 2011
[2] Robert J Goldston and Paul H Rutherford, *Introduction to plasma Physics*, Institute of Physics Publishing Bristol and Philadelphia, 1995
[3] Weston Stacey, *Fusion*, Wiley VCH Verlag, 2010
[4] John Wesson with contribution from D. J. Campbell, *Tokamaks*, Oxford : Clarendon Press, 2004
[5] ITER web site: http://www.iter.org
[6] N.Mitchell, A. Devred, P. Libeyre, B. Lim and F. Savary, "The ITER Magnets: Design and Construction Status", *in IEEE Transactions on Applied Superconductivity*, no.99, November 2011.
[7] N. Mitchell, P. Bauer, D. Bessette, A. Devred, R. Gallix, C. Jong, J. Knaster, P. Libeyre, B. Lim, A. Sahu and F. Simon, "Status of the ITER magnets" in *Fusion Engineering and Design*, vol.84, n. 2-6, pp. 113-121, June 2009.
[8] A. Foussat et al, "Overview of the ITER Correction Coils Design", *in IEEE Transaction on Applied Superconductivity,* vol. 20, no. 3, June 2010.
[9] R. S. Hemsworth, A. Tanga and V. Antoni, "Status of ITER neutral beam injection system (invited)", *in Review of Scientific Instruments*, vol. 79, no. 2, Feb. 2008.
[10] J. Tao, I. Benfatto, J.K. Goff, A. Mankani, F. Milani, I. Song, H. Tan and J. Thomsen, "ITER Coil Power Supply and Distribution System" in *IEEE/NPSS 24th Symposium on Fusion Engineering (SOFE)*, 2011.
[11] A.D. Mankani, I. Benfatto, J. Tao, J.K. Goff, J. Hourtoule, J. Gascon, D. Cardoso-Rodrigues, and B. Gadeau, "The ITER reactive power compensation and harmonic filtering (RPC & HF) system: Stability & performance" in *IEEE/NPSS 24th Symposium on Fusion Engineering (SOFE)*, 2011.

Analytical models for stability analysis in high power ac/dc converters applied to the ITER case

3 The Simplified Power Supply System (SPSS)

A Simplified Power Supply System (SPSS) (Figure 3-1) has been worked out to reproduce as much as possible the active and reactive power consumption equivalent to the ITER one in order to make easier the development of the analytical models. Nevertheless the analytical approaches worked out and described in this thesis can be easily applied to the whole ITER power supply system, to take into account all the details.

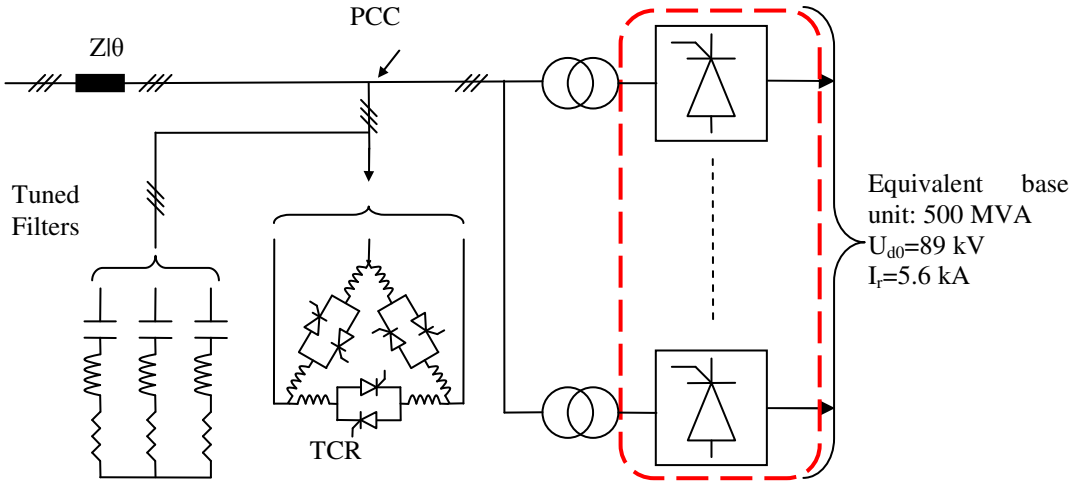

Figure 3-1 The Simplified Power Supply System (SPSS) used in the development of the model

The SPSS consists of one busbar at 66 kV only, which supplies one ac/dc converter base unit with rated power of about 500 MVA (this value is obtained considering the average distribution of the loads among the three 66 kV busbars, for instance in the design of the PPEN the loads connected to a 66 kV busbar consist of 5 PF and 2 CS ac/dc converter base units) and the reactive compensation system described in the paragraph 2.2.

All the values of main parameters of the SPSS are calculated respect to the same voltage level of 66 kV; therefore the transformer ratio of the ac/dc converter base unit is equal to 1.

The equivalent series impedance Z of the grid has been calculated in order to reproduce as much as possible the real voltage drop at the 66 kV busbar, where the short circuit impedance of the grid (multiplied by the number of the busbars equal to 3 and by a diversity/utilization factor equal to 0.8) and of the step down transformer are lumped together in the impedance Z.

The total impedance Z results:

$$Z = 3 \cdot 0.8 \cdot \frac{U^2}{S_{SC}} + v_{SC-PS} \cdot \frac{U^2}{S_{400}} = 3 \cdot 0.8 \cdot \frac{66000^2}{12 \cdot 10^9} + 0.12 \cdot \frac{66000^2}{300 \cdot 10^6} = 2.6136 \ \Omega. \qquad \text{(eq. 3-1)}$$

Where S_{SC} is the short circuit power of the grid (12 GVA), S_{400} is the nominal power and $v_{SC\text{-}PS}$ is the short circuit voltage between the primary and secondary winding of the step down transformer 400 kV/66 kV (see chapter 2 for more details)

The short circuit resistance R_Z is supposed equal to the 10 % of the reactance X_Z and they result:

$$R_Z = \frac{Z}{\sqrt{1^2 + 10^2}} = \frac{2.6136}{\sqrt{101}} = 0.2601 \ \Omega \qquad \text{(eq. 3-2)}$$

$$X_Z = \frac{Z}{\sqrt{0.1^2 + 1^2}} = \frac{2.6136}{\sqrt{1.01}} = 2.6006\ \Omega \qquad \text{(eq. 3-3)}$$

Therefore the inductance L_Z is:

$$L_Z = \frac{Z}{2\pi \cdot f} = \frac{2.6006}{2\pi \cdot 50} = 8.278\ \text{mH} \qquad \text{(eq. 3-4)}$$

Downstream of this Z impedance, at the Point of Common Coupling (PCC) with all the subsystems, the short circuit power is equal to 1.67 GVA. The limit of nominal power of 300 MVA due to the step-down transformer has been neglected allowing a more exhaustive analysis also for unusual operating conditions.
The ac/dc conversion system of the SPSS is the union of 5 PF and 2 CS ac/dc converter base units which the main data are given in the Table 2-2. The calculation of the main data of the ac/dc conversion system of the SPSS is described below, considering that the transformer ratio of the SPSS ac/dc converter base unit is equal to 1 and the per-unit values of the PF and CS ac/dc converter base unit are the same also for the SPSS one; the Figure 3-2 shows the used nomenclature related to one subunit (only a 6 pulses ac/dc converter):

- The equivalent rated dc output current $I_{N\text{-}SPSS}$ is:

$$I_{r-SPSS} = \left(I_{r-PF} \cdot 5 + I_{N-CS} \cdot 2\right) \cdot \frac{U_{2N}}{U_{2N-SPSS}} = \left(55000 \cdot 5 + 45000 \cdot 2\right) \cdot \frac{1.012}{66} = 5.6\ \text{kA} \qquad \text{(eq. 3-5)}$$

Where $U_{2N\text{-}SPSS}$ and U_{2N} are the nominal voltages of the secondary winding of the transformer of the SPSS and PF-CS ac/dc converter base unit respectively, and $I_{r\text{-}PF}$ and $I_{r\text{-}CS}$ are the rated dc output currents.

- The no-load dc voltage $U_{d0\text{-}SPSS}$ is:

$$U_{d0-SPSS} = \frac{3 \cdot \sqrt{2} \cdot U_{2N-SPSS}}{\pi} = \frac{3 \cdot \sqrt{2} \cdot 66000}{\pi} = 89.1\ \text{kV} \qquad \text{(eq. 3-6)}$$

- The rated power of the transformer $S_{N\text{-}SPSS}$

$$S_{N-SPSS} = S_{N-PF} \cdot 5 + S_{N-CS} = \left(39 \cdot 5 + 32 \cdot 2\right) \cdot 10^6 = 259\,\text{MVA} \qquad \text{(eq. 3-7)}$$

- The leakage inductance $L_{ac/dc}$ of the ac/dc converter transformer is:

$$L_{ac/dc} = x_{SC} \cdot \frac{U_{1N-SPSS}^2}{S_{N-SPSS}} \cdot \frac{1}{2\pi \cdot f} = 0.175 \cdot \frac{66000^2}{\left(39 \cdot 5 + 32 \cdot 2\right) \cdot 10^6} \cdot \frac{1}{2\pi \cdot 50} = 9.369\ \text{mH} \qquad \text{(eq. 3-8)}$$

Where x_{SC} is the per-unit value of the reactance of the PF and CS ac/dc converter transformers.

- The total winding resistance $R_{ac/dc}$ of the ac/dc converter transformer results:

$$R_{ac/dc} = 2 \cdot r_W \cdot \frac{U_{1N}^2}{S_N} = 2 \cdot 0.0023 \cdot \frac{66000^2}{\left(39 \cdot 5 + 32 \cdot 2\right) \cdot 10^6} = 77.37\ \text{m}\Omega \qquad \text{(eq. 3-9)}$$

Where r_W is the per-unit value of the resistance of the PF and CS ac/dc converter transformers.

- The inductance L_i and the resistance R_i of the inter-phase reactors are assumed:

$$L_i = 94.59\,\text{mH} \qquad \text{(eq. 3-10)}$$

$$R_i = 47.3\ \text{m}\Omega \qquad \text{(eq. 3-11)}$$

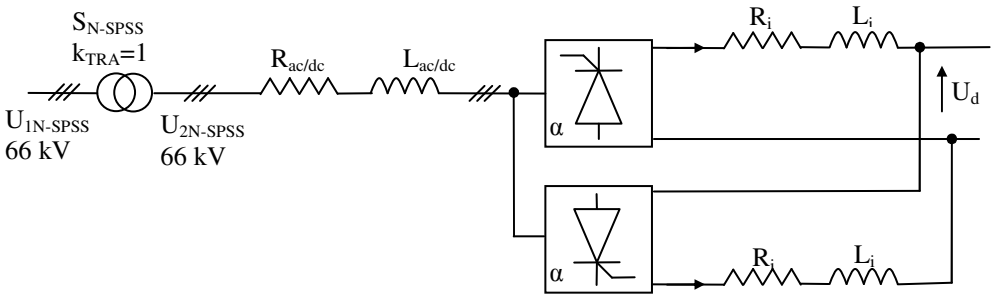

Figure 3-2 A subunit of the ac/dc conversion system considered in the SSPS

4 Quasi-Static Model used to investigate the power and voltage stabilities of the ac/dc converter system

The Quasi-Static Model is proposed in the literature [1]-[4] to calculate indexes often used to evaluate the strength of the ac system connected to High Voltage Direct Current systems: Critical Short Circuit Ratio (CSCR) [5] and Voltage Sensitivity Factor (VSF) and here it is fitted to the ITER Simplified Power Supply System (SPSS).
This model is based on the steady state equations of the system considering only the fundamental component of the ac variables and the average values of the dc ones; it doesn't describe dynamic transients. It evaluates how a small variation of a parameter can perturb an equilibrium condition, and result in a new equilibrium condition.
The equations of the model are derived by the power flow equations as a function of some relevant parameters in order to carry out sensitivity analysis.
Only the 12 pulse operating mode has been considered and the two parallel ac/dc converters are lumped in only one, neglecting the effect of the winding resistances of the transformer and of the interphase reactors between the converters and with a leakage inductance of the ac/dc converter transformer L_{ac/dc_12} equal to $L_{ac/dc}/2$
The nomenclature used in the Quasi-Static Model of the SPSS is (Figure 4-1):

- f is the frequency at 50 Hz
- U_S is the rms value of the phase to phase voltage source;
- U is the rms value of the phase to phase voltage at the point of common coupling (PCC)
- δ is the phase angle of the phase to phase voltage U at the point of common coupling (PCC) with respect to Us;
- Z is the magnitude of the short circuit impedance of the grid
- θ is the argument of the short circuit impedance of the grid
- α is the firing angle of the converter;
- L_{ac/dc_12} is the equivalent inductance of the ac/dc converter transformer
- I_{dc} is the output current of the ac/dc converter
- R_C is the equivalent resistance of the impedance at 50 Hz of the Tuned Filter written in parallel configuration
- C_{50} is the equivalent capacitance of the impedance at 50 Hz the Tuned Filter written in parallel configuration
- B_C is the value of susceptance which lumps together the effect of the TCR and of the Tuned Filters and at any equilibrium point it is equal to:

  $B_C = \frac{Q_{dc}}{U^2}$ if $Q_{dc} < 2\pi \cdot f \cdot C_{50} \cdot U^2$ (TCR not saturated)

  $B_C = 2\pi \cdot f \cdot C_{50}$ if $Q_{dc} > 2\pi \cdot f \cdot C_{50} \cdot U^2$ (TCR switched off)

  where Qdc is the ac/dc converter power consume
- U_{dc}: dc output voltage:

  $$U_{dc} = \frac{3 \cdot \sqrt{2}}{\pi} \cdot U \cdot \cos\alpha - 6 \cdot f \cdot L_{ac/dc\_12} \cdot I_{dc} \qquad \text{(eq. 4-1)}$$

- u: the overlap angle:

  $$u = \arccos\left(\cos\alpha - \frac{4 \cdot \pi \cdot f \cdot L_{ac/dc\_12}}{\sqrt{2} \cdot U} \cdot I_{dc} \right) - \alpha \qquad \text{(eq. 4-2)}$$

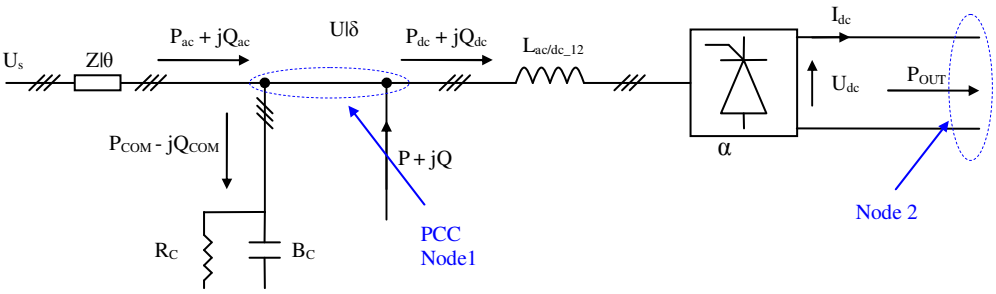

Figure 4-1 Quasi Static Model with the respective notation

The power equations of the Quasi-Static Model are:

- ac/dc converter power equations:

active power $P_{dc} = U_{dc} \cdot I_{dc}$ (eq. 4-3)

reactive power $Q_{dc} = P_{dc} \cdot \frac{(2u + \sin 2\alpha - \sin(2\alpha + 2u))}{\cos 2\alpha - \cos(2\alpha + 2u)}$ (eq. 4-4)

where U_{dc} and u have to be replaced in equations (4-3) and (4-4) by (4-1) and (4-2) respectively

- ac line power equations (phasor diagram of the ac line voltage is shown in the Figure 4-2):

active power $P_{ac} = \frac{(U \cdot U_S \cdot \cos(\delta + \theta) - U^2 \cdot \cos\theta)}{Z}$ (eq. 4-5)

reactive power $Q_{ac} = \frac{(U \cdot U_S \cdot \sin(\delta + \theta) - U^2 \cdot \sin\theta)}{Z}$ (eq. 4-6)

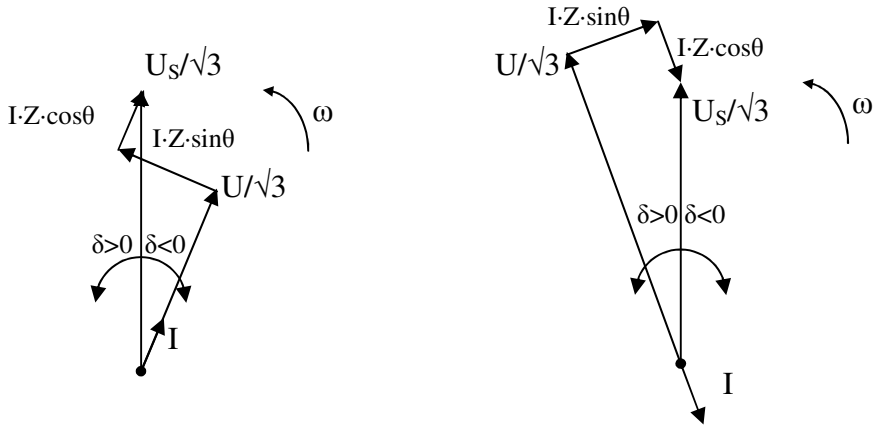

Figure 4-2 Phasor diagram of the ac line voltages

- reactive power compensation system equations:

active power $P_{COM} = \frac{U^2}{R_C}$ (eq. 4-7)

reactive power $Q_{COM} = B_C \cdot U^2$ (eq. 4-8)

- P and Q are the active and reactive power injected in the ac busbar as disturbance.
- P_{OUT} is the output power of the ac/dc converter

The Quasi-Static Model of the SPSS may be represented by a mathematical model based on algebraic equations of independent variables:

$$0 = g(x, xp) \quad \text{(eq. 4-9)}$$

Where x is the vector of three independent variables of the system and xp is the vector of input disturbance variable and g is the system of algebraic equations. The variables in x and xp may be set in order to obtain a desired parameter for the sensitivity analysis; the variables as a whole are: U, δ, I_{dc}, α, P_{OUT}, P, Q, U_S.

The algebraic equations g(U, δ, I_{dc}, α, P_{OUT}, P, Q, U_S) are achieved from the power-flow equations at each node (see Figure 4-1):

$$\begin{bmatrix} 0 \\ 0 \\ 0 \end{bmatrix} = \begin{bmatrix} P_{OUT} - P_{dc} \\ P_{ac} - P_{dc} + P - P_{COM} \\ Q_{ac} - Q_{dc} + Q + Q_{COM} \end{bmatrix} = \begin{bmatrix} g_1(U, \delta, I_{dc}, \alpha, P_{OUT}, P, Q, U_S) \\ g_2(U, \delta, I_{dc}, \alpha, P_{OUT}, P, Q, U_S) \\ g_3(U, \delta, I_{dc}, \alpha, P_{OUT}, P, Q, U_S) \end{bmatrix} = g(U, \delta, I_{dc}, \alpha, P_{OUT}, P, Q, U_S) \quad \text{(eq. 4-10)}$$

At an equilibrium point (x_0, xp_0) the differential algebraic system becomes:

$$0 = g(x_0, xp_0) \quad \text{(eq. 4-11)}$$

The algebraic equation system is linearized at the equilibrium point making possible the sensitivity analysis:

$$0 = G_x(x_0, xp_0) \cdot \Delta x + G_{xp}(x_0, xp_0) \cdot \Delta xp \quad \text{(eq. 4-12)}$$

Where G_x and G_{xp} are the Jacobian sub-matrices of g with respect to x and xp as shown below (they are obtained by symbolic calculation with Matlab tool):

$$G_x = \frac{\partial g}{\partial x}, G_{xp} = \frac{\partial g}{\partial xp} \quad \text{(eq. 4-13)}$$

In the following sections by using the jacobian matrixes calculated for the Quasi Static Model, the strength of the ac system which supplies the SPSS is evaluated in terms of power and voltage stability.

4.1 Power stability analysis

The ac/dc conversion system is considered stable in power if the output power P_{OUT} of the ac/dc converter rises with the increase of the output dc current I_{dc} in the condition of minimum firing angle α. A first evaluation of the power stability is considered by calculating Short Circuit Ratio (SCR) defined as the ratio between the short circuit power N_{SC} at the ac converter bus and the nominal dc power of the ac/dc converter $P_{N\text{-}dc}$:

$$SCR = \frac{N_{SC}}{P_{N-dc}} \quad \text{(eq. 4-14)}$$

and comparing it with the value of the Critical Short Circuit Ratio (CSCR) defined as the ratio between the short circuit power N_{SC} and the Maximum Available Power (MAP) at the ac converter bus:

$$CSCR = \frac{N_{SC}}{MAP} = \frac{1667}{486} = 3.43 \quad \text{(eq. 4-15)}$$

If SCR < CSCR the ac system is considered weak. In the standard IEEE 1204 [5] the reference value of the CSCR is 3. Considering the short circuit power (1.7 GVA) and the rated power of the ac/dc converter (500 MVA) of the SPSS the SCR results 3.4, not so far from 3.

With the Quasi-Static Model this issue may be studied in detail, evaluating the sign of the derivative of the output power P_{OUT} respect to dc current I_{dc} of the ac/dc converter at the operating condition with the nominal current of 5.6 kA; if the sign is positive the

system is power stable, if it is negative is power instable; the zero value indicates the MAP operating condition.
For the calculation of $\partial P_{OUT}/\partial I_{dc}$ by the quasi static model, the firing angle (α=0), the susceptance B_C, the injected active and reactive powers (P=0, Q=0) and the source voltage U_S (at 66 kV) are kept constant, and the vectors Δx and Δxp are:

$$\Delta x = (\Delta U, \Delta\delta, \Delta P_{OUT})^t \qquad \Delta xp = \Delta I_{dc} \qquad \text{(eq. 4-16)}$$

The equation of the quasi static model for each equilibrium point may be written:

$$G_x(x_0, xp_0)\cdot(\Delta U, \Delta\delta, \Delta P_{OUT})^t + G_{xp}(x_0, xp_0)\cdot\Delta I_{dc} = 0 \qquad \text{(eq. 4-17)}$$

If G_x^{-1} exists, the previous equation results:

$$(\Delta U, \Delta\delta, \Delta P_{OUT})^t = -G_x^{-1}(x_0, xp_0)\cdot G_{xp}(x_0, xp_0)\cdot\Delta I_{dc} = 0 \qquad \text{(eq. 4-18)}$$

The parameter $\partial P_{OUT}/\partial I_{dc}$ is equal to the matrix element 3,1:

$$\frac{\partial P_{OUT}}{\partial I_{dc}} = \left(-G_x^{-1}(x_0, xp_0)\cdot G_{xp}(x_0, xp_0)\right)_{3,1} \qquad \text{(eq. 4-19)}$$

The curves of the parameter $\partial P_{OUT}/\partial I_{dc}$ and of the power P_{OUT} versus the dc current I_{dc} of the SPSS are shown respectively in the Figure 4-3 a) and b).
At the nominal dc current of the 5.6 kA the parameter $\partial P_{OUT}/\partial I_{dc}$ has positive sign and it may be concluded that the ac/dc conversion system operates in power stability. The MAP results 486 MW at the dc current of 8 kA so the CSCR of the SPSS is 1.7/0.486=3.5, and considering the real power (net of the ac voltage drops) P_{OUT} of 423 MW at the nominal current the SCR results equal to 4; these values are slightly higher than the ones given in the literature.

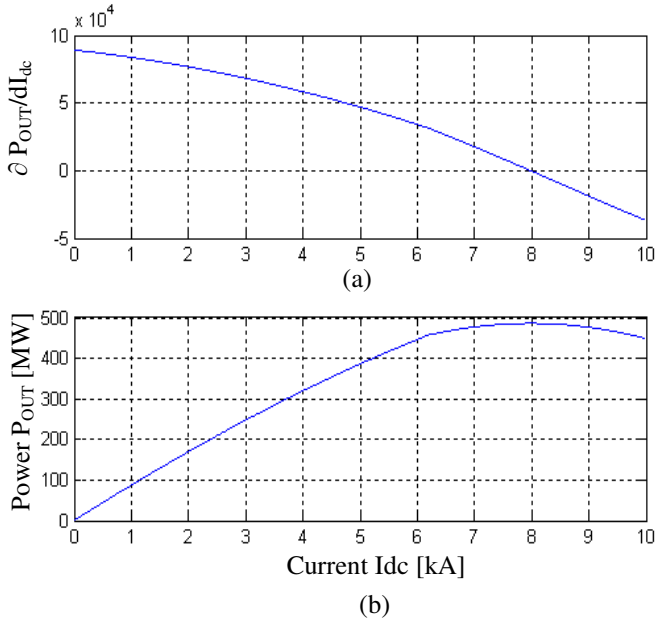

Figure 4-3 (a) Curve of the parameter $\partial P_{OUT}/\partial I_{dc}$ versus dc current I_{dc}, (b) The output power P_{OUT} versus dc current I_{dc}

4.2 Voltage stability analysis

The busbar voltage U at the PCC is very sensitive to the variation of the reactive power. The Voltage Sensitivity Factor index defined as the derivative of the voltage U respect to the reactive power Q injected in the ac busbar can be an useful indicator of the voltage stability. The more this index is low, the more the system may be considered

voltage stable. A possible cause of injection of reactive power Q can be due to a control error in the reactive power compensation system.
For the calculation of the VSF by using the quasi static model, the dc current I_{dc}, the power P_{OUT}, the susceptance BC, the injected active power (P=0) and the source voltage US (at 66 kV) are kept constant in the neighborhood of the equilibrium point, and the vectors Δx and Δxp are:

$$\Delta x = (\Delta U, \Delta\delta, \Delta\alpha)^t$$
$$\Delta xp = \Delta Q \qquad \text{(eq. 4-20)}$$

The equation of the quasi static model for each equilibrium point may be written:

$$G_x(x_0, xp_0)\cdot(\Delta U, \Delta\delta, \Delta\alpha)^t + G_{xp}(x_0, xp_0)\cdot\Delta Q = 0 \qquad \text{(eq. 4-21)}$$

If G_x^{-1} exists, the previous equation results:

$$(\Delta U, \Delta\delta, \Delta\alpha)^t = -G_x^{-1}(x_0, xp_0)\cdot G_{xp}(x_0, xp_0)\cdot\Delta Q = 0 \qquad \text{(eq. 4-22)}$$

The parameter ∂U/∂Q is equal to the matrix element 1,1:

$$\frac{\partial U}{\partial Q} = \left(-G_x^{-1}(x_0, xp_0)\cdot G_{xp}(x_0, xp_0)\right)_{1,1} \qquad \text{(eq. 4-23)}$$

Usually the VSF is given in per unit value defined as:

$$VSF = \frac{\partial U / U_{nom}}{\partial Q / Q_{comp,nom}} \qquad \text{(eq. 4-24)}$$

where $Q_{comp,nom}$ is the nominal reactive power of the Tuned Filters (250 Mvar) and U_{nom} is the nominal voltage of the converter bus bar (66 kV).
The surface of the VSF (Figure 4-4) and of the busbar voltage U (Figure 4-5) versus the active power P_{dc} reactive power Q_{dc} plane have been plotted for all operating points of the SPSS limiting the dc current to the rated value of 5.6 kA and the reactive power demand from the grid to 67 Mvar.

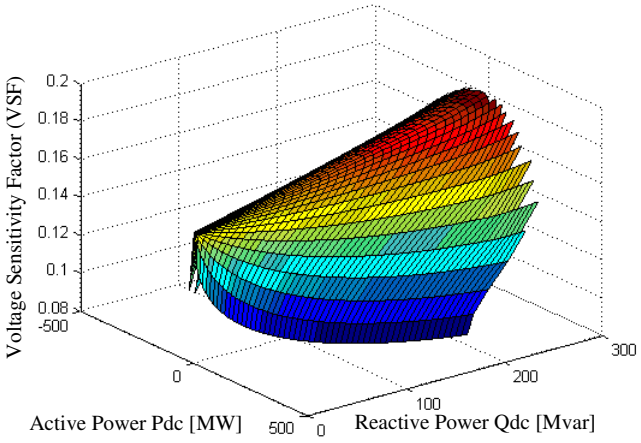

Figure 4-4 Voltage sensitivity Factor for all the operating conditions

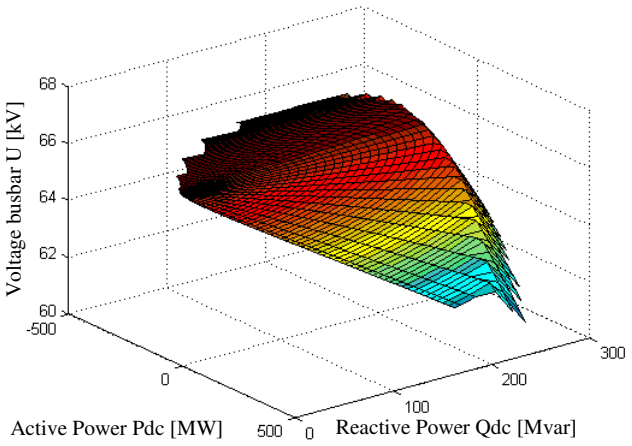

Figure 4-5 Voltage busbar U for all the operating conditions

It may be noted that the VSF is enough limited in all the possible operating condition of the SPSS with a maximum value of 0.2, and also the variation range of the voltage busbar U is low and so no voltage instability has been found.

5 The Dynamic Model

The Dynamic Model is based on the state space formulation of the Simplified Power Supply System (SPSS see chapter 3), allowing the study of the dynamic stability of the system by the eigenvalue analysis and the calculation of the subsystem participation factors to identify the causes of the instabilities [6]-[8].
The Simplified Power Supply System (SPSS) can be divided in three subsystems: the Tuned Filters, the TCR and the ac/dc converter which are connected at the same busbar downstream of the short circuit impedance.
The active subsystems of the SPSS can be considered as a current source controlled by two types of inputs: the former is the busbar voltage on the Point of Common Coupling (PCC) with all the subsystems and the latter represents the inputs for the control of the subsystem. The Tuned Filters subsystem doesn't have any control and the output currents can be written as a linear function of the PCC voltage, while the TCR and the ac/dc converter have their control system and their output currents are non-linear function of the inputs. It is assumed to implement Phase Locked Loop to synchronize the TCR and ac/dc converter control systems to the ac input voltages. Figure 5-1 shows the notation used in the Dynamic Model.
Considering the nature non linear and discrete of the ac/dc converter and of the TCR system, the building of the state space matrix of the whole system is not an easy task. The identified approach for this study has similarities with the one previous presented Jovcic in [9]-[11]. In this approach the discrete phenomena have been approximated with continuous transfer functions. So a non-linear algebraic-differential equation system based on the equations related the fundamental components for ac system and mean ones for the dc system may be written. Moreover the ac variables have been represented in dq frame by Park's transformation [12], so the ac and dc system has the same frequency frame making possible the small signal analysis around an equilibrium point.
Considering the limit due to the approximation of the discrete transfer functions by continuous ones, the Dynamic Model under study aims to investigate phenomena with range frequency less than 100 Hz.
The next paragraph describes the applied general method to achieve the Dynamic Model of each subsystem based on the approach at the state space formulation for each subsystem. Then the transfer functions and analytical equations used to define the Dynamic Model of the each subsystem (TCR, Tuned Filters and ac/dc conversion system) are illustrated. Some components, as for example the Phase Locked Loop, are used in several subsystems, and they are described at first. Finally the building of the state matrix of the whole system is shown and a stability analysis of the SPSS has been carried out. Models of the subsystems and of the whole system SPSS have been built by a simulation program (PSIM) capable to reproduce the system instantaneous waveforms allowing the validation of the equivalent Dynamic Models (run in Matlab Simulink program, state space tool) in frequency and time domain by a comparison between the simulation results.

5.1 The building of the Dynamic Model of each subsystem

Adopting a modular approach, for each subsystem (Tuned Filter, TCR and ac/dc converter) a non linear algebraic-differential equation system with n state variables can be written:

- Differential equation system:

$$\begin{bmatrix} f_1(\dot{x}_{subsys}, x_{subsys}, e_d, e_q, inp_{subsys}) \\ \dots \\ f\dots(\dot{x}_{subsys}, x_{subsys}, e_d, e_q, inp_{subsys}) \\ \dots \\ f_n(\dot{x}_{subsys}, x_{subsys}, e_d, e_q, inp_{subsys}) \end{bmatrix} = f_{subsys}(\dot{x}_{subsys}, x_{subsys}, e_d, e_q, inp_{subsys}) = 0 \quad \text{(eq. 5-1)}$$

- Algebraic equation system

$$id_{subsys=} = g_{subsys}(x_{subsys})$$
$$iq_{subsys=} = g_{subsys}(x_{subsys}) \quad \text{(eq. 5-2)}$$

Where f and g are the differential and algebraic equation systems respectively, x indicates the state vector, $\dot{x}$ is the vector of the derivative of x, inp is the vector of the input variables and id and iq are the flowing current of the considered subsystem, while e_d and e_q are respectively the d and q components of the voltage on the Point of Common Coupling (PCC) with all the subsystems. It is highlighted that g is given as function of the state variables only and the feed through (or feed forward) matrix results equal to a zeros matrix due to the nature of the subsystems. Applying the small signal analysis to the non linear algebraic-differential equation system around an equilibrium point p = ($\dot{x}_0$, x_0, e_{d0}, e_{q0}, inp_0) results:

$$f_{\dot{x}} \cdot \Delta\dot{x} + f_x \cdot \Delta x + f_e \cdot [\Delta e_d, \Delta e_q]^T + f_{inp} \cdot \Delta inp = 0$$
$$[\Delta id, \Delta iq]^T = g_x \cdot \Delta x$$

Where the matrixes $f_{\dot{x}}$, f_x, f_e, f_{inp} and g_x are the Jacobian matrixes at the equilibrium point p defined as:

$$f_{\dot{x}} = \left.\frac{\partial f}{\partial \dot{x}}\right|_p \quad f_x = \left.\frac{\partial f}{\partial x}\right|_p \quad f_e = \left.\frac{\partial f}{\partial (ed, eq)}\right|_p \quad f_{inp} = \left.\frac{\partial f}{\partial inp}\right|_p \quad g_x = \left.\frac{\partial (id, iq)}{\partial x}\right|_p \quad \text{(eq. 5-3)}$$

Finally it is possible to define the Dynamic Model of the subsystem written as a state space matrix:

$$[\Delta\dot{x}_{subsys}] = A_{subsys} \cdot [\Delta x_{subsys}] + B_{e\_subsyst} \cdot \begin{bmatrix} e_d \\ e_q \end{bmatrix} + B_{i\_subsyst} \cdot [inp_{subsys}] \quad \text{(eq. 5-4)}$$
$$[\Delta i_{subsys}] = C_{subsys} \cdot [\Delta x_{subsys}]$$

where the state matrix A_{subsyt} is:

$$A_{subsys} = -f_{\dot{x}}^{-1} \cdot f_x$$

B_e is the input matrix related to the PCC voltage:

$$B_e = -f_{\dot{x}}^{-1} \cdot f_e$$

B_{i_subsyt} is the input matrix of the input variables:

$$B_{i\_subsyst} = -f_{\dot{x}}^{-1} \cdot f_i$$

and C_{subsyt} is the output matrix of currents:

$$C_{subsyst} = g_x$$

The Jacobian Matrixes have been calculated by using the Symbolic Calculation Tool of Matlab.

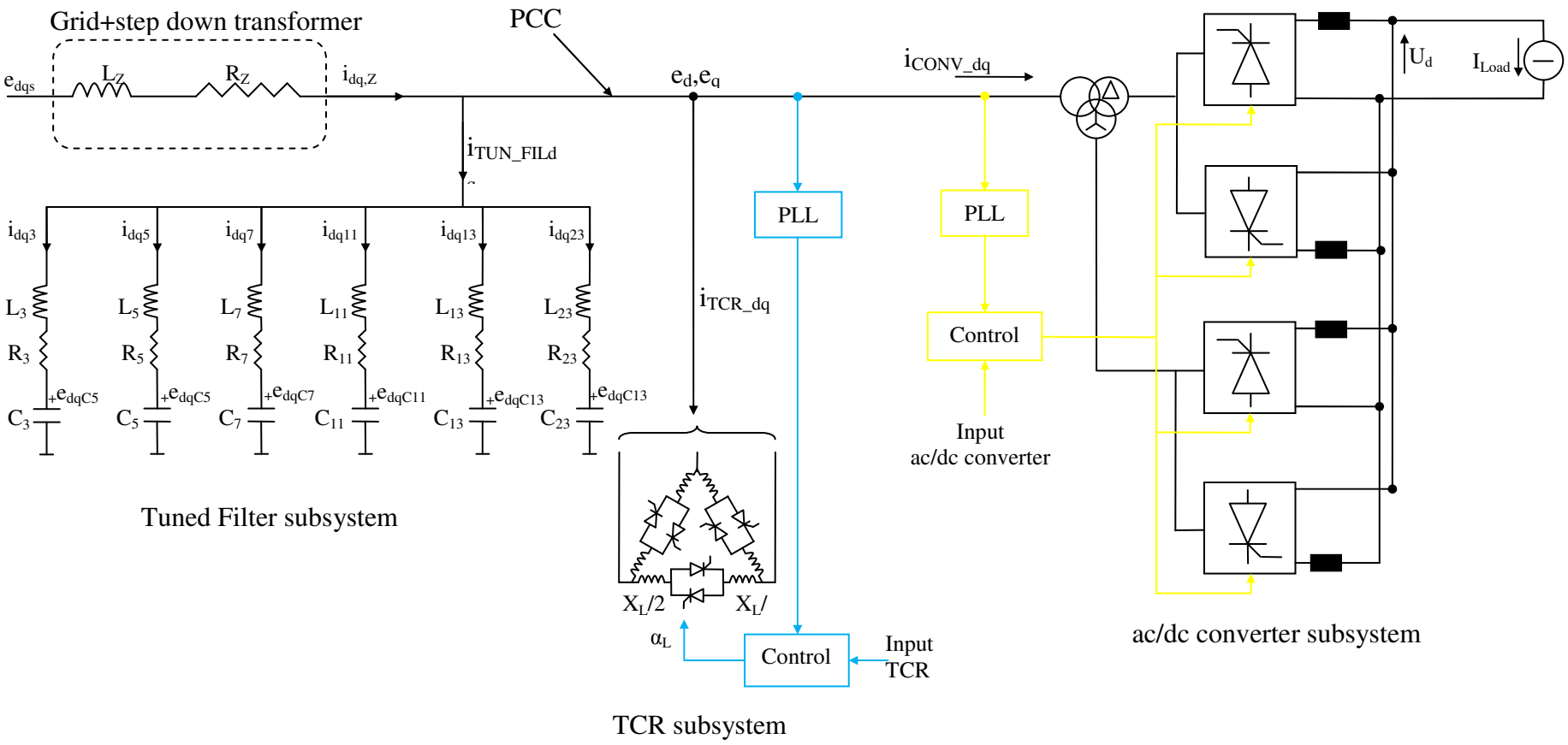

Figure 5-1 Notation used in the Dynamic Model

5.2 The Phase Locked Loop

In the Figure 5-2 it is shown the block scheme of the Phase Locked Loop [13].

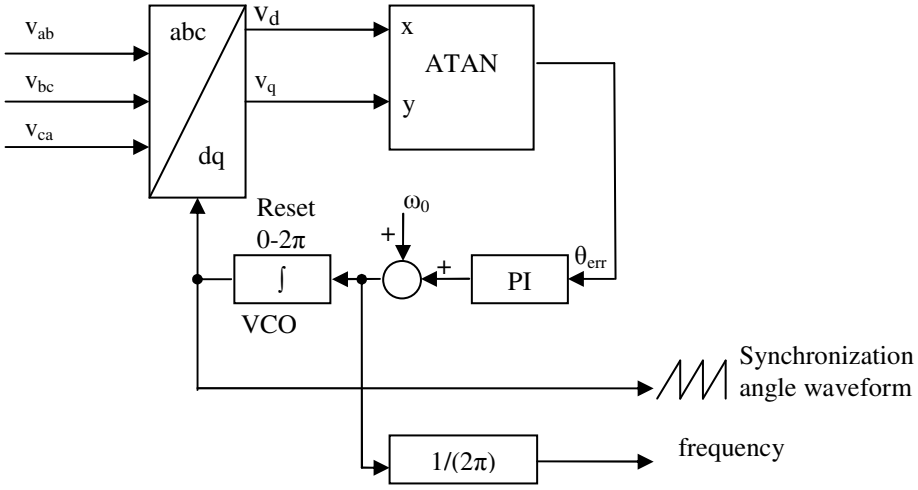

Figure 5-2 Bolck scheme of the Phase Locked Loop

The three input line to line voltage are transformed into d-q components and then the error angle is calculated and it is corrected by the PI controller. The Voltage Controlled Oscillator (VCO) integrates the angular frequency providing the reference angle locked on the fundamental component.

5.2.1 The analytical model equations of the PLL in dq frame

The block scheme of the PLL in dq frame is shown in the Figure 5-3.

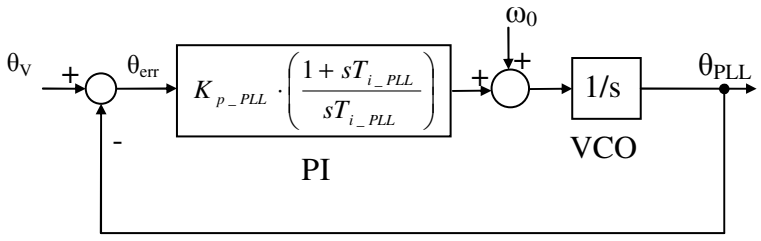

Figure 5-3 Block scheme of the PLL control

Defining in variable in dq frame:

- θ_V is the angle written as function of the dq components of the busbar voltage e_d and e_q at the PCC (see Figure 5-4)

$$\theta_V = \arctan\left(\frac{e_q}{e_d}\right) \qquad \text{(eq. 5-5)}$$

- The output of the integrator θ_{PLL}
- The output of the integrator of the PI controller = w_{1_PLL}

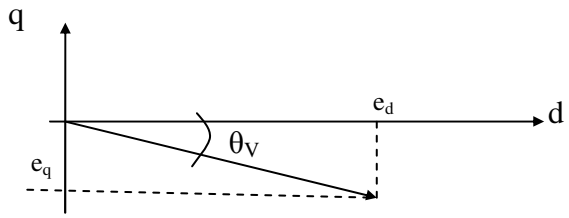

Figure 5-4 Diagram of the angle voltage θ_V related to the d-q component of the voltage e_d and e_q

The state equations result

$$\left(k_{p\_PLL}\cdot\left(\arctan\left(\frac{e_q}{e_d}\right)-\theta_{PLL}\right)\right)-T_{i\_PLL}\cdot\frac{dw_{1\_PLL}}{dt}=0 \qquad \text{(eq. 5-6)}$$

$$\left(k_{p\_PLL}\cdot\left(\arctan\left(\frac{e_q}{e_d}\right)-\theta_{PLL}\right)+w_{1\_PLL}\right)-\frac{d\theta_{PLL}}{dt}=0 \qquad \text{(eq. 5-7)}$$

The response of the PLL to a variation of the phase angle of the busbar voltage depends principally from the proportional gain k_{p_PLL} of the PI controller, while the response to the variation of the frequency from f_0 depends from the time constant T_{i_PLL}.
For this study the bandwidth of angle control is set to 650 Hz (this value of bandwidth has been assumed because the harmonics are filtered until more than the 13th component, i.e. 650 Hz, and to increase interaction phenomena between subsystem in order to validate the models) and the one of the frequency control is set to 50 Hz and the parameters of the PI controller result:
$k_{p\_PLL}= 2\cdot\pi\cdot650$
$T_{i\_PLL}= 1/(2\cdot\pi\cdot50)$
The bandwidth of angle control is enough higher than the one of the frequency control to avoid interaction between the two control loops that produces overshoot in the output angle θ_{PLL}.

5.3 The analytical model equations of the mean value calculation

The measures to be utilized as feedback signals in the control loops need to be filtered. For example the dc output voltage on the dc load is filtered by a block (called mean block) with time constant of 3.333 ms. The transfer function of the mean block is shown in the Figure 5-5.

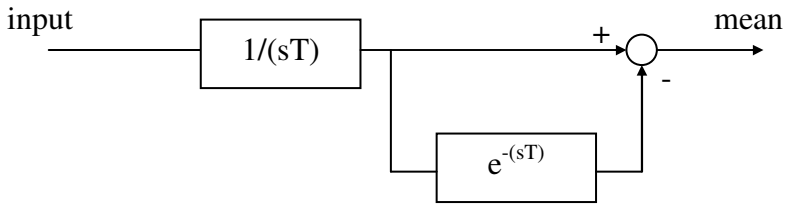

Figure 5-5 Block scheme of the mean value calculation

The transfer function G_M of the mean block in s-domain can be written:

$$G_M(s)=\frac{1-e^{-sT_i}}{sT_i} \qquad \text{(eq. 5-8)}$$

where T_i is the integration time.

Writing the transfer function G_M as function of jω results:

$$G_M(s) = \frac{1 - e^{-j\omega T_i}}{j\omega T_i} \cong \frac{1 - \cos(\omega T_i) + j\sin(\omega T_i)}{j\omega T_i} \quad \text{(eq. 5-9)}$$

The magnitude of the transfer function G_M is:

$$|G_M(j\omega)| = \frac{\sqrt{(1-\cos(\omega T_i))^2 + (\sin(\omega T_i))^2}}{\omega T_i} = \frac{\sqrt{1+(\cos(\omega T_i))^2 + (\sin(\omega T_i))^2 - 2\cdot\cos(\omega T)}}{\omega T_i} = \quad \text{(eq. 5-10)}$$

$$= \frac{\sqrt{2-2\cdot\cos(\omega T_i)}}{\omega T_i} = \frac{2\sqrt{\frac{1-\cos(\omega T_i)}{2}}}{\omega T_i} = \frac{\sin\left(\frac{\omega T_i}{2}\right)}{\frac{\omega T_i}{2}}$$

and considering the numerator and the denominator phase of G_M equal to (π+ωT)/2 and π /2 respectively, the phase of G_M results

$$\varphi_{GM}(\omega) = \frac{\pi}{2} + \frac{\omega T_i}{2} - \frac{\pi}{2} = \frac{\omega T_i}{2} \quad \text{(eq. 5-11)}$$

For frequency range lower than $1/T_i$ the mean block can be represented with the transfer function of a time delay equal to $T_i/2$ and in the following sections it has been represented as a low pass filter with a constant time equal to $T_i/2$:

$$G_M(s) = \frac{1 - e^{-sT_i}}{sT_i} \cong e^{-s\frac{T}{2}} \cong \frac{1}{1 + s\frac{T_i}{2}} \quad \text{(eq. 5-12)}$$

A frequency spectrum analysis with the aim to verify of the approximation of the mean block with integration time Ti of 3.333 ms by the respective low pass filter has been carried out. The result is shown in the Figure 5-6 in terms of magnitude ratio and phase error between the outputs of the low pass filter and of the mean block applying to the input sinusoidal waveforms at several frequency values. It should be noted that the approximation is accurate for frequency range lower than 300 Hz, which is the frequency value equal to the reciprocal of the integration time Ti.

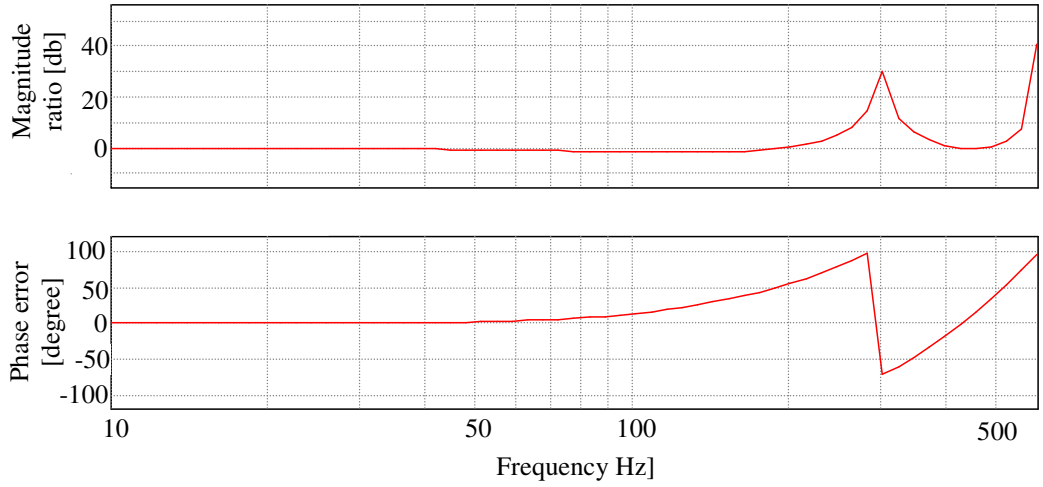

Figure 5-6 Magnitude ratio and phase error between the outputs of the low pass filter and of the mean block in the frequency domain

5.4 The analytical model equations of the Tuned Filters Subsystems

This Tuned filter subsystem is a linear and continuous system. The analytical equations are the state equations of the inductors and capacitors written in dq frame and they are written below:

- 3rd harmonic filter

$$e_d - e_{C3d} + \omega \cdot L_3 \cdot i_{3q} - R_3 \cdot i_{3d} - L_3 \cdot \frac{di_{3d}}{dt} = 0$$

$$e_q - e_{C3q} - \omega \cdot L_3 \cdot i_{3d} - R_3 \cdot i_{3q} - L_3 \cdot \frac{di_{3q}}{dt} = 0 \qquad \text{(eq. 5-13)}$$

$$i_{3d} + \omega \cdot C_3 \cdot e_{C3q} - C_3 \cdot \frac{de_{C3d}}{dt} = 0$$

$$i_{3q} - \omega \cdot C_3 \cdot e_{C3d} - C_3 \cdot \frac{de_{C3q}}{dt} = 0 \qquad \text{(eq. 5-14)}$$

- 5th harmonic filter

$$e_d - e_{C5d} + \omega \cdot L_5 \cdot i_{5q} - R_5 \cdot i_{5d} - L_5 \cdot \frac{di_{5d}}{dt} = 0$$

$$e_q - e_{C5q} - \omega \cdot L_5 \cdot i_{5d} - R_5 \cdot i_{5q} - L_5 \cdot \frac{di_{5q}}{dt} = 0 \qquad \text{(eq. 5-15)}$$

$$i_{5d} + \omega \cdot C_5 \cdot e_{C5q} - C_5 \cdot \frac{de_{C5d}}{dt} = 0$$

$$i_{5q} - \omega \cdot C_5 \cdot e_{C5d} - C_5 \cdot \frac{de_{C5q}}{dt} = 0 \qquad \text{(eq. 5-16)}$$

- 7th harmonic filter

$$e_d - e_{C7d} + \omega \cdot L_7 \cdot i_{7q} - R_7 \cdot i_{7d} - L_7 \cdot \frac{di_{7d}}{dt} = 0$$

$$e_q - e_{C7q} - \omega \cdot L_7 \cdot i_{7d} - R_7 \cdot i_{7q} - L_7 \cdot \frac{di_{7q}}{dt} = 0 \qquad \text{(eq. 5-17)}$$

$$i_{7d} + \omega \cdot C_7 \cdot e_{C7q} - C_7 \cdot \frac{de_{C7d}}{dt} = 0$$

$$i_{7q} - \omega \cdot C_7 \cdot e_{C7d} - C_7 \cdot \frac{de_{C7q}}{dt} = 0 \qquad \text{(eq. 5-18)}$$

- 11th harmonic filter

$$e_d - e_{C11d} + \omega \cdot L_{11} \cdot i_{11q} - R_{11} \cdot i_{11d} - L_{11} \cdot \frac{di_{11d}}{dt} = 0$$

$$e_q - e_{C11q} - \omega \cdot L_{11} \cdot i_{11d} - R_{11} \cdot i_{11q} - L_1 \cdot \frac{di_{11q}}{dt} = 0 \qquad \text{(eq. 5-19)}$$

$$i_{11d} + \omega \cdot C_{11} \cdot e_{C11q} - C_5 \cdot \frac{de_{C11d}}{dt} = 0$$

$$i_{11q} - \omega \cdot C_{11} \cdot e_{C11d} - C_{11} \cdot \frac{de_{C11q}}{dt} = 0 \qquad \text{(eq. 5-20)}$$

- 13th harmonic filter

$$e_d - e_{C13d} + \omega \cdot L_{13} \cdot i_{13q} - R_{13} \cdot i_{13d} - L_{13} \cdot \frac{di_{13d}}{dt} = 0$$

$$e_q - e_{C13q} - \omega \cdot L_{13} \cdot i_{13d} - R_{13} \cdot i_{13q} - L_{13} \cdot \frac{di_{13q}}{dt} = 0 \qquad \text{(eq. 5-21)}$$

$$i_{13d} + \omega \cdot C_{13} \cdot e_{C13q} - C_{13} \cdot \frac{de_{C13d}}{dt} = 0$$
$$i_{13q} - \omega \cdot C_{13} \cdot e_{C13d} - C_{13} \cdot \frac{de_{C13q}}{dt} = 0 \qquad \text{(eq. 5-22)}$$

- 23th harmonic filter

$$e_d - e_{C23d} + \omega \cdot L_{23} \cdot i_{23q} - R_{23} \cdot i_{23d} - L_{23} \cdot \frac{di_{23d}}{dt} = 0$$
$$e_q - e_{C23q} - \omega \cdot L_{23} \cdot i_{23d} - R_{23} \cdot i_{23q} - L_{23} \cdot \frac{di_{23q}}{dt} = 0 \qquad \text{(eq. 5-23)}$$

$$i_{23d} + \omega \cdot C_{23} \cdot e_{C23q} - C_{23} \cdot \frac{de_{C23d}}{dt} = 0$$
$$i_{23q} - \omega \cdot C_{13} \cdot e_{C23d} - C_{23} \cdot \frac{de_{C23q}}{dt} = 0 \qquad \text{(eq. 5-24)}$$

5.4.1 The Dynamic Model of the Tuned Filters subsystem

The Dynamic Model of the Tuned Filter subsystem has been represented by a state space matrix where:

- the inputs are the dq component of voltage busbar (e_d, e_q),
- the outputs are the total current of the tuned filters (i_{filt_d}, i_{filt_q}).
- No inputs control.

The Tuned Filter equations from eqs. 5-13 to 5-24 are used to build the state space matrix of the system.
The vector of the state variable x results:

- i_{3d}, i_{3q}, e_{C3d}, e_{C3q}, i_{5d}, i_{5q}, e_{C5d}, e_{C5q}, i_{7d}, i_{7q}, e_{C7d}, e_{C7q}, i_{11d}, i_{11q}, e_{C11d}, e_{C11q}, i_{13d}, i_{13q}, e_{C13d}, e_{C13q}, i_{23d}, i_{23q}, e_{C23d}, e_{C23q}

And the output vector consists of the output currents of the Tuned Filters equal to:

- $i_{Tun\_Fil\_d}=i_{3d}+i_{5d}+i_{7d}+i_{11d}+i_{13d}+i_{23d}$
- $i_{Tun\_Fil\_q}=i_{3q}+i_{5q}+i_{7q}+i_{11q}+i_{13q}+i_{23q}$

Considering the method described in the paragraph 5.1, the Dynamic Model of the Tuned Filters Subsystem is:

$$\left[\Delta \dot{x}_{Tun\_Fil}\right] = A_{Tun\_Fil} \cdot \left[\Delta x_{Tun\_Fil}\right] + B_{e\_Tun\_Fil} \cdot \begin{bmatrix} e_d \\ e_q \end{bmatrix} \qquad \text{(eq. 5-25)}$$
$$\left[\Delta i_{Tun\_Filt}\right] = C_{Tun\_Fil} \cdot \left[\Delta x_{Tun\_Fil}\right]$$

Where the matrix $B_{i\_TUN\_FIL}$ is a zero matrix because there are no control inputs, so it is not included.

5.5 The TCR subsystem

The block scheme of the TCR system is shown in the Figure 5-7. The TCR system is controlled to minimize the reactive power demand from the grid; it operates in feed-forward mode, i.e. the reference signal to control the firing angle α_L of the TCR system is calculated using the measurement of the reactive power of the ac/dc conversion system corrected on the basis of the measurement of the busbar voltage. The relation between the firing angle α_L and the inductance L of the TCR at the fundamental component is:

$$\frac{1}{L(\alpha_L)} = \frac{3}{L_r} \frac{(2\pi - 2\alpha_L + \sin(2\alpha_L))}{\pi} \qquad \text{(eq. 5-26)}$$

where L_r is the inductance of each phase branch of the TCR and the angle α_L is related to the zero cross of the respective phase voltage on the TCR and it may vary from $\pi/2$ rad (maximum consume of reactive power) to a π rad (consume of reactive power equal to 0). It may be noted that the relation is not linear, but it can be easily linearized by look-up table.
In dq frame the inputs of the TCR system are the measures of dq components of the ac/dc converter current and the dq components of the busbar voltage e_d and e_q, while the output variables are the TCR current i_{TCRdq}.
In the following paragraphs the analytical equations used to build the state space matrix for the small signal analysis are illustrated dividing the TCR system in two parts: the former (on the left of the Figure 5-7) explains the analytical equation describing the TCR dynamic, while the latter (on the right of the Figure 5-7) explains the feed forward calculation. The interface between the two parts is the reference signal of the TCR ref_{TCR}.

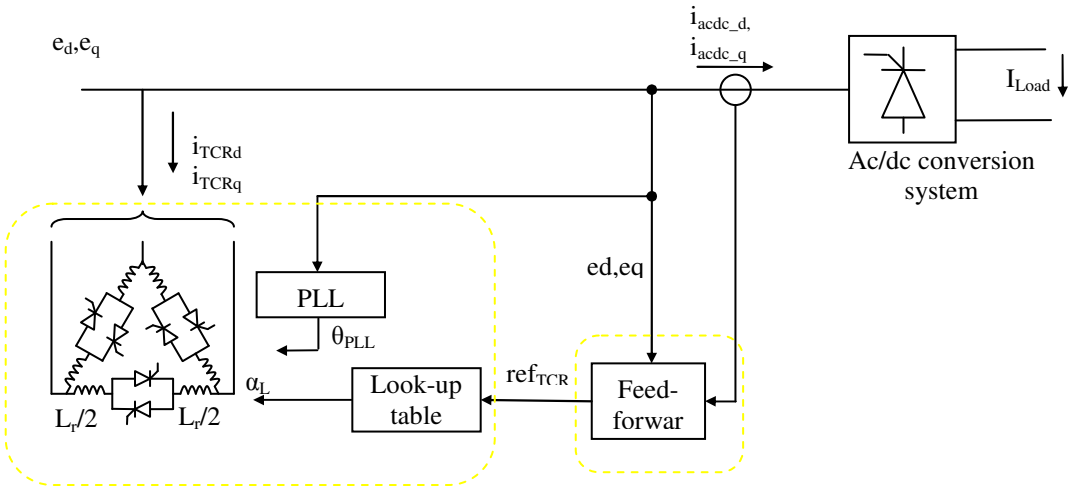

Figure 5-7 The block scheme of the TCR subsystem

5.5.1 TCR dynamic modeling

In literature [14]-[18] the continuous models of the TCR system is represented with the two transfer function $G_1(s)$ and $G_2(s)$ (Figure 5-8):

$$G_1(s) = e^{-sTd}$$

$$G_2(s) = \frac{1}{1+sT_b} \qquad \text{(eq. 5-27)}$$

where $G_1(s)$ is related to the time delay T_d of firing angle alpha assumed as the average time between two switching instants (of about one ms) and $G_2(s)$ is a low pass filter with time constant Tb, which models the TCR switching sequence accounting for the three phases arrangement represented by a low pass filter with time constant T_b (value between 3 and 6 ms).
The dq components of the TCR current (i_{TCRd} and i_{TCRq}) are calculated by the system G_3 of differential equations:

$$\begin{bmatrix} \frac{di_{TCRd}}{dt} \\ \frac{di_{TCRq}}{dt} \end{bmatrix} = \begin{bmatrix} 0 & \omega \\ -\omega & 0 \end{bmatrix} \cdot \begin{bmatrix} i_{TCRd} \\ i_{TCRq} \end{bmatrix} + \begin{bmatrix} out_{G2d} \\ out_{G2q} \end{bmatrix} \qquad \text{(eq. 5-28)}$$

Where out_{G2d} and out_{G2q} are the output d-q components of the transfer function $G_2(s)$.

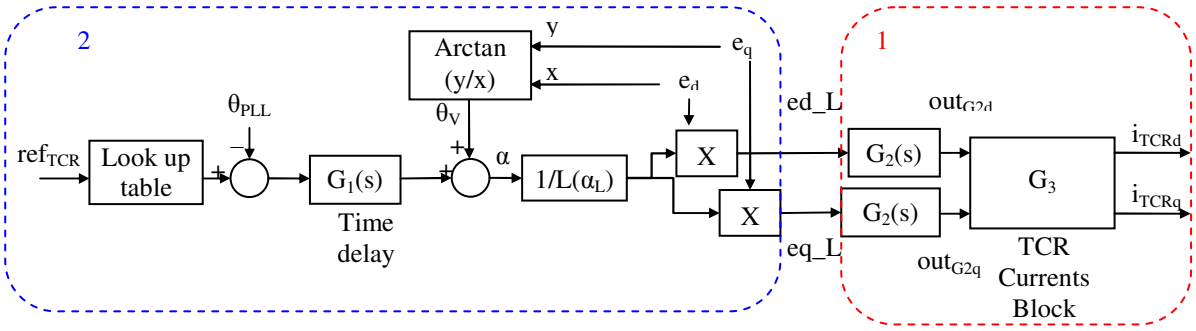

Figure 5-8 The transfer function of the TCR subsystem

These equations show an un-damped homogeneous component at angular frequency of -ω in dq frame, which is inconsistent with the real operation of the TCR system; the introduction of the angular frequency ω depend on the change from the ac to dq frame, it is related to the frequency of the grid of 50 Hz and it results equal to $2 \cdot \pi \cdot f = 2 \cdot \pi \cdot 50 \approx 314$ rad/s. Therefore the existing continuous models in literature are accurate for frequency range lower than about 25 Hz.

The modelling of the TCR dynamic has been divided in two parts (see the Figure 5-8) to make easier understanding it where the interface signals are ed_L and eq_L.

5.5.1.1 Modeling of the part 1 of the TCR system

For this study a slightly different approach has been thought in order to eliminate the un-damped homogeneous component, such to increase the frequency range. The modelling of the TCR dynamic inside the red dashed box is improved and the new one is represented in the block scheme of Figure 5-9. In the model of TCR worked out for this study, a band-stop filter with center angular frequency ω_0 equal to ω is put in series between the input signals (ed_L, eq_L) and before TCR current block G_3 eliminating the un-damped homogeneous component. With this solution the angular frequency at + ω and -ω are eliminated but in the real case just the one at -ω is eliminated. So in parallel to the previous block a pass-band is put in series to the inputs (ed_L, eq_L) and before TCR current block G_3, but the output of the TCR current block are manipulated in order to eliminate only the component at -ω.

In the dq reference frame the direct I_f and reverse I_b sequences can be written:

$$\begin{aligned} i_d &= I_f \cdot \cos(\omega t + \varphi_f) + I_b \cdot \cos(-\omega t + \varphi_b) \\ i_q &= I_f \cdot \sin(\omega t + \varphi_f) + I_b \cdot \sin(-\omega t + \varphi_b) \end{aligned} \qquad \text{(eq. 5-29)}$$

And the derivatives are

$$\begin{aligned} \frac{di_d}{dt} &= -\omega \cdot I_f \cdot \sin(\omega t + \varphi_f) + \omega \cdot I_b \cdot \sin(-\omega t + \varphi_b) \\ \frac{di_q}{dt} &= \omega \cdot I_f \cdot \cos(\omega t + \varphi_f) - \omega \cdot I_b \cdot \cos(-\omega t + \varphi_b) \end{aligned} \qquad \text{(eq. 5-30)}$$

The reverse component at -ω can be eliminated combining the dq component with the respective derivative, obtaining just the direct sequence I_f as explained in the following equations:

$$out_d = \frac{i_d}{2} + \frac{di_q}{dt} \cdot \frac{1}{2 \cdot \omega} =$$
$$= \frac{1}{2}\left(I_f \cdot \cos(\omega t + \varphi_f) + I_b \cdot \cos(-\omega t + \varphi_b)\right) + \frac{1}{2 \cdot \omega}\left(\omega \cdot I_f \cdot \cos(\omega t + \varphi_f) - \omega \cdot I_b \cdot \cos(-\omega t + \varphi_b)\right) =$$
$$= I_f \cdot \cos(\omega t + \varphi_f) \qquad \text{(eq. 5-31)}$$

$$out_q = \frac{i_q}{2} - \frac{di_d}{dt} \cdot \frac{1}{2 \cdot \omega} =$$
$$= \frac{1}{2}\left(I_f \cdot \sin(\omega t + \varphi_f) + I_b \cdot \sin(-\omega t + \varphi_b)\right) - \frac{1}{2 \cdot \omega}\left(-\omega \cdot I_f \cdot \sin(\omega t + \varphi_f) + \omega \cdot I_b \cdot \sin(-\omega t + \varphi_b)\right) =$$
$$= I_f \cdot \sin(\omega t + \varphi_f)$$

The components out_d and out_q are equal only to the direct sequence.

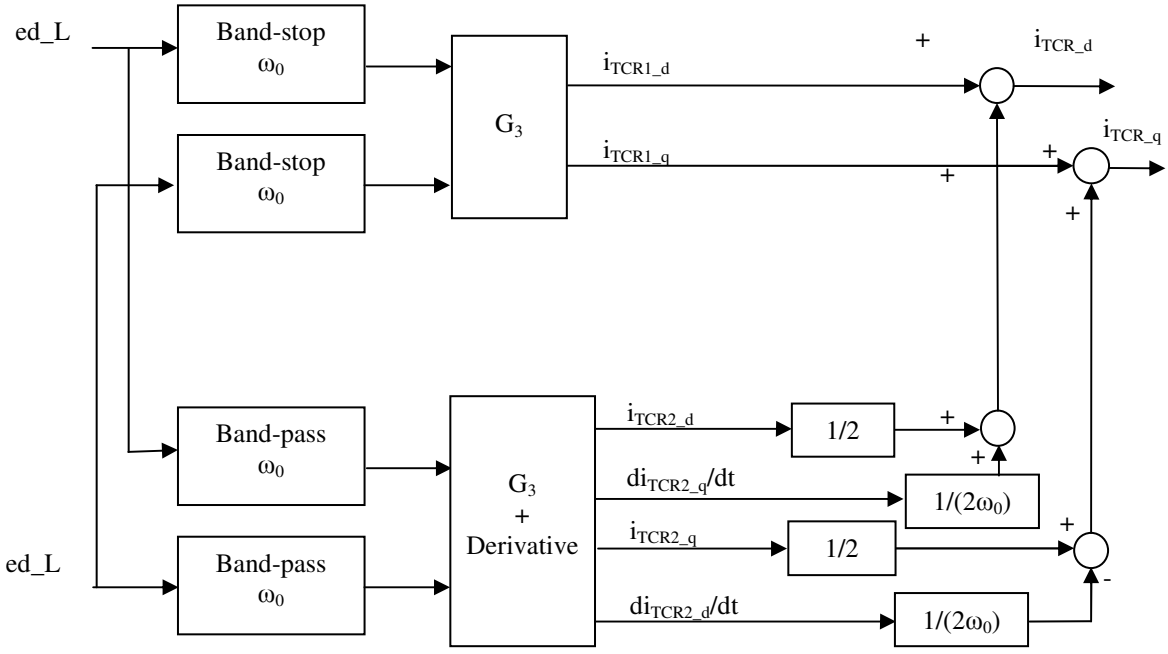

Figure 5-9 Bolck scheme of TCR dynamic with the elimination of the un-damped homogeneous component

The block scheme of Figure 5-9 can be represented by the equations reported below:

- the band-stop and the band-pass filters equation may be written manipulating the same two state variables ($e_{TCRban1}$ and $e_{TCRban2}$) for d and q components.
- the center angular frequency ω_0 is $2 \cdot \pi \cdot 50 = 314$ rad/s (i.e. 50 Hz), while a good accuracy of the TCR model has been found *by* trial and error method with the bandwidth (called Ban) of the band-pass and band-stop filter equal to $2 \cdot \pi \cdot 100$ rad/s (or 100 Hz)

The analytical equations used in the state space formulation of the Dynamic Model are:

- state equations of the filters for d component (state variables $e_{TCRban1\_d}$ and $e_{TCRban2\_d}$)

$$
\begin{aligned}
&-Ban\cdot e_{TCRban1\_d}-\omega_0^2\cdot e_{TCRban2\_d}+\omega_0^2\cdot ed\_L-\frac{d\left(e_{TCRban1\_d}\right)}{dt}=0\\
&e_{TCRban1\_d}-\frac{d\left(e_{TCRban2\_d}\right)}{dt}=0
\end{aligned}
\qquad \text{(eq. 5-32)}
$$

- state equations of the filters for q component (state variables $e_{TCRban1\_q}$ and $e_{TCRban2\_q}$)

$$
\begin{aligned}
&-Ban\cdot e_{TCRban1\_q}-\omega_0^2\cdot e_{TCRban2\_q}+\omega_0^2\cdot eq\_L-\frac{d\left(e_{TCRban1\_q}\right)}{dt}=0\\
&e_{TCRban1\_q}-\frac{d\left(e_{TCRban2\_q}\right)}{dt}=0
\end{aligned}
\qquad \text{(eq. 5-33)}
$$

- state equations of dq component of the output current (i_{TCR1_d} and i_{TCR1_q} and they are the state variables) of the TCR with the band-stop filter

$$
\begin{aligned}
&ed\_L-\frac{Ban}{\omega_0^2}\cdot e_{TCRban1\_d}+\omega_0\cdot i_{TCR1\_q}-\frac{d\left(i_{TCR1\_d}\right)}{dt}=0\\
&eq\_L-\frac{Ban}{\omega_0^2}\cdot e_{TCRban1\_q}-\omega_0\cdot i_{TCR1\_d}-\frac{d\left(i_{TCR1\_q}\right)}{dt}=0
\end{aligned}
\qquad \text{(eq. 5-34)}
$$

- state equations of dq component of the output current (i_{TCR2_d} and i_{TCR2_q} and they are the state variables) of the TCR with the band-pass filter

$$
\begin{aligned}
&\frac{Ban}{\omega_0^2}\cdot e_{TCRban1\_d}+\omega_0\cdot i_{TCR2\_q}-\frac{d\left(i_{TCR2\_d}\right)}{dt}=0\\
&\frac{Ban}{\omega_0^2}\cdot e_{TCRban1\_q}-\omega_0\cdot i_{TCR2\_d}-\frac{d\left(i_{TCR2\_q}\right)}{dt}=0
\end{aligned}
\qquad \text{(eq. 5-35)}
$$

- The output current (i_{TCRd} and i_{TCRq}) in dq frame of the TCR system result:

$$
\begin{aligned}
&i_{TCRd}=i_{TCR1\_d}+\frac{i_{TCR2\_d}}{2}+\left(\frac{Ban}{\omega_0^2}\cdot e_{TCRban1\_q}-\omega_0\cdot i_{TCR2\_d}\right)\cdot\frac{1}{2\cdot\omega_0}\\
&i_{TCRq}=i_{TCR1\_d}+\frac{i_{TCR2\_q}}{2}+\left(\frac{Ban}{\omega_0^2}\cdot e_{TCRban1\_d}-\omega_0\cdot i_{TCR2\_q}\right)\cdot\frac{1}{2\cdot\omega_0}
\end{aligned}
\qquad \text{(eq. 5-36)}
$$

5.5.1.2 Modeling of part 2 of the TCR system

The time delay of firing angle alpha assumed as the average time between two switching instant of the TCR system has been accounted by a transfer function G_d with a mean time delay T_{COM} of 1.667 ms (the minimum delay is 0 and the maximum one is 3.333 ms in 6 pulses configuration with grid frequency at 50 Hz):

$$
G_d(s)=e^{-sT_{COM}}=\frac{1}{1+sT_{COM}+\frac{\left(sT_{COM}\right)^2}{2!}+\frac{\left(sT_{COM}\right)^3}{3!}.....}\cong\frac{1}{1+sT_{COM}}
\qquad \text{(eq. 5-37)}
$$

and in this study it has been approximated by series Taylor stopped at the first order (see the arrow a in the Figure 5-10).

The look up table $\alpha_L(1/L)$, which means the inverse function of $1/L(\alpha_L)$ (given at pag. 42), cannot be written by an analytical function. To overcame this problem it would be necessary to move upstream the function $1/L(\alpha_L)$ but it is not possible because this function is not linear. Therefore it is necessary approximate the function $1/L(\alpha_L)$ by a linearization around the equilibrium point α_{L1} (which must be calculated from each operating condition). The result is a constant con_α_{L1}:

$$con\_\alpha_{L1} = \frac{\partial(1/L(\alpha_L))}{\partial\alpha_L}\bigg|_{\alpha L1} = \frac{3}{L_r}\cdot\frac{-2+2\cos(2\cdot\alpha_{L1})}{\pi} \qquad \text{(eq. 5-38)}$$

and the block con_α_{L1} can be move upstream as shown in the in the Figure 5-10 (see the arrow b).

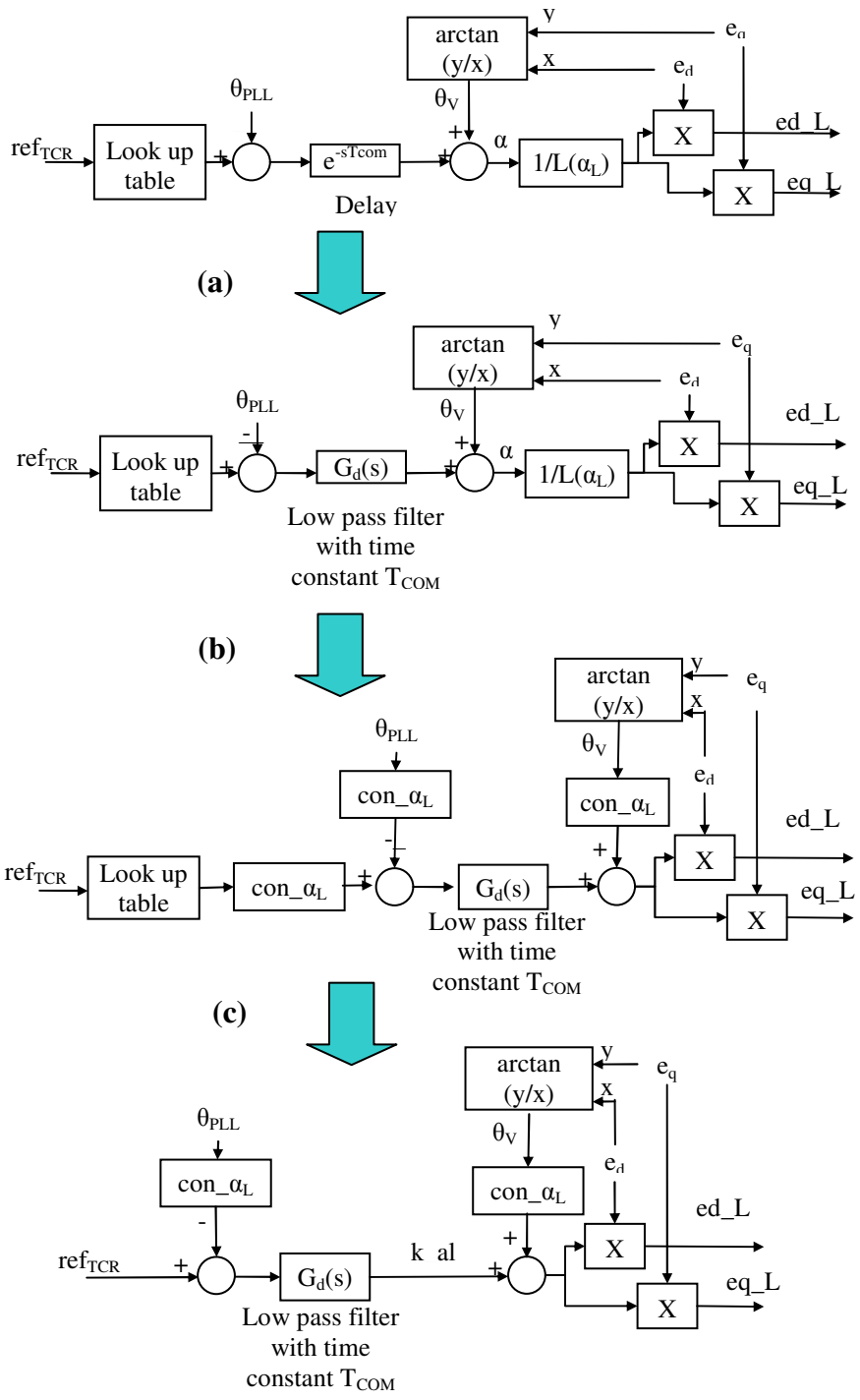

Figure 5-10 Bolck scheme of the simplification of the TCR dynamic related to the the time delay of firing angle alpha

Then considering that the look up table is the inversion function of $1/L(\alpha_L)$ and applying the inversion function theorem, the product of the derivatives of the two functions $1/L(\alpha_L)$ and $\alpha_L(1/L)$ around the equilibrium point α_{L1} results:

$$\left.\frac{\partial(1/L(\alpha_L))}{\partial\alpha_L}\right|_{\alpha_{L1}} \cdot \left.\frac{\partial(\alpha_L(1/L))}{\partial 1/L}\right|_{1/L_1} = 1 \qquad \text{(eq. 5-39)}$$

where L_1 is the inductance value resulting by the function $1/L(\alpha_L)$

$$L_1 = \frac{L_r}{3} \cdot \frac{\pi}{(2\pi - 2\alpha_{L1} + \sin(2\alpha_{L1}))} \qquad \text{(eq. 5-40)}$$

Therefore at small signals the series of the look up table and of the con_α_{L1} blocks can be neglected, because for each equilibrium point the product of the transfer functions of this series is always equal to 1 (see the arrow c in the Figure 5-10).
Finally the effects of the PLL by the output angle θ_{PLL} and of the variation of voltage phase angle θ_V =arctan(eq/ed) have been considered as shown in the figure.
The state equation considered in the analytical model of this part is:

$$-k\_al + ref_{TCR} - \theta_{PLL} \cdot (-2 + 2 \cdot \cos(2 \cdot \alpha_{L1})) - T_{COM} \cdot \frac{d(k\_al)}{dt} = 0 \qquad \text{(eq. 5-41)}$$

And output ed_L and eq_L signals are:

$$ed\_L = \left(k\_al + \arctan\left(\frac{e_q}{e_d}\right) \cdot (-2 + 2 \cdot \cos(2 \cdot \alpha_{L1}))\right) \cdot ed$$
$$eq\_L = \left(k\_al + \arctan\left(\frac{e_q}{e_d}\right) \cdot (-2 + 2 \cdot \cos(2 \cdot \alpha_{L1}))\right) \cdot eq \qquad \text{(eq. 5-42)}$$

where k_al is the state variable that considers the response of the TCR.
Applying the method described in the paragraph 5.1, the Dynamic Model of the TCR system described so far has been built to evaluate the accuracy of the approximation of the transfer functions considered above.
The state variables are: $e_{TCRban1\_d}$, $e_{TCRban2\_d}$, $e_{TCRban1\_q}$, $e_{TCRban2\_q}$, i_{TCR1_d}, i_{TCR1_q}, i_{TCR2_d}, i_{TCR2_q} and k_al and also the state variables of the PLL θ_{PLL} and w_{1_PLL}.
The input variable are ref_{TCR} and the voltage ed and eq.
The output variables are the TCR currents i_{TCRd} and i_{TCRq}.
The analytical equation used to calculate the Jacobian Matrix are the ones from eq. 5-32 to 5-42 (replacing the auxiliary variables where necessary) and the PLL ones given in the paragraph 5.2.1 .
A frequency analysis of the responses of the Dynamic Model and of the equivalent PSIM model has been worked out at the equilibrium point with voltage equal to 66 kV and the input of the TCR (ref_{TCR}) equal to 0.5 (i.e. the TCR system consumes half reactive power of the rated one) applying to the input of the TCR models some sinusoidal waveforms at several frequencies with magnitude equal to 0.05 (5 %). This frequency analysis has been achieved measuring magnitude and phase of the d and q components of the TCR current (i_{TCRd}, i_{TCRq}) both for the Dynamic and PSIM models by the Fast Fourier Transformer (FFT) at the same frequency of the sinusoidal waveform applied to the ref_{TCR} and then the direct and reverse sequences has been calculated. The magnitude ratio and phase error between the TCR currents of Dynamic and PSIM

models given both for direct and for reverse sequences as function of the frequency values applied to the ref_{TCR} are shown in the Figure 5-11.

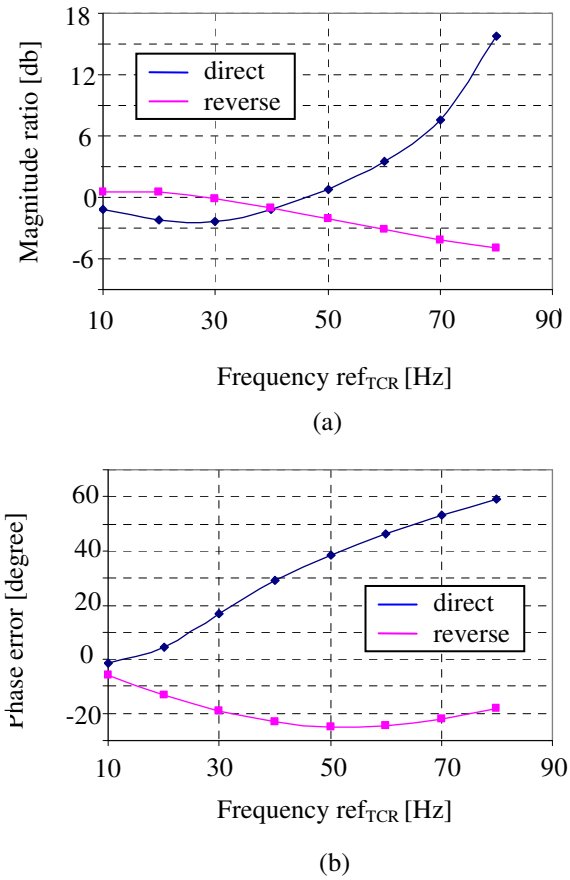

Figure 5-11 The magnitude ratio and phase error between the TCR currents of Dynamic and PSIM models given both for direct (blue line) and for reverse (purple) sequences as function of the frequency values applied to the ref_{TCR}.

The accuracy of the TCR Dynamic Model has been verified by a comparison with the PSIM model of the TCR for frequency range lower than 50 Hz. The results described by the Figure 5-11 shows that the magnitude ratio is included between ±3 db and the phase error is included between ±45 degree for both the direct and reverse sequences of the TCR currents.

5.5.2 Calculation of the reactive power consumed from the ac/dc conversion system and of the reference input applied to the TCR system

5.5.2.1 The calculation of the reactive power consumed by the ac/dc conversion system in the ac frame and of the TCR reference

The reactive power consumed from the load is calculated by using the Fast Fourier Transformer (FFT) applied to voltages and currents, in this manner only the component at 50 Hz is achieved in terms of rms value (U for the voltage and I for the current) and phase angle (φ). The reactive power results:

$$Q_{acdc}=U_{ab}\cdot I_a\cdot\sin(\varphi_{ab}-\varphi_a)+ U_{cb}\cdot I_c\cdot\sin(\varphi_{cb}-\varphi_c) \qquad \text{(eq. 5-43)}$$

And the nomenclature is shown in the Figure 5-12.

The reactive power is then filtered with Low Pass Filter (LPF in the Figure 5-12) with time constant equal to 5 ms.
The input signal ref_{TCR} for the TCR system described in the previous section results:

$$ref_{TCR} = \left(2\pi \cdot 50 \cdot C_{50} - \frac{Q_{acdc\_f}}{U_{mean}^2} \right) \cdot \frac{2\pi \cdot 50 \cdot Lr}{3} \qquad \text{(eq. 5-44)}$$

Where C_{50} is the capacitance at 50 Hz of the impedance in parallel configuration R//C of the whole Tuned Filters, L_r is the inductance of the TCR inductor (L_r =112.174 mH), U_{mean} is the average value between the three line voltages after the FFT at 50 Hz and the Q_{acdc_f} is the reactive power after the low pass filter.

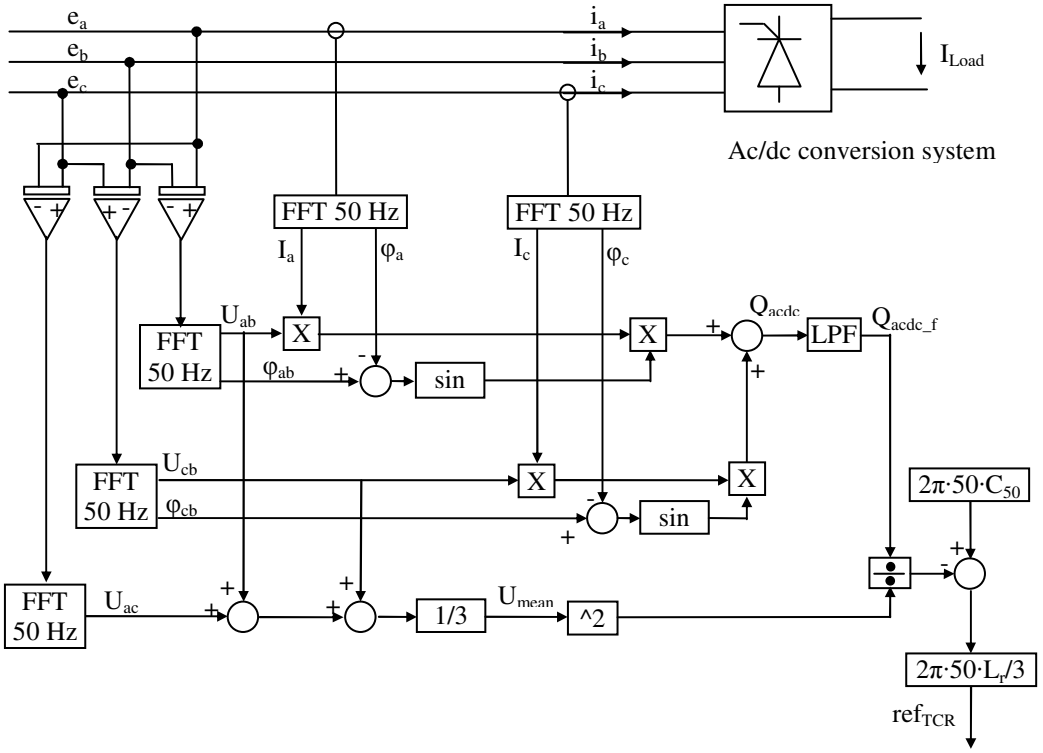

Figure 5-12 Calculation of the reactive power consumed by the ac/dc conversion system in the ac frame and of the reference TCR system

5.5.2.2 The analytical model of the calculation of the reactive power consumed by the ac/dc conversion system in the dq frame and of the TCR reference

In the dq frame the reactive power is equal to:

$$Q_{acdc}=eq \cdot id - ed \cdot iq \qquad \text{(eq. 5-45)}$$

Considering the FFT block of the calculation of the reactive power in ac frame illustrated in the previous paragraph, the quasi equivalent configuration in dq frame is shown in the Figure 5-13.
The d-q components of voltage and current are filtered by a mean block with integration time equal to 20 ms. It is quasi equivalent because in the case of a reverse sequence at 50 Hz in ac frame the FFT at 50 Hz doesn't modify it, while in dq frame the considered reverse sequence becomes a sequence with frequency equal to -100 Hz and it is completely eliminated.
The mean block has been approximated by a low pass filter with time constant T_{VIQ_fft} = 0.02/2=0.01 s/rad (see paragraph 5.3); so the analytical model equations of mean value

of voltage and current in in dq frame result (state variables are: e_{d_f}, e_{q_f}, $i_{acdc\_d\_f}$, and $i_{acdc\_q\_f}$,

$$-e_{d\_f} + e_d - T_{VIQ\_fft} \cdot \frac{d(e_{d\_f})}{dt} = 0 \qquad \text{(eq. 5-46)}$$

$$-e_{q\_f} + e_q - T_{VIQ\_fft} \cdot \frac{d(e_{q\_f})}{dt} = 0 \qquad \text{(eq. 5-47)}$$

$$-i_{acdc\_d\_f} + i_{acdc\_d} - T_{VIQ\_fft} \cdot \frac{d(i_{acdc\_d\_f})}{dt} = 0 \qquad \text{(eq. 5-48)}$$

$$-i_{acdc\_q\_f} + i_{acdc\_q} - T_{VIQ\_fft} \cdot \frac{d(i_{acdc\_q\_f})}{dt} = 0 \qquad \text{(eq. 5-49)}$$

Where ed and eq are busbar voltages in dq frame and i_{acdc_d} and i_{acdc_d} are the currents due to the ac/dc conversion system, while with subscript "$_f$" indicates the variable after the mean block.

The reactive power Q_{acdc} is

$$Q_{acdc} = \frac{3}{2} \cdot \left(e_{q\_f} \cdot i_{acdc\_d\_f} - e_{d\_f} \cdot i_{acdc\_q\_f}\right) \qquad \text{(eq. 5-50)}$$

And it is filtered by Low Pass filter with time constant T_{Qdc_f} equal to 0.005 s/rad and the state equation of the Low Pass filter results:

$$(-Q_{acdc\_f} + Q_{acdc}) - T_{Qdc\_f} \cdot \frac{d(Q_{acdc\_f})}{dt} = 0 \qquad \text{(eq. 5-51)}$$

where Q_{acdc_f} is the state variable.

Finally the input reference ref_{TCR} of the TCR system results

$$ref_{TCR} = \left(2\pi \cdot 50 \cdot C_{50} - \frac{Q_{acdc\_f}}{\frac{3}{2} \cdot \left(e_{d\_f}^2 + e_{q\_f}^2\right)}\right) \cdot \frac{2\pi \cdot 50 \cdot Lr}{3} \qquad \text{(eq. 5-52)}$$

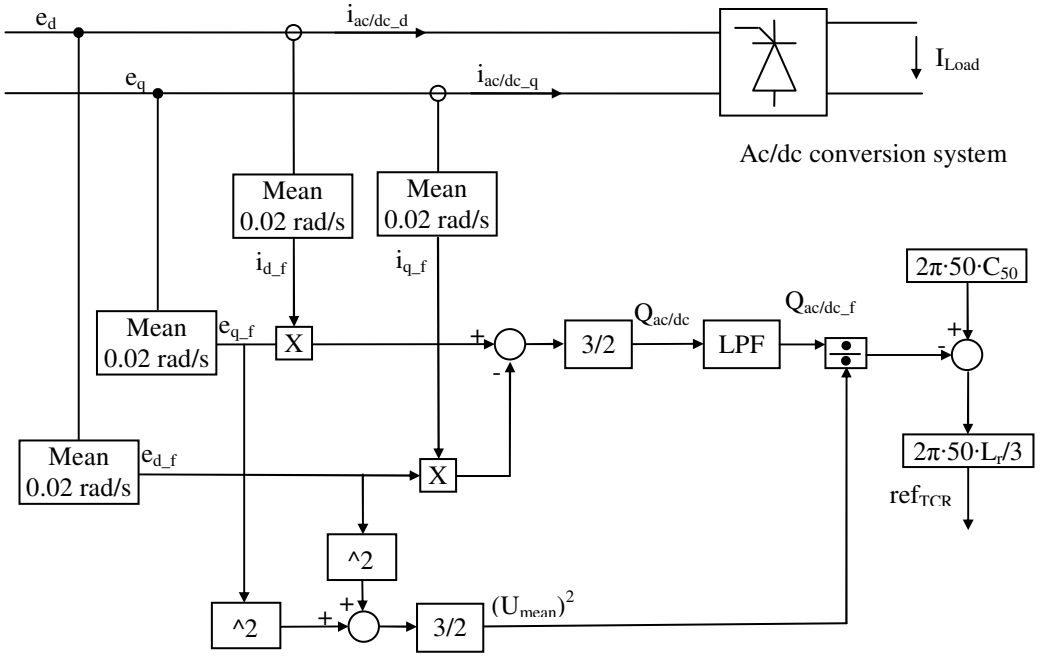

Figure 5-13 Calculation of the reactive power consumed by the ac/dc conversion system in the dq frame and of the reference TCR system

The accuracy limit in the frequency domain of the Dynamic Model of the calculation of the reference of the TCR system is principally due to the approximation of the mean block by the low pass filter, so the frequency range of validity of this part of the TCR system is lower than 50 Hz (see paragraph 5.3).

5.5.3 The Dynamic Model of the TCR system (included the PLL)

The Dynamic Model of the TCR system (included the PLL) has been has been represented by a state space matrix where:

- the inputs are the dq component of voltage busbar (e_d, e_q)
- the inputs of the control are the current of the ac/dc conversion system (i_{acdc_d}, i_{acdc_q}),
- the outputs are the TCR currents (i_{TCRd}, i_{TCRq}).

The equation of the PLL (see paragraph 5.2.1) and of the TCR system from equation 5-32 to 5-42 and from 5-46 to 5-52 (replacing the auxiliary variables where necessary) are used to build the Jacobian matrix of the system (see paragraph 5.1). The state variables are listed below:

- PLL = w_{1_PLL}, θ_{PLL}
- TCR = e_{d_f}, e_{q_f}, $i_{acdc\_d\_f}$, $i_{acdc\_q\_f}$, Q_{dc_f}, i_{TCR1_d}, i_{TCR1_q}, i_{TCR2_d}, i_{TCR2_q}, $e_{TCR\_ban1\_d}$, $e_{TCR\_ban2\_d}$, $e_{TCR\_ban1\_q}$, $e_{TCR\_ban2\_q}$, $k_{\_al}$

Considering the method described in the paragraph 5.1, the Dynamic Model of the TCR Subsystem is:

$$[\Delta \dot{x}_{TCR}] = A_{TCR} \cdot [\Delta x_{TCR}] + B_{e\_TCR} \cdot \begin{bmatrix} \Delta e_d \\ \Delta e_q \end{bmatrix} + B_{inp\_TCR} \cdot \begin{bmatrix} \Delta_{iacdc\_d} \\ \Delta_{iacdc\_d} \end{bmatrix} \qquad \text{(eq. 5-53)}$$

$$[\Delta i_{TCR}] = C_{TCR} \cdot [\Delta x_{TCR}]$$

In the Figure 5-15 is shown a comparison between the waveforms of the TCR currents at small signals (Δi_{TCRd} and Δi_{TCRq}) between PSIM and Dynamic Models after that a step function (Figure 5-14) to the busbar voltage (Δe_d and Δe_q) has been applied (at the equilibrium point with voltage busbar U=66 kV and reactive power consumed by the TCR Q_{TCR}=185 Mvar).

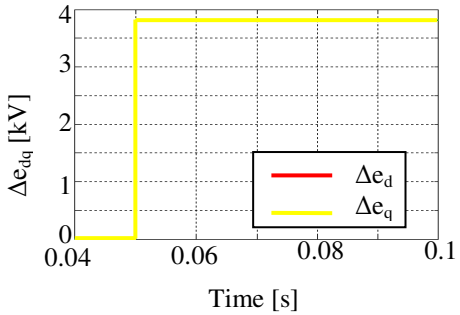

Figure 5-14 Step function applied to the busbar voltage (Δe_d and Δe_q)

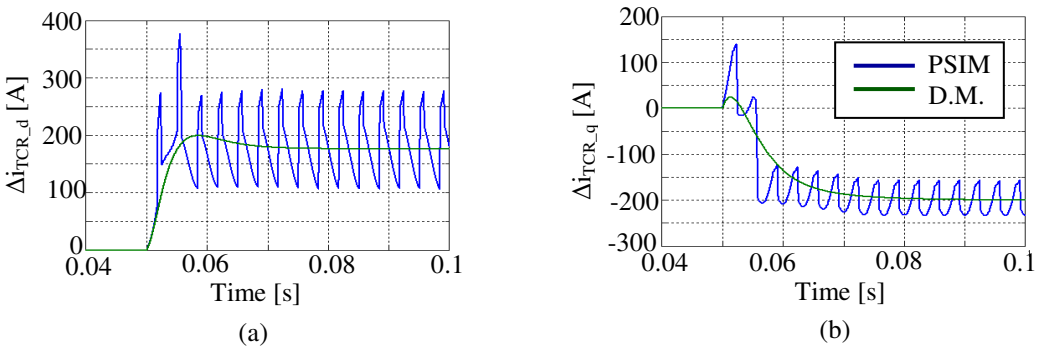

Figure 5-15 Comparison between the waveforms of the TCR currents at small signals (Δi_{TCRd} and Δi_{TCRq}) between PSIM (blue line) and Dynamic (green line) Models after a step function applied to the busbar voltage (Δe_d and Δe_q)

The high frequency oscillating components of the current in the PSIM model (blue line) are due to the switching phenomena not considered in the Dynamic Model (green line). Nevertheless it may be noted that the waveforms of the TCR currents achieved by the Dynamic Model show a good agreement with that achieved by PSIM models. Considering the frequency analysis carried out in the previous paragraph, the TCR subsystem can be considered accurate for range frequency less than 50 Hz.

5.6 The ac/dc conversion subsystem

The Dynamic model of the ac/dc converter base unit of the SPSS is illustrated in this section. The ac/dc converter base unit may operate in three modes as discussed in the paragraph 2.1:

- 6 pulses operation
- 12 pulses operation
- circulating mode

The data of the ac/dc converter base unit used in the SPSS are given in the paragraph 3. The analytical equations used in the development of the Dynamic Model are based on the classical ones at rms values of the fundamental component at 50 Hz for the ac system and mean value for the dc system; these ac variables have been replaced by the ones related to dq frame. The load current I_{Load} has been assumed as a source current, and for each equilibrium point it is assumed as constant value (the superconducting coil have an high inductance), neglecting the dynamic of the load.
For each operating mode a different Dynamic Model has to be defined and they are described in the following sections.

5.6.1 The ac/dc converter in 6 pulse operation

The operation of the ac/dc converter in 6 pulses mode means that only one ac/dc converter of the base unit (subunit) is operating. The block scheme of one subunit is shown in the Figure 5-16.

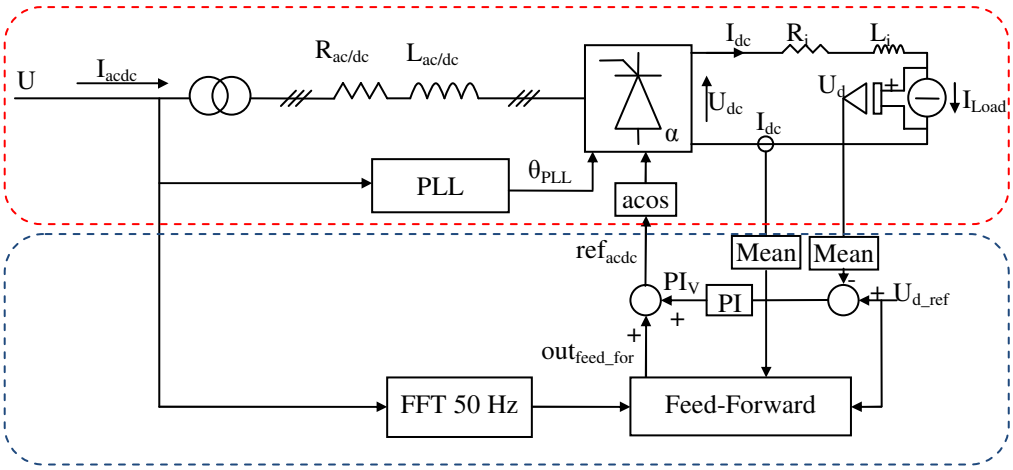

Figure 5-16 Block scheme of the ac/dc converter in 6 pulse operating mode

In the Figure 5-16 the ac/dc converter transformer is represented by the leakage inductance $L_{ac/dc}$ and the resistance $R_{ac/dc}$ of the windings and transformation ratio equal to k_{tra}, while R_i and L_i are the resistance and the inductance of the interphase reactor. The ac/dc converter is voltage controlled principally in feed forward mode, and a PI controller is used to correct the small errors.
The study of the ac/dc converter operating in 6 pulses operation has been divided in two parts: the former describes the dynamic of the ac/dc converter and the latter is focused on the control system.

5.6.1.1 The Dynamic Model of the ac/dc converter in 6 pulses operation

5.6.1.1.1 The output voltage on the load U_d in 6 pulses operation

The ac/dc converter can be simplified as in the Figure 5-17, moving the resistance of the transformer winding R_{acdc} downstream of the ac/dc converter (this assumption has been described more in detail below). The inputs are the d and q components of the busbar voltage (e_d and e_q) and the reference signal ref_{acdc}, while the outputs are the d and q components of the current of the ac/dc converter i_{acdc_d} and i_{acdc_q} and the voltage U_d on the load.

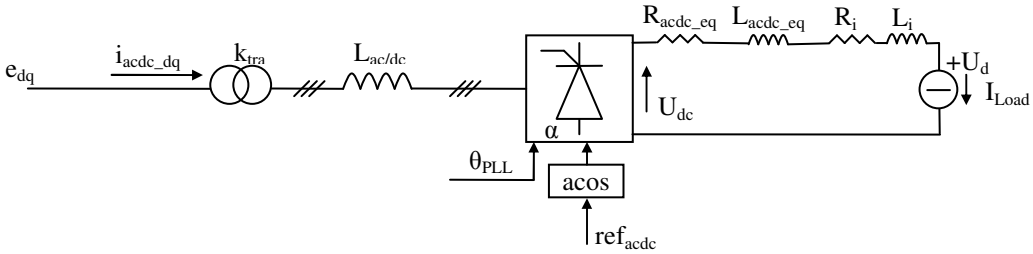

Figure 5-17 The simplified block scheme of the ac/dc converter

The transfer function of the output voltage U_d is shown in the Figure 5-18. The dynamic response of the ac/dc converter may be assumed for frequency range lower than the switching frequency as a time delay T_{dc} equal to an half switching time [19]-[20], and considering the 6 pulses operation of the ac/dc converter the switching time results 1/(50·6) = 3.33 ms and the time delay T_{dc} results 3.33/2=1.67 ms. Nevertheless this transfer function is not continuous, so it has been developed in Taylor series and

stopped to the first order, resulting in the transfer function of a low pass filter with constant time equal to T_{dc}.

$$e^{-sT_{dc}} = \frac{1}{1 + sT_{dc} + \frac{(sT_{dc})^2}{2!} + \frac{(sT_{dc})^3}{3!} .....} \cong \frac{1}{1 + sT_{dc}} \qquad \text{(eq. 5-54)}$$

and the dynamic response of the ac/dc converter can be describe by the state equation

$$-a + \arccos(ref_{acdc}) - \theta_{PLL} - \frac{d(a)}{dt} \cdot T_{dc} = 0 \qquad \text{(eq. 5-55)}$$

where a is the state variable of the low pass filter, ref_{acdc} is the input reference and θ_{PLL} is the output angle of the PLL.

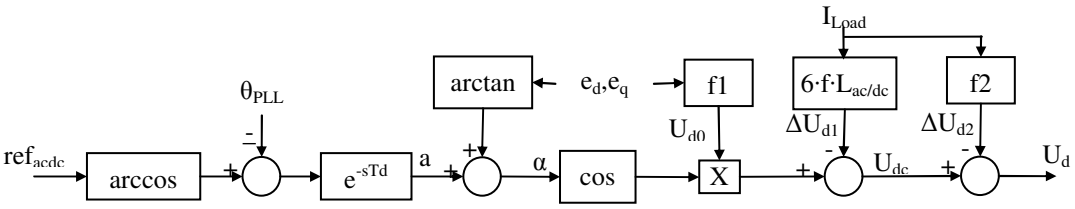

Figure 5-18 The transfer function of the output voltage U_d

The output voltage U_{dc} is given by:

$$U_{dc} \cong \frac{3 \cdot \sqrt{2}}{\pi \cdot k_{tra}} \cdot U \cdot \cos\alpha - 6 \cdot f \cdot L_{ac/dc} \cdot I_{Load} \qquad \text{(eq. 5-56)}$$

The relation between the rms value U of the fundamental component at 50 Hz of the voltage busbar U and the respective voltages in dq frame is

$$U = \sqrt{\frac{3}{2}\left(e_d^2 + e_q^2\right)} \qquad \text{(eq. 5-57)}$$

And the firing angle α (θ_V is the phase displacement of the voltage given as arctan(eq/ ed) results:

$$\alpha = a + \theta_V = a + \arctan\left(\frac{e_q}{e_d}\right) \qquad \text{(eq. 5-58)}$$

So the analytical equation of the output voltage U_{dc} of the ac/dc converter in dq frame variables replacing the firing angle α by equation 5-58 results:

$$U_{dc} \cong U_{d0} \cdot \cos\left(a + \arctan\left(\frac{e_q}{e_d}\right)\right) - 6 \cdot f \cdot L_{ac/dc} \cdot I_{Load} \qquad \text{(eq. 5-59)}$$

Where the no load voltage U_{d0} is (called function f1 in the Figure 5-18)

$$U_{d0} \cong \frac{3 \cdot \sqrt{2}}{\pi \cdot k_{tra}} \cdot \sqrt{\frac{3}{2}\left(e_d^2 + e_q^2\right)} \qquad \text{(eq. 5-60)}$$

The resistance and inductance of the step down transformer has been moved to the dc side to make easier the calculation. It should be noted that, when the ac/dc converter operates with two switched on thyristors, the equivalent resistance seen from the dc side is equal to 2 $R_{ac/dc}$, while, when three thyristors are switched on, the phases 1 and 2 are in parallel and in series with the one of the phase 3 (during the overlap angle), the equivalent resistance is equal to 1.5 $R_{ac/dc}$. The same reasoning can be carried out for the equivalent inductance.

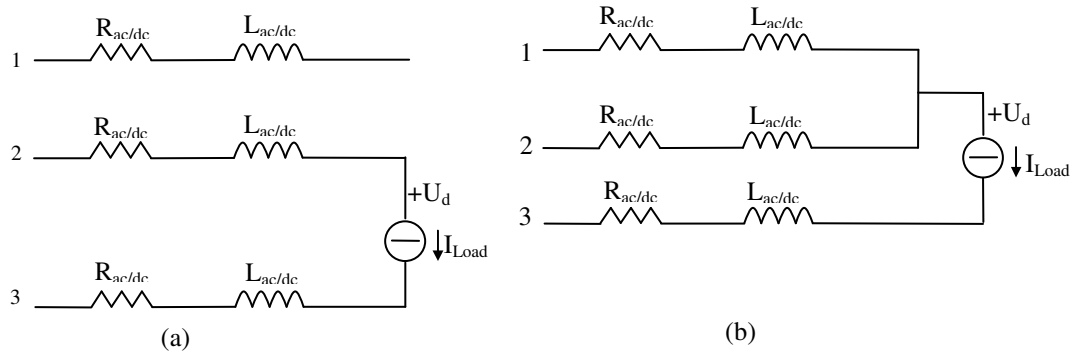

Figure 5-19 Two and three thyristor counduction of the ac/dc converter

Considering that the switching period is 60 electrical degrees (π/3), the equivalent resistance R_{acdc_eq} is equal to:

$$R_{acdc\_eq} = R_{ac/dc} \cdot \frac{\left(2 \cdot \left(\frac{\pi}{3} - u\right) + 1.5 \cdot u\right)}{\frac{\pi}{3}} \qquad \text{(eq. 5-61)}$$

And the equivalent inductance L_{acdc_eq}

$$L_{acdc\_eq} = L_{ac/dc} \cdot \frac{\left(2 \cdot \left(\frac{\pi}{3} - u\right) + 1.5 \cdot u\right)}{\frac{\pi}{3}} \qquad \text{(eq. 5-62)}$$

where u is the overlap angle due to the inductance of the step down transformer. It is considered as the output of a low pass filter with time constant T_{dc} and the state equation is:

$$-u + \left(\arccos\left(\cos(\hat{\alpha}) - \frac{4 \cdot f \cdot \pi \cdot L_{ac/dc} \cdot I_{Load} \cdot k_{tra}}{\sqrt{3\left(e_d^2 + e_q^2\right)}}\right) - (\hat{\alpha})\right) - \frac{d(u)}{dt} \cdot T_{dc} = 0 \qquad \text{(eq. 5-63)}$$

Where

$$\hat{\alpha} = \arccos(ref_{acdc}) - \theta_{PLL} + \theta_V = \arccos(ref_{acdc}) - \theta_{PLL} + \arctan\left(\frac{e_q}{e_d}\right) \qquad \text{(eq. 5-64)}$$

Considering that the load current is imposed and constant, in the calculation of the voltage U_d on the dc load the inductance L_{acdc_eq} can be neglected and it results:

$$U_d = U_{dc} - \left(R_i + R_{ac/dc} \cdot \frac{\left(2 \cdot \left(\frac{\pi}{3} - u\right) + 1.5 \cdot u\right)}{\frac{\pi}{3}}\right) \cdot I_{Load} \qquad \text{(eq. 5-65)}$$

This approximation in the Figure 5-18 is considered by function f2.

5.6.1.1.2 The dq components of the ac/dc converter in 6 pulses operation

Also for the current the dynamic response is represented by a delay with time constant equal to T_{dc} and modelled by a low pass filters.
Some new state variables have to be introduced to describe the transfer function of the currents of the ac/dc converter:

- e_{d_c} and e_{q_c} are the busbar voltage filtered with a low pass filter with time constant T_{dc}:

$$-e_{d\_c} + e_d - T_{dc} \cdot \frac{d(e_{d\_c})}{dt} = 0 \qquad \text{(eq. 5-66)}$$

$$-e_{q\_c} + e_q - T_{dc} \cdot \frac{d(e_{q\_c})}{dt} = 0 \qquad \text{(eq. 5-67)}$$

- the firing angle $\overline{\alpha}$ is the sum of the state variable a and of the angle voltage $\overline{\theta}_V$

$$\overline{\alpha} = a + \overline{\theta}_V \qquad \text{(eq. 5-68)}$$

where

$$\overline{\theta}_V = \arctan\left(\frac{e_{q\_c}}{e_{d\_c}}\right) \qquad \text{(eq. 5-69)}$$

The active and reactive components i_{at} and i_{re} of current of the ac/dc converter are obtained by the power equations:

$$i_{at} = \frac{Pdc}{\sqrt{\frac{3}{2}} \cdot U}$$
$$i_{re} = \frac{Qdc}{\sqrt{\frac{3}{2}} \cdot U} \qquad \text{(eq. 5-70)}$$

Where Pdc and Qdc are the active and reactive power consume of the ac/dc converter:

$$Pdc = U_{dc} \cdot I_{Load} = \left(\frac{3 \cdot \sqrt{2}}{\pi \cdot k_{tra}} \cdot U \cdot \cos\overline{\alpha} - 6 \cdot f \cdot L_{ac/dc} \cdot I_{Load}\right) \cdot I_{Load} =$$
$$= \frac{3 \cdot \sqrt{2}}{\pi \cdot k_{tra}} \cdot U \cdot I_{Load} \cdot \frac{1}{2} \cdot \left(\cos(\overline{\alpha}) + \cos(\overline{\alpha} + u)\right) \qquad \text{(eq. 5-71)}$$

$$Qdc = Pdc \cdot \tan(\varphi) \qquad \text{(eq. 5-72)}$$

Where φ indicates the angle phase between the busbar voltage and the current and the tangent results:

$$\tan(\varphi) = \frac{\left(2u + \sin(2\overline{\alpha}) - \sin(2\overline{\alpha} + 2u)\right)}{\cos(2\overline{\alpha}) - \cos(2\overline{\alpha} + 2u)} \qquad \text{(eq. 5-73)}$$

The active component of the current results:

$$i_{at} = \frac{Pdc}{\sqrt{\frac{3}{2}} \cdot U} = \frac{\frac{3 \cdot \sqrt{2}}{\pi \cdot k_{tra}} \cdot U \cdot I_{Load} \cdot \frac{1}{2} \cdot \left(\cos(\overline{\alpha}) + \cos(\overline{\alpha} + u)\right)}{\sqrt{\frac{3}{2}} \cdot U} =$$
$$= \frac{2}{\sqrt{3} \cdot \pi \cdot k_{tra}} \cdot I_{Load} \cdot \frac{1}{2} \cdot \left(\cos(\overline{\alpha}) + \cos(\overline{\alpha} + u)\right) \qquad \text{(eq. 5-74)}$$

And the reactive one results

$$i_{re} = \frac{Qdc}{\sqrt{\frac{3}{2}} \cdot U} = \frac{Pdc}{\sqrt{\frac{3}{2}} \cdot U} \tan(\varphi) = i_{at} \frac{(2u + \sin(2\overline{\alpha}) - \sin(2\overline{\alpha} + 2u))}{\cos(2\overline{\alpha}) - \cos(2\overline{\alpha} + 2u)} =$$
$$= \frac{2}{\sqrt{3} \cdot \pi \cdot k_{tra}} \cdot I_{Load} \cdot \frac{1}{2} \cdot (\cos(\overline{\alpha}) + \cos(\overline{\alpha} + u)) \cdot \frac{(2u + \sin(2\overline{\alpha}) - \sin(2\overline{\alpha} + 2u))}{\cos(2\overline{\alpha}) - \cos(2\overline{\alpha} + 2u)} \quad \text{(eq. 5-75)}$$

The active and reactive component have to be rotate to be synchronous with the dq frame, and the d and q components of the current of the ac/dc converter i_{acdc_d} and i_{acdc_q} result:

$$i_{acdc\_d} = i_{at} \cdot \cos\overline{\theta}_V + i_{re} \cdot \sin\overline{\theta}_V$$
$$i_{acdc\_q} = i_{at} \cdot \sin\overline{\theta}_V - i_{re} \cdot \cos\overline{\theta}_V \quad \text{(eq. 5-76)}$$

Applying the method described in the paragraph 5.1, the Dynamic Model of the ac/dc converter in 6 pulses configuration described so far has been built to evaluate the accuracy of the approximation of the transfer functions considered above.
The state variables are: a, u, e_{d_c}, e_{q_c} and also the state variables of the PLL θ_{PLL} and w_{1_PLL}.
The input variable is ref_{acdc} and the voltage e_d and e_q.
The output variables are the ac/dc converter currents i_{acdc_d} and i_{acdc_q} and the voltage U_d on the load.
The analytical equations used to calculate the Jacobian Matrixes are the state equations 5-55, 5-63, 5-66, 5-67 and the PLL ones given in the paragraph 5.2.1, while and the outputs are given from the equations 5-65 and 5-76 (replacing the auxiliary variables where necessary). The feed-forward matrix is not a zero matrix, because the output voltage U_d is dependent on the voltage busbar e_d and e_q.
A frequency analysis of the responses of the Dynamic Model and of the equivalent PSIM model has been worked out at the equilibrium point with the busbar voltage at 66 kV, the load current at 2.5 kA and the input of the ac/dc converter (ref_{acdc}) equal to 0.5, and applying to the input of the ac/dc converter some sinusoidal waveforms at several frequencies with magnitude equal to 0.05 (5 %). This frequency analysis has been achieved measuring magnitude and phase at the small signals of the d and q components of the ac/dc converter currents (Δi_{acdc_d}, Δi_{acdc_q}) and the voltage ΔU_d on the load both for the Dynamic and PSIM models by the Fast Fourier Transformer (FFT) at the same frequency of the sinusoidal waveform applied to the ref_{acdc}.
The magnitude ratio and phase error between the ac/dc converter currents of Dynamic and PSIM models given both for direct and for reverse sequences as function of the frequency values applied to the ref_{acdc} are shown in the Figure 5-20.
The magnitude ratio and phase error between the ac/dc converter voltage ΔU_d on the load of Dynamic and PSIM models given as function of the frequency values applied to the ref_{acdc} are shown in the Figure 5-21.
The Dynamic Model may be considered accurate with the PSIM model for frequency range lower than 90 Hz, where the magnitude ratio is included between ± 3 db and the phase error is included between ± 45 degree for both the direct and reverse sequences of the currents and of the voltage on the load.

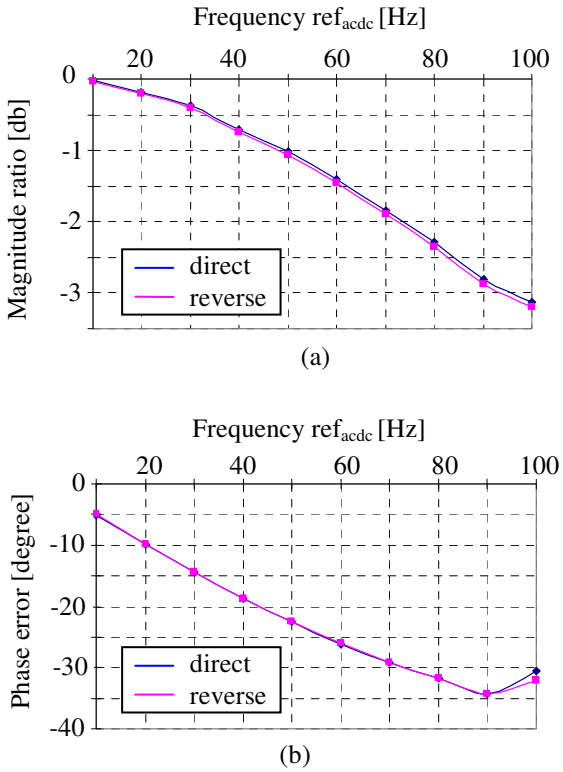

Figure 5-20 The magnitude ratio (a) and phase error (b) between the ac/dc converter currents of Dynamic and PSIM models given both for direct (blue line) and for reverse (purple line) sequences as function of the frequency values applied to the ref$_{acdc}$

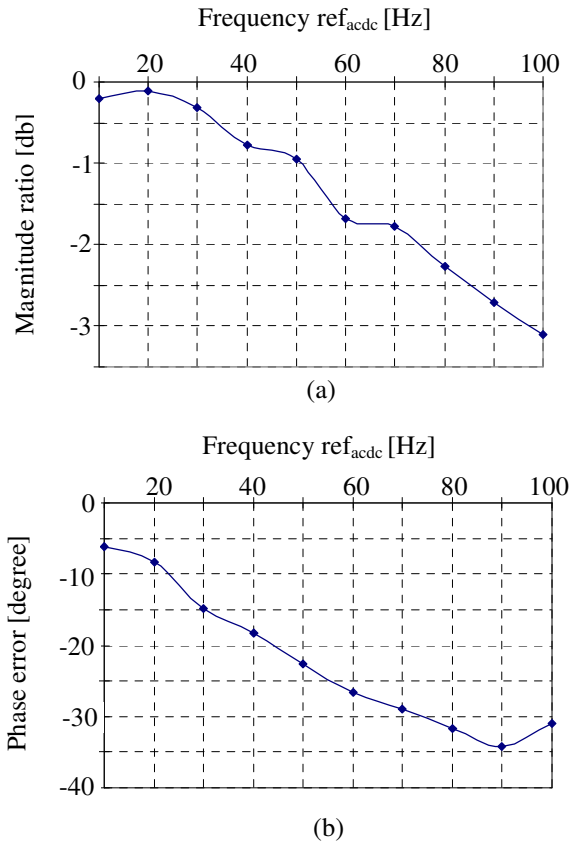

Figure 5-21 The magnitude ratio (a) and phase error (b) between the ac/dc converter voltage ΔU_d on the load of Dynamic and PSIM models given as function of the frequency values applied to the ref_{acdc}

5.6.1.2 The control system of the ac/dc converter in 6 pulses operation

The block scheme of the control system of the ac/dc converter in 6 pulses operation is shown in the Figure 5-22.

The output of the feed-forward block is obtained by the steady-state equation of the output voltage of the ac/dc converter:

$$out_{feed-for} = \frac{U_{d\_ref} + (Ri + 2 \cdot R_{ac/dc}) \cdot I_{dc1\_mean} + 6 \cdot f \cdot L_{ac/dc} \cdot I_{dc\_mean}}{U_{d0\_f}}$$

Where U_{d_ref} is the reference value of the voltage on the load, U_{d0_f} is the no load voltage of the ac/dc converter calculated by the FFT component at 50 Hz of the busbar voltage U, and I_{dc_mean} is the mean value of the output current of the ac/dc converter with an integration time of 3.333 ms. The effect two or three conducting thyristors has been approximated considering only the condition of two conducting thyristors

The FFT at 50 Hz of the bus bar voltage is quasi-equivalent to a calculation of the mean value with integration time of 0.02 s of the busbar voltage e_d and e_q in dq frame (see paragraph 5.5.2.2), and it may be considered as a low pass filter with time constant equal to 0.02/2 = 0.01 s/rad, so the voltage U_{d0_f} results

$$-U_{d0\_f} + \frac{3 \cdot \sqrt{2}}{\pi \cdot k_{tra}} \sqrt{\frac{3}{2} \cdot \left(e_d^2 + e_q^2\right)} - T_{Ud0\_f} \cdot \frac{d(U_{d0\_f})}{dt} = 0 \qquad \text{(eq. 5-77)}$$

Where T_{Ud0} is equal to 0.02/2=0.01 s/rad (see paragraph 5.3).

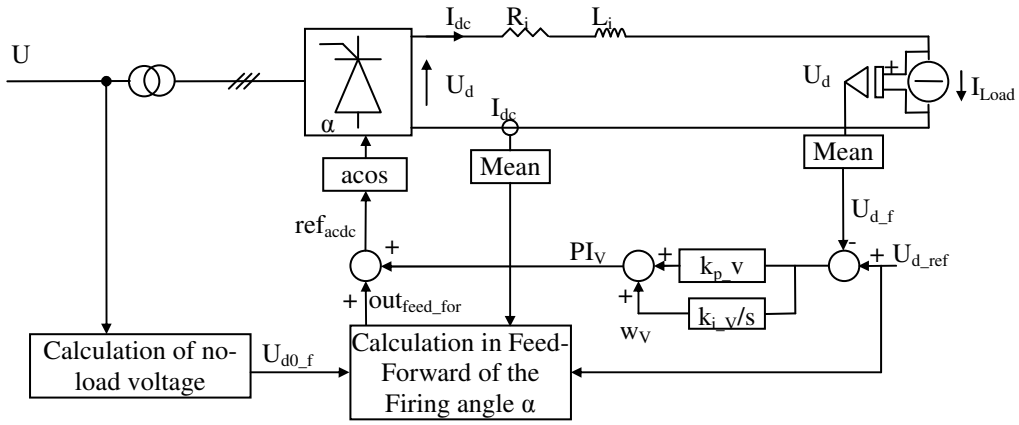

Figure 5-22 Block scheme of the control system of the ac/dc converter in 6 pulses operation

The measure of the output dc current of the ac/dc converter is achieved by calculating the mean value with an integration time of 3.3333 ms. Considering that the output dc current is imposed by the current source at small signal analysis the contribute of this measure is zero, so in this case it is neglected and the output of the feed forward block results:

$$out_{feed-for} = \frac{U_{d\_ref} + (R_i + 2 \cdot R_{ac/dc}) \cdot I_{Load} + 6 \cdot f \cdot L_{ac/dc} \cdot I_{Load}}{U_{d0\_f}} \qquad \text{(eq. 5-78)}$$

The PI controller is used to correct the small errors introduced by the feed forward calculation.

The feedback signal of the dc voltage on the load is filtered by a mean block with time constant equal to 3.333 ms and in the analytical model it is simplified by a low pass filter (see paragraph 5.3), whose the relative state equation (state variable U_{d_f}) is:

$$-U_{d\_f} + U_d - \frac{d(U_{d\_f})}{dt} \cdot T_{U_{d\_f}} = 0 \qquad \text{(eq. 5-79)}$$

The PI controller has one state variable w_v which is the output of the integrator:

$$k_{i\_V} \cdot (U_{d\_ref} - U_{d\_f}) - \frac{d(w_v)}{dt} = 0 \qquad \text{(eq. 5-80)}$$

The output of the PI controller results:

$$PI_V = k_{p\_V} \cdot (U_{d\_ref} - U_{d\_f}) + w_V$$

where k_{p_V} and k_{i_V} are the proportional and integral gains respectively of the PI controller. For this study they have been set: $k_{p\_V} = 0$, $k_{i\_V} = 1.06 \cdot 10^{-3}$.

The reference input ref_{acdc} is the sum of the outputs of the feed-forward block and of the PI controller:

$$ref_{acdc} = out_{feed-for} + PI_V$$

The accuracy limit in the frequency domain of the Dynamic Model of the control system of the ac/dc conversion system is principally due to the approximation of the mean block by the low pass filter (eq 5-77), so the frequency range of validity of this part is lower than 50 Hz (see paragraph 5.3).

5.6.1.3 The state space matrix of the ac/dc converter in 6 pulse configuration

The Dynamic Model of the ac/dc converter in 6 pulses configuration (included the PLL) has been represented by a state space matrix where:

- the inputs are the dq component of voltage busbar (e_d, e_q)
- the inputs of the control is the voltage reference U_{d_ref}
- the outputs are the ac/dc converter currents (i_{acdc_d}, i_{acdc_q}).

The equations of the PLL (see paragraph 5.2.1) and of the ac/dc converter in 6 pulses operation (described above) are used to build the Jacobian matrix of the system (see paragraph 5.1). The state variables are listed below:

- PLL = w_{1_PLL}, θ_{PLL}
- ac/dc converter = a, u, e_{d_c}, e_{q_c}, w_V, U_{d_f}, U_{d0_f}

Considering the method described in the paragraph 5.1, the Dynamic Model of the ac/dc converter in 6 pulses configuration is:

$$\left[\Delta \dot{x}_{acdc\_6}\right] = A_{acdc} \cdot \left[\Delta x_{acdc\_6}\right] + B_{e\_acdc\_6} \cdot \begin{bmatrix} \Delta e_d \\ \Delta e_q \end{bmatrix} + B_{inp\_acdc\_6} \cdot \Delta U_{d\_ref} \qquad \text{(eq. 5-81)}$$

$$\left[\Delta i_{acdc\_6}\right] = C_{acdc} \cdot \left[\Delta x_{acdc\_6}\right]$$

Adding another row to the matrix C_{acdc}, also the measure of the voltage on the load U_{d_f} can be observed.

In the following figures are shown a comparison of the waveforms of the measure of the voltage on the load (ΔU_{d_f} see Figure 5-24) and of the ac/dc converter currents (Δi_{acdc_d} and Δi_{acdc_q} Figure 5-25) and between PSIM and Dynamic Models after that a step function to the busbar voltage (Δe_d and Δe_q see Figure 5-23) has been applied (at the equilibrium point Ud=40 kV, Id=2 kA). All the waveforms are show the variation from the equilibrium point.

The high frequency oscillating components of the ac/dc converter current in the PSIM model (blue line) are due to the switching phenomena not considered in the Dynamic Model (green line); nevertheless it may be noted that the waveforms of the ac/dc converter currents obtained by the Dynamic Model show a good agreement with the ones described by PSIM models (Figure 5-25). Also the waveforms of the measure of the voltage show a good agreement between the models (Figure 5-24).

Considering the frequency analysis carried out in the previous paragraph, the Dynamic Model of the ac/dc converter in 6 pulses configuration can be considered accurate for range frequency less than 50 Hz (limit due principally to the control system see paragraph 5.6.1.2).

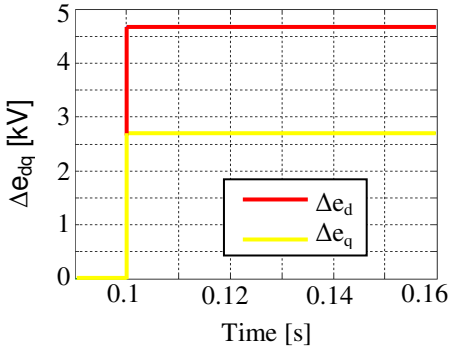

Figure 5-23 Step function applied to the busbar voltage (Δe_d and Δe_q)

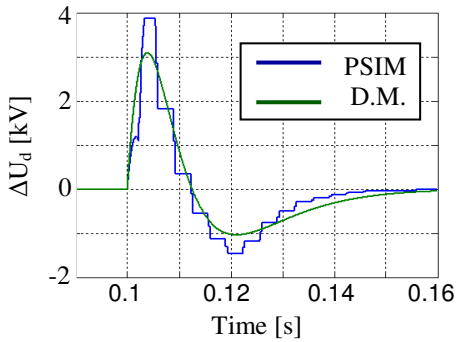

Figure 5-24 Comparison between the waveforms of the measure of the voltage ΔU_{d_f} on the load of the ac/dc converter between PSIM (blue line) and Dynamic (green line) Models after a step function applied to the busbar voltage (Δe_d and Δe_q)

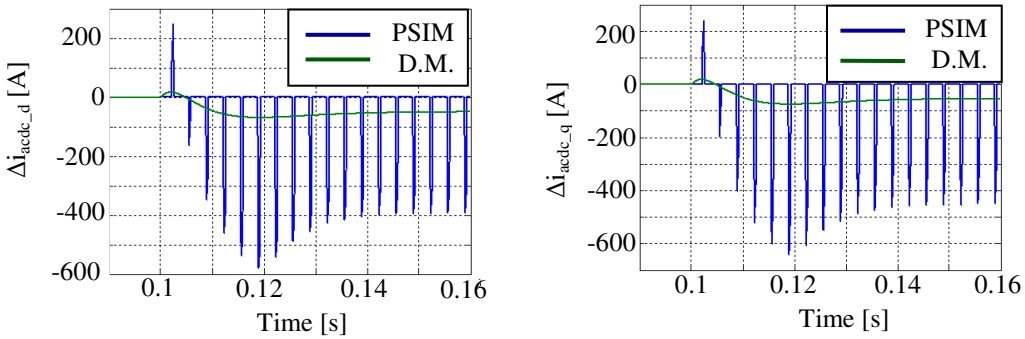

Figure 5-25 Comparison between the waveforms of the ac/dc converter currents at small signals (Δi_{acdc_d} and Δi_{acdc_q}) between PSIM (blue line) and Dynamic (green line) Models after a step function applied to the busbar voltage (Δe_d and Δe_q)

5.6.2 The ac/dc converter base unit in 12 pulse operation

The ac/dc converter in 12 pulse configuration means that two converters of the unit base are operating in parallel. The block scheme of the unit in 12 pulses operation is shown in the Figure 5-26.

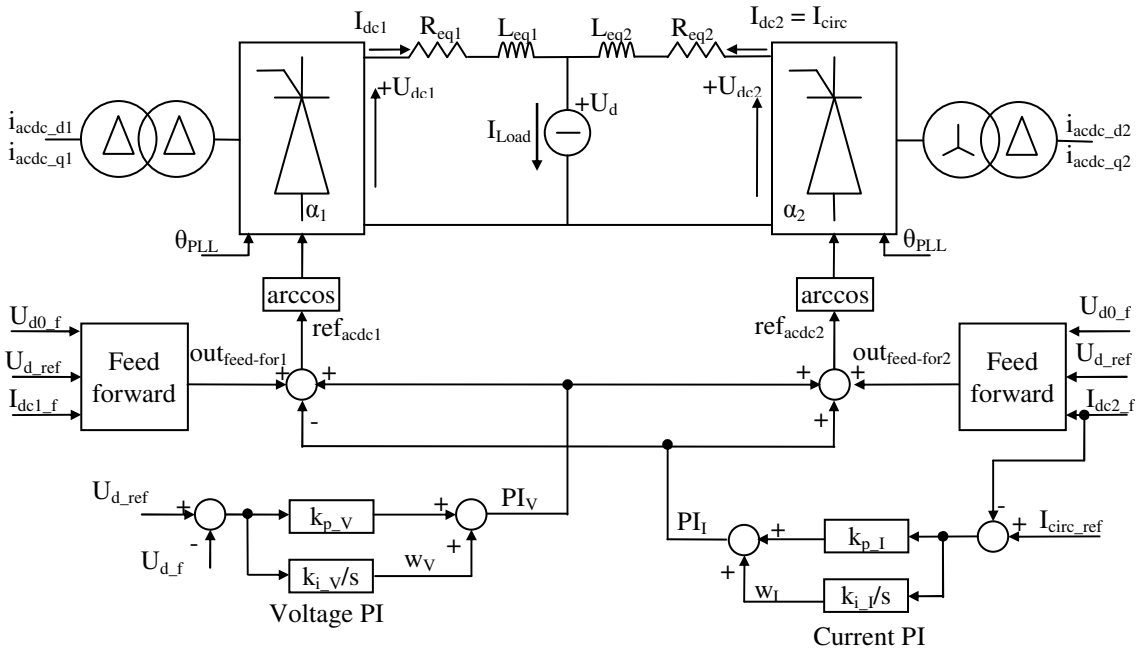

Figure 5-26 Block scheme of the ac/dc converter in 12 pulses operating mode

The differences respect to the 6 pulses configuration are the dynamic response, the control to balance the circulating current between the two parallel ac/dc converters and that the output currents I_{dc1} and I_{dc2} of the ac/dc converters are not imposed by the load current I_{Load} but they are dependent from the circulating current I_{circ}:

$I_{dc1}=I_{Load}-I_{circ}$
$I_{dc2}=I_{circ}$

The inputs are the d and q components of the busbar voltage (e_d and e_q), the voltage reference U_{d_ref}, and the reference of the circulating current I_{circ_ref}, while the outputs are the sum i_{acdc_d} and i_{acdc_q} of the d and q components of the currents of the two ac/dc converters i_{acdc_d1} and i_{acdc_q1}, i_{acdc_d2} and i_{acdc_q2}:

- $i_{acdc\_d} = i_{acdc\_d1} + i_{acdc\_d2}$
- $i_{acdc\_q} = i_{acdc\_q1} + i_{acdc\_q2}$

The equations considered in the 6 pulse converter model can be used also in the 12 pulses model, adding a subscript 1 and 2 to consider the two different converters.

5.6.2.1 The dynamic of the ac/dc converter in 12 pulses opearation

5.6.2.1.1 The output voltage on the load U_d in 12 pulses operation

In the 6 pulses converter the dynamic response of the ac/dc converter has been assumed for frequency range lower than the switching frequency as a time delay equal to an half switching time (see paragraph 5.6.1.1). This is true also for the 12 pulses ac/dc converter, i.e. an ac/dc converter connected to a six-phase system, while in ITER case the 12 pulse configuration is given from the parallel of two 6 pulses ac/dc converters connected to a three-phase systems. Nevertheless the assumption of the transfer function given as a time delay equal to an half switching time has been considered valid

also for the ac/dc converter unit base in 12 pulses configuration because the Dynamic Model aims to investigate phenomena with range frequency less than 100 Hz. Therefore in the 12 pulses operation of the ac/dc converter base unit the switching time results 1/(50·12) = 1.667 ms and the time delay results 0.833 ms. For both the two parallel ac/dc converters the delay has been approximated by two low pass filters with time constant equal to T_{dc1}= T_{dc2}=0.833 as done for a 6 pulses ac/dc converter.
The dynamic response of the two ac/dc converters can be described by the state equations:

$$\begin{aligned} &-a_1+\arccos\left(ref_{acdc1}\right)-\theta_{PLL}-\frac{d\left(a_1\right)}{dt}\cdot T_{dc1}=0 \\ &-a_2+\arccos\left(ref_{acdc2}\right)-\theta_{PLL}-\frac{d\left(a_2\right)}{dt}\cdot T_{dc2}=0 \end{aligned} \qquad \text{(eq. 5-82)}$$

where a_1 and a_2 are the state variables of the low pass filters, ref_{acdc1} and ref_{acdc2} are the input references and θ_{PLL} is the output angle of the PLL.
The output voltages U_{dc1} and U_{dc2} are:

$$U_{dc1}=\frac{3\cdot\sqrt{2}}{\pi\cdot k_{tra}}\cdot\sqrt{\frac{3}{2}\left(e_d^2+e_q^2\right)}\cdot\cos\left(a_1+\arctan\left(\frac{e_q}{e_d}\right)\right)-6\cdot f\cdot L_{ac/dc}\cdot\left(I_{Load}-I_{circ\_c1}\right) \quad \text{(eq. 5-83)}$$

$$U_{dc2}=\frac{3\cdot\sqrt{2}}{\pi\cdot k_{tra}}\cdot\sqrt{\frac{3}{2}\left(e_d^2+e_q^2\right)}\cdot\cos\left(a_2+\arctan\left(\frac{e_q}{e_d}\right)\right)-6\cdot f\cdot L_{ac/dc}\cdot\left(I_{circ\_c2}\right) \quad \text{(eq. 5-84)}$$

where I_{circ_c} is the filtered circulating current I_{circ} by of a low pass filter, because the drop voltage due the switching of the thyristors is based on average values. The related state equations of the two converters result:

$$-I_{circ\_c1}+I_{circ}-\frac{d\left(I_{circ\_c1}\right)}{dt}\cdot T_{dc1}=0 \quad \text{(eq. 5-85)}$$

$$-I_{circ\_c2}+I_{circ}-\frac{d\left(I_{circ\_c2}\right)}{dt}\cdot T_{dc2}=0 \quad \text{(eq. 5-86)}$$

The state equation related to the circulating current I_{circ} (I_{Load} is a constant around the equilibrium point and its time derivative is always equal to zero) is:

$$U_{dc1}-R_{eq1}\cdot\left(I_{Load}-I_{circ}\right)-L_{eq1}\cdot\frac{d\left(-I_{circ}\right)}{dt}+R_{eq2}\cdot\left(I_{circ}\right)+L_{eq2}\cdot\frac{d\left(I_{circ}\right)}{dt}-U_{dc2}=0 \quad \text{(eq. 5-87)}$$

Where L_{eq1}, L_{eq2} and R_{eq1}, R_{eq2} are respectively the sum of the inductances and the resistances of the step down transformer at the dc side and the interphase reactor:

$$L_{eq1}=L_{ac/dc}\cdot\frac{\left(2\cdot\left(\frac{\pi}{3}-u_1\right)+1.5\cdot u_1\right)}{\frac{\pi}{3}}+L_i \quad \text{(eq. 5-88)}$$

$$L_{eq2}=L_{ac/dc}\cdot\frac{\left(2\cdot\left(\frac{\pi}{3}-u_2\right)+1.5\cdot u_2\right)}{\frac{\pi}{3}}+L_i \quad \text{(eq. 5-89)}$$

$$R_{eq1} = R_{ac/dc} \cdot \frac{\left(2 \cdot \left(\frac{\pi}{3} - u_1\right) + 1.5 \cdot u_1\right)}{\frac{\pi}{3}} + R_i \qquad \text{(eq. 5-90)}$$

$$R_{eq2} = R_{ac/dc} \cdot \frac{\left(2 \cdot \left(\frac{\pi}{3} - u_2\right) + 1.5 \cdot u_2\right)}{\frac{\pi}{3}} + R_i \qquad \text{(eq. 5-91)}$$

u_1 and u_2 are the overlap angles due to the inductance of the step down transformer related to the two ac/dc converters and they are considered as the output of the low pass filter with time constant $T_{dc1}=T_{dc2}$ and the state equations are:

$$\begin{aligned} &-u_1 + \left(\arccos\left(\cos(\hat{\alpha}_1) - \frac{4 \cdot f \cdot \pi \cdot L_{ac/dc} \cdot (I_{Load} - I_{circ}) \cdot k_{tra}}{\sqrt{3\left(e_d^2 + e_q^2\right)}}\right) - (\hat{\alpha}_1)\right) - \frac{d(u_1)}{dt} \cdot T_{dc1} = 0 \\ &-u_2 + \left(\arccos\left(\cos(\hat{\alpha}_2) - \frac{4 \cdot f \cdot \pi \cdot L_{ac/dc} \cdot I_{circ} \cdot k_{tra}}{\sqrt{3\left(e_d^2 + e_q^2\right)}}\right) - (\hat{\alpha}_2)\right) - \frac{d(u_2)}{dt} \cdot T_{dc2} = 0 \end{aligned} \qquad \text{(eq. 5-92)}$$

Where

$$\begin{aligned} \hat{\alpha}_1 &= \arccos(ref_{acdc1}) - \theta_{PLL} + \arctan\left(\frac{e_q}{e_d}\right) \\ \hat{\alpha}_2 &= \arccos(ref_{acdc2}) - \theta_{PLL} + \arctan\left(\frac{e_q}{e_d}\right) \end{aligned} \qquad \text{(eq. 5-93)}$$

The voltage U_d on the dc load results:

$$U_d = U_{dc1} - R_{eq1} \cdot (I_{Load} - I_{circ}) - L_{eq1} \cdot \frac{d(-I_{circ})}{dt} \qquad \text{(eq. 5-94)}$$

5.6.2.1.2 <u>The dq components of the ac/dc converter in 12 pulses operation</u>

As done in 6 pulses operation the dynamic response of the currents of the ac/dc converter are represented by low pass filters with time constant equal to $T_{dc1} = T_{dc2}$. Some new state and auxiliary variables have to be introduced to describe the transfer function of the output currents of the ac/dc converter:

- e_{d_c1}, e_{q_c1} and e_{d_c2}, e_{q_c2} are the busbar voltage filtered with a low pass filters with time constant T_{dc1} and T_{dc2} respectively:

$$\begin{aligned} &-e_{d\_c1} + e_d - T_{dc1} \cdot \frac{d(e_{d\_c1})}{dt} = 0 \\ &-e_{q\_c1} + e_q - T_{dc1} \cdot \frac{d(e_{q\_c1})}{dt} = 0 \\ &-e_{d\_c2} + e_d - T_{dc2} \cdot \frac{d(e_{d\_c2})}{dt} = 0 \\ &-e_{q\_c2} + e_q - T_{dc2} \cdot \frac{d(e_{q\_c2})}{dt} = 0 \end{aligned} \qquad \text{(eq. 5-95)}$$

- the firing angle $\overline{\alpha}_1$ is the sum of the state variable a_1 and of the angle voltage $\overline{\theta}_{V1}$ for the ac/dc converter 1 and and $\overline{\alpha}_2$ is the same for the ac/dc converter 2

$$\overline{\alpha}_1 = a_1 + \overline{\theta}_{V1}$$
$$\overline{\alpha}_2 = a_2 + \overline{\theta}_{V2} \qquad \text{(eq. 5-96)}$$

where

$$\overline{\theta}_{V1} = \arctan\left(\frac{e_{q\_c1}}{e_{d\_c1}}\right)$$
$$\overline{\theta}_{V2} = \arctan\left(\frac{e_{q\_c2}}{e_{d\_c2}}\right) \qquad \text{(eq. 5-97)}$$

The active component of the currents of the converter 1 and 2 result:

$$i_{at1} = \frac{2}{\sqrt{3}\cdot\pi\cdot k_{tra}}\cdot\left(I_{Load} - I_{circ}\right)\cdot\frac{1}{2}\cdot\left(\cos\left(\overline{\alpha}_1\right) + \cos\left(\overline{\alpha}_1 + u_1\right)\right)$$
$$i_{at2} = \frac{2}{\sqrt{3}\cdot\pi\cdot k_{tra}}\cdot I_{circ}\cdot\frac{1}{2}\cdot\left(\cos\left(\overline{\alpha}_2\right) + \cos\left(\overline{\alpha}_2 + u_2\right)\right) \qquad \text{(eq. 5-98)}$$

And the reactive ones result

$$i_{re1} = \frac{2}{\sqrt{3}\cdot\pi\cdot k_{tra}}\cdot\left(I_{Load} - I_{circ}\right)\cdot\frac{1}{2}\cdot\left(\cos\left(\overline{\alpha}_1\right) + \cos\left(\overline{\alpha}_1 + u_1\right)\right)\cdot\frac{\left(2u_1 + \sin\left(2\overline{\alpha}_1\right) - \sin\left(2\overline{\alpha}_1 + 2u_1\right)\right)}{\cos\left(2\overline{\alpha}_1\right) - \cos\left(2\overline{\alpha}_1 + 2u_1\right)}$$
$$i_{re2} = \frac{2}{\sqrt{3}\cdot\pi\cdot k_{tra}}\cdot I_{circ}\cdot\frac{1}{2}\cdot\left(\cos\left(\overline{\alpha}_2\right) + \cos\left(\overline{\alpha}_2 + u_2\right)\right)\cdot\frac{\left(2u_2 + \sin\left(2\overline{\alpha}_2\right) - \sin\left(2\overline{\alpha}_2 + 2u_2\right)\right)}{\cos\left(2\overline{\alpha}_2\right) - \cos\left(2\overline{\alpha}_2 + 2u_2\right)} \qquad \text{(eq. 5-99)}$$

The active and reactive components have to be rotate to be synchronous with the dq frame, and the d and q components of the current of the ac/dc converter in 12 pulses configuration i_{acdc_d} and i_{acdc_q} result:

$$i_{acdc\_d} = i_{acdc\_d1} + i_{acdc\_d2} = i_{at1}\cdot\cos\overline{\theta}_{V1} + i_{re1}\cdot\sin\overline{\theta}_{V1} + i_{at2}\cdot\cos\overline{\theta}_{V2} + i_{re2}\cdot\sin\overline{\theta}_{V2}$$
$$i_{acdc\_q} = i_{acdc\_q1} + i_{acdc\_q2} = i_{at1}\cdot\sin\overline{\theta}_{V1} - i_{re1}\cdot\cos\overline{\theta}_{V1} + i_{at2}\cdot\sin\overline{\theta}_{V2} - i_{re2}\cdot\cos\overline{\theta}_{V2} \qquad \text{(eq. 5-100)}$$

5.6.2.2 The control system of the ac/dc converter base unit in 12 pulses configuration

The output of the feed-forward block is achieved by the steady-state equation of the output voltage U_d for both the two ac/dc converters:

$$out_{feed-for1} = \frac{U_{d\_ref} + (Ri + 2\cdot R_{ac/dc})\cdot I_{dc1\_mean} + 6\cdot f\cdot L_{ac/dc}\cdot I_{dc\_mean1}}{U_{d0\_f}}$$
$$out_{feed-for2} = \frac{U_{d\_ref} + (Ri + 2\cdot R_{ac/dc})\cdot I_{dc1\_mean} + 6\cdot f\cdot L_{ac/dc}\cdot I_{dc\_mean2}}{U_{d0\_f}} \qquad \text{(eq. 5-101)}$$

Where U_{d_ref} is the reference value of the voltage on the load, U_{d0_f} is the no load voltage of the ac/dc converter calculating by the FFT component at 50 Hz of the busbar voltage U, and I_{dc_mean1} and I_{dc_mean2} are the mean values of the output currents of the ac/dc converters with an integration time of 3.333ms.

As done in 6 pulses configuration, the FFT at 50 Hz of the bus bar voltage is quasi-equivalent to a calculation of the mean value with integration time of 0.02 s of the busbar voltage e_d and e_q in dq frame (see paragraph 5.5.2.2), and it may be considered as a low pass filter with time constant equal to 0.02/2 = 0.01 s/rad, so the voltage U_{d0_f} results

$$-U_{d0\_f}+\frac{3\cdot\sqrt{2}}{\pi\cdot k_{tra}}\sqrt{\frac{3}{2}\cdot\left(e_d^2+e_q^2\right)}-T_{Ud0\_f}\cdot\frac{d(U_{d0\_f})}{dt}=0 \quad \text{(eq. 5-102)}$$

Where T_{Ud0} is equal to 0.02/2=0.01 s/rad (see paragraph 5.3).
The feedback of the output dc currents of the two ac/dc converter is achieved by calculating the mean value with an integration time of 3.333 ms. Considering that the load current is imposed, just the circulating current may vary, and approximating the mean block by a low pass filter of time constant T_{Idc_f} equal to 3.333/2=1.667 s/rad, it yields:

$$-I_{circ\_f}+I_{circ}-\frac{d\left(I_{circ\_f}\right)}{dt}\cdot T_{Idc\_f}=0 \quad \text{(eq. 5-103)}$$

And the outputs of the feed forward block results

$$\begin{aligned} out_{feed-for1}&=\frac{U_{d\_ref}+(Ri+2\cdot R_{ac/dc})\cdot\left(I_{Load}-I_{circ\_f}\right)+6\cdot f\cdot L_{ac/dc}\cdot\left(I_{Load}-I_{circ\_f}\right)}{U_{d0\_f}} \\ out_{feed-for2}&=\frac{U_{d\_ref}+(Ri+2\cdot R_{ac/dc})\cdot I_{circ\_f}+6\cdot f\cdot L_{ac/dc}\cdot I_{circ\_f}}{U_{d0\_f}} \end{aligned} \quad \text{(eq. 5-104)}$$

The feedback signal of the dc voltage on the load is filtered by a mean block with time constant equal to 3.333 ms and in the analytical model it is simplified by a low pass filter (see paragraph 5.3), whose the relative state equation (state variable U_{d_f}) is:

$$-U_{d\_f}+U_d-\frac{d\left(U_{d\_f}\right)}{dt}\cdot T_{U_{d\_f}}=0 \quad \text{(eq. 5-105)}$$

The PI controller of the voltage U_d has one state variable w_v which is the output of the integrator:

$$k_{i\_V}\cdot\left(U_{d\_ref}-U_{d\_f}\right)-\frac{d\left(w_v\right)}{dt}=0 \quad \text{(eq. 5-106)}$$

The output of the PI controller results:

$$PI_V=k_{p\_V}\cdot\left(U_{d\_ref}-U_{d\_f}\right)+w_V \quad \text{(eq. 5-107)}$$

where k_{p_V} and k_{i_V} are the proportional and integral gains respectively of the PI voltage controller.
The PI controller of the circulating current I_{circ} has one state variable w_I which is the output of the integrator:

$$k_{i\_V}\cdot\left(I_{circ\_ref}-I_{circ\_f}\right)-\frac{d\left(w_I\right)}{dt}=0 \quad \text{(eq. 5-108)}$$

The output of the PI controller results:

$$PI_I=k_{p\_I}\cdot\left(I_{circ\_ref}-I_{circ\_f}\right)+w_I \quad \text{(eq. 5-109)}$$

where k_{p_I} and k_{i_I} are the proportional and integral gains respectively of the PI controller. For this study they have been set: $k_{p\_V}=0$, $k_{i\_V}=1.06\cdot10^{-3}$ and $k_{p\_I}=1.2\cdot10^{-4}$, $k_{i\_I}=2.14\cdot10^{-4}$.
The reference inputs ref_{acdc1} and ref_{acdc2} are:

$$\begin{aligned} ref_{acdc1}&=out_{feed-for1}+PI_V-PI_I \\ ref_{acdc2}&=out_{feed-for2}+PI_V+PI_I \end{aligned} \quad \text{(eq. 5-110)}$$

5.6.2.3 The state space matrix of the ac/dc converter in 12 pulses operation

The Dynamic Model of the ac/dc converter in 12 pulses operation (included the PLL) has been represented by a state space matrix where:

- the inputs are the dq component of busbar voltage (e_d, e_q)
- the inputs of the control are the voltage reference U_{d_ref} and the circulating reference I_{circ_ref}
- the outputs are the ac/dc converter currents (i_{acdc_d}, i_{acdc_q}).

The equations of the PLL (see paragraph 5.2.1) and of the ac/dc converter in 12 pulses configuration (see above) are used to build the Jacobian matrix of the system (see paragraph 5.1). The state variables are listed below:

- PLL = w_{1_PLL}, θ_{PLL}
- ac/dc converter = a_1, u_1, a_2, u_2, I_{circ}, w_V, w_I, U_{d_f}, U_{d0_f}, I_{circ_f}, e_{d_c1}, e_{q_c1}, I_{cir_c1}, e_{d_c2}, e_{q_c2}, I_{cir_c2},

The analytical equations have to been written just as function of the state variables and of the input variables, replacing the auxiliary variables where necessary.
Considering the method described in the paragraph 5.1, the Dynamic Model of the ac/dc converter in 12 pulses configuration is:

$$\begin{aligned}\left[\Delta \dot{x}_{acdc\_12}\right] &= A_{acdc\_12} \cdot \left[\Delta x_{acdc\_12}\right] + B_{e\_acdc\_12} \cdot \begin{bmatrix}\Delta e_d \\ \Delta e_q\end{bmatrix} + B_{inp\_acdc\_12} \cdot \begin{bmatrix}\Delta U_{d\_ref} \\ \Delta I_{circ\_ref}\end{bmatrix} \\ \left[\Delta i_{acdc\_12}\right] &= C_{acdc\_12} \cdot \left[\Delta x_{acdc\_12}\right]\end{aligned} \qquad \text{(eq. 5-111)}$$

In the following figures are shown a comparison of the waveforms of the measure of the voltage on the load (ΔU_{d_f} see Figure 5-28), of the measure of the circulating current (ΔI_{circ} see Figure 5-29) and of the ac/dc converter currents (Δi_{acdc_d} and Δi_{acdc_q} see Figure 5-30), between PSIM and Dynamic Models after that a two several step functions have been applied at the same time to the busbar voltage (Δe_d and Δe_q see Figure 5-27) and to the circulating current (at the equilibrium point U_d =20 kV, I_{Load} = 4 kA, I_{cir} = 2 kA). The waveforms indicate the variation from the equilibrium point.
The high frequency oscillating components of the current Δi_{acdc_d} and Δi_{acdc_q} in the PSIM model (blue line) are due to the switching phenomena not considered in the Dynamic Model (green line), nevertheless it may be noted that the waveforms of the currents obtained by the Dynamic Model show a good agreement with that achieved by PSIM models (Figure 5-30). Also the waveforms of the voltage measure on the load ΔU_{d_f} and of the the circulating current ΔI_{circ_f} show a good agreement between the two models. The Dynamic Model of the ac/dc converter in 12 pulses operating mode can be considered accurate for frequency range equal to the 6 pulses one (i.e. <50 Hz limit due principally to the control system), because the approximations are similar.

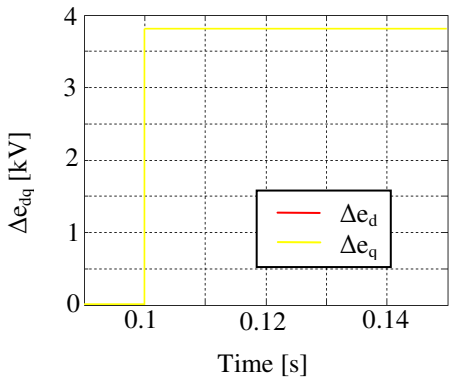

Figure 5-27 Step function applied to the busbar voltage (Δe_d and Δe_q)

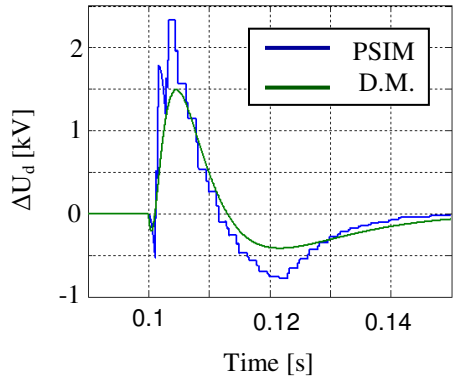

Figure 5-28 Comparison between the waveforms of the measure of the voltage on the load ΔU_{d_f} of the ac/dc converter between PSIM (blue line) and Dynamic (green line) Models after a step function applied to the busbar voltage (Δe_d and Δe_q) and to the circulating current reference

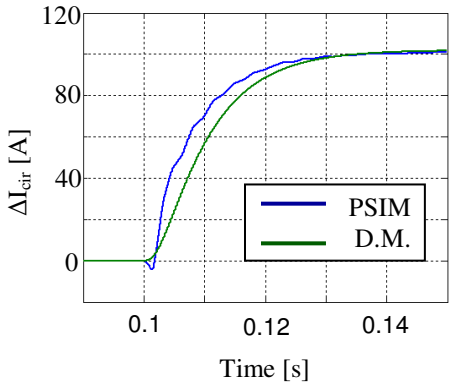

Figure 5-29 Comparison between the waveforms of the measure of the circulating current ΔI_{cir} of the ac/dc converter between PSIM (blue line) and Dynamic (green line) Models after two several step functions applied at the sime time to the busbar voltage (Δe_d and Δe_q) and to the circulating current reference

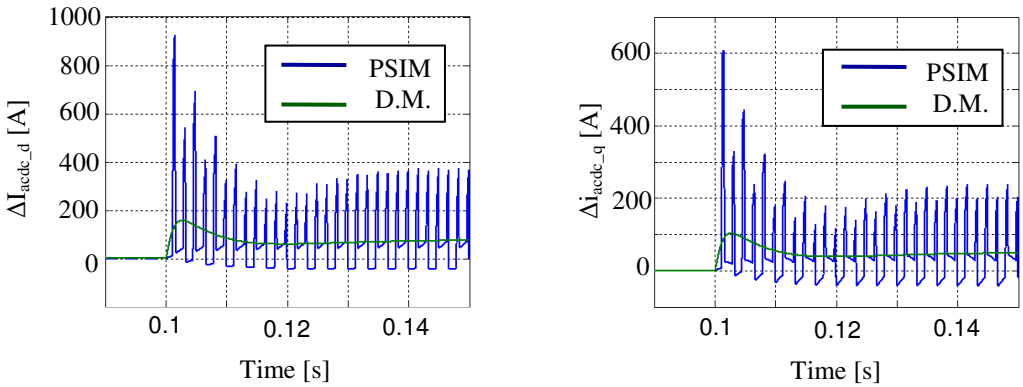

Figure 5-30 Comparison between the waveforms of the ac/dc converter currents at small signals (Δi_{acdc_d} and Δi_{acdc_q}) between PSIM (blue line) and Dynamic (green line) Models after two several step functions applied at the sime time to the busbar voltage (Δe_d and Δe_q) and to the circulating current reference

5.6.3 The ac/dc converter base unit in circulating mode

In circulating mode operation the dc output current of an ac/dc converter is the sum of the load current I_{Load} and the current I_{circ} flowing in the anti-parallel one. The block scheme of the unit in circulating mode operation is shown in the Figure 5-31

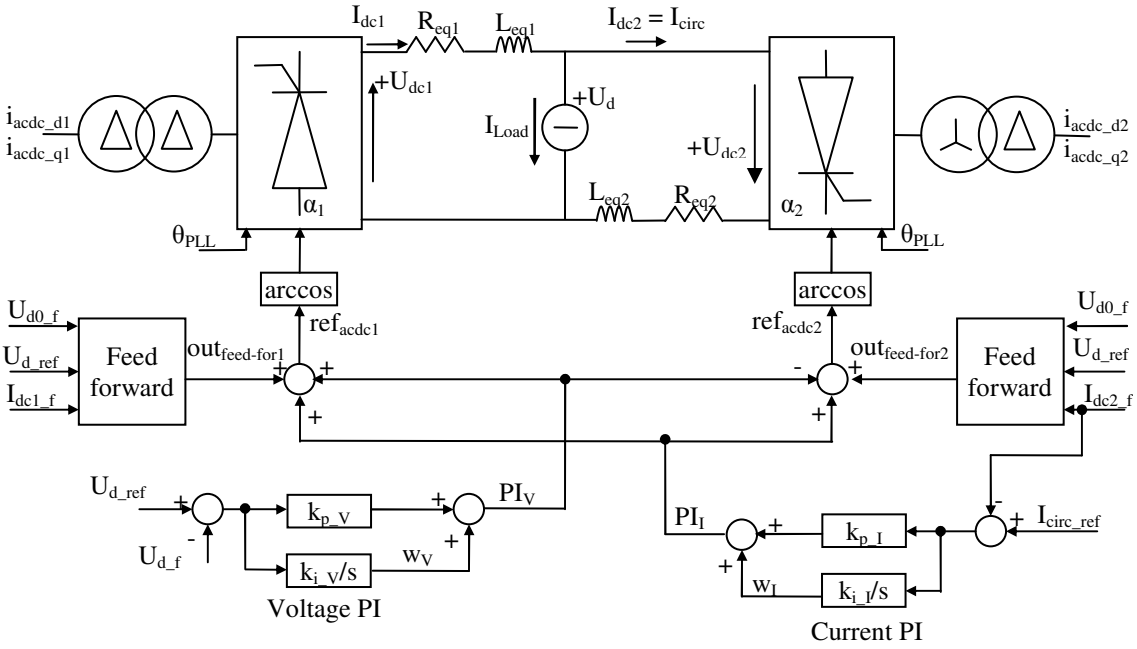

Figure 5-31 Block scheme of the ac/dc converter in circulating mode

The equations considered in the 12 pulse ac/dc converter model can be used also in the circulating operation model, but taking into account the different dynamic response and of the sign of the circulating current I_{circ} between the two anti-parallel ac/dc converters and that the output dc currents I_{dc1} and I_{dc2} of the ac/dc converters are:

$I_{dc1}=I_{Load}+I_{circ}$

$I_{dc2}=I_{circ}$

The inputs are the d and q components of the busbar voltage (e_d and e_q), the voltage reference U_{d_ref}, and the reference of the circulating current I_{circ_ref}, while the outputs are

the sum i_{acdc_d} and i_{acdc_q} of the d and q components of the currents of the two ac/dc converters i_{acdc_d1} and i_{acdc_q1}, i_{acdc_d2} and i_{acdc_q2}:

- $i_{acdc\_d} = i_{acdc\_d1} + i_{acdc\_d2}$
- $i_{acdc\_q} = i_{acdc\_q1} + i_{acdc\_q2}$

5.6.3.1 The dynamic of the ac/dc converter base unit operating circulating mode

5.6.3.1.1 The output voltage on the load U_d in circulating mode

The time between two switching instants of the ac/dc converter base unit operating circulating mode is not constant but it depends from the alpha firing angle (α_1 and α_2) of the two converters which are different; indeed if one operate as rectifier (firing angle < 90 degree), the other one operate as inverter (firing angle > 90 degree). The switching time instants for the two anti-parallel ac/dc converters (t_1 an t_2) are:

$$t_1(k) = \alpha_1 \frac{0.01}{\pi} + k \cdot T_{SW}$$
$$t_2(k) = T_{SD} + \alpha_2 \frac{0.01}{\pi} + k \cdot T_{SW} \qquad \text{for k=0,1,2,..} \qquad \text{(eq. 5-112)}$$

Where T_{SW} is the time between two switching of one ac/dc converter (6 pulses operation) which is 1/50/6 = 3.333 ms, $T_{SD} = T_{SW}/2$ indicates the time difference between synchronization reference of the firing angles of the two ac/dc converters in anti-parallel due to the difference connections of the secondary windings (star and delta) and the firing angles are given in radians. The Figure 5-32 shows several switching pattern of the two converters, indicating with T_1 and T_2 the interval time between two switching instants of the base unit.
For instance, with the ac/dc converter unit in circulating mode if

$$\alpha_1 = \alpha_2 + k \cdot T_{SW} \frac{\pi}{0.01} \text{ for k = 0,1,2,..} \qquad \text{(eq. 5-113)}$$

A switching occur each $T_{SW}/2$ ($T_1=T_2=T_{SW}/2$ see figure) and it has an equivalent dynamic response to the 12 pulses operation, while if

$$\alpha_1 = \left(\alpha_2 + T_{SD} \frac{\pi}{0.01} \right) + k \cdot T_{SW} \frac{\pi}{0.01} \text{ for k = 0,1,2,..} \qquad \text{(eq. 5-114)}$$

the two converters switch at the same instant with time intervals equal to T_{SW} (T1=0, $T2=T_{SW}$) and the unit base has an equivalent dynamic response to the 6 pulses operation; therefore the dynamic response of the ac/dc converter base unit in circulating mode change with the operating point.
Considering that time interval T_1 and T_2 generally are not equal, a mean value (calculated for each operating point indicated with subscript "$_0$") has been considered for the time delays T_{dc1} and T_{dc2} of the transfer functions used to describe the dynamic of the two converters:

$$T_{dc1} = T_{dc2} = \frac{1}{2} \cdot \frac{T_{SW}}{2} \cdot \left(\frac{\max(T_1, T_2)}{T_{SW}/2} \right) \qquad \text{(eq. 5-115)}$$

where the function "max" take the maximum value between T_1 and T_2
and written as function of the firing angle α_{1_0} and α_{2_0} it yields:

$$T_{dc1} = T_{dc2} = \frac{1}{2} \cdot \frac{T_{SW}}{2} \cdot \left(0.5 + \left| \frac{|\alpha_{1\_0} - \alpha_{2\_0}|}{\pi/3} - round\left(\frac{|\alpha_{1\_0} - \alpha_{2\_0}|}{\pi/3} \right) \right| \right) \qquad \text{(eq. 5-116)}$$

where the function "round(X)" rounds the elements of X to the nearest integers. For both the two anti-parallel ac/dc converters the delay has been approximated by two low pass filters with time constant equal to $T_{dc1} = T_{dc2}$.
The dynamic response of the two ac/dc converters can be described by the state equations:

$$\begin{aligned} -a_1 + \arccos\left(ref_{acdc1}\right) - \theta_{PLL} - \frac{d\left(a_1\right)}{dt} \cdot T_{dc1} = 0 \\ -a_2 + \arccos\left(ref_{acdc2}\right) - \theta_{PLL} - \frac{d\left(a_2\right)}{dt} \cdot T_{dc2} = 0 \end{aligned} \qquad \text{(eq. 5-117)}$$

where a_1 and a_2 are the state variables of the low pass filters, ref_{acdc1} and ref_{acdc2} are the input references and θ_{PLL} is the output angle of the PLL.

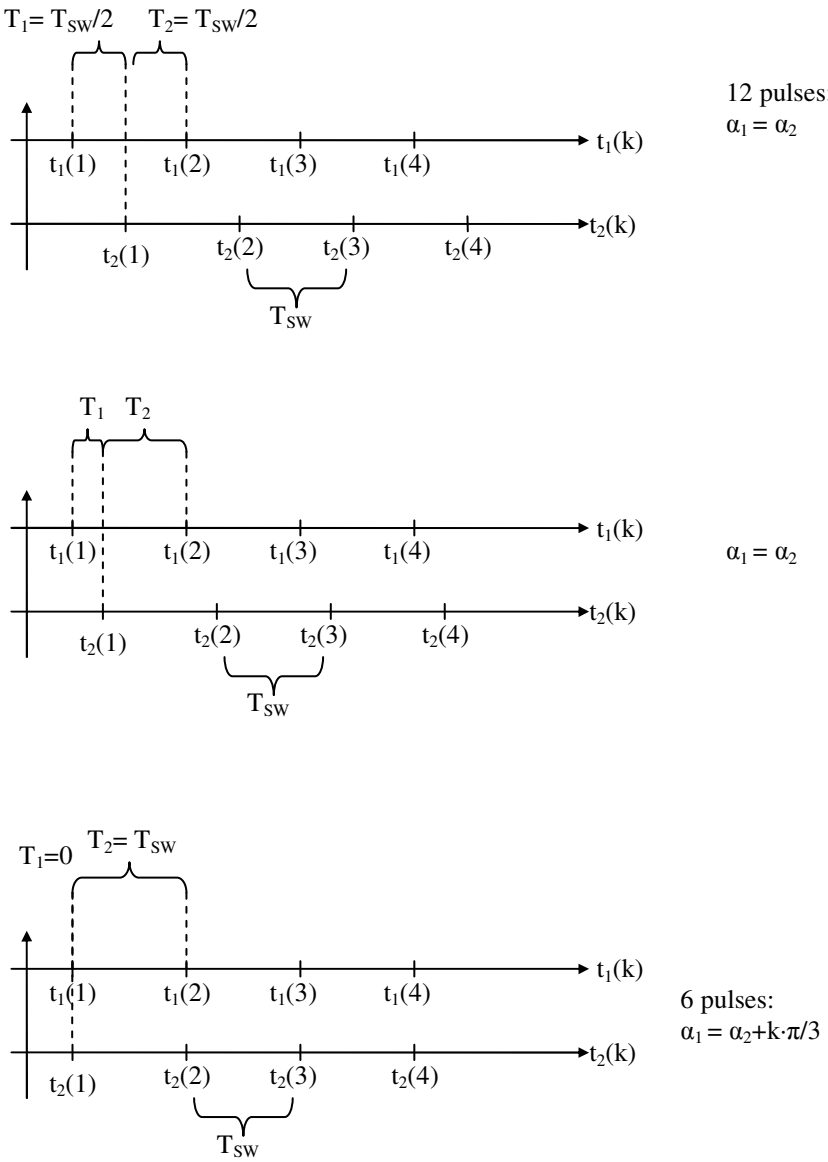

Figure 5-32 Several switching patterns of the two converters, indicating with T_1 and T_2 the interval time between two switching instants of the base unit

The output voltages U_{dc1} and U_{dc2} are:

$$U_{dc1} = \frac{3 \cdot \sqrt{2}}{\pi \cdot k_{tra}} \cdot \sqrt{\frac{3}{2}\left(e_d^2 + e_q^2\right)} \cdot \cos\left(a_1 + \arctan\left(\frac{e_q}{e_d}\right)\right) - 6 \cdot f \cdot L_{ac/dc} \cdot \left(I_{dc\_load} + I_{circ\_c1}\right) \qquad \text{(eq. 5-118)}$$

$$U_{dc2} = \frac{3 \cdot \sqrt{2}}{\pi \cdot k_{tra}} \cdot \sqrt{\frac{3}{2}\left(e_d^2 + e_q^2\right)} \cdot \cos\left(a_2 + \arctan\left(\frac{e_q}{e_d}\right)\right) - 6 \cdot f \cdot L_{ac/dc} \cdot \left(I_{circ\_c2}\right) \quad \text{(eq. 5-119)}$$

where I_{circ_c} is the filtered circulating current I_{circ} by of a low pass filter, because the drop voltage due the switching of the thyristors is based on average values. The related state equations of the two converters result:

$$-I_{circ\_c1} + I_{circ} - \frac{d\left(I_{circ\_c1}\right)}{dt} \cdot T_{dc1} = 0 \quad \text{(eq. 5-120)}$$

$$-I_{circ\_c2} + I_{circ} - \frac{d\left(I_{circ\_c2}\right)}{dt} \cdot T_{dc2} = 0 \quad \text{(eq. 5-121)}$$

The state equation related to the circulating current I_{circ} (I_{Load} is a constant around the equilibrium point and its time derivative is always equal to zero) is:

$$U_{dc1} - R_{eq1} \cdot \left(I_{Load} + I_{circ}\right) - L_{eq1} \cdot \frac{d\left(I_{circ}\right)}{dt} - R_{eq2} \cdot \left(I_{circ}\right) - L_{eq2} \cdot \frac{d\left(I_{circ}\right)}{dt} + U_{dc2} = 0 \quad \text{(eq. 5-122)}$$

Where L_{eq1}, L_{eq2} and R_{eq1}, R_{eq2} are respectively the sum among the inductances and the resistances of the step down transformer seen from the dc side and the interphase reactor for the two converters:

$$L_{eq1} = L_{ac/dc} \cdot \frac{\left(2 \cdot \left(\frac{\pi}{3} - u_1\right) + 1.5 \cdot u_1\right)}{\frac{\pi}{3}} + L_i \quad \text{(eq. 5-123)}$$

$$L_{eq2} = L_{ac/dc} \cdot \frac{\left(2 \cdot \left(\frac{\pi}{3} - u_2\right) + 1.5 \cdot u_2\right)}{\frac{\pi}{3}} + L_i \quad \text{(eq. 5-124)}$$

$$R_{eq1} = R_{ac/dc} \cdot \frac{\left(2 \cdot \left(\frac{\pi}{3} - u_1\right) + 1.5 \cdot u_1\right)}{\frac{\pi}{3}} + R_i \quad \text{(eq. 5-125)}$$

$$R_{eq2} = R_{ac/dc} \cdot \frac{\left(2 \cdot \left(\frac{\pi}{3} - u_2\right) + 1.5 \cdot u_2\right)}{\frac{\pi}{3}} + R_i \quad \text{(eq. 5-126)}$$

u_1 and u_2 are the overlap angles due to the inductance of the step down transformer related to the two ac/dc converters and they are considered as the output of the low pass filter with time constant T_{dc1}=T_{dc2} and the state equations are:

$$\begin{aligned} &-u_1 + \left(\arccos\left(\cos\left(\hat{\alpha}_1\right) - \frac{4 \cdot f \cdot \pi \cdot L_{ac/dc} \cdot \left(I_{Load} + I_{circ}\right) \cdot k_{tra}}{\sqrt{3\left(e_d^2 + e_q^2\right)}}\right) - \left(\hat{\alpha}_1\right)\right) - \frac{d\left(u_1\right)}{dt} \cdot T_{dc1} = 0 \\ &-u_2 + \left(\arccos\left(\cos\left(\hat{\alpha}_2\right) - \frac{4 \cdot f \cdot \pi \cdot L_{ac/dc} \cdot I_{circ} \cdot k_{tra}}{\sqrt{3\left(e_d^2 + e_q^2\right)}}\right) - \left(\hat{\alpha}_2\right)\right) - \frac{d\left(u_2\right)}{dt} \cdot T_{dc2} = 0 \end{aligned} \quad \text{(eq. 5-127)}$$

Where

$$\hat{\alpha}_1 = \arccos\left(ref_{acdc1}\right) - \theta_{PLL} + \arctan\left(\frac{e_q}{e_d}\right)$$
$$\hat{\alpha}_2 = \arccos\left(ref_{acdc2}\right) - \theta_{PLL} + \arctan\left(\frac{e_q}{e_d}\right) \qquad \text{(eq. 5-128)}$$

The voltage U_d on the dc load results:

$$U_d = U_{dc1} - R_{eq1} \cdot \left(I_{Load} + I_{circ}\right) - L_{eq1} \cdot \frac{d\left(I_{circ}\right)}{dt} \qquad \text{(eq. 5-129)}$$

5.6.3.1.2 The dq components of the ac/dc converter in circulating mode

As done in 6 pulses configuration the dynamic response of the currents of the ac/dc converter are represented by low pass filters with time constant equal to $T_{dc1} = T_{dc2}$. Some new state and auxiliary variables have to be introduced to describe the transfer function of the output currents of the ac/dc converter:

- e_{d_c1}, e_{q_c1} and e_{d_c2}, e_{q_c2} are the busbar voltage filtered with a low pass filters with time constant T_{dc1} and T_{dc2} respectively:

$$\begin{aligned} &-e_{d\_c1} + e_d - T_{dc1} \cdot \frac{d(e_{d\_c1})}{dt} = 0 \\ &-e_{q\_c1} + e_q - T_{dc1} \cdot \frac{d(e_{q\_c1})}{dt} = 0 \\ &-e_{d\_c2} + e_d - T_{dc2} \cdot \frac{d(e_{d\_c2})}{dt} = 0 \\ &-e_{q\_c2} + e_q - T_{dc2} \cdot \frac{d(e_{q\_c2})}{dt} = 0 \end{aligned} \qquad \text{(eq. 5-130)}$$

- the firing angle $\overline{\alpha}_1$ is the sum of the state variable a_1 and of the angle voltage $\overline{\theta}_{V1}$ for the ac/dc converter 1 and and $\overline{\alpha}_2$ is the same for the ac/dc converter 2

$$\begin{aligned} \overline{\alpha}_1 &= a_1 + \overline{\theta}_{V1} \\ \overline{\alpha}_2 &= a_2 + \overline{\theta}_{V2} \end{aligned} \qquad \text{(eq. 5-131)}$$

where

$$\begin{aligned} \overline{\theta}_{V1} &= \arctan\left(\frac{e_{q\_c1}}{e_{d\_c1}}\right) \\ \overline{\theta}_{V2} &= \arctan\left(\frac{e_{q\_c2}}{e_{d\_c2}}\right) \end{aligned} \qquad \text{(eq. 5-132)}$$

The active component of the currents of the converter 1 and 2 result:

$$\begin{aligned} i_{at1} &= \frac{2}{\sqrt{3} \cdot \pi \cdot k_{tra}} \cdot \left(I_{Load} + I_{circ}\right) \cdot \frac{1}{2} \cdot \left(\cos\left(\overline{\alpha}_1\right) + \cos\left(\overline{\alpha}_1 + u_1\right)\right) \\ i_{at2} &= \frac{2}{\sqrt{3} \cdot \pi \cdot k_{tra}} \cdot I_{circ} \cdot \frac{1}{2} \cdot \left(\cos\left(\overline{\alpha}_2\right) + \cos\left(\overline{\alpha}_2 + u_2\right)\right) \end{aligned} \qquad \text{(eq. 5-133)}$$

And the reactive ones result

$$i_{re1} = \frac{2}{\sqrt{3}\cdot\pi\cdot k_{tra}}\cdot\left(I_{Load}+I_{circ}\right)\cdot\frac{1}{2}\cdot\left(\cos\left(\overline{\alpha}_1\right)+\cos\left(\overline{\alpha}_1+u_1\right)\right)\cdot\frac{\left(2u_1+\sin\left(2\overline{\alpha}_1\right)-\sin\left(2\overline{\alpha}_1+2u_1\right)\right)}{\cos\left(2\overline{\alpha}_1\right)-\cos\left(2\overline{\alpha}_1+2u_1\right)}$$
$$i_{re2} = \frac{2}{\sqrt{3}\cdot\pi\cdot k_{tra}}\cdot I_{circ}\cdot\frac{1}{2}\cdot\left(\cos\left(\overline{\alpha}_2\right)+\cos\left(\overline{\alpha}_2+u_2\right)\right)\cdot\frac{\left(2u_2+\sin\left(2\overline{\alpha}_2\right)-\sin\left(2\overline{\alpha}_2+2u_2\right)\right)}{\cos\left(2\overline{\alpha}_2\right)-\cos\left(2\overline{\alpha}_2+2u_2\right)} \quad \text{(eq. 5-134)}$$

The active and reactive components have to be rotate to be synchronous with the dq frame, and the d and q components of the current of the ac/dc converter in 12 pulses configuration i_{acdc_d} and i_{acdc_q} result:

$$i_{acdc\_d} = i_{acdc\_d1} + i_{acdc\_d2} = i_{at1}\cdot\cos\overline{\theta}_{V1} + i_{re1}\cdot\sin\overline{\theta}_{V1} + i_{at2}\cdot\cos\overline{\theta}_{V2} + i_{re2}\cdot\sin\overline{\theta}_{V2}$$
$$i_{acdc\_q} = i_{acdc\_q1} + i_{acdc\_q2} = i_{at1}\cdot\sin\overline{\theta}_{V1} - i_{re1}\cdot\cos\overline{\theta}_{V1} + i_{at2}\cdot\sin\overline{\theta}_{V2} - i_{re2}\cdot\cos\overline{\theta}_{V2} \quad \text{(eq. 5-135)}$$

5.6.3.2 The control system of the ac/dc converter base unit in circulating mode operations

The output of the feed-forward block is achieved by the steady-state equation of the output voltage U_d for both the two ac/dc converters:

$$out_{feed-for1} = \frac{U_{d\_ref} + (R_i + 2\cdot R_{ac/dc})\cdot I_{dc1\_mean} + 6\cdot f\cdot L_{ac/dc}\cdot I_{dc\_mean1}}{U_{d0\_f}}$$
$$out_{feed-for2} = \frac{-U_{d\_ref} + (R_i + 2\cdot R_{ac/dc})\cdot I_{dc1\_mean} + 6\cdot f\cdot L_{ac/dc}\cdot I_{dc\_mean2}}{U_{d0\_f}} \quad \text{(eq. 5-136)}$$

Where U_{d_ref} is the reference value of the voltage on the load, U_{d0_f} is the no load voltage of the ac/dc converter calculated by the FFT component at 50 Hz of the busbar voltage U, and I_{dc_mean1} and I_{dc_mean2} are the mean values of the output currents of the ac/dc converters with an integration time of 3.333ms.

As done in 6 pulses configuration, the FFT at 50 Hz of the bus bar voltage is quasi-equivalent to a calculation of the mean value with integration time of 0.02 s of the busbar voltage ed and eq in dq frame (see paragraph 5.5.2.2), and it may be considered as a low pass filter with time constant equal to 0.02/2 = 0.01 s/rad, so the voltage U_{d0_f} results

$$-U_{d0\_f} + \frac{3\cdot\sqrt{2}}{\pi\cdot k_{tra}}\sqrt{\frac{3}{2}\cdot\left(e_d^2+e_q^2\right)} - T_{Ud0\_f}\cdot\frac{d(U_{d0\_f})}{dt} = 0 \quad \text{(eq. 5-137)}$$

Where T_{Ud0} is equal to 0.02/2=0.01 s/rad (see paragraph 5.3).

The feedback of the output dc currents of the two ac/dc converter is achieved by calculating the mean value with an integration time of 3.333 ms. Considering that the load current is imposed, just the circulating current may vary, and approximating the mean block by a low pass filter of time constant T_{Idc_f} equal to 3.333/2=1.667 s/rad, it yields:

$$-I_{circ\_f} + I_{circ} - \frac{d\left(I_{circ\_f}\right)}{dt}\cdot T_{Idc\_f} = 0 \quad \text{(eq. 5-138)}$$

And the outputs of the feed forward block results

$$out_{feed-for1} = \frac{U_{d\_ref} + (R_i + 2\cdot R_{ac/dc})\cdot\left(I_{Load}+I_{circ\_f}\right) + 6\cdot f\cdot L_{ac/dc}\cdot\left(I_{Load}+I_{circ\_f}\right)}{U_{d0\_f}}$$
$$out_{feed-for2} = \frac{-U_{d\_ref} + (R_i + 2\cdot R_{ac/dc})\cdot I_{circ\_f} + 6\cdot f\cdot L_{ac/dc}\cdot I_{circ\_f}}{U_{d0\_f}}$$

The feedback signal of the dc voltage on the load is filtered by a mean block with time constant equal to 3.333 ms and in the analytical model it is simplified by a low pass filter (see paragraph 5.3), whose the relative state equation (state variable U_{d_f}) is:

$$-U_{d\_f} + U_d - \frac{d(U_{d\_f})}{dt} \cdot T_{U_{d\_f}} = 0 \qquad \text{(eq. 5-139)}$$

The PI controller of the voltage U_d has one state variable w_v which is the output of the integrator:

$$k_{i\_V} \cdot (U_{d\_ref} - U_{d\_f}) - \frac{d(w_v)}{dt} = 0 \qquad \text{(eq. 5-140)}$$

The output of the PI controller results:

$$PI_V = k_{p\_V} \cdot (U_{d\_ref} - U_{d\_f}) + w_V$$

where k_{p_V} and k_{i_V} are the proportional and integral gains respectively of the PI voltage controller.

The PI controller of the circulating current I_{circ} has one state variable w_I which is the output of the integrator:

$$k_{i\_V} \cdot (I_{circ\_ref} - I_{circ\_f}) - \frac{d(w_I)}{dt} = 0 \qquad \text{(eq. 5-141)}$$

The output of the PI controller results:

$$PI_I = k_{p\_I} \cdot (I_{circ\_ref} - I_{circ\_f}) + w_I$$

where k_{p_I} and k_{i_I} are the proportional and integral gains respectively of the PI controller.

The reference inputs ref_{acdc1} and ref_{acdc2} are:

$$\begin{aligned} ref_{acdc1} &= out_{feed-for1} + PI_V + PI_I \\ ref_{acdc2} &= out_{feed-for2} - PI_V + PI_I \end{aligned} \qquad \text{(eq. 5-142)}$$

5.6.3.3 The state space matrix of the ac/dc converter in circulating mode

The Dynamic Model of the ac/dc converter in circulating mode (included the PLL) has been represented by a state space matrix where:

- the inputs are the dq component of busbar voltage (e_d, e_q)
- the inputs of the control are the voltage reference U_{d_ref} and the circulating reference I_{circ_ref}
- the outputs are the ac/dc converter currents (i_{acdc_d}, i_{acdc_q}).

The equations of the PLL (see paragraph 5.2.1) and of the ac/dc converter in circulating mode operation (see above) are used to build the Jacobian matrix of the system (see paragraph 5.1). The state variables are listed below:

- PLL = w_{1_PLL}, θ_{PLL}
- ac/dc converter = a_1, u_1, a_2, u_2, I_{circ}, w_V, w_I, U_{d_f}, U_{d0_f}, I_{circ_f}, e_{d_c1}, e_{q_c1}, I_{cir_c1}, e_{d_c2}, e_{q_c2}, I_{cir_c2},

The analytical equations have to been written just as function of the state variables and of the input variables, replacing the auxiliary variables where necessary.

Considering the method described in the paragraph 5.1, the Dynamic Model of the ac/dc converter in 12 pulses configuration is:

$$\begin{aligned} [\Delta \dot{x}_{acdc\_circ}] &= A_{acdc\_circ} \cdot [\Delta x_{acdc\_circ}] + B_{e\_acdc\_circ} \cdot \begin{bmatrix} \Delta e_d \\ \Delta e_q \end{bmatrix} + B_{inp\_acdc\_circ} \cdot \begin{bmatrix} \Delta U_{d\_ref} \\ \Delta I_{circ\_ref} \end{bmatrix} \\ [\Delta i_{acdc\_circ}] &= C_{acdc\_circ} \cdot [\Delta x_{acdc\_circ}] \end{aligned} \qquad \text{(eq. 5-143)}$$

In the following figures are shown a comparison of the waveforms of the measure of the voltage on the load (ΔU_{d_f} see Figure 5-34), of the measure of the circulating current (ΔI_{circ_f} see Figure 5-35) and of the ac/dc converter currents (Δi_{acdc_d} and Δi_{acdc_q} see Figure 5-36), between PSIM and Dynamic Models of the ac/dc converter in circulating mode after that two several step functions have been applied at the same time to the busbar voltage (Δe_d and Δe_q see Figure 5-33) and to the circulating current (at the equilibrium point U_d =-30 kV, I_{Load} = 840 kA, I_{cir} = 840 kA). All the figures represent the variation from the equilibrium point.
The high frequency oscillating components of the current Δi_{acdc_d} and Δi_{acdc_q} in the PSIM model (blue line) are due to the switching phenomena not considered in the Dynamic Model (green line), nevertheless it may be noted that the waveforms of the currents obtained by the Dynamic Model show a good agreement with that achieved by PSIM models (Figure 5-30). Also the waveforms of the voltage measure on the load ΔU_{d_f} show a good agreement between the two models. The waveforms of the measure of the circulating current ΔI_{circ_f} show a good agreement between the two models, but with a small error due to the switching phenomena not considered in the Dynamic Model.
The Dynamic Model of the ac/dc converter in circulating mode can be considered accurate for frequency range equal to the 6 pulses one (i.e. <50 Hz limit due principally to the control system), because the approximations are similar.

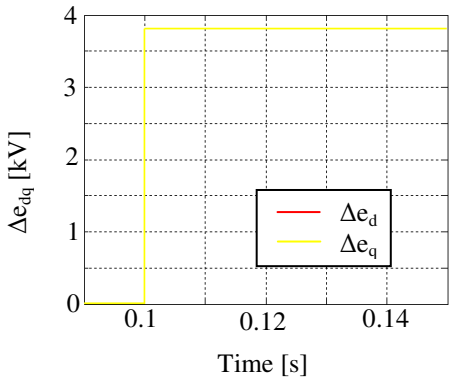

Figure 5-33 Step function applied to the busbar voltage (Δe_d and Δe_q)

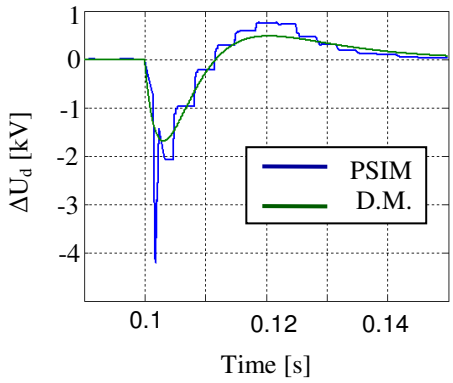

Figure 5-34 Comparison between the waveforms of the measure of the voltage on the load ΔU_{d_f} of the ac/dc converter between PSIM (blue line) and Dynamic (green line) Models after a step function applied to the busbar voltage (Δe_d and Δe_q) and to the circulating current reference

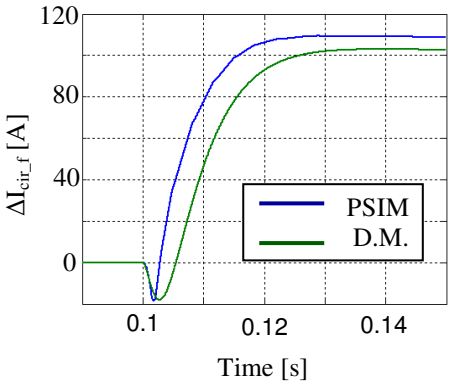

Figure 5-35 Comparison between the waveforms of the measure of the circulating current ΔI_{cir} of the ac/dc converter between PSIM (blue line) and Dynamic (green line) Models after two several step functions applied at the sime time to the busbar voltage (Δe_d and Δe_q) and to the circulating current reference

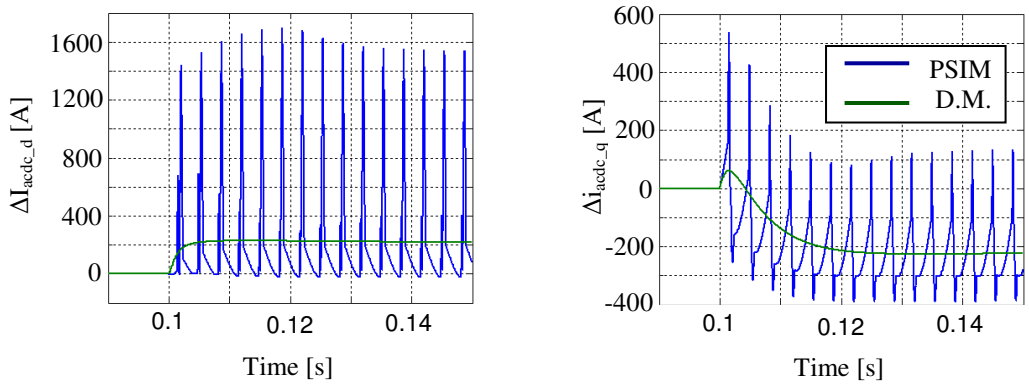

Figure 5-36 Comparison between the waveforms of the ac/dc converter currents at small signals (Δi_{acdc_d} and Δi_{acdc_q}) between PSIM (blue line) and Dynamic (green line) Models after two several step functions applied at the sime time to the busbar voltage (Δe_d and Δe_q) and to the circulating current reference

5.7 The state space matrix of the Dynamic Model of the SSPS

The state space matrix consisting of the union of the three subsystems (Tuned Filters, TCR, ac/dc converter base unit) at small signal analysis is given by the union of the matrixes calculated in the previous sections:

$$\begin{bmatrix}\Delta\dot{x}_{TUN\_FIL}\\ \Delta\dot{x}_{TCR}\\ \Delta\dot{x}_{CONV}\end{bmatrix}=\begin{bmatrix}A_{TUN\_FIL} & 0 & 0\\ 0 & A_{TCR} & B_{i\_TCR}\cdot C_{CONV}\\ 0 & 0 & A_{CONV}\end{bmatrix}\cdot\begin{bmatrix}\Delta x_{TUN\_FIL}\\ \Delta x_{TCR}\\ \Delta x_{CONV}\end{bmatrix}+\begin{bmatrix}B_{e\_TUN\_FIL}\\ B_{e\_TCR}\\ B_{e\_CONV}\end{bmatrix}\cdot\begin{bmatrix}e_d\\ e_q\end{bmatrix}+\begin{bmatrix}0 & 0 & 0\\ 0 & 0 & 0\\ 0 & 0 & B_{i\_CONV}\end{bmatrix}\cdot\begin{bmatrix}0\\ 0\\ inp_{CONV}\end{bmatrix} \quad \text{(eq. 5-144)}$$

$$\begin{bmatrix}\Delta i_{Zd}\\ \Delta i_{Zq}\end{bmatrix}=\begin{bmatrix}C_{TUN\_FIL} & C_{TCR} & C_{CONV}\end{bmatrix}\cdot\begin{bmatrix}\Delta x_{TUN\_FIL}\\ \Delta x_{TCR}\\ \Delta x_{CONV}\end{bmatrix}$$

where $x_{...}$ is the vector of the state variables and $inp_{...}$ is the vector of the input ones indicated for each subsystem by a different subscripts:

- "TUN_FIL" means the Tuned Filter subsystem,
- "TCR" means the TCR subsystem
- "CONV" indicates one of the possible operating modes of the ac/dc converter base unit: 12 pulses or 6 pulses or circulating modes

e_d and e_q are the voltage bus bar, and i_{Zd} and i_{Zq} are the current provided from the grid given in dq component and it is the sum of the current of all the subsystem:

$\Delta i_{Zd}=\Delta i_{TUN\_FILd}+\Delta i_{TCRd}+\Delta i_{CONVd}$

$\Delta i_{Zq}=\Delta i_{TUN\_FILq}+\Delta i_{TCRq}+\Delta i_{CONVq}$

The matrix product $B_{i\_TCR}\cdot C_{CONV}$ considers that the dq current of the ac/dc converter are the inputs of the TCR system.

The following matrixes have been defined to make easier the explanation:

$$A_d=\begin{bmatrix}A_{TUN\_FIL} & 0 & 0\\ 0 & A_{TCR} & B_{i\_TCR}\cdot C_{CONV}\\ 0 & 0 & A_{CONV}\end{bmatrix}$$

$$B_e=\begin{bmatrix}B_{e\_TUN\_FIL}\\ B_{e\_TCR}\\ B_{e\_CONV}\end{bmatrix} \quad \text{(eq. 5-145)}$$

$$C=\begin{bmatrix}C_{TUN\_FIL} & C_{TCR} & C_{CONV}\end{bmatrix}$$

The matrix related to the inputs reference has been reduced in order to delete the zeros:

$$\begin{bmatrix}0 & 0 & 0\\ 0 & 0 & 0\\ 0 & 0 & B_{i\_CONV}\end{bmatrix}\cdot\begin{bmatrix}0\\ 0\\ inp_{CONV}\end{bmatrix}\Rightarrow\begin{bmatrix}0\\ 0\\ B_{i\_CONV}\end{bmatrix}\cdot inp_{i\_CONV}=B_{inp}\cdot inp_{i\_CONV} \quad \text{(eq. 5-146)}$$

The new matrix considering the previous definitions becomes:

$$\begin{bmatrix}\Delta\dot{x}_{TUN\_FIL}\\ \Delta\dot{x}_{TCR}\\ \Delta\dot{x}_{CONV}\end{bmatrix}=A_d\cdot\begin{bmatrix}\Delta x_{TUN\_FIL}\\ \Delta x_{TCR}\\ \Delta x_{CONV}\end{bmatrix}+B_e\cdot\begin{bmatrix}\Delta e_d\\ \Delta e_q\end{bmatrix}+B_{inp}\cdot\Delta inp_{CONV} \quad \text{(eq. 5-147)}$$

$$\begin{bmatrix}\Delta i_{Zd}\\ \Delta i_{Zq}\end{bmatrix}=C\cdot\begin{bmatrix}\Delta x_{TUN\_FIL}\\ \Delta x_{TCR}\\ \Delta x_{CONV}\end{bmatrix}$$

All the subsystems are coupled each other by the short circuit impedance Z of the grid and the related equations in the dq frame are:

$$\begin{aligned}e_{Sd}-e_d+\omega\cdot L_Z\cdot i_{Zq}-R_Z\cdot i_{Zd}-L_Z\cdot\frac{di_{Zd}}{dt}=0\\ e_{Sq}-e_q-\omega\cdot L_Z\cdot i_{Zd}-R_Z\cdot i_{Zq}-L_Z\cdot\frac{di_{Zq}}{dt}=0\end{aligned} \quad \text{(eq. 5-148)}$$

Where e_{Sd} and e_{Sq} are the d-q components for the source voltage of the grid, R_Z and L_Z are the resistance and the inductance of the short circuit impedance respectively.

From equation at the small signal analysis the d-q component of the busbar voltage e_d and e_q result:

$$\begin{bmatrix} \Delta e_d \\ \Delta e_q \end{bmatrix} = \begin{bmatrix} -R_Z & \omega \cdot L_Z \\ -\omega \cdot L_Z & -R_Z \end{bmatrix} \cdot \begin{bmatrix} \Delta i_{Zd} \\ \Delta i_{Zq} \end{bmatrix} + \begin{bmatrix} -L_Z & 0 \\ 0 & -L_Z \end{bmatrix} \cdot \begin{bmatrix} \frac{d(\Delta i_{Zd})}{dt} \\ \frac{d(\Delta i_{Zq})}{dt} \end{bmatrix} + \begin{bmatrix} \Delta e_{Sd} \\ \Delta e_{Sq} \end{bmatrix} \quad \text{(eq. 5-149)}$$

And the matrix and the matrix R_M and L_M are defined:

$$R_M = \begin{bmatrix} -R_Z & \omega \cdot L_Z \\ -\omega \cdot L_Z & -R_Z \end{bmatrix}$$
$$L_M = \begin{bmatrix} -L_Z & 0 \\ 0 & -L_Z \end{bmatrix} \quad \text{(eq. 5-150)}$$

The state space matrix of the Dynamic Model of the whole Simplified Power Supply System results:

$$\begin{bmatrix} \Delta \dot{x}_{TUN\_FIL} \\ \Delta \dot{x}_{TCR} \\ \Delta \dot{x}_{CONV} \end{bmatrix} = A_{SPSS} \cdot \begin{bmatrix} \Delta x_{TUN\_FIL} \\ \Delta x_{TCR} \\ \Delta x_{CONV} \end{bmatrix} + B_{SPSS} \cdot \begin{bmatrix} \Delta e_{Sd} \\ \Delta e_{Sq} \\ \Delta inp_{CONV} \end{bmatrix} \quad \text{(eq. 5-151)}$$

$$\begin{bmatrix} \Delta i_{TUN\_FIL} \\ \Delta i_{TCR} \\ \Delta i_{CONV} \end{bmatrix} = C_{SPSS} \cdot \begin{bmatrix} \Delta x_{TUN\_FIL} \\ \Delta x_{TCR} \\ \Delta x_{CONV} \end{bmatrix}$$

Where the state matrix A_{SPSS} results:

$$A_{SPSS} = \left[I - B_e \cdot L_M \cdot C \right]^{-1} \cdot \left[A_d + B_e \cdot R_M \cdot C \right] \quad \text{(eq. 5-152)}$$

where I is the Identity Matrix.

The input matrix B_{SPSS} is:

$$B_{SPSS} = \left[I - B_e \cdot L_M \cdot C \right]^{-1} \cdot \left[B_e \quad B_{inp} \right] \quad \text{(eq. 5-153)}$$

The output matrix C_{SPSS} is built in order to observe the currents of the subsystems:

$$C_{SPSS} = \begin{bmatrix} C_{TUN\_FIL} & 0 & 0 \\ 0 & C_{TCR} & 0 \\ 0 & 0 & C_{out} \end{bmatrix} \quad \text{(eq. 5-154)}$$

Naturally other variables may be observed beyond the currents of the subsystems, adding some rows to the matrix C_{SPSS} and if necessary adding the feed-forward matrix.

The following figures show a comparison between the simulation results of the Dynamic Model of the SPSS with the ac/dc converter in 6 pulses operating mode run in Matlab simulink and of the PSIM equivalent model at the equilibrium point with the source voltage = 66 kV, output voltage of the converter U_d = 20 kV and applying a step function of 4.5 kV (about 5 % of U_{d0}) to the voltage reference of the ac/dc converter.

The figures from Figure 5-37 to Figure 5-41 show the following waveforms both for Dynamic and PSIM models: the dc output voltage ΔU_{d_mean} (i.e. downstream of the filtering block of the mean value), the currents in dq frame of ac/dc conversion, Tuned Filters and TCR subsystems, and finally the busbar voltages Δe_d and Δe_q. All the figures represent the variation from the equilibrium point.

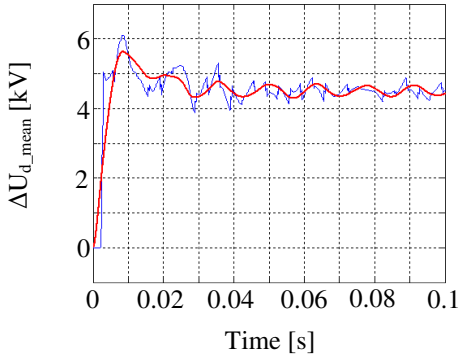

Figure 5-37 Waveforms of the measurement ΔU_{d_mean} of dc voltage on the load both for Dynamic (red line) and PSIM models (blue line) in consequence of a step function of 4.5 kV (about 5 % of U_{d0}) to the voltage reference of the ac/dc converter

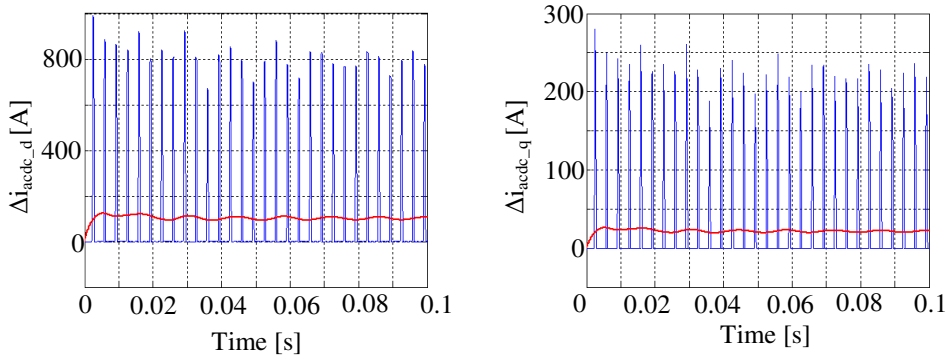

Figure 5-38 Waveforms of the d and q components of the ac/dc converter current (Δi_{acdc_d} and Δi_{acdc_q}) both for Dynamic (red line) and PSIM models (blue line) in consequence of a step function of 4.5 kV (about 5 % of U_{d0}) to the voltage reference of the ac/dc converter

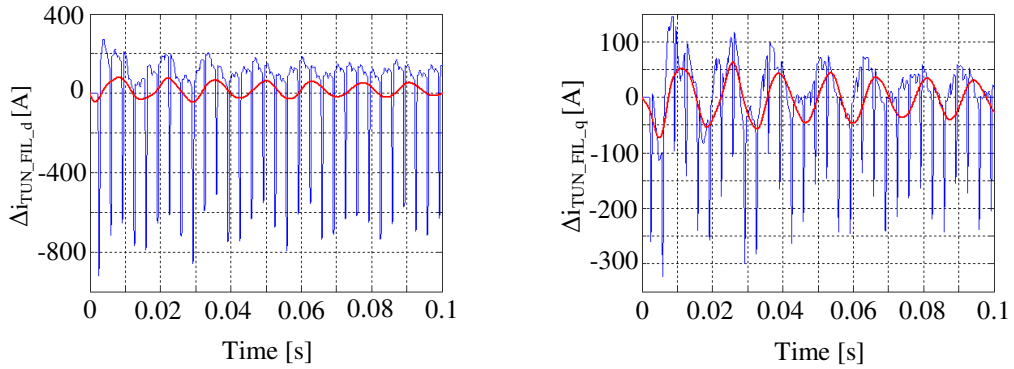

Figure 5-39 Waveforms of the d and q components of the Tuned Filters ($\Delta i_{TUN\_FIL\_d}$ and $\Delta i_{TUN\_FIL\_q}$) both for Dynamic (red line) and PSIM models (blue line) in consequence of a step function of 4.5 kV (about 5 % of U_{d0}) to the voltage reference of the ac/dc converter

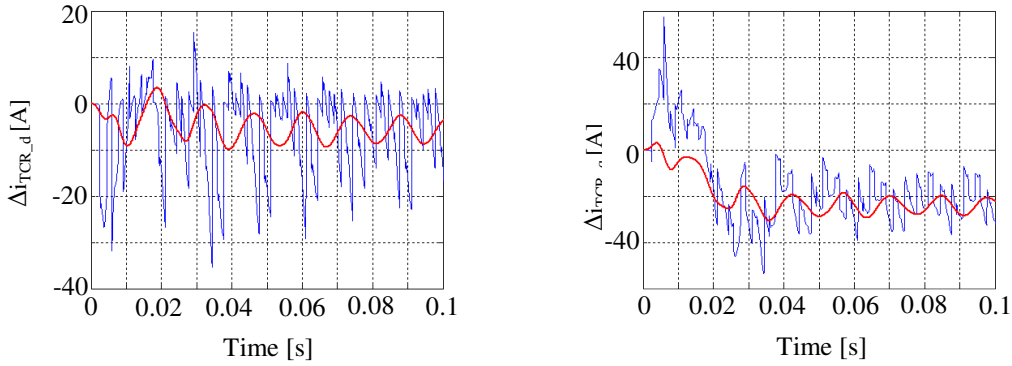

Figure 5-40 Waveforms of the d and q components of the TCR subsystem (Δi_{TCR_d} and Δi_{TCR_q}) both for Dynamic (red line) and PSIM models (blue line) in consequence of a step function of 4.5 kV (about 5 % of U_{d0}) to the voltage reference of the ac/dc converter

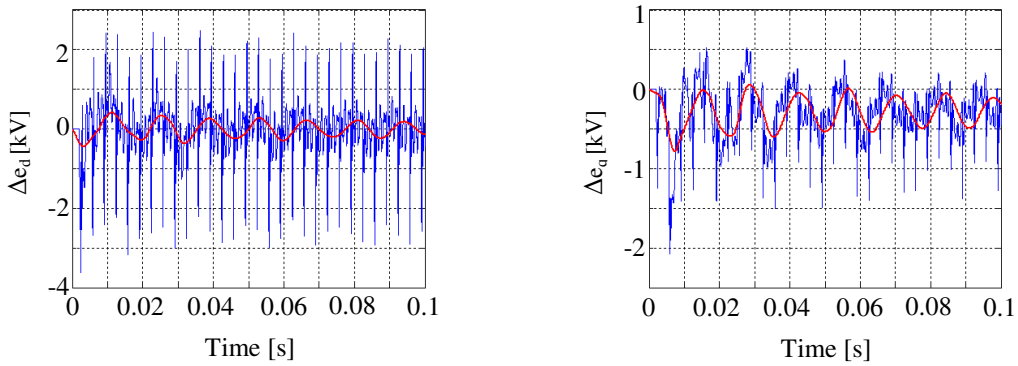

Figure 5-41 Waveforms of the busbar voltage Δe_d and Δe_q both for Dynamic (red line) and PSIM models (blue line) in consequence of a step function of 4.5 kV (about 5 % of U_{d0}) to the voltage reference of the ac/dc converter

The figure shows a good agreement between the waveforms achieved by the Dynamic Model and the PSIM one. The high frequency harmonics in the waveforms obtained by PSIM model are due to the switching frequency, which is not considered by the Dynamic Model.

Considering the analysis carried out in the previous model, the Dynamic Model may be considered accurate for frequency range lower than 50 Hz. This limit is principally given from the TCR model and to the control system where the FFT a 50 Hz has been used, while the ac/dc conversion system model shows a good accuracy up to a frequency of about 100 Hz. Therefore in the frequency range between 50 and 100 Hz the system might be not so accurate, but anyway it may give some information about the stability.

5.8 The stability analysis of the Dynamic Model of the SPSS

The stability analysis of the Dynamic Model of the SSPS has been carried out by the calculation of the eigenvalues of the state matrix A_{SPSS}. The system is stable if the real part of the eigenvalues is less than zero [6]-[8].

The stability analysis of SSPS has been studied considering all the three operating modes of the ac/dc converter for different dc voltage and current of the load. Below just the stability analysis of the Dynamic Model of the SPSS with the ac/dc converter base unit in 6 pulses operation has been illustrated in detail, because the other cases are similar.

All the operating points (up to either the ac/dc converter of TCR controls saturate) have been investigated also for not-usual operating conditions of ITER, in order to validate the Dynamic Model; therefore the instable conditions found in this analysis don't mean that the ITER power supply system is instable too.
The parameters of the control systems have been set:

- The PLL parameters (same values for TCR and ac/dc converter): $k_{p\_PLL}= 2\cdot\pi\cdot650$, $T_{i\_PLL}= 1/(2\cdot\pi\cdot50)$
- The voltage PI controller of the ac/dc converter: $k_{p\_V} = 0$ and $k_{i\_V} = 1.06\cdot10^{-3}$

The Figure 5-42 and Figure 5-43 show the damping ratio ζ and the resonance frequency f_n of the eigenvalues λ of the state matrix A_{SPSS} as function of the dc load current I_{Load} and at the fixed output dc voltage U_d equal to 20 kV, where:

- The damping ratio ζ= -(real part λ) / $\sqrt{}$((real part λ)^2+ (imaginary part λ)^2)
- The resonance frequency f_r (Hz) =(imaginary part λ) / (2π)

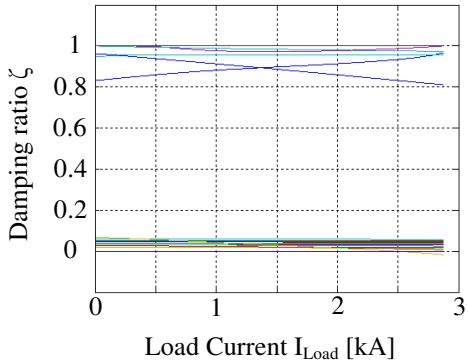

Figure 5-42 The damping ratio ζ of the eigenvalues λ of the state matrix A_{SPSS} versus the load current I_{Load}

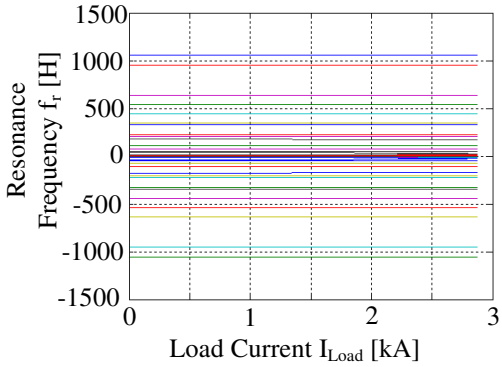

Figure 5-43 The resonance frequency f_r of the eigenvalues λ of the state matrix A_{SPSS} versus the load current I_{Load}

The system is stable when the damping ratio ζ is higher than zero. The Figure 5-44 shows a zoom of the Figure 5-42 near the point where the damping ratio of some eigenvalues becomes negative and consequently the system is instable.

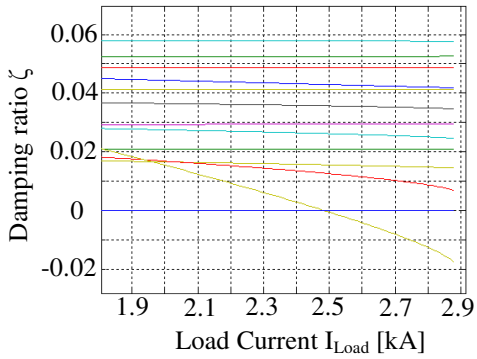

Figure 5-44 Zoom of the damping ratio ζ of the eigenvalues λ of the state matrix A_{SPSS} versus the load current I_{Load}

From the Figure 5-44 it can be noted that there are two lines with damping ratio $\zeta \leq 0$. The blue line is related to four eigenvalues (the four lines are superimposed) of the TCR subsystem equal to i314 and they have damping ratio equal to 0. As explained in the paragraph 5.5.1.1 this mode has been damped and it doesn't appear in the currents of the TCR, but is limited to some auxiliary states, which are not relevant for the stability of the system and it is neglected.
The yellow line cross the axis of the dc load current I_{Load} at about 2490 A and the value of the eigenvalue at this point is 0.136 ± i457 where the resonance frequency is 72.73 Hz. Therefore, by the eigenvalue analysis of the state matrix of the Dynamic Model of the SPSS, the system should be instable for dc load current higher than 2490 A. The verification of the result obtained by the Dynamic Model has been carried out by the PSIM one and the simulation results are shown in the Figure 5-45 and Figure 5-46.

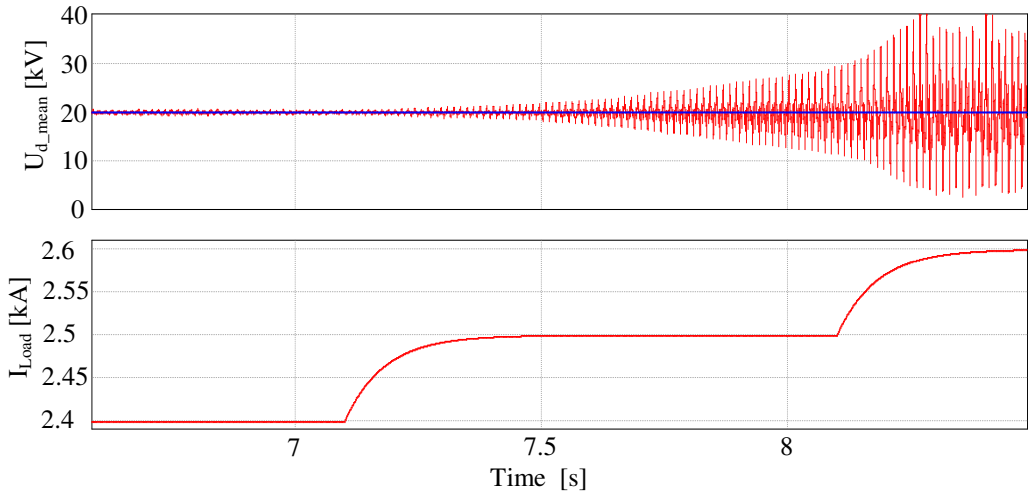

Figure 5-45 The waveforms of the measurements of the dc voltage U_{d_mean} (red line while the blue line ie the voltage reference signal) and load current I_{Load} during the instable condition

(a)

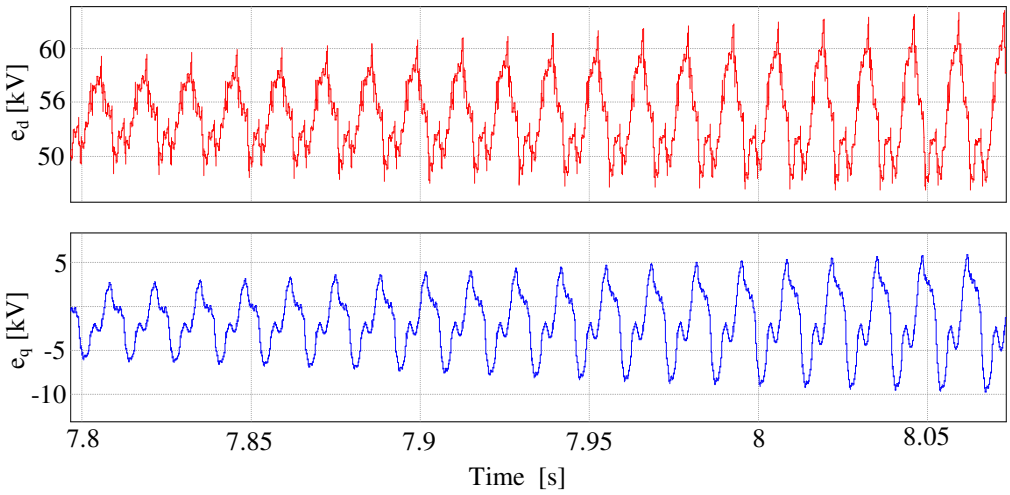

Figure 5-46 Waveforms of the busbar voltages ed and eq during the instable condition

The Figure 5-45 shows the waveforms of the measurements of the dc voltage U_{d_mean} (is the red line, while the blue line is the voltage reference signal) varying slowly the load current I_{Load}. It may be seen that the voltage start to oscillate for a load current higher than 2500 A, this means the system is instable. The frequency of the instability can be roughly calculated by the waveforms of the busbar voltages e_d and e_q (Figure 5-46) and, by considering the cycle of the two consecutive peaks and the lag of the voltage e_q related to e_d, it results a direct sequence of about 76 Hz, which is equivalent to 126 Hz in ac frame. It is highlighted that there is a good agreement between the results obtained by the Dynamic Model and the PSIM model in terms of both the threshold of the load current beyond which the system is instable and of frequency of instability.
In the Table 5-1 is shown the comparison between Dynamic Model and the PSIM model in terms of thresholds of the load current beyond which the system is unstable for 6 pulses operating mode of the ac/dc converter for different values of the output voltages Ud. The Dynamic Model is valid up to a maximum value of the load current, beyond which either TCR or the ac/dc converter controllers are saturated, and this current limit is indicated in the third column of table. In the saturation case a new Dynamic Model of the SPSS should be built.
The Dynamic Model is not so accurate at maximum firing alpha (80 kV) of the ac/dc converter because its transfer function is strongly not linear. Moreover it should be considered that the instability frequency is at 74 Hz which is not so far from the maximum limit of the 100 Hz, beyond which the results of the Dynamic Models are not valid. However a good agreement has been found among the results of Dynamic and PSIM models with the ac/dc converter in 6 pulse mode.

Table 5-1 Comparison between Dynamic Model and the PSIM model in terms of thresholds of the load current beyond which the system is unstable for 6 pulses operating mode of the ac/dc converter

Voltage on the load [kV]	Thresholds of dc load current related to the stability of the SPSS [A]		Threshold of dc load current related to the saturation of the controllers [A]
	Dynamic model	PSIM	PSIM
-80	1190	500	3550
-70	1320	1000	4560
-60	1400	1300	3790
-50	1480	1600	3400

-40	1560	1700	3150
-30	1650	1800	2990
-20	1750	1600	2890
-10	1880	1600	2830
0	2040	1900	2810
10	2240	2500	2830
20	2490	2500	2880
30	2810	2700	2980
40	3140*	2800	3140
50	3400*	3300	3400
60	never	never	3870
70	never	never	4960
80	never	never	2450

* the damping ratio ζ related to the mode is higher than zero but it is near to zero (ζ <0.014)

5.8.1 The participation of the state variables in the instable mode

The analysis of the participation factors allows identifying the states which contribute the instabilities, providing some insight about solving them.

The methods given in the literature deals with the analysis of the participation factors just of the diagonalizable matrix. In the case under study the state matrix A_{SPSS} is not diagonalizable; this is due in particular to the eigenvalues of the second order filter used in the TCR subsystem modelling. Therefore these methods cannot be directly applied to the matrix A_{SPSS}; the attempt to extend them also to matrixes not diagonalizable will be the subject of future works.

Nevertheless in the case under study the subsystem participation factors related to unstable eigenvalue have been roughly calculated the same, considering that the instable eigenvalue is distinct and that the no-distinct eigenvalue are principally due to the states of the TCR subsystem.

The method described in [7] has been used for the calculation of the participation factors in this study, in order to obtain some insights. The participation factor of the j-th variable in the i-th mode is defined as the product of the j-th components of the right v_{ji} and left w_{ij} eigenvectors corresponding to the i-th mode:

$$p_{ji} = v_i^j w_i^j \qquad \text{(eq. 5-155)}$$

Where the eigenvector are normalized such that:

$$w_i^T v_i = 1 \qquad \text{(eq. 5-156)}$$

So the sum of participation factor related to one distinct eigenvalue is equal to 1.

The subsystem participation p_{Si} is the sum of the participation factors (the real part in case of complex conjugate eigenvalues) of the variables that describe a subsystem S in an i-th mode.

$$p_{Si} = \sum_{j \in S} p_{ji} \qquad \text{(eq. 5-157)}$$

The participation factors of the subsystems are:

- p_{TUN_FIL}= 0.9778
- p_{TCR} = 0.0182
- p_{CONV} = 0.0039

From the rough analysis of the subsystem participation factor it yields that the state of the Tuned Filter subsystem more contributes to the instability. This result can be validated by considering the amplification factor A_f of the harmonics defined as:

$$A_f(f) = \frac{I_{Source}}{I_{TCR+CON}} = \left| \frac{Z(f) // Z_{Filt}(f)}{Z(f)} \right| \qquad \text{(eq. 5-158)}$$

where $Z_{Filt}(f)$ is the impedance of the tuned filters and Z(f) is the impedance of the grid at the frequency f (Figure 5-47).

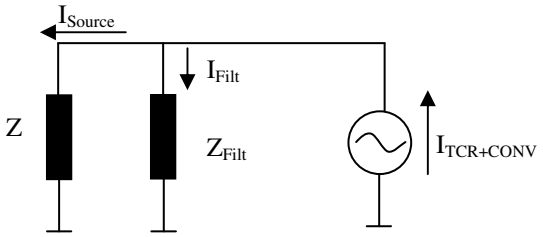

Figure 5-47 Block scheme for the calculation of the Amplification Factor A_f

The amplification factor A_f describes the effect of the injection of a current harmonic of the TCR + ac/dc conversion subsystems ($I_{TCR+CONV}$) into the grid: the higher A_f value is, the higher is the interaction phenomena between the grid and the subsystems at the considered frequency. It can be noted in the Figure 5-48 that the peak value of A_f is just at the frequency of 120 Hz in the ac frame, which is the frequency of the instable mode. It may be hazarded the guess that the main contribution to the unstable mode is given from the state variables of the tuned filters.

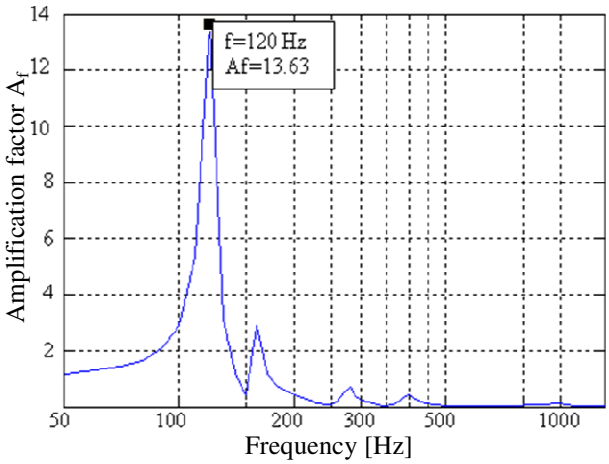

Figure 5-48 Amplification factor A_f of current harmonics among the short circuit impedance of the grid and the Tuned Filters

5.8.2 Example of setting of the parameters of the controller

The advantage of Dynamic Model respect to the program of simulation transient as PSIM is that the effect of the change in any parameters on the system stability can be studied without run the simulations, saving a lot of time. For instance the gains of the PLL have been reduced respect to the previous analysis and they are:

- The PLL parameters (same values for TCR and ac/dc converter): $k_{p\_PLL}= 2\cdot\pi\cdot10$, $T_{i\_PLL}= 1/(2\cdot\pi\cdot0.77)$

Then the eigenvalues analysis (in few seconds) has been carried out; the results show that the frequency of the instable mode is about 66 Hz and in the Table 5-2 are shown the new thresholds of the load current beyond which the SPSS with ac/dc converter in 6 pulses operating mode is unstable and they are verified by PSIM program (hours).

Table 5-2 Comparison between Dynamic Model and the PSIM model in terms of thresholds of the load current beyond which the system is unstable for 6 pulses operating mode of the ac/dc converter

Voltage on the load [kV]	Thresholds of dc load current related to the stability of the SPSS [A]		Threshold of dc load current related to the saturation of the controllers [A]
	Dynamic model	PSIM	PSIM
-80	never	never	3550
-70	never	never	4560
-60	never	never	3790
-50	never	never	3400
-40	never	never	3150
-30	never	never	2990
-20	never	never	2890
-10	never	never	2830
0	never	never	2810
10	2830*	2800	2830
20	2880*	2900	2880
30	2980*	2900	2980
40	3140*	3000	3140
50	3400*	3300	3400
60	3850	3700	3870
70	never	never	4960
80	never	never	2450

* the damping ratio ζ related to the instable mode is higher than zero but it is near to zero (ζ <0.01)

From the results given in the Table 5-2 it can be noted that with low gains of the PLL system is more stable, in particular when the converter operates as inverter.
It is then highlighted that the Dynamic Model is a very effective tool in the assessment of the control system and it may be used also for sensitivity analysis of the eigenvalues respect to the main control parameters.

5.8.3 Verification of the Dynamic Model of SPSS with ac/dc converter opearating in 12 pulses and circulating operating modes.

A verification of the Dynamic Model of the SPSS with the ac/dc converters operating in 12 pulses and circulating mode has been carried out. The following parameters of the control systems have been set:

- The PLL parameters (same values for TCR and ac/dc converter): $k_{p\_PLL}= 2\cdot\pi\cdot650$, $T_{i\_PLL}= 1/(2\cdot\pi\cdot50)$
- The voltage PI controller of the ac/dc converter: $k_{p\_V} = 0$ and $k_{i\_V} = 1.06\cdot10^{-3}$
- The current PI controller of the ac/dc converter: $k_{p\_I} = 1.2\cdot10^{-4}$ and $k_{i\_I}= 2.14\cdot10^{-4}$

In the Table 5-3 is shown the comparison between Dynamic Model and the PSIM model in terms of thresholds of the load current beyond which the system is unstable for 12 pulses operating mode of the ac/dc converter.

Table 5-3 Comparison between the Dynamic Model and PSIM model in terms of thresholds of the load current beyond which the system is unstable for 12 pulses operating mode of the ac/dc converter

Voltage on the load [kV]	Thresholds of dc load current related to the stability of the SPSS [A]		Threshold of dc load current related to the saturation of the controllers [A]
	Dynamic model	PSIM	
-80	1010	600	6010

-70	1180	900	4520
-60	1310	1300	3790
-50	1440	1500	3400
-40	1570	2000	3150
-30	1720	2400	2990
-20	1890	2500	2890
-10	2090	2600	2830
0	2320	2800	2810
10	2580	never	2820
20	2850	never	2870
30	never	never	2970
40	never	never	3130
50	never	never	3380
60	never	never	3820
70	never	never	4840
80	never	3760	3820

In the Table 5-4 and Table 5-5are shown the comparison between Dynamic Model and the PSIM model with the ac/dc converter operating in circulating current mode in terms of the thresholds of the circulating current beyond which the system is unstable with a constant load current I_{Load}=0 A and I_{Load}=840 A.

Table 5-4 Comparison between Dynamic Model and the PSIM model in terms of thresholds of the circulating current beyond which the system is unstable for circulating mode of the ac/dc converter

Voltage on the load [kV]	Thresholds of circulating current related to the stability of the SPSS [A]		Threshold of circulating current related to the saturation of the controllers [A]
	Dynamic model	PSIM	
-80	1160	1000	3020
-70	1570	1900	2280
-60	1710	1700	1900
-50	1690	1600	1700
-40	1570*	1550	1570
-30	never	never	1490
-20	never	never	1440
-10	never	never	1410
0	never	never	1400
10	never	never	1410
20	never	never	1440
30	never	never	1490
40	1570*	never	1570
50	1690	1650	1700
60	1710	1700	1900
70	1570	1700	2280
80	1160	1200	3020

* the damping ratio ζ related to the instable mode is higher than zero but it is near to zero (ζ <0.01)

Table 5-5 Comparison between Dynamic Model and the PSIM model in terms of thresholds of the circulating current beyond which the system is unstable for circulating mode of the ac/dc converter

Voltage on the load [kV]	Thresholds of circulating current related to the stability of the SPSS [A]		Threshold of circulating current related to the saturation of the controllers [A]
	Dynamic model	PSIM	
-80	350	0	2720
-70	840	600	1850

-60	1060	1000	1480
-50	1120	1100	1280
-40	1150	1100	1150
-30	never	never	1070
-20	never	never	1020
-10	never	never	990
0	never	never	980
10	never	never	990
20	never	never	1020
30	never	never	1070
40	never	never	1150
50	never	never	1280
60	1470	1400	1490
70	1480	1400	1880
80	1080	1600	2030

The Dynamic Model with 12 pulses and circulating operating modes of the ac/dc converter are not so accurate at maximum and minimum firing alpha (± 80 kV) of the ac/dc converter because their transfer functions are strongly not linear. A good agreement has been found among the results of Dynamic and PSIM model in circulating operating mode of the ac/dc converter, while in the 12 pulses case the accuracy is lower.

6 Conclusions

Two analytical models have been developed in the first part of PhD thesis allowing the study of the stability of ITER Pulsed Power Electrical Network.

Each one has been developed on a simplified equivalent scheme (called Simplified Power Supply System SPSS) of the ITER power supply system in order to make easier the development of the analytical models.

The Quasi-Static Model has been worked out to evaluate the strength of the ac network supplying the ITER SPSS by sensitivity analysis. The parameters SCR and VSF indicate that the ac system of ITER SPSS is not weak and no critical condition has been found from the static point of view. Moreover it also allows performing further studies identifying other indexes in dependence of the interaction phenomena to be investigated.

The Dynamic model has allowed the study of the dynamic stability based on the approach of the state space formulation at small signal analysis of the SPSS. The Dynamic Model of each subsystem has been described in detail and validated by comparison with the simulation results obtained by a program (PSIM) capable to reproduce the system instantaneous waveforms.
From the frequency analysis, the dynamic model is accurate for frequency range less than 50 Hz, but it may be used to obtain some insight about the system stability also for frequency range up to 100 Hz.

Some unstable operating conditions have been identified, with a frequency of the unstable mode near to 70 Hz in dq frame (120 Hz in ac frame). The cause of this unstable mode has been identified by a rough analysis of the participation factors, and it yields that the unstable mode is due principally to the Tuned Filter subsystem. It has been verified that the peak of the resonance frequency between tuned Filters and the grid impedance is just to 120 Hz.

The Dynamic Model may be a useful tool to set the control parameters; indeed the effect of their variation may be observed without run numerical simulations of the overall system, saving a lot of computation time. An example has been described in this thesis, varying the gains of the PI controller of the PLL. It yields that with lower gain of the PI controller of the PLL, the system is more stable.

This model may be easily implemented with more detail to the whole ITER power supply system and it can be a very useful tool to aid the design and the verification of practicability of different operating scenarios.

References

[1] B. Franken and G. Andersson, "Analysis of HVDC converters connected to weak AC systems", *in IEEE Transactions on Power Systems*, vol. 5, no. 1, pp. 235-242, Feb. 1990.

[2] O.B. Nayak, A.M. Gole, D.G. Chapman and J.B. Davies, "Control sensitivity indices for stability analysis of HVDC systems", IEEE Transactions on Power Delivery, vol. 12, n. 4, pp. 2054-2060, Oct. 1995.

[3] Denis Lee Hau Aik and G. Andersson, "Impact of dynamic system modelling on the power stability of HVDC systems", *in IEEE Transactions on Power Delivery*, vol. 14, no. 4, pp. 1427-1437, Oct 1999

[4] Denis Lee Hau Aik and G. Andersson, "Nonlinear dynamics of HVDC systems", *in IEEE Transactions on Power Delivery*, vol. 14, no. 4, pp. 1417-1426, Oct 1999

[5] *IEEE Guide for Planning DC Links Terminating at AC Locations Having Low Short-Circuit Capacities*, IEEE Standard. 1204-1997

[6] L. Rouco, "Eigenvalue-based methods for analysis and control of power system oscillations," in IEE Colloquium on Power System Dynamics Stabilisation, 23-24 Feb 1998

[7] I.J.Perez-Arriaga, G.C.Verghese and F.C. Schweppe, "Selective Modal Analysis with Applications to Electric Power Systems, PART I: Heuristic Introduction", *in IEEE Transactions on Power Apparatus and Systems*, vol. PAS-101, no. 9, pp. 3117-3125, September 1982.

[8] W.A. Hashlamoun, M.A. Hassouneh and E.H. Abed, "New Results on Modal Participation Factors: Revealing a Previously Unknown Dichotomy", *in IEEE Transactions on Automatic Control*, vol. 54, no. 7, pp. 1439-1449, July 2009.

[9] D. Jovcic, N. Pahalawaththa, M. Zavahir, "Analytical modelling of HVDC-HVAC systems", in IEEE Transactions on Power Delivery, vol. 14, no. 2, pp. 506-511, 1999

[10] D. Jovcic, N. Pahalawaththa, M. Zavahir, "Small signal analysis of HVDC-HVAC interactions", in IEEE Transactions on Power Delivery, vol. 14, no. 2, pp. 525-530, 1999

[11] D. Jovcic, N. Pahalawaththa, M. Zavahir, "Novel current controller design for elimination of dominant oscillatory mode on an HVDC line", *in IEEE Transactions on Power Delivery*, vol. 14, no. 2, pp. 543-548, 1999

[12] Giovanni Martinelli and Augusto Morini, *Lezioni di Teoria unificata delle macchine elettriche rotanti*, SG Editoriali Padova, 1992

[13] F. Blaabjerg, R. Teodorescu, M. Liserre and A. V. Timbus, "Overview of Control and Grid Synchronization for Distributed Power generation Systems" *in IEEE Transaction on Industrial Electronics,* October 2006.

[14] IEEE Special Stability Controls Working Group, "Static VAr compensator models for power flow and dynamic performance simulation", *IEEE Transactions on Power Systems*, vol. 9, n. 1, pp. 229-240, Feb.1994.

[15] A.E. Hammad and M. El-Sadek, "Application of a Thyristor Controlled Var Compensator for Damping Subsynchronous Oscillations in Power Systems", *IEEE Transactions on Power Apparatus and Systems*, vol. PAS-103, n. 1, pp. 198-212, Jan. 1984.

[16] M.R. Iravani and M. Parniani, "Computer analysis of small-signal stability of power systems including network dynamics", *IEE Proceedings- Generation, Transmission and Distribution*, vol.142, n. 6, pp. 613-617, Nov. 1995.

[17] D. Jovcic, N. Pahalawaththa, M. Zavahir and H.A. Hassan, "SVC dynamic analytical model", in *IEEE Transactions on Power Delivery*, vol. 18, n.4, Oct. 2003.

[18] D. Jovcic, G.N. Pillai, “Analytical modeling of TCSC dynamics”, *in IEEE Transactions on Power Delivery*, vol, 20, n. 1, pp.1097-1104, April 2005
[19] P.K. Kalra, “An approach for handling the nonlinearities of HVDC system for stability analysis”, *in IEEE Transactions on Power Electronics,* vol. 5, no. 3, pp. 371 - 377, July 1990.
[20] E. Parrish and E. McVey, “A theoretical model for single-phase silicon-controlled rectifier systems”, *IEEE Transactions on Automatic Contro*l, vol. 12, n. 5, pp. 577-579, 1967.

Study of Active-Front-End design for the Acceleration Grid Power Supply of ITER Neutral Beam Injector

Acronyms

AFE	Active Front-End
AGPS	Accelerator Grid Power Supply
CBPWM	Carrier Based PWM
CC	Current Control
CHB	Cascade H-Bridge
DCG	Direct Current Generator
FC	Flying Capacitor
f_{SW}	switching frequency
IGCT	Integrated Gate-Commutated Thyristor
m	modulation index
NPC	Neutral Point Clamped
PCC	Point of Common Coupling
PLL	Phase Locked Loop
PWM	Pulse Width Modulation
RPC & HF	Reactive Power Compensation & Harmonic Filtering
SAFE	Synchronous AFE
SHEPWM	Selective Harmonic Elimination PWM
TCR	Thyristor Controlled Reactor
V_{dc}	dc link voltage
VSC	Voltage Source Converter
ZSS	Zero Sequence Signal

7 Reference Design of the Accelerator Grid Power Supply System

In the AGPS reference scheme (Figure 7-1) defined in the Annex B to Procurement Arrangement [1], a step down transformer connected to the 66 kV ITER electrical network (see chapter 2) feeds the ac/dc conversion system, which supplies the five Neutral Point Clamped (NPC) inverter systems connected in parallel at the input side. Each one feeds the primary side of a three-phase step-up transformer and the secondary side is connected to a three-phase diode bridge rectifier with a dc filter connected in parallel. The diodes rectifier are connected in series at the output side in order to increase the absolute value of the dc voltage up to the required value (-1 MV for deuterium, -870 kV for Hydrogen). The NPC inverter, the step-up transformer, the diode bridge rectifier and dc filter of each acceleration stage form the Direct Current Generator (DCG). A Transmission Line connects the diode rectifiers to the NBI grids.

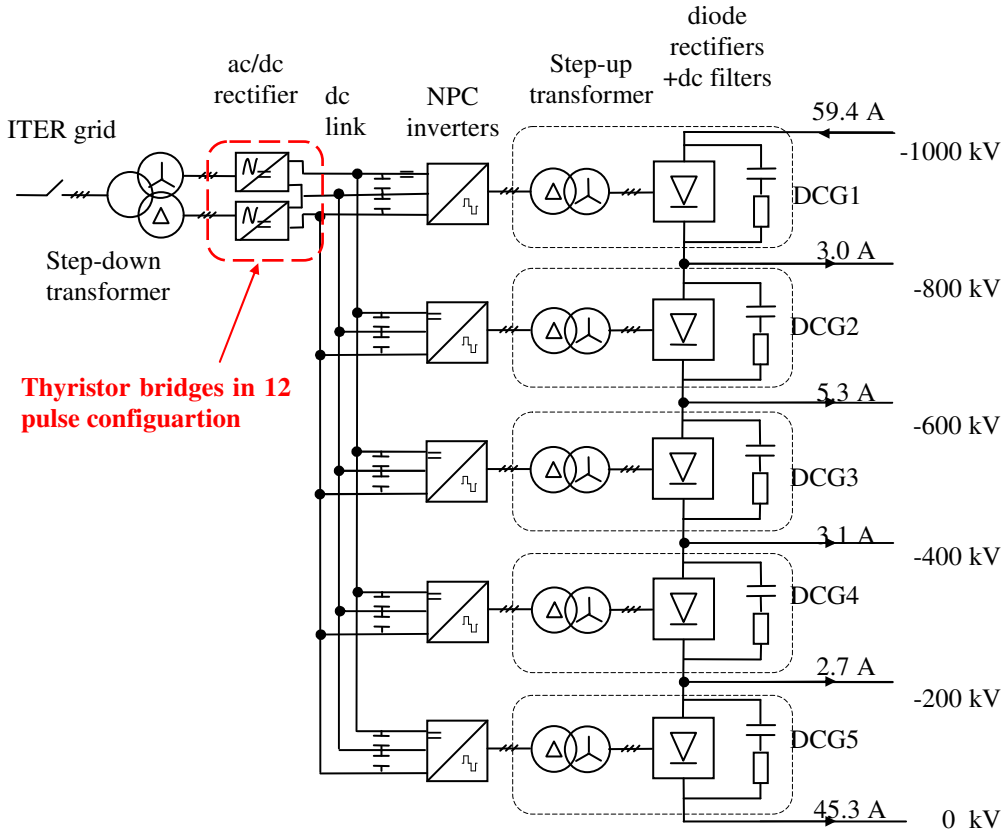

Figure 7-1 - AGPS reference scheme (the current and voltage values are referred to Deuterium operation) with MAMuG configuration.

The ac/dc conversion system has to produce a nominal dc-link voltage (V_{dc}) on the capacitor bank equal to 6.5 kV, which supplies the five NPC inverters, and has to supply a nominal power of about 54 MW.
When the ac/dc rectifier system is required to supply the nominal voltage value of 6.5 kV, it shall assure that value stay within the required accuracy of ± 6% in steady state conditions, also for example when the ITER grid voltage varies inside the tolerance range (62kV-72kV). In transient conditions, as for example after the switch-

off of the dc/ac inverter system caused by the breakdown protection, the dc-link voltage shall remains inside the range 6.5 kV ± 10%.
The ac/dc conversion system shall be arranged to assure at least a 12-pulse operation and it shall be compatible with the NPC inverter scheme, i.e. it shall provide a central point at the output for the connection with the neutral point of the inverter. Therefore, the ac/dc conversion system shall be composed al least of two bridges connected at the output.

7.1 Calculation of the main design parameters

In the technical note TW6-THHN-NBD1 [2] the main design parameters of the ac/dc conversion system have been calculated and they are quoted below.

7.1.1 Step down transformer and ac/dc conversion system

The maximum no-load voltage at the output of the ac/dc conversion system $E_{D0,ac/dc}$ is related to the no-load secondary winding voltage of the step-down transformers $V_{20,SD}$ by means of the following equation:

$$E_{D0,ac/dc}=1.35\cdot V_{20,SD} \qquad \text{(eq. 7-1)}$$

When the system is operating at full voltage and current, the ac/dc conversion system is supplying the output voltage $E_{D,ac/dc}$, which corresponds to half of the dc-link voltage value V_{dc}. It is:

$$E_{D0,ac/dc}=\frac{E_{D,ac/dc}}{1-\frac{V_{XSC}}{2}-V_{RSC}}=\frac{V_{dc}/2}{1-\frac{V_{XSC}}{2}-V_{RSC}} \qquad \text{(eq. 7-2)}$$

where V_{XSC} is the per-unit inductive short-circuit voltage of the step-down transformer and V_{RSC} the resistive one, which is usually negligible. In the following, V_{XSC} has been assumed equal to 10%.
From eq. 7-1 and 7-2, the no-load secondary winding voltage of the step-down transformers $V_{20,SD}$ can be obtained:

$$V_{20,SD}=\frac{V_{dc}/2}{1.35\cdot\left(1-\frac{V_{XSC}}{2}\right)-(1-\Delta v)} \qquad \text{(eq. 7-3)}$$

where the term (1-Δv) accounts for the rated minimum voltage of the distribution grid with respect to the nominal value.
With a maximum dc-link voltage V_{dc} of 6500 V and Δv=6%, we obtain:

$$V_{20,SD}=\frac{6500/2}{1.35\cdot\left(1-\frac{0.1}{2}\right)-(1-0.06)}=2696\cong 2700[V] \qquad \text{(eq. 7-4)}$$

The ac/dc conversion system nominal output current is:

$$I_D=\frac{P_{out}}{V_{dc}} \qquad \text{(eq. 7-5)}$$

where P_{out} is the output power of the ac/dc conversion system (52 MW for Deuterium operation). Keeping a 10% margin to take into account the power losses, it results:

$$I_D = \frac{1.1 \cdot 52 \cdot 10^6}{6500} = 8.8[kA] \quad \text{(eq. 7-6)}$$

Assuming a three winding configuration, the r.m.s. nominal line current for each secondary winding of each step-down transformer is given by:

$$I_{2,SD} = I_{D0} \cdot \sqrt{\frac{2}{3}} \cdot \frac{1}{2} = 8800 \cdot 0.816 \cdot 0.5 = 3591[A] \quad \text{(eq. 7-7)}$$

The secondary winding equivalent short-circuit impedance of each step-down transformer is:

$$Z_{SC,SD} = 0.1 \cdot \frac{V_{20,SD}}{\sqrt{3} \cdot I_{2,SD}} = 0.1 \cdot \frac{2700}{\sqrt{3} \cdot 3591} = 0.043[\Omega] \quad \text{(eq. 7-8)}$$

The rated power for each secondary winding of the step-down transformers is:

$$P_{SD} = \sqrt{3} \cdot V_{20,SD} \cdot I_{2,SD} = \sqrt{3} \cdot 2700 \cdot 3591 = 16.8[MVA] \quad \text{(eq. 7-9)}$$

The total rated power of each step-down transformer shall be therefore of 33.6 MVA.

7.1.2 Rating of the dc link capacitor banks

The NPC inverter is fed by a dc link with a common central point and two capacitor banks connected between this central point and the positive and negative terminals respectively. The output terminals of the ac/dc conversion system have to be connected to a choke inductance, in order to guarantee the limitation of the current derivative in case of short-circuit on the dc link. Actually, the choke inductance value depends also on the dc link capacitance value, and the choice of both parameters must be performed considering other several aspects, such as:

- The over-voltage at the load disconnection
- The dc link voltage ripple
- The voltage level at which the current flow in the converter becomes discontinuous

Overall dynamic response expected from the converter here, only a rough estimation of the capacitance needed is performed, leaving the task of refining and verifying the value to the simulations. The target for the design presented here is to limit the over-voltage at load disconnection (i.e. beam off) to less than 10% of the nominal dc link voltage, i.e. to less than 650V. At load disconnection, the firing signals to the thyristors of the ac/dc conversion system are removed; the thyristors, which were conducting before the removal of the firing signals, keep conducting until the current reaches zero. Therefore, the overvoltage on the dc link is determined by the amount of charge flowing into the capacitor in this time interval, or, from another point of view, by the energy stored in the inductances of the system (choke inductance and transformer inductance) plus the energy coming from the grid.

Using a simplified approach and neglecting the energy coming from the grid, it is possible to show that the over-voltage at load disconnection is roughly estimated as follows:

$$\Delta V = I_{d,CONV} \cdot \sqrt{\frac{L_{OFF}}{C}} \quad \text{(eq. 7-10)}$$

where $I_{d,CONV}$ is the converter nominal current (8000A), L_{OFF} the total inductance seen at the ac connection of the ac/dc converter (which can be shown to be four times the phase inductance of each transformer), C the total dc link capacitance.

Therefore:

$$C = \frac{I^2{}_{d,CONV}}{\Delta V^2} \cdot L_{OFF} = \frac{8000^2}{650^2} \cdot 276 \cdot 10^{-6} = 42[mF] \qquad \text{(eq. 7-11)}$$

which corresponds to about 8.4 mF per inverter at 6500V. The calculation does not include choke inductances placed on the dc side of the converter. Should a choke inductance be necessary, the capacitance value has to be increased; we can round up the calculated value to 10 mF, obtaining a total dc link capacitance of 50 mF to account for this possibility. This value will be used as a starting point in the models to simulate more precisely the dc link over-voltage obtained during the beam off.

8 Active Front-End ac/dc Converter and respective control scheme for NBI AGPS

8.1 Choice of the topology of AFE Converter for AGPS

The ac/dc converter AGPS has to provide a rating power of 54.7 MW, therefore it needs of high power converters. In literature several converter topologies of high power applications are presented and they may be classified in direct e indirect [3]-[4]. The former usually connects the load directly to the source through power semiconductors, for example cycloconverter and matrix converter. The latter transfers the power into two stage, rectification and inversion, and is usually linked by an energy storage component, for example Current Source Converter, High Power two-level or Multilevel Voltage Source Converter (VSC). The use of Multilevel VSCs seems a good solution for the AGPS ac/dc conversion section, because they may operate as an active rectifier, with the advantages of the control of the dc link voltage and power factor; moreover using the Pulse Width Modulation (PWM) with a closed-loop current control, the total harmonic distortion of the input currents is lower in a multilevel than in a two level converter. The three level Neutral-Point Clamped (NPC), the four-level Flying Capacitor (FC) and the Cascade H-Bridge (CHB) converters are the most established and commercialized. A short description of these topologies is given below:

- The three level NPC converter is of particular interest for the medium voltage application, since all semiconductors operate at a commutation voltage of half the dc-link voltage. Respect to a two level VSC with two device per switch position and operating at the same dc link voltage, the NPC VSC has two additional diodes per phase leg, connected at the midpoint of the series capacitors, called Neutral Point (Figure 8-1). This enables the three level characteristic of the topology: $\pm V_{dc}/2$ and 0.

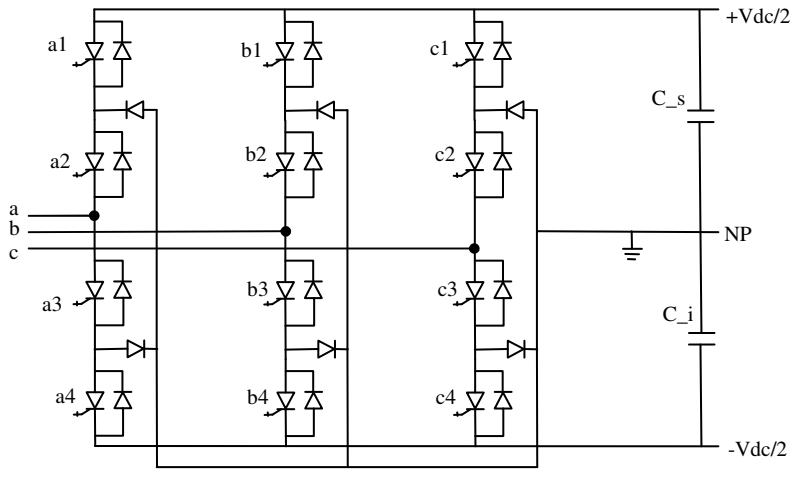

Figure 8-1 The topology of the three-level NPC converter.

With the IGCT semiconductors, this converter may supply a maximum power of 10 MVA. The main structural drawback of the 3L NPC VSC is the unequal loss distribution, concentrated especially in the internal switches. To improve the loss distribution, active switches may be placed in parallel to the clamping

diodes. The corresponding circuit configuration is called three level Active NPC VSC (Figure 8-2).

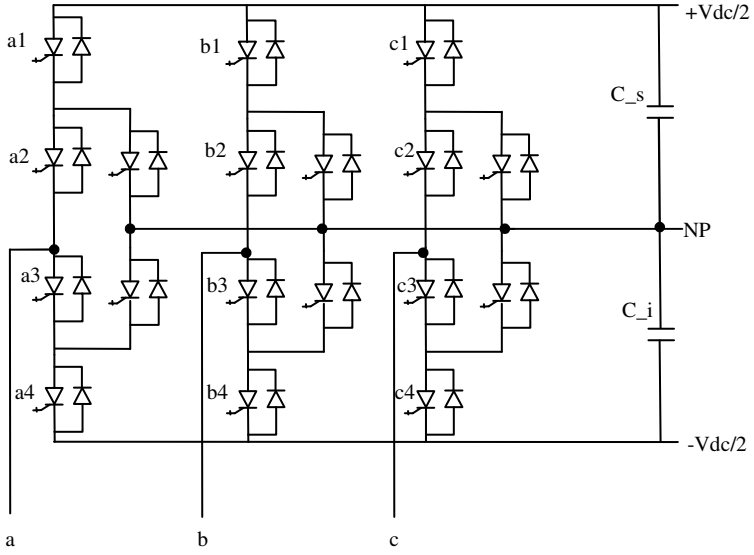

Figure 8-2 The topology of the three-level ANPC converter.

The more equal semiconductor junction temperature distribution enables a substantial increase of the power, until 16 MVA [5].

- The four-level FC converter consist of three multicells (Figure 8-3), one for each phase, which give at the output a three phase voltage and at the input they are connected in parallel to the same dc link (Figure 8-4).

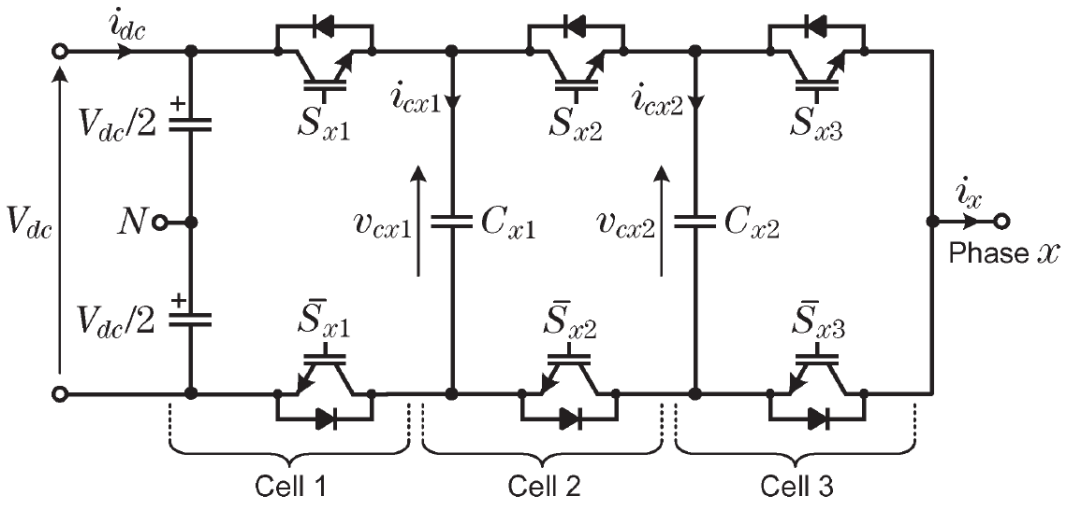

Figure 8-3 Multicell layout of one phase leg of 4L FC-VSC [3].

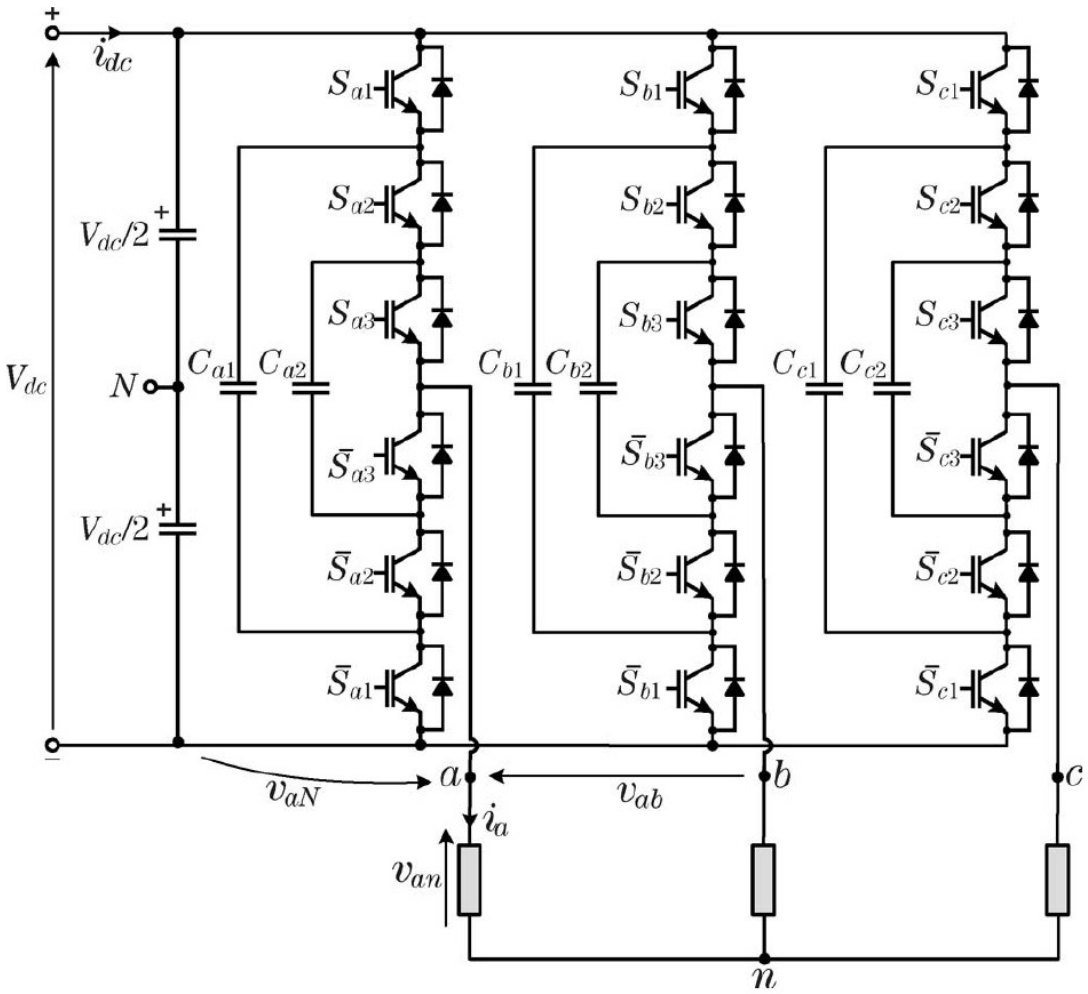

Figure 8-4 Layout of 4L FC-VSC [3].

One converter phase leg has a series connection of three commutation cell. The nominal voltage of the Flying Capacitors C_{x1} and C_{x2} are 2/3 V_{dc} and 1/3 V_{dc} respectively. With this topology four voltage level are achieve: $\pm V_{dc}/2$ and $\pm V_{dc}/6$. The four-level FC converter becomes cheaper than 3L NPC VSC for switching frequency f_{SW}>1500 Hz [4].

- The Cascaded H-Bridge (CHB) multilevel converter is composed of the series of H-bridge power cells. Each cell includes a single–phase 3L H-bridge inverter, a capacitive dc-link, a rectifier (non-regenerative or regenerative for AFE applications) and an independent or isolated voltage source provided by transformer secondaries or batteries.
  The level number achievable with k cells is equal to 2k+1. Hence with high voltage ratings a lot cells have to be utilized, increasing the level number and the output voltage quality.

Regard to the ac/dc section of AGPS, the switching frequency of the AFE rectifier necessary to comply with the technical specifications is less than 1500 Hz (see the next section); the installation of the step up transformers on the ac side is necessary, because of the very high voltage (1 MV) of the beam accelerator, and only 3 level square wave output voltage at 150 Hz is required. For these reasons the three-level NPC converter topology has been considered the most suitable design solution both for the rectifier and the inverter stages of the AGPS system based on AFE approach with a nominal dc link voltage of 6500 V.

8.2 Control scheme of 3L NPC converter

In this section a control scheme for active front-end three-level NPC converter is described. It has to be able to perform two important duties [6]-[7]:

- the first one is to keep the dc bus voltage constant, balanced and equal to a defined reference value;
- the second one is to force the power distribution system current to be sinusoidal and in phase with the respective phase-to-neutral voltage, independently of the load connected to the dc link.

The block diagram of the control scheme is shown in Figure 8-5. There are different blocks and each one has a given function:

- the current controller forces the line current to be sinusoidal and with a unity power factor;
- the reference angle detector needs to obtain a reference for the synchronous frame transformation;
- the total voltage controller keep the dc link voltage constant and equal to a given reference value;
- the differential voltage controller maintains the voltage across each capacitor constant and balanced; this goal is achieved by changing the amplitude of each triangular carrier waveforms;
- the filter reduces the current harmonics injected in the grid supply.

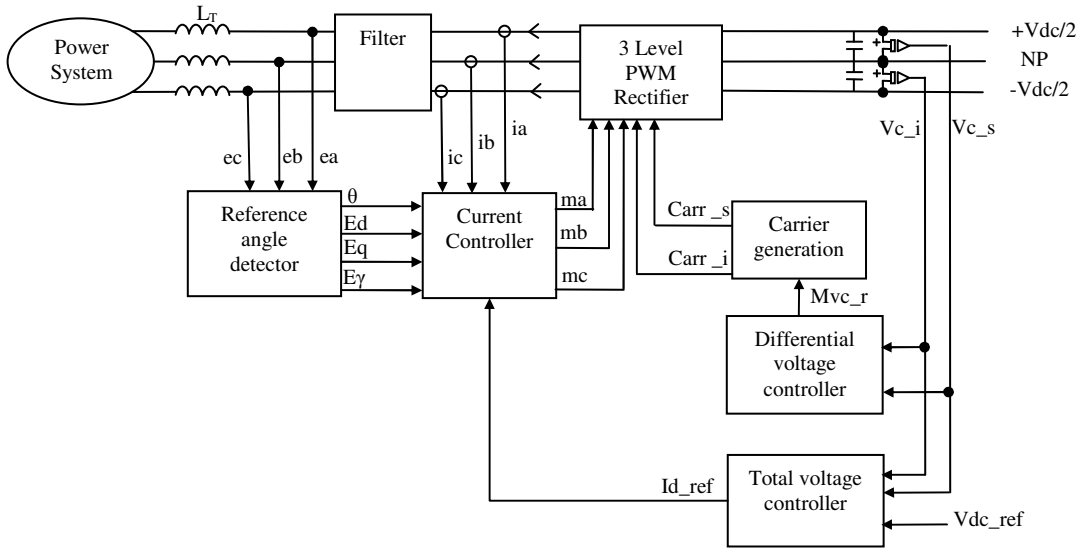

Figure 8-5 The block diagram of the three-level converter control.

In the following sections a more complete description is given for each block.

8.3 Current controller of PWM VSC

The main task of the Current Control (CC) in a PWM converter is to force the currents to follow the reference signals. It compares the reference signals with the measured instantaneous values of the phase currents and it generates the switching states for the converter power devices, so as to reduce the current error. Several CC techniques are present in the industrial applications. They may be classified in two main groups: linear (PI stationary and synchronous, state feedback and predictive with constant switching frequency) or non linear controllers (hysteresis, Delta Modulation, on-line optimized control, neural networks and fuzzy logic) [8]-[10].

For the ac/dc converter of AGPS a linear controller is proposed, because in contrast to the non linear controller they can be used with the open loop modulator (sinusoidal PWM, space vector modulator, etc…), which present the advantage of constant switching frequency f_{SW}, very important for High Power ac/dc VSC to guarantee safe operation of semiconductor power switches.
For this study a synchronous PI controller has been chosen and is illustrated below, but before the mathematical model of the three-level VSC is introduced [11]. For sake of simplicity, the dc link capacitors have been replaced by constant voltage sources and only the fundamental components of voltage and current are considered. Initially the transformer short circuit inductance L_{SC} is neglected. The power circuit of the three-phase Voltage Sources Converter is shown in Figure 8-6.

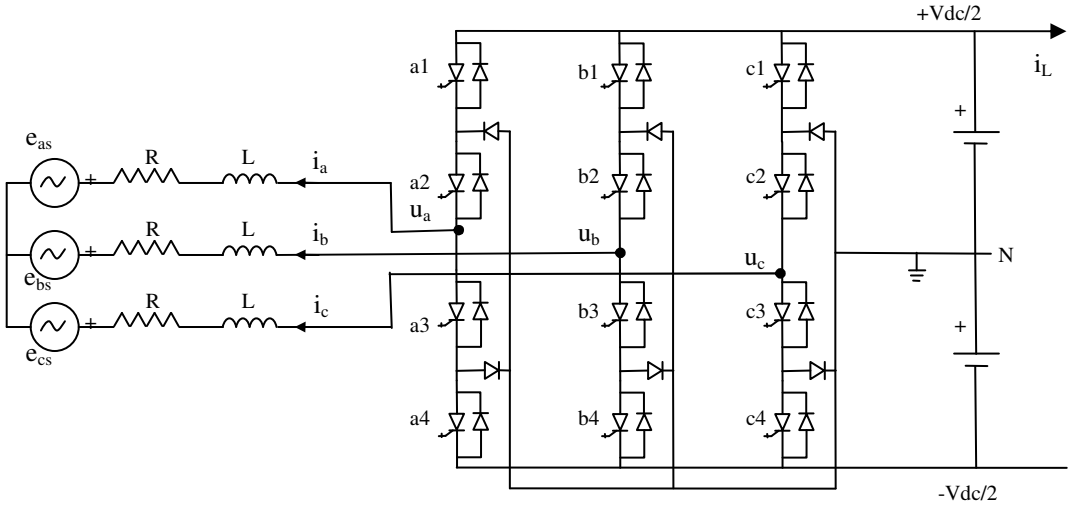

Figure 8-6 Voltage Source Converter power topology

The phase voltages of the grid are:

$$\begin{bmatrix} e_{as} \\ e_{bs} \\ e_{cs} \end{bmatrix} = \begin{bmatrix} E_M \cdot \cos(\omega \cdot t) \\ E_M \cdot \cos(\omega \cdot t - \frac{2\pi}{3}) \\ E_M \cdot \cos(\omega \cdot t - \frac{4\pi}{3}) \end{bmatrix} \qquad \text{(eq. 8-1)}$$

while the phase voltages of the three-level converter are:

$$\begin{bmatrix} u_a \\ u_b \\ u_c \end{bmatrix} = \begin{bmatrix} S_a \\ S_b \\ S_c \end{bmatrix} \cdot \frac{V_{dc}}{2} \qquad \text{(eq. 8-2)}$$

where S_x (x=a,b,c) are the switching states of each phase leg; when the switching state is +1, it generates $+V_{dc}/2$, when the switching state is -1, it generates $-V_{dc}/2$, and if the switching state is 0, it generates a zero-level voltage because it is connected to the neutral point. The two pair of switches of one phase leg $S_{x,k}$ and $S_{x,k+2}$ (k=1,2) receive

inverted gate signals to enable a proper modulation and to avoid forbidden switches states.
If only the phase voltage fundamental components are considered, it can be written:

$$\begin{bmatrix} u_{as} \\ u_{bs} \\ u_{cs} \end{bmatrix} = \begin{bmatrix} m \cdot \cos(\omega \cdot t + \alpha) \\ m \cdot \cos(\omega \cdot t - \frac{2\pi}{3} + \alpha) \\ m \cdot \cos(\omega \cdot t - \frac{4\pi}{3} + \alpha) \end{bmatrix} \cdot \frac{V_{dc}}{2} \qquad \text{(eq. 8-3)}$$

where m is the modulation index and α is the displacement angle among the phase voltage of the grid and the phase voltage fundamental component of the VSC.
The following equations describe the operation of the VSC in the stationary frame:

$$L \cdot \begin{bmatrix} d(i_a)/dt \\ d(i_b)/dt \\ d(i_c)/dt \end{bmatrix} + R \cdot \begin{bmatrix} i_a \\ i_b \\ i_c \end{bmatrix} = \begin{bmatrix} u_{as} \\ u_{bs} \\ u_{cs} \end{bmatrix} - \begin{bmatrix} e_{as} \\ e_{bs} \\ e_{cs} \end{bmatrix} \qquad \text{(eq. 8-4)}$$

Applying the Park's transformation from three-phase system abc to rotating frame dq:

$$\begin{bmatrix} x_d \\ x_q \\ x_o \end{bmatrix} = \frac{2}{3} \cdot \begin{bmatrix} \cos(\omega \cdot t + \theta) & \cos(\omega \cdot t + \theta - \frac{2\pi}{3}) & \cos(\omega \cdot t + \theta - \frac{4\pi}{3}) \\ -sen(\omega \cdot t + \theta) & -sen(\omega \cdot t + \theta - \frac{2\pi}{3}) & -sen(\omega \cdot t + \theta - \frac{4\pi}{3}) \\ \frac{1}{2} & \frac{1}{2} & \frac{1}{2} \end{bmatrix} \cdot \begin{bmatrix} x_a \\ x_b \\ x_c \end{bmatrix} \qquad \text{(eq. 8-5)}$$

to the equations 8-4, yields

$$L \cdot \frac{d(i_d)}{dt} - L \cdot \omega \cdot i_q + R \cdot i_d = u_d - E_M \qquad \text{(eq. 8-6)}$$

$$L \cdot \frac{d(i_q)}{dt} + L \cdot \omega \cdot i_d + R \cdot i_q = u_q \qquad \text{(eq. 8-7)}$$

$$L \cdot \frac{d(i_o)}{dt} + R \cdot i_o = u_o \qquad \text{(eq. 8-8)}$$

Note that the grid phase voltages are transformed in only d-component because the θ reference it is chosen in the order to achieve e_q = 0 V and e_d= E_M. In the synchronous rotating d-q frame the active and reactive power may be written respectively as:

$$P = \frac{3}{2}\left(e_d \cdot i_d + e_q \cdot i_q\right); \qquad \text{(eq. 8-9)}$$

$$Q = \frac{3}{2}\left(e_q \cdot i_d - e_d \cdot i_q\right). \qquad \text{(eq. 8-10)}$$

As it may be noted, the active power is set by the control of the current i_d, while the reactive power is set by control of the current i_q. In particular with this reference system of the phase current, if i_d<0 the VSC is adsorbing active power, while if i_d>0 it is providing active power to the grid.

The current i_0 control the homopolar current, if the transformer star point is ground connected, and it avoids circulating current between more parallel converters.
The small-signal linearization of the currents and voltages:

$$i_d = I_d + \hat{i}_d \quad \text{(eq. 8-11)}$$

$$i_q = I_q + \hat{i}_q \quad \text{(eq. 8-12)}$$

$$i_o = I_o + \hat{i}_o \quad \text{(eq. 8-13)}$$

$$u_d = U_d + \hat{u}_d \quad \text{(eq. 8-14)}$$

$$u_q = U_q + \hat{u}_q \quad \text{(eq. 8-15)}$$

$$u_o = U_o + \hat{u}_o \quad \text{(eq. 8-16)}$$

leads to:

$$L \cdot \frac{d(\hat{i}_d)}{dt} - L \cdot \omega \cdot \hat{i}_q + R \cdot \hat{i}_d = \hat{u}_d \quad \text{(eq. 8-17)}$$

$$L \cdot \frac{d(\hat{i}_q)}{dt} + L \cdot \omega \cdot \hat{i}_d + R \cdot \hat{i}_q = \hat{u}_q \quad \text{(eq. 8-18)}$$

$$L \cdot \frac{d(\hat{i}_o)}{dt} + R \cdot \hat{i}_o = \hat{u}_o \quad \text{(eq. 8-19)}$$

The equations 8-17, 8-18 and 8-19 can be transformed in the Laplace domain (s-domain) as:

$$(sL + R) \cdot \hat{i}_d = \hat{u}_d + L \cdot \omega \cdot \hat{i}_q \quad \text{(eq. 8-20)}$$

$$(sL + R) \cdot \hat{i}_q = \hat{u}_q - L \cdot \omega \cdot \hat{i}_d \quad \text{(eq. 8-21)}$$

$$(sL + R) \cdot \hat{i}_0 = \hat{u}_0 \quad \text{(eq. 8-22)}$$

In the Figure 8-7 the block scheme, which describes the model of the VSC, is shown.

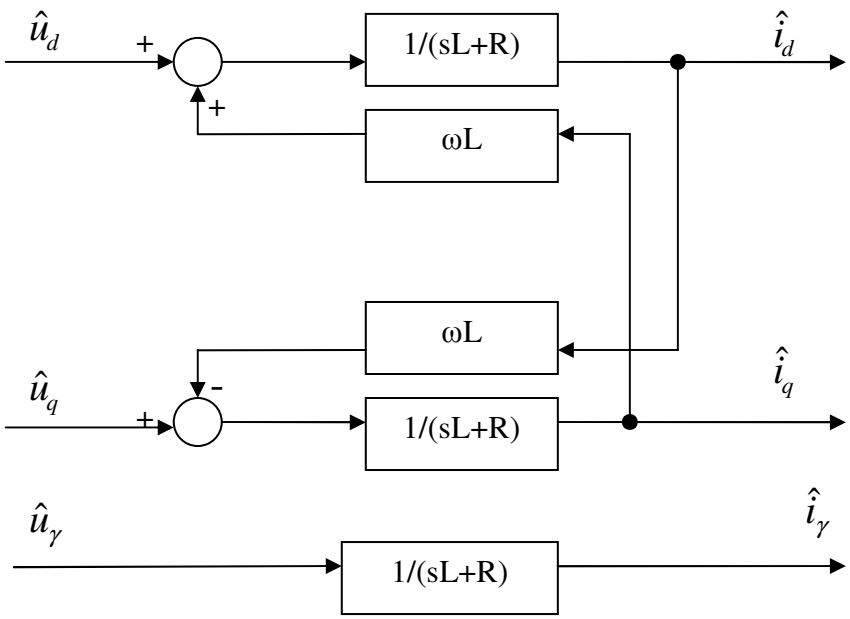

Figure 8-7 The block diagram of the VSC model

It can be seen that there is a cross-coupling between d and q components because of the ωL part. The cross-coupling can affect the dynamic performance of the regulator. Therefore, it is very important to decouple the coupling term for a better performance. Multiplying the eq. 8-21 with the complex number j and adding to eq. 8-20, yields

$$(sL+R)\cdot(\hat{i}_d + j\cdot\hat{i}_q) = (\hat{u}_d + j\cdot\hat{u}_q) + L\cdot\omega\cdot(\hat{i}_q - j\cdot\hat{i}_d) \qquad \text{(eq. 8-23)}$$

this can be rewritten as:

$$(sL+R+j\cdot\omega\cdot L)\cdot\bar{i} = \bar{u} \qquad \text{(eq. 8-24)}$$

where:

$$\bar{u} = \hat{u}_d + j\cdot\hat{u}_q$$
$$\bar{i} = \hat{i}_d + j\cdot\hat{i}_q$$

Therefore transfer function G(s) of the VSC is:

$$G(s) = \frac{\bar{i}}{\bar{u}} = \frac{1}{(sL+R+j\cdot\omega\cdot L)} \qquad \text{(eq. 8-25)}$$

The transfer function G'(s) without the coupling term ωL should be achieved:

$$G'(s) = \frac{\bar{i}}{\bar{u}'} = \frac{1}{(sL+R)} \qquad \text{(eq. 8-26)}$$

Two different methods are proposed in [11]: "feedforward" or "feedback" decoupling methods.
In this AGPS study, the method used to decouple the component d-q is "feedback method".
The current control loop of the VSC with "feedback" decoupling method is shown in the Figure 8-8.

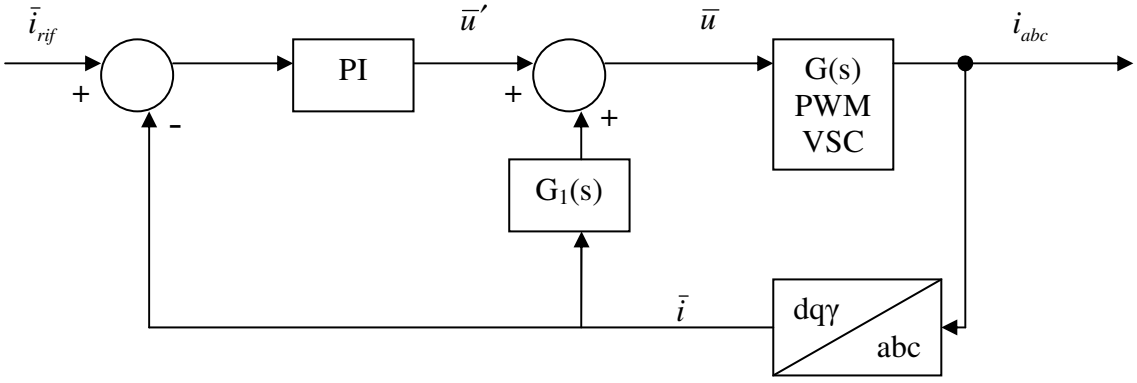

Figure 8-8 Current control of the VSC.

To achieve the decoupling among d-q components, the term $G_1(s)$ have to be calculated.

From the Figure 8-8, it may be written:

$$G(s)\cdot\left[\bar{u}' + G_1(s)\cdot\bar{i}\right] = \bar{i} \qquad \text{(eq. 8-27)}$$

and it follows:

$$\left[1 - G(s)\cdot G_1(s)\right]\cdot\bar{i} = G(s)\cdot\bar{u}' \qquad \text{(eq. 8-28)}$$

Finally we have:

$$\frac{\bar{i}}{\bar{u}'} = G'(s) = \frac{G(s)}{1 - G(s)\cdot G_1(s)} \qquad \text{(eq. 8-29)}$$

Putting in the transfer functions G(s) e G'(s), yields:

$$\frac{1}{(sL+R)} = \frac{1}{(sL+R+j\cdot\omega\cdot L) - G_1(s)} \qquad \text{(eq. 8-30)}$$

The transfer function $G_1(s)$ to decouple d-q components results:

$$G_1(s) = j\cdot\omega\cdot L \qquad \text{(eq. 8-31)}$$

The complete diagram of the current control of the VSC with the feedback decoupling method at the small-signal linearization is shown in Figure 8-9.

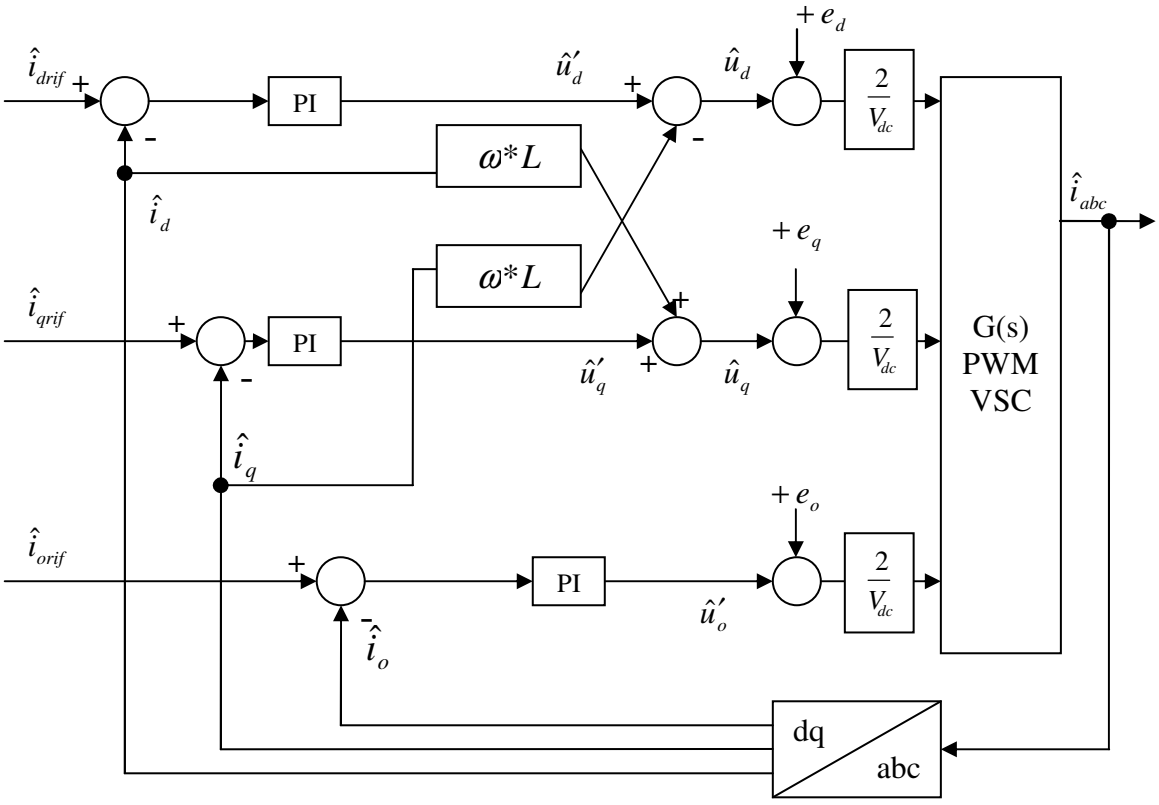

Figure 8-9 Complete diagram of the current control of the VSC with the feedback decoupling method at the small-signal linearization.

It may be noted that the grid voltages are feed-forwarded, because they are not constant but they change with different loads, due to the presence of the transformer short circuit impedance (R_{SC}, L_{SC}). The output signals of the current controller are normalized respect to $V_{dc}/2$.
Therefore with the d-q components decoupled, the transfer function G'(s) is the same for the three components:

$$G'(s) = \frac{\bar{i}}{\bar{u}'} = \frac{1}{(sL+R)} \qquad \text{(eq. 8-32)}$$

Using the Internal Model Control principle to design the current controller [12], yields:

$$G_{PI}(s) = \frac{1}{G'(s)} \cdot \frac{W_d(s)}{1-W_d(s)} \qquad \text{(eq. 8-33)}$$

Where:

$G_{PI}(s) = K_P + \frac{K_I}{s}$ is the transfer function of the PI controller;

$W_d(s) = \frac{1}{1+T_C \cdot s}$ is the transfer function of the current control loop.

It yields:

$$G_{PI}(s) = (sL+R) \cdot \frac{1}{1+T_C \cdot s - 1} = \frac{L}{T_C} + \frac{R}{T_C \cdot s} = L \cdot \alpha_C + \frac{R \cdot \alpha_C}{s} \qquad \text{(eq. 8-34)}$$

where α_C is the bandwidth of the current control loop.
The proportional and integral gains become:

$$K_P = L \cdot \alpha_C \qquad \text{(eq. 8-35)}$$

$$K_I = R \cdot \alpha_C \qquad \text{(eq. 8-36)}$$

The digital processing (Figure 8-10) have to be considered to determine the maximum value of bandwidth α_C [13]-[14].

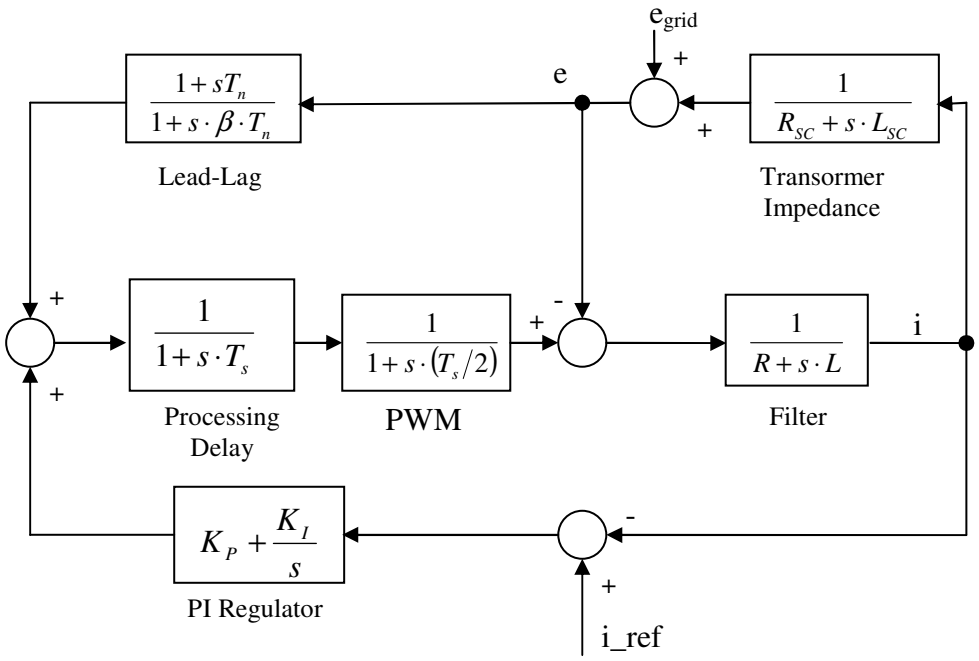

Figure 8-10 Converter current control loop including the processing and PWM delays.

It should be noted that there is a delay equal to the sampling time T_S in the system for the digital processing, plus 0,5 T_S delay is implicitly introduced by discretization of the system plant using a zero th-order hold, as is commonly used to describe continuous systems controlled by PWM. The total delay of the current loop is:

$$G_{delay,total} = \frac{1}{1+1{,}5 \cdot s \cdot T_S + 0{,}5 \cdot s^2 \cdot T_S^2} \approx \frac{1}{1+1{,}5 \cdot s \cdot T_S} \qquad \text{(eq. 8-37)}$$

Hence the maximum of bandwidth α_C is:

$\alpha_C = \frac{1}{1{,}5 \cdot a \cdot T_s}$ with a≥2 (method of the symmetric optimum).

Nevertheless for T_S very small, the bandwidth α_C should be always less of the $(2*\pi*f_{SW})/2$. Usually the sampling frequency $f_S=1/T_S$ is twice the switching frequency f_{SW} in a double edge unsymmetrical PWM.

Furthermore it is not possible to achieve a completely decoupled system due to the current control loop delay. The current control is improved if a Lead-Lag block is added to the voltage grid:

$G_{Lead-Lag} = \frac{1+sT_n}{1+s \cdot \beta \cdot T_n}$.

The time constant T_n should be equal to $1.5 \cdot T_S$, while β should be ≤ 1, founding a good compromise between compensation and noise amplification.

8.3.1 Pulsed Width Modulation Strategies

Several PWM techniques are used for the two-level power converters, but they may be used for three level converters too. They may be classified in Carrier Based PWM (CBPWM), in Space Vector Modulation (SVM) and in off line pre-programmed PWM switching pattern.

Between CBPWM strategies, the most used are [9], [15]:

- Sinusoidal PWM: sinusoidal modulation is based on two triangular carrier signals. The common carrier signals are compared with three reference sinusoidal signals and the logical signals are generated to define the switching instant of the switch. The maximum value of the modulation index m (defined as pick value of the reference sinusoidal signal/(V_{dc}/2)) may be equal to 1.
- CB-PWM with Zero Sequence Signal (ZSS-CB-PWM): This strategy may be used if the neutral point on the ac side of the power converter is not connected with the dc side midpoint 0, in this manner the phase currents depend only on the voltage difference between phases, and homopolar sequence current can not circulate. It consists in inserting an additional Zero Sequence Signal ZSS of the third harmonic, which does not produce the line voltage distortion. It may be divided in two group: continuous and discontinuous. The most known continuous modulation is the method with sinusoidal ZSS with 1/6 amplitude, which correspond to the maximum linear range (m=1.15); the most known discontinuous modulation is Optimal Sinusoidal PWM (OSPWM), where each phase voltage is clamped to either + V_{dc}/2 or –V_{dc}/2 for one-third of each half-cycle [16].

Several reference signals of the CBPWM strategies and the respective ZSS are shown in Figure 8-11.

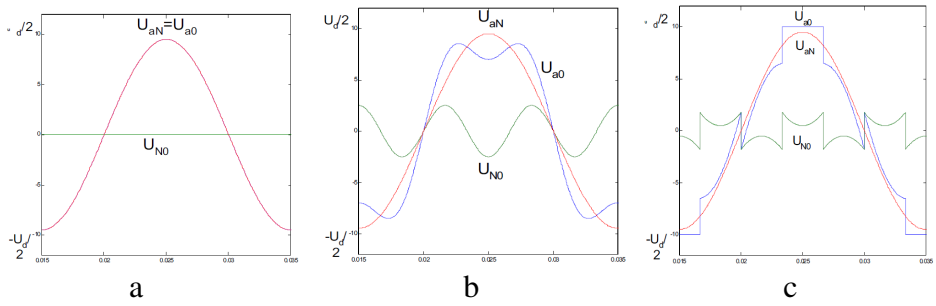

Figure 8-11 a) SPWM; b) modulation with 3-th harmonic; c) OSPWM [16].

In CBPWM technique for NPC VSC, the switch firing signals for each phase are produced by comparing the respective modulation signal with two carrier triangular waveforms (Figure 8-12).

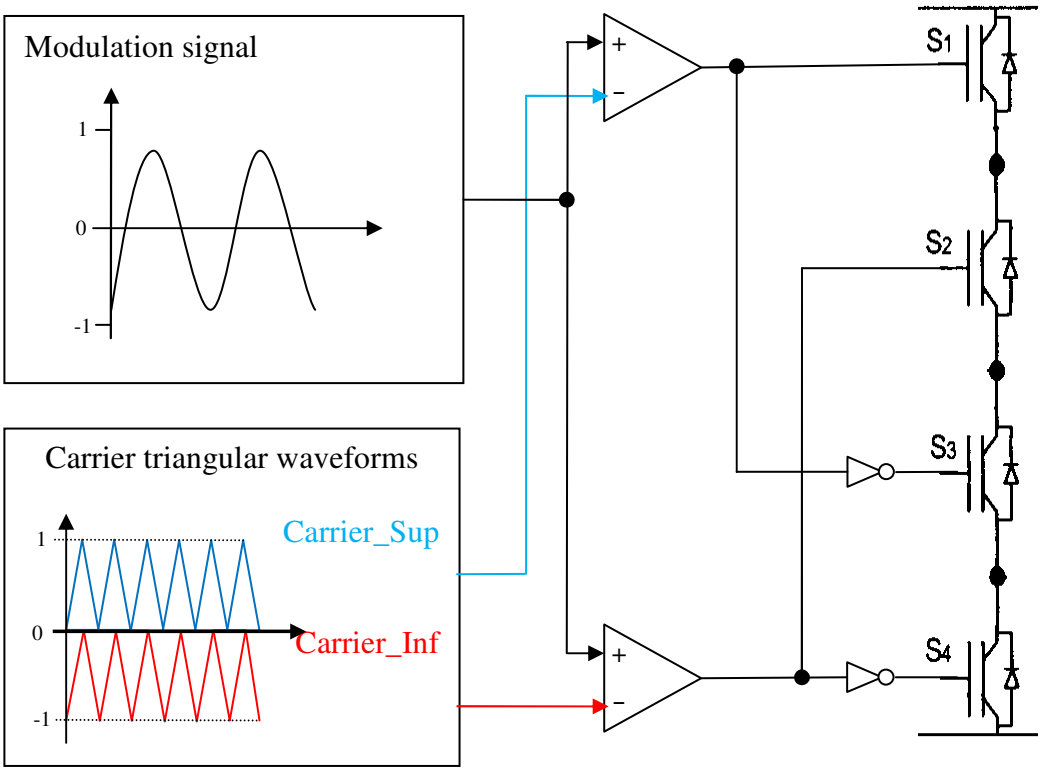

Figure 8-12 Switch gating signals for one phase leg.

The SVM [3] has been extended for the three-level NPC VSC. It is a bit more complex than in a two level VSC. There are 27 different switching states and their voltage vectors are shown in Figure 8-13. There are some switching states with redundant space-vector representation, which are used for neutral point balance purposes.

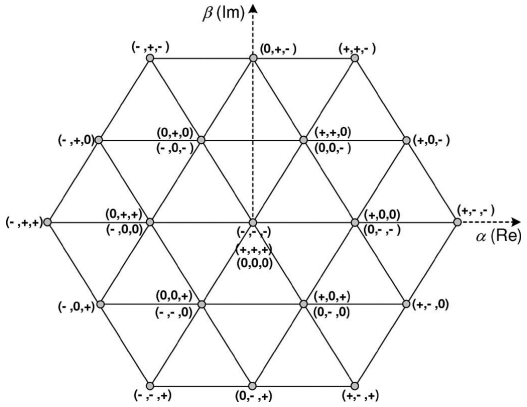

Figure 8-13 Voltage space vectors generated by a NPC-VSC [3].

The most used off-line strategy is Selective Harmonic Elimination Pulse Width Modulation (SHEPWM) [17]. It is based on the calculation of pre-programmed PWM switching pattern to obtain output voltages with zero content in some specific harmonics. Several modifications of this strategy are presented in literature to mitigate the non-eliminate harmonics [18]-[19] or to reduce the voltage total harmonic distortion [20].
For this study ZSS CBPWM with 1/6 amplitude of the fundamental is used.

8.4 The reference angle detector

The current control used for this study operates in d-q rotating frame, therefore it needs of a detector to calculate the reference angle θ_{dq} [10]. The different methods to extract the phase angle are:

- Zero-Crossing Method detects when the grid phase voltage cross the zero value, this technique is poor in presence of harmonics or notches.
- Filtering of Grid Voltage may be used in different frame (Figure 8-14), it is better than zero-crossing method, but the use of filter introduce a delay in the processed signal and it may be unacceptable.

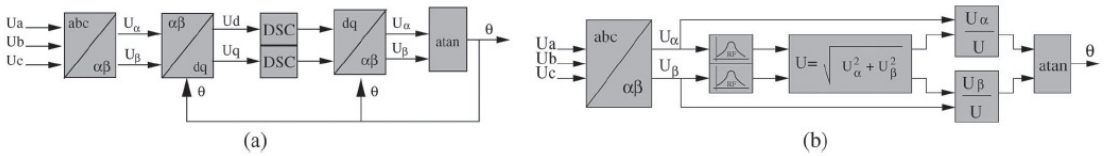

Figure 8-14 Synchronization method using (a) filtering on the *dq* synchronous rotating reference frame and (b) filtering on *αβ* stationary frame [10].

- Phase-Locked Loop (PLL) technique is the state of the art method to extract phase angle of the grid voltages and it is the method used for this study.

In the Figure 8-15 it is shown how the reference angle for synchronous rotating d-q frame locked on the fundamental is obtained [21] and this method has been used in the control system of the AFE design of the ac/dc conversion system under study.

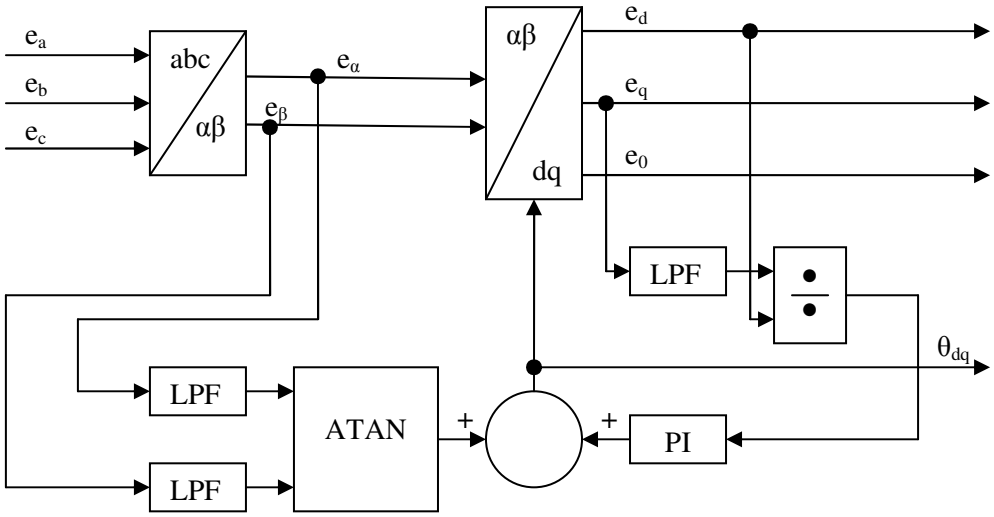

Figure 8-15 Scheme of the reference angle detector for the d-q transformation [21].

The three input phases are transformed into α-β components and then are heavily filtered (with the Low Pass Filters) before performing the angle detection in order to avoid the injection of the low order harmonics, which might be present into the input voltage. A PI controller monitors the relative q-component of the voltage and it corrects the displacement angle introduced by the filters.
By this reference angle detector, E_q is 0 V and E_d results:

$$E_d = E_M ; \qquad \text{(eq. 8-38)}$$

where E_M is the maximum value of phase voltage fundamental component.

8.5 The dc-link voltage controller

Considering the input-output balance power of an AFE rectifier in a synchronous rotating d-q frame and neglecting the losses, the following equation may be write [21]:

$$\frac{3}{2}\left\{e_d \cdot i_d + e_q \cdot i_q\right\} = v_{dc} \cdot C \frac{dv_{dc}}{dt} + v_{dc} \cdot i_L \qquad \text{(eq. 8-39)}$$

where the first part is the active power provide to the converter, while the second one is the sum between the power changed with the dc link capacitor and that of the load, which drains a current i_L. For the sake of the simplicity, the phase current reference system is opposite respect to the one used to describe the current control, namely $i_d>0$ when an active power is provided to the converter.
The small linearization leads to:

$$\frac{3}{2}\left\{\left(E_d + \hat{e}_d\right)\cdot\left(I_d + \hat{i}_d\right) + \left(E_q + \hat{e}_q\right)\cdot\left(I_q + \hat{i}_q\right)\right\} = \left(V_{dc} + \hat{v}_{dc}\right)\cdot C\frac{d\left(V_{dc} + \hat{v}_{dc}\right)}{dt} + \left(V_{dc} + \hat{v}_{dc}\right)\cdot\left(I_L + \hat{i}_L\right) \qquad \text{(eq. 8-40)}$$

To obtain the dc link voltage control, the transfer function has to be found; hence the other perturbations may be neglected:

$$\frac{3}{2}\left\{E_d \cdot I_d + E_d \cdot \hat{i}_d + E_q \cdot I_q\right\} = V_{dc} \cdot C \frac{d\hat{v}_{dc}}{dt} + V_{dc} \cdot I_L + \hat{v}_{dc} \cdot I_L \qquad \text{(eq. 8-41)}$$

where the second order signal perturbations have also been assumed zero.

In steady state yields:

$$\frac{3}{2}\left\{E_d \cdot I_d + E_q \cdot I_q\right\} = V_{dc} \cdot I_L \qquad \text{(eq. 8-42)}$$

it results in:

$$\frac{3}{2}\left\{E_d \cdot \hat{i}_d\right\} = V_{dc} \cdot C\frac{d\hat{v}_{dc}}{dt} + \hat{v}_{dc} \cdot I_L \qquad \text{(eq. 8-43)}$$

Indicating the load equivalent resistance $R_L=V_{dc}/I_L$ and to assuming $V_{dc}=\sqrt{3}\cdot E_d$ in order not to increase too much the switch losses, in the Laplace-domain the transfer function is:

$$\frac{\hat{v}_{dc}}{\hat{i}_d} = \frac{\sqrt{3}}{2} \cdot \frac{R_L}{(R_L C \cdot s + 1)} \qquad \text{(eq. 8-44)}$$

The PI regulator $[K_{Vdc}\cdot(1+s\cdot T_{Vdc})/(s\cdot T_{Vdc})]$ of the linear controller for the dc link voltage loop can be designed using the symmetrical optimum principle:

$$T_{Vdc} = R_L \cdot C$$

$$K_{Vdc} = \alpha_{Vdc} \cdot \frac{2 \cdot T_{V\,dc}}{\sqrt{3} \cdot R_L} = \alpha_{Vdc} \cdot \frac{2 \cdot C}{\sqrt{3}} \qquad \text{(eq. 8-45)}$$

$$\alpha_{Vdc} = \frac{\alpha_C}{\gamma}, \gamma \geq 2$$

where α_{Vdc} is the bandwidth of dc link voltage controller.
In the Figure 8-16 the dc link voltage loop is reported with also the transfer function of the inner current control.

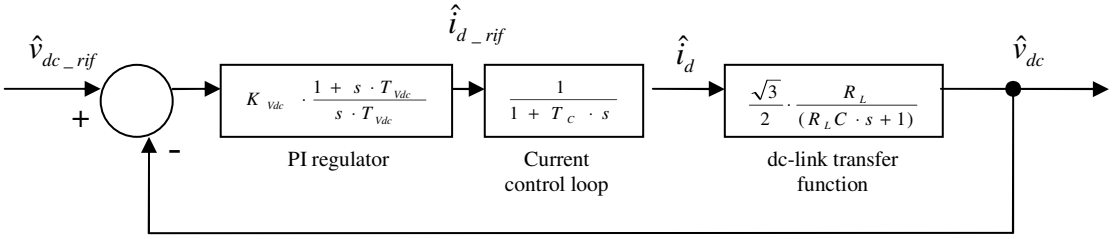

Figure 8-16 Scheme of the voltage dc-link voltage control loop.

This type of control may become unstable during regenerative operation ($R_L<0$), because the open loop transfer function has a negative pole. This problem is reduced with a big dc-link capacitance. In [22] a non-linear control of the dc voltage loop is proposed, which overcomes this problem adding a current sensor in the dc link. Nevertheless the ac/dc converter of the AGPS has to operate only in rectifier operation and the linear control is chosen.

8.6 The differential voltage controller

The algorithm used to generate the triangular carrier wave form is shown in Figure 8-17 [6]-[7].

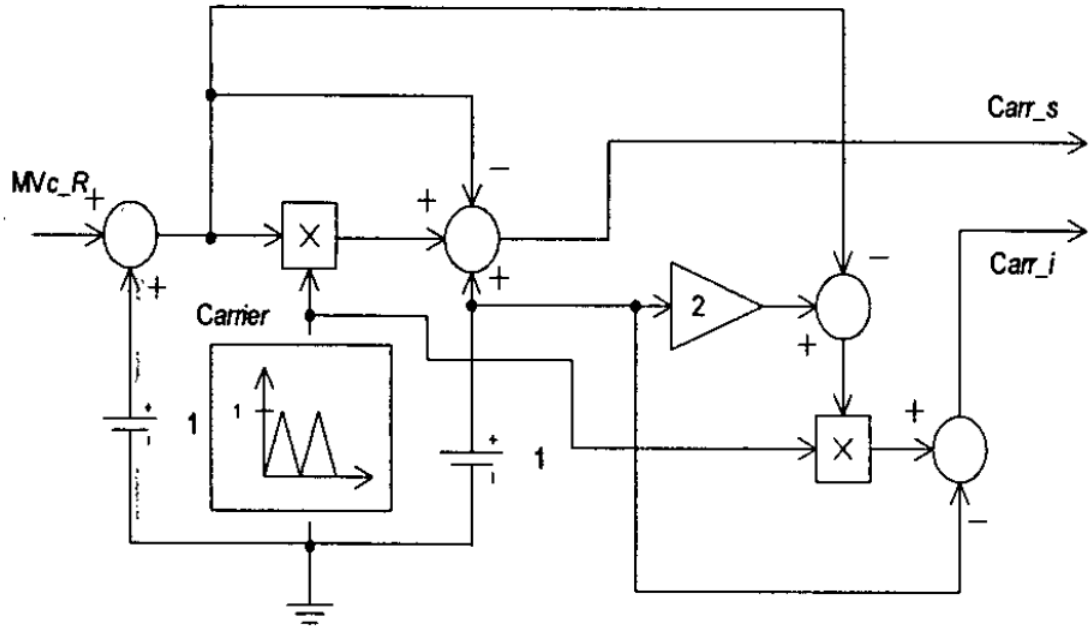

Figure 8-17 Scheme of the carrier generation [6].

The two triangular carrier waveforms are in phase and their amplitudes are complementary, namely the upper one has 1 and 0 extreme values, while the lower one has 0 and -1 extreme values. The control of the voltage balance between the two capacitors is obtained by the modification of the triangular carrier waveforms. In particular, when a voltage across one capacitor must be increased, the respective carrier waveform increases by the variation of the common extreme 0, while the complementary one is reduced in the same proportion. The variation of the carrier waveforms amplitudes is commanded by the signal MVc_R, which is given by PI regulator. The control of the voltage balance between the two capacitors is shown in Figure 8-18.

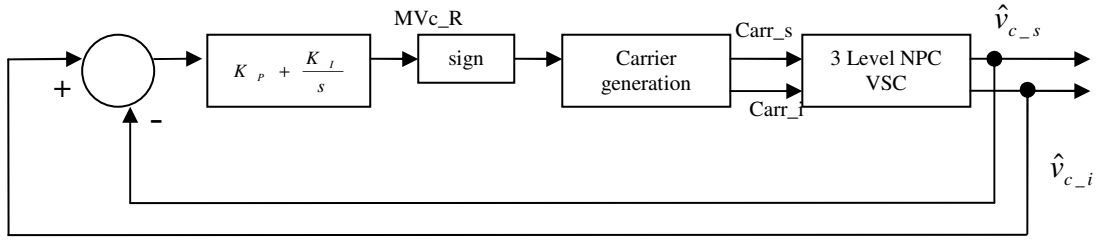

Figure 8-18 Block diagram of control of the voltage balance between the two capacitors.

It should be noted that this control is good only in rectifier operation (sign = +); in regenerative operation it may be used by changing the sign to the MVc_R signal (sign = -)

8.7 The input filter of AFE - VSC

The input filter of AFE-VSC has to be designed to meet the harmonic distortion limit according to IEEE-519-1992 [23]

There are three topologies of filter used for AFE VSC:

- L filter consists on just an inductive filter connected in series with the converter (Figure 8-19). During the design of this component, the main aim is to avoid the saturation in the inductors, with consequent higher losses.

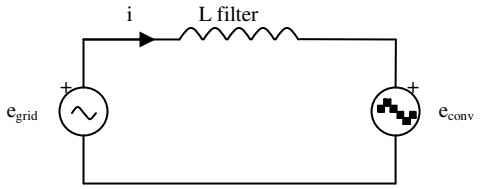

Figure 8-19 Equivalent single phase of L filter.

- LCL filter aims to reduce high-order harmonics on the grid side (Figure 8-20). The resonant frequency of the impedance seen to the side converter should be in a range between ten times the line frequency and one half of the switching frequency, to avoid resonance problems in lower and upper parts of the harmonic spectrum. In [14] and [24] the description of the LCL filter design is given. For high power converter with low switching frequency the design of LCL filter becomes very difficult, or it may be used together with tuned filters with SHEPWM strategy [17].

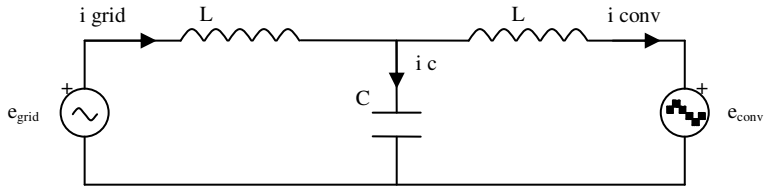

Figure 8-20 Equivalent single phase of LCL filter.

- Tuned filter with LC filter are used in high power converters with SHEPWM strategy to minimize the non eliminated harmonics [20].

In the case of L filter, the value of the inductance is limited to achieve a good tracking of the current reference signal [14]. The maximum value of the L filter may be calculated by considering the steady state equation:

$$\overline{E}_{grid} - \overline{E}_{conv} = j\omega L \cdot \overline{I} \qquad \text{(eq. 8-46)}$$

Where E_{grid} is the peak value of the phase voltage grid, E_{conv}=m·Vdc/2 and I is the peak value of the current.

The phasor diagram in condition of unity power factor is shown in Figure 8-21.

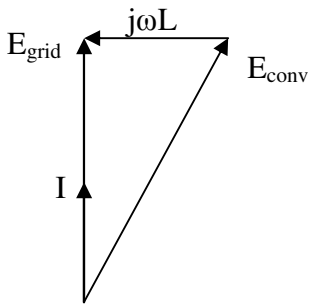

Figure 8-21 The phasor diagram in condition of unity power factor.

The upper limit of the L filter is given:

$$L_{MAX} = \frac{\sqrt{\left(\frac{m_{\max} \cdot Vdc}{2}\right)^2 - E_{grid}^2}}{\omega I} \qquad \text{(eq. 8-47)}$$

The peak to peak ripple current for a two level converter is given by [25]:

$$\hat{i}_{ripple} = \frac{m \cdot Vdc}{8 \cdot \sqrt{3} \cdot f_{SW} \cdot L} \qquad \text{(eq. 8-48)}$$

For a NPC converter, in the case the neutral point of the converter is isolated from the neutral of the grid, the equation 3-39 becomes:

$$\hat{i}_{ripple} = \frac{m \cdot \frac{V_{dc}}{2}}{8 \cdot \sqrt{3} \cdot f_{SW} \cdot L} \qquad \text{(eq. 8-49)}$$

In closed loop systems, the modulation index under no load condition is:

$$m = \frac{E_{grid}}{V_{dc}/2} \qquad \text{(eq. 8-50)}$$

and the ripple current may be calculated without to consider the dc link voltage:

$$\hat{i}_{ripple} = \frac{E_{grid}}{8 \cdot \sqrt{3} \cdot f_{SW} \cdot L} \qquad \text{(eq. 8-51)}$$

8.7.1 Synchronous Active Front-End

When n converters have to operate in parallel, namely they are connected to the same point in ac side and to the same dc link, it is possible reduce the harmonic current injected in the grid by shifting the each triangular carrier of a phase equal to 1/n of the switching period [26]-[28]. This technique, called Synchronous Active Front-End takes the advantage of minimizing the size of the filter. The principle schemes of SAFE control and power circuit are shown in Figure 8-22 and Figure 8-23. This technique should be used with continuous modulation strategy, because with the discontinuous one the phase shift between the switching signals of the paralleled module generate a zero sequence current which is dangerous for the converters [29]. Moreover it should be noted that the grid current has low THD, while the ripple current into the side converter depends principally on the decoupling inductances L_f.

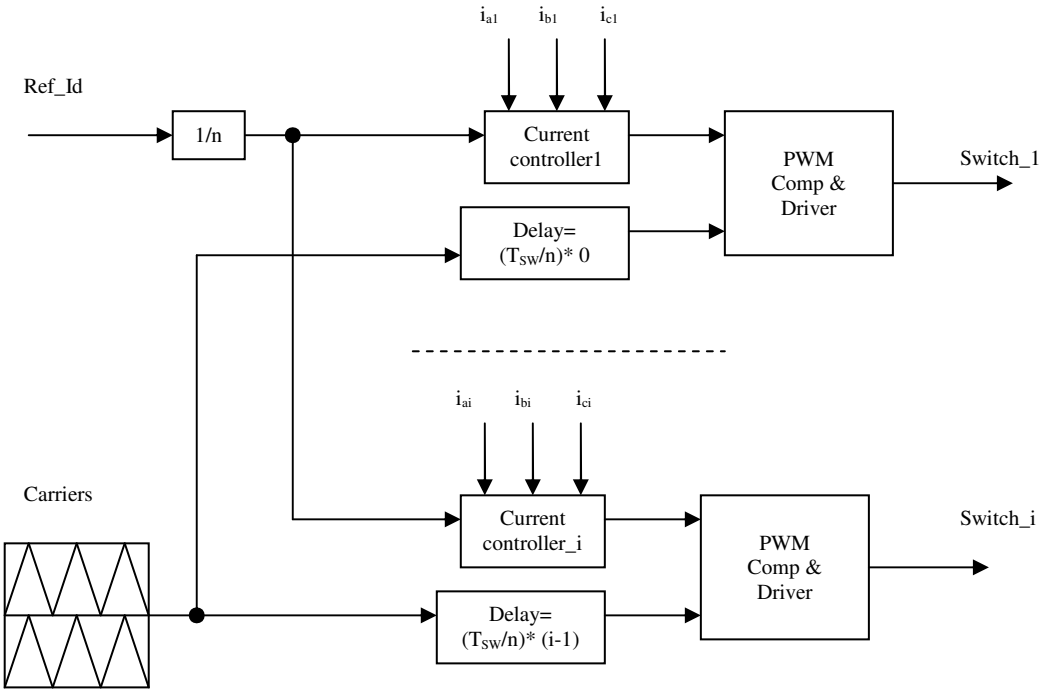

Figure 8-22 The principle scheme of Syncronous AFE control (i=1,…,n): control section.

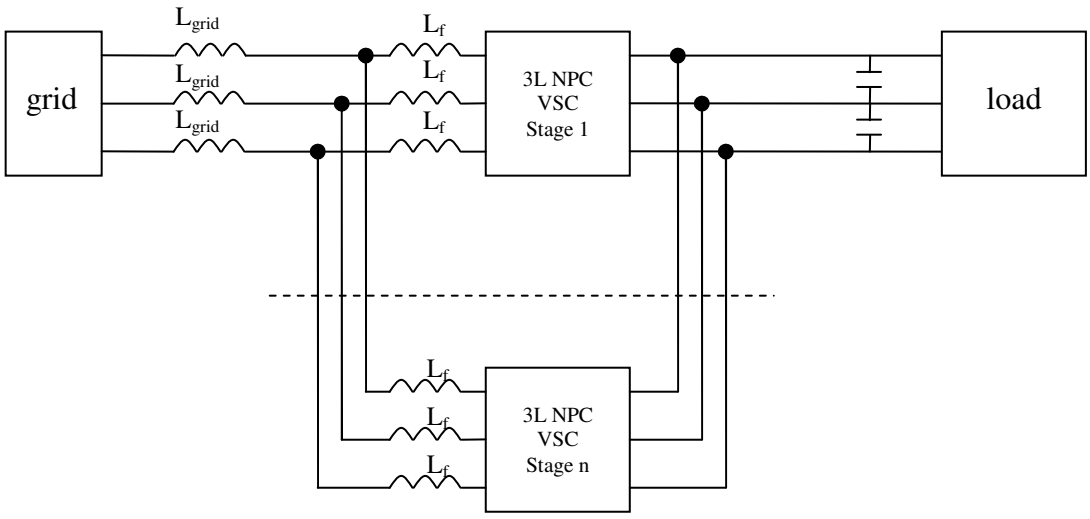

Figure 8-23 The principle scheme of Syncronous AFE control (i=1,…,n): power section.

8.7.1.1 Circulation of current harmonics among two Voltage Source Converter with independent and common neutral point in SAFE configuration (i.e. with shifted carrier waveforms)

The two cases, without and with the connection of the two neutral points between the two converters are compared. The two converters have the same modulation signal with m=1 and the respective carrier have a displacement of phase is 180 electirical degrees (Figure 8-24).

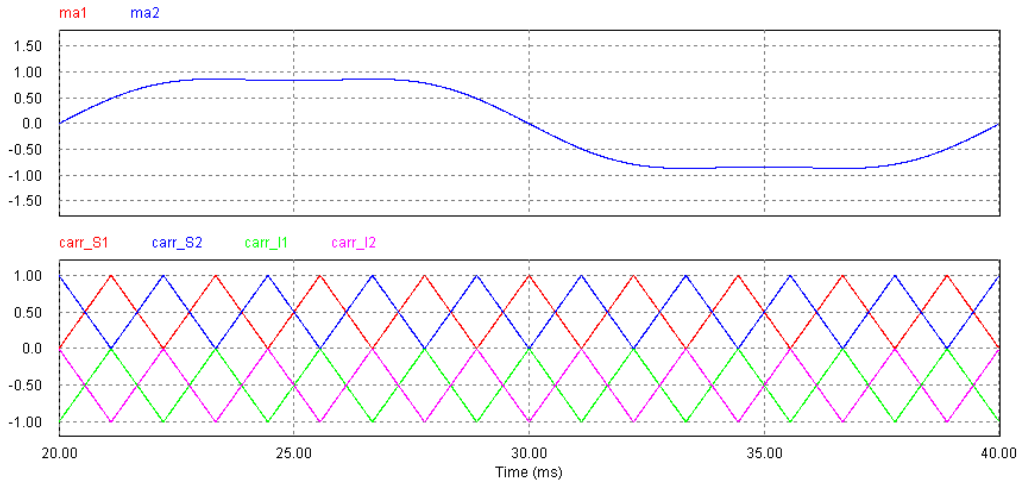

Figure 8-24 Modulation signals and carrier waveforms.

a) Without the connection between the neutral points

The PSIM model without connection between the neutral points of the two converters is shown in the Figure 8-25.

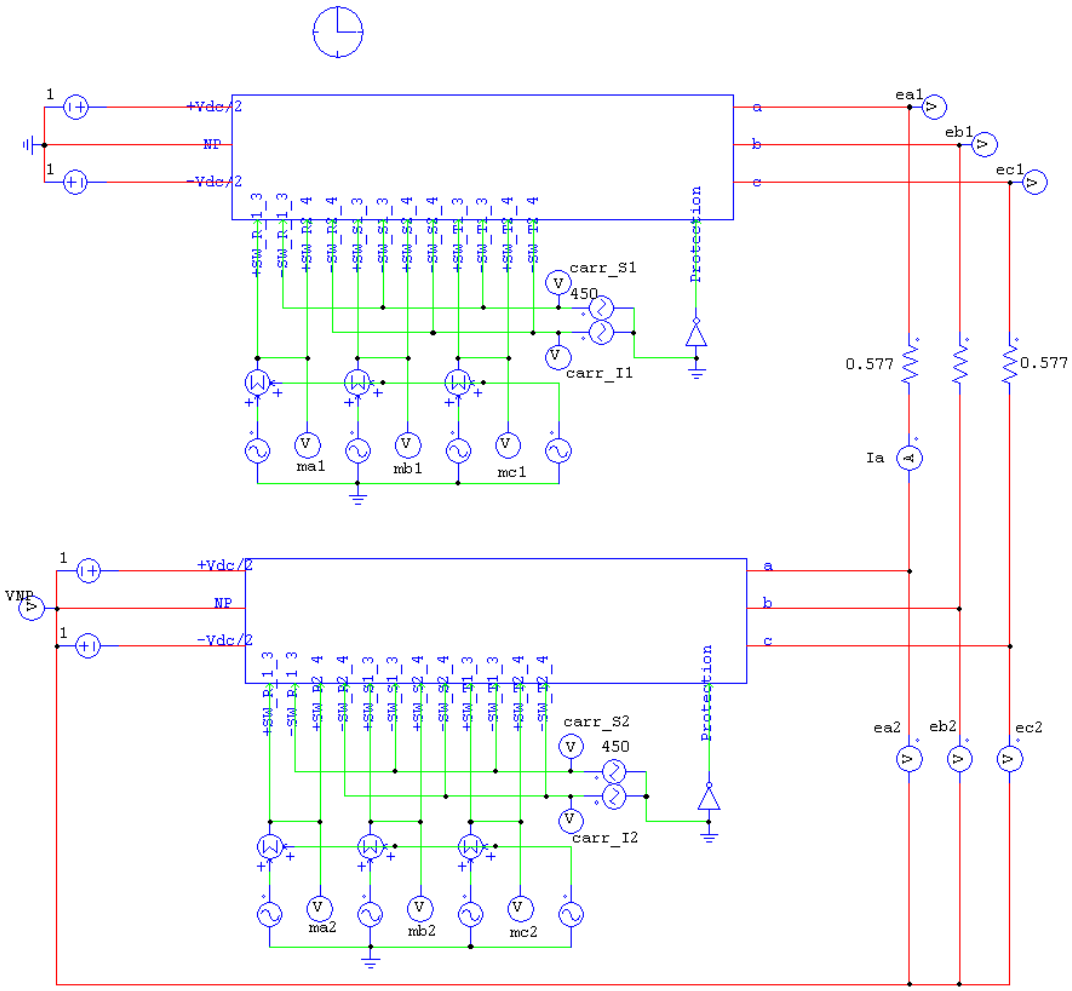

Figure 8-25 The PSIM model without the connection between the neutral points.

The amplitude of voltage source in the dc link is 1 V, the carrier/switching frequency is 450 Hz and the resistance limits the current ripple and its value is $1/\sqrt{3}=0.577\ \Omega$.

The waveforms of the phase to neutral (ea1, ea2) and phase to phase (vab1=ea1-eb1, vab2=ea2-eb2) voltages of the two converters, difference between the phase to phase voltages (vab1-vab2) of the two converters, the ripple current Ia in the resistance, the difference between the phase to neutral voltages (ea1-ea2) and the voltage VNP between the two neutral points are shown in the Figure 8-26.
The respective harmonic components are shown in the Figure 8-27.

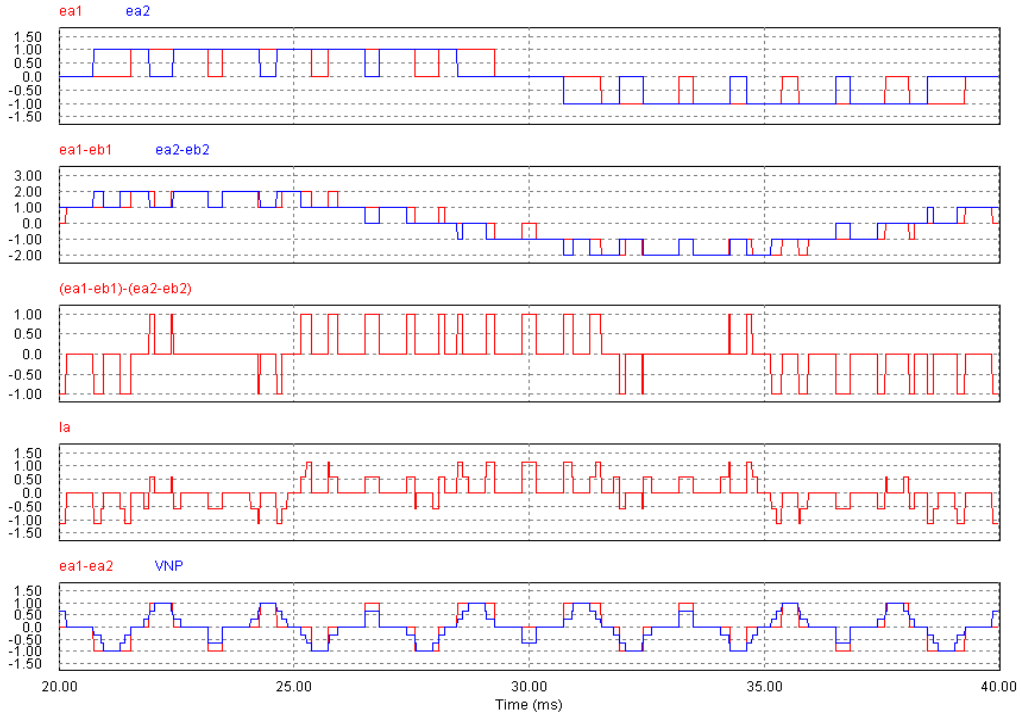

Figure 8-26 The waveforms of: (1st row) the phase to neutral (ea1, ea2) and (2st row) phase to phase (vab1=ea1-eb1, vab2=ea2-eb2) voltages of the two converters, difference between the phase to phase voltages vab1-vab2=(ea1-eb1)-(ea2-eb2) of the two converters, the ripple current Ia in the resistance, the difference between the phase to neutral voltages (ea1-ea2) and the voltage VNP between the two neutral points.

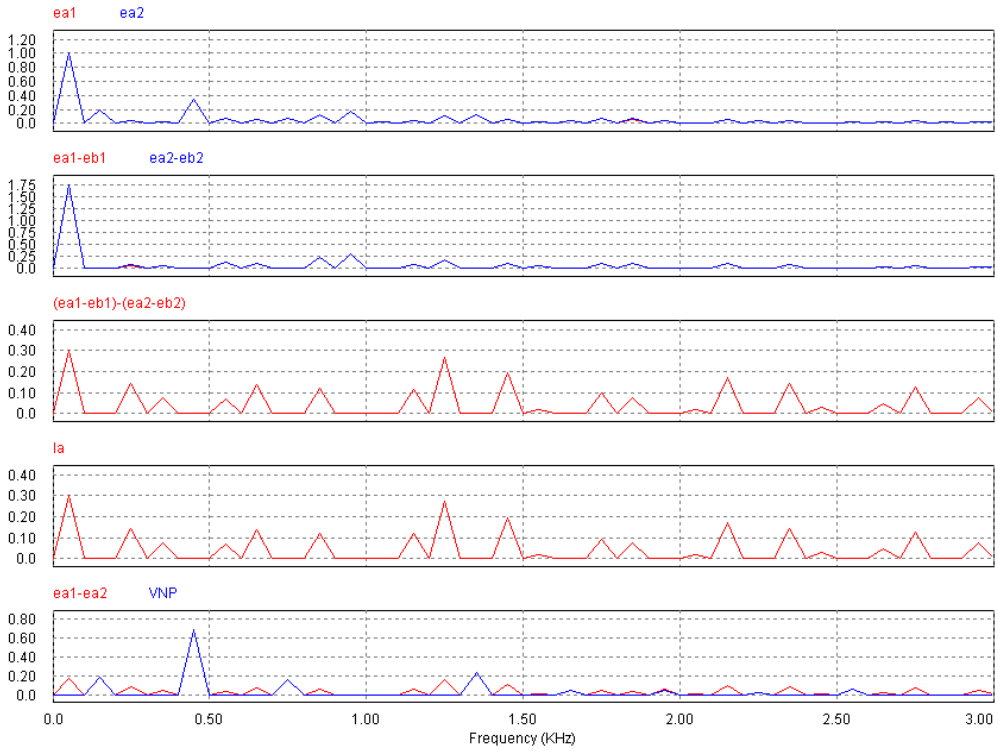

Figure 8-27 The harmonic components of: (1st row) the phase to neutral (ea1, ea2) and (2st row) phase to phase (vab1=ea1-eb1, vab2=ea2-eb2) voltages of the two converters, difference between the phase to phase voltages vab1-vab2=(ea1-eb1)-(ea2-eb2) of the two converters, the ripple current Ia in the resistance, the difference between the phase to neutral voltages (ea1-ea2) and the voltage VNP between the two neutral points.

The phase to phase voltages vab1 and vab2 don't have the harmonic components multiples or submultiples of the switching frequency 450 Hz of a factor 3, on the contrary of the phase to neutral voltages ea1 and ea2; hence the harmonic components of the phase to neutral voltage multiplies of a factor 3 o 1/3 are homopolar sequences. The ripple current Ia in the resistance has the same harmonic content of the difference of the phase to phase voltages between the two converters (vab1-vab2). The voltage between the two neutral points VNP has only the harmonic components multiplies of 3 or 1/3 of the switching frequency, i.e the homopolar sequences; it should be noted that the amplitude of the component at switching frequency in the voltage VNP is twice the amplitude of the respective harmonic component in the voltages ea1 and ea2, it means that the harmonics component at the switching frequency have a displacement of phase of 180 electrical degrees.

2) With the connection between the neutral points.
The PSIM model is the same illustrated before but with the connection between the neutral points of the two converters is shown in the Figure 8-28.

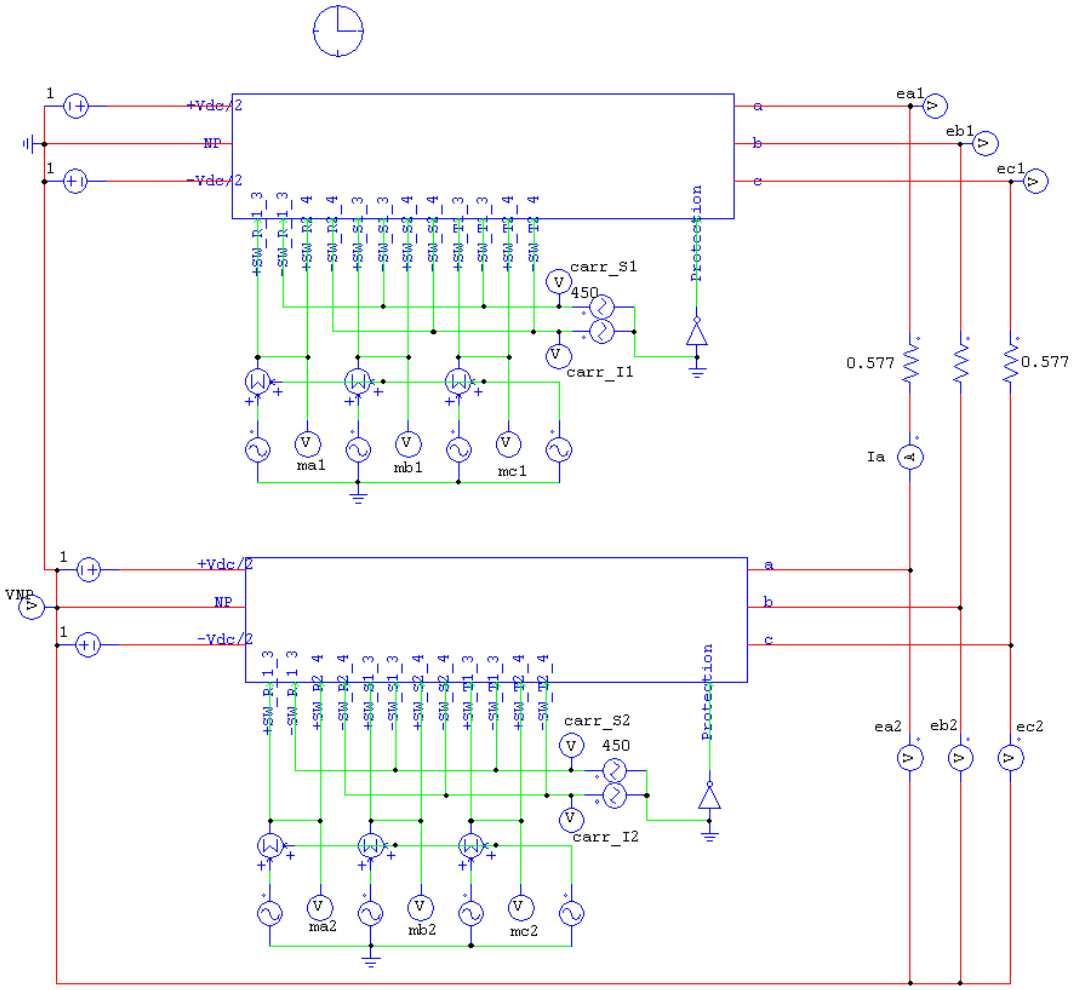

Figure 8-28 The PSIM model with the connection between the neutral points.

The amplitude of voltage source in the dc link is 1 V, the carrier/switching frequency is 450 Hz and the resistance limits the current ripple and its value is $1/\sqrt{3}=0.577\ \Omega$.
The waveforms of the phase to neutral (ea1, ea2) and phase to phase (vab1=ea1-eb1, vab2=ea2-eb2) voltages of the two converters, difference between the phase to phase voltages (vab1-vab2) of the two converters, the ripple current Ia in the resistance, the difference between the phase to neutral voltages (ea1-ea2) and the voltage VNP between the two neutral points are shown in the Figure 8-29.
The respective harmonic components are shown in the Figure 8-30.

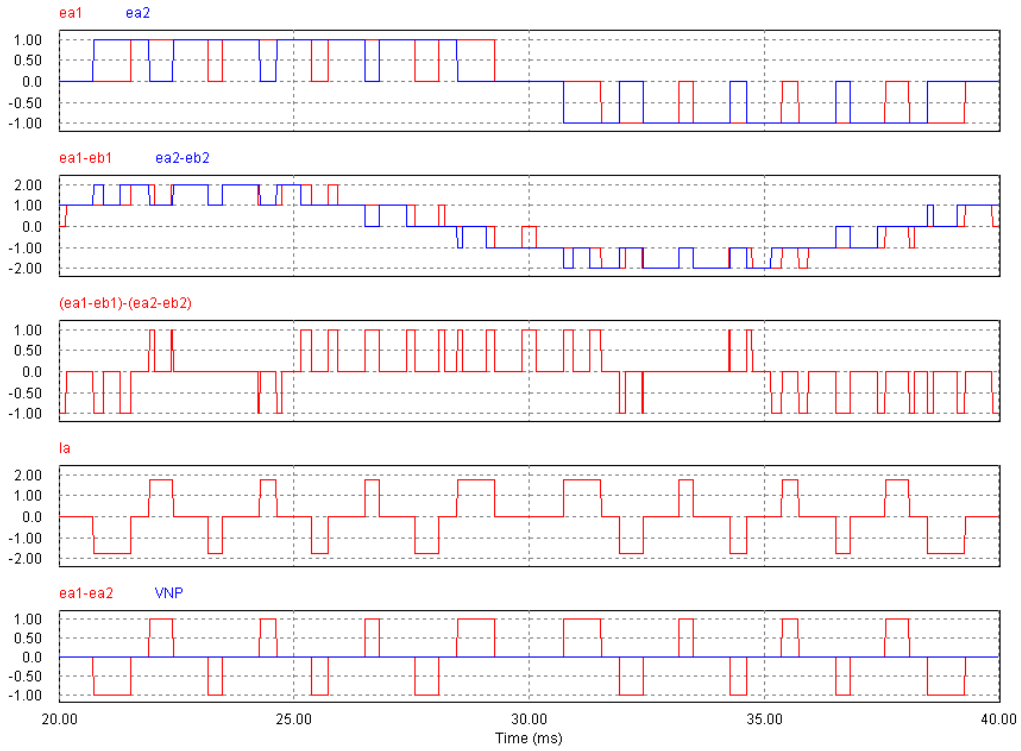

Figure 8-29 The waveforms of: (1st row) the phase to neutral (ea1, ea2) and (2st row) phase to phase (vab1=ea1-eb1, vab2=ea2-eb2) voltages of the two converters, difference between the phase to phase voltages vab1-vab2=(ea1-eb1)-(ea2-eb2) of the two converters, the ripple current Ia in the resistance, the difference between the phase to neutral voltages (ea1-ea2) and the voltage VNP between the two neutral points.

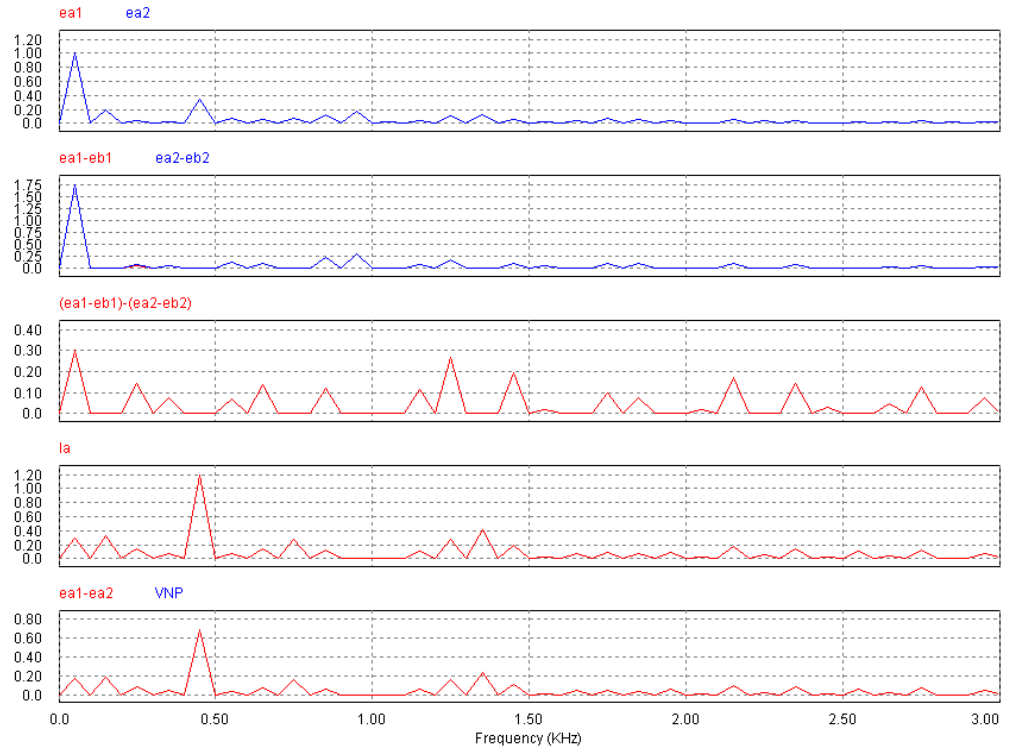

Figure 8-30 The harmonic components of: (1st row) the phase to neutral (ea1, ea2) and (2st row) phase to phase (vab1=ea1-eb1, vab2=ea2-eb2) voltages of the two converters, difference between the phase to phase voltages vab1-vab2=(ea1-eb1)-(ea2-eb2) of the two converters, the ripple current Ia in the

resistance, the difference between the phase to neutral voltages (ea1-ea2) and the voltage VNP between the two neutral points.

With the connection between the two neutral points the biggest harmonic component of the current ripple in the resistance is at 450 Hz. If the carrier waveforms of two converters connected to the same dc link have a displacement of phase, the current ripple in the switches increases a lot and also the losses.

9 Design of the ac/dc section of AGPS based on Active Front-End approach

The input data, which have to be considered during the design of the ac/dc conversion section of AGPS, are [1]:

- Rating power = 54.7 MW;
- dc-link voltage:
  - Nominal value = 6.5 kV;
  - Maximum variation under stationary regimes = ± 6 %;
  - Maximum variation under transients = ± 10 %;
- Grid voltage:
  - Nominal value: 66 kV;
  - Maximum value: 72 kV;
  - Minimum value: 62 kV;
- Short circuit capacity of the 66 kV line is in the range from 1.7 GVA to 2 GVA.
- The dc link capacitance value is 50 mF, the same one used in the analysis of the technical note TW6-THHN-NBD1 in order to compare the two ac/dc conversion topologies. Moreover in this study the dc link is split in five independent parts, one for each acceleration stage; so the capacitance is 10 mF per stage. It should be noted that the capacitance is split uniformly between the stages to achieve a modular system, even if the load of each stage is not the same.

The AGPS ac/dc conversion section topology (Figure 9-1) proposed in this study is based on NPC VSC topology (see paragraph 8.1) in the Synchronous Active Front End configuration by using CBPWM modulation strategy with Zero Sequence Signal with 1/6 amplitude of the fundamental (1/6 ZSS CBPWM) (see paragraph 8.3.1). It should be noted that there is only a two windings transformer and it is used an L filter.

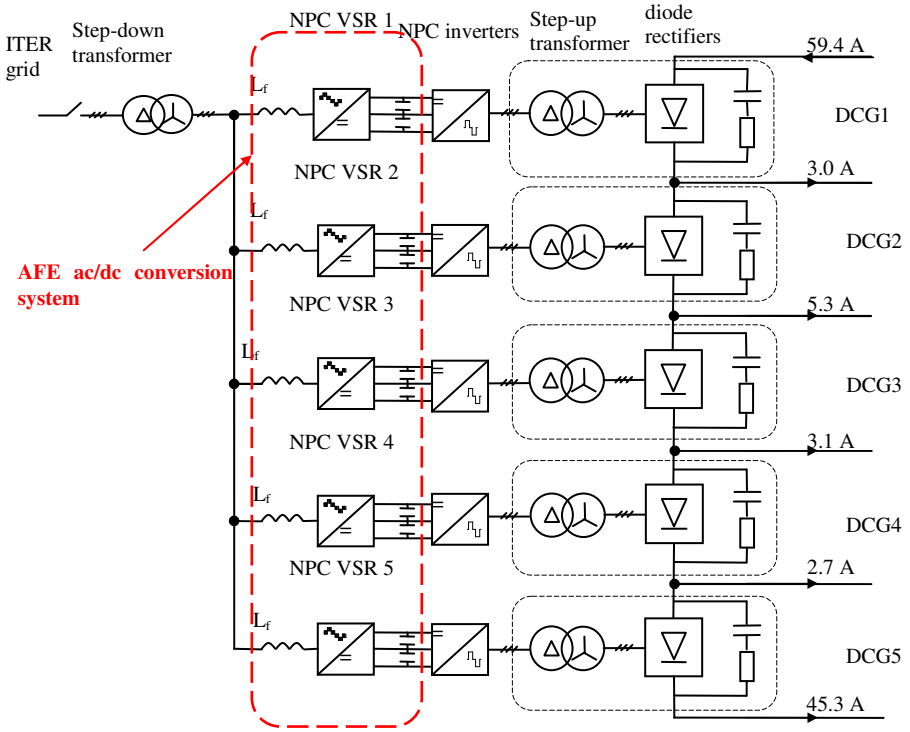

Figure 9-1 Ac/dc section of AGPS based on Synchronous Active Front-End approach.

If two converters are connected to the same acceleration stage, i.e at the same dc link, the switch losses increase a lot when the carrier waveforms have a displacement of phase. So each acceleration stage has two NPC VSCs which operate with the same carrier waveforms, while the carrier waveforms of different stages have a displacement of phase. A short description of the phenomena is given in the paragraph 8.7.1.1.
Hence the displacement of phase of carrier waveforms is applied only between the converters of different acceleration stages to reduce the ripple of the current injected into the grid; anyway a good reduction of the harmonic in the grid current is achieved (see paragraph 9.5)

The following steps have been carried out to design SAFE conversion section:

- Choice of the transformer secondary voltage and of the L filter;
- Choice of the switching frequency;
- Description of the model used to optimize the control parameters;
- Thermal analysis on the switches to determine the number of parallel converters;
- To verify that the current harmonic injected into the grid are below the limits request in IEEE 519-1992 [23];
- Fault Analysis

Initially only the first stage 1000-800 kV is considered to make easier the study, because it has the greater power consumption.

9.1 Choice of the transformer secondary voltage and of the L filter

The turn ratio n of the transformer has to be chosen in order to have a high secondary voltage so as to reduce the current phase, with consequent minimize of the losses on the switches. Nevertheless the limit imposed from the equation 8-47 of the L filter calculation has to be considered. A small L filter involves high current harmonics and high ripple current; moreover the inductance L_f has to decouple the parallel converters.
A good compromise has been found with this transformer:

- Three-phase delta/star transformer;
- Turn ratio n = 30;
- Voltage ratio k = n/√3 = 30/√3= 17.32;
- Rated power S_N = 60 MVA;
- Rated primary voltage V_{1N}= 66 kV;
- Rated secondary voltage V_{2N}= V_{1N} /k = 3811 V;
- Short circuit power $p_{SC\%}$ = 0,6 %;
- Short circuit voltage $v_{SC\%}$ = 10 %;

The rated secondary current is:

$$I_{2N} = \frac{S_N}{\sqrt{3} \cdot V_{2N}} = \frac{60 \cdot 10^6}{\sqrt{3} \cdot 3811} = 9091[A] \qquad \text{(eq. 9-1)}$$

The transformer short circuit impedance is:

$$Z_{SC,2} = \frac{v_{SC\%}}{100} \cdot \frac{V_{2N}}{\sqrt{3} \cdot I_{2N}} = 0{,}1 \cdot \frac{3811}{\sqrt{3} \cdot 9091} = 24{,}2[m\Omega] \qquad \text{(eq. 9-2)}$$

The transformer short circuit resistance is:

$$R_{SC,2} = \frac{p_{SC\%}}{100} \cdot \frac{S_N}{3 \cdot I_{2N}^2} = 0{,}006 \cdot \frac{60 \cdot 10^6}{3 \cdot 9091^2} = 1{,}452[m\Omega] \qquad \text{(eq. 9-3)}$$

The transformer short circuit inductance is:

$$L_{SC,2} = \frac{\sqrt{Z_{SC,2}^2 - R_{SC,2}^2}}{2 \cdot \pi \cdot f} = \frac{\sqrt{24{,}2^2 - 1{,}452^2} * 10^{-3}}{2 \cdot \pi \cdot 50} = 0{,}0769[mH] \quad \text{(eq. 9-4)}$$

The base impedance is:

$$Z_{B,2} = \frac{V_{2N}}{\sqrt{3} \cdot I_{2N}} = \frac{3811}{\sqrt{3} \cdot 9091} = 242[m\Omega] \quad \text{(eq. 9-5)}$$

And the base inductance is:

$$L_{B,2} = \frac{Z_{B,2}}{2 \cdot \pi \cdot f} = \frac{242 \cdot 10^{-3}}{2 \cdot \pi \cdot 50} = 0.77[mH] \quad \text{(eq. 9-6)}$$

The maximum total inductance ($L_{TOT,M} = L_{SC,2} + L_{f,M}$) is calculated for the first acceleration stage DCG1 (1000-800 Kv), i.e. the stage with greater power consumption; by considering:

- the modulation strategy is 1/6 ZSS CBPWM with a maximum modulation index m_{max}=1.1547;
- a margin of -5 % on dc-link voltage to avoid over modulation, V_{dc}=6500 V;
- the maximum grid voltage effective value 72 kV has to be used, hence the maximum secondary phase voltage peak value $E_{2,PEAK}$ is:

$$E_{2,PEAK} = \frac{V_{1,MAX}}{k} \cdot \frac{\sqrt{2}}{\sqrt{3}} = \frac{72000}{17.32} \cdot \frac{\sqrt{2}}{\sqrt{3}} = 3394[V] \quad \text{(eq. 9-7)}$$

- only the first stage is considered in the computation, so an equivalent impedance transformer has to be calculated. The equivalence factor ke is achieved by the acceleration grid currents shown in the eq 9-8:

$$ke = \frac{\sum I_{AG,i}}{I_{AG,1}} = \frac{59.4 + 56.4 + 51.1 + 48 + 45.3}{59.4} = \frac{260.2}{59.4} = 4.38 \quad \text{(eq. 9-8)}$$

the equivalent transformer resistance and inductance are respectively:

$$R_{SC,e} = R_{SC,2} \cdot ke = 1{,}452 \cdot 4.38 = 6.36[m\Omega]$$
$$L_{SC,e} = L_{SC,2} \cdot ke = 0.0769 \cdot 4.38 = 0.337[mH] \quad \text{(eq. 9-9)}$$

and the equivalent base inductance is

$$L_{B,e} = L_{B,2} \cdot ke = 0.77 \cdot 4.38 = 3.374[mH] \quad \text{(eq. 9-10)}$$

- the secondary phase current peak value of the first stage is calculated with a margin of +5% on the acceleration grid current and at maximum grid voltage, is given by:

$$I_{2,PEAK} = \frac{E_{AG} \cdot I_{AG,1} \cdot 1.05}{\sqrt{3}} \cdot \frac{k}{V_{1,MAX}} \cdot \sqrt{2} = \quad \text{(eq. 9-11)}$$
$$= \frac{2 \cdot 10^5 \cdot 59.4 \cdot 1.05}{\sqrt{3}} \cdot \frac{17.32}{72000} \cdot \sqrt{2} = 2450\ [A]$$

The maximum total inductance value for the first acceleration stage DCG1 results (eq. 8-38):

$$L_{TOTM,e} = \frac{\sqrt{\left(\frac{m_{max} \cdot Vdc \cdot 0.95}{2}\right)^2 - E_{2,PEAK}^2}}{\omega \cdot I_{2,PEAK}} = \frac{\sqrt{\left(\frac{1.1547 \cdot 6500 \cdot 0.95}{2}\right)^2 - 3394^2}}{2 \cdot \pi \cdot 50 \cdot 2450} = 1.417[mH] \quad \text{(eq. 9-12)}$$

The maximum filter inductance $L_{fM,e}$ is:

$$L_{fM,e} = L_{TOTM,e} - L_{SC,e} = 1.418 - 0.337 = 1.081[mH] \quad \text{(eq. 9-13)}$$

In percent it is:

$$L_{fM,e\%} = \frac{L_{fM,e}}{L_{B,e}} \cdot 100 = \frac{1.081}{3.373} \cdot 100 = 32\% \qquad \text{(eq. 9-14)}$$

In the Table 9-1 the L filter values for several turn ratios are shown.

Table 9-1 The L filter values for several turn ratios.

Turn ratio	V_{2N}	L_{Be}	$L_{SC,e}$	$L_{TOTM,e}$	$L_{fM,e}$	$L_{fM,e\%}$
n	[V]	[mH]	[mH]	[mH]	[mH]	%
28	4083	3.874	0,387	impossible		
29	3942	3.611	0,360	0,831	0,470	13
30	3811	3.374	0,337	1,417	1,081	32
31	3688	3.160	0,315	1,743	1,427	45

The turn ratio 30 has been chosen to achieve enough margins in the design of the inductance $L_{f,e}$; by increasing $L_{f,e}$ the ripple current into the side converter is reduced and the switching losses too. Nevertheless a big $L_{f,e}$ means a huge and expensive filter.
For this study $L_{f,e}$ has been chosen equal to **0.54** mH (16 %). This value is also used in the other stage to comply with the modularity principle.
For each acceleration stage, the value of the L_f filter of a single converter is:

$$L_f = Nc \cdot L_{f,e} \qquad \text{(eq. 9-15)}$$

where N_C is the number of parallel NPC converters.

9.2 Choice of the switching frequency

The bandwidth of the inner current control of the NPC VSC has to be determined by considering the limits imposed to the dc link voltage during transient condition [1]. They are ± 10 % of the dc link voltage. The more critical transient for the control is the sudden beam off event consequent a grid breakdown. In this case the NPC VSC output dc current has to be taken at 0 in the shorter possible time, in order to avoid overvoltages on the dc link capacitors.
The power of the first acceleration stage (with a margin of +5% on the current) is:

$$P_{DCG1} = E_{DCG1} \cdot I_{DCG11} \cdot 1.05 = 200000 \cdot 59.4 \cdot 1.05 = 12{,}474[MW] \qquad \text{(eq. 9-16)}$$

The dc link output current $I_{dc,1}$ at 6500 V is:

$$I_{dc,1} = \frac{P_{DCG1}}{V_{dc}} = \frac{12.474 \cdot 10^6}{6500} = 1919[A] \qquad \text{(eq. 9-17)}$$

The current control action on $I_{dc,1}$ may be approximated with a negative ramp (Figure 9-2).

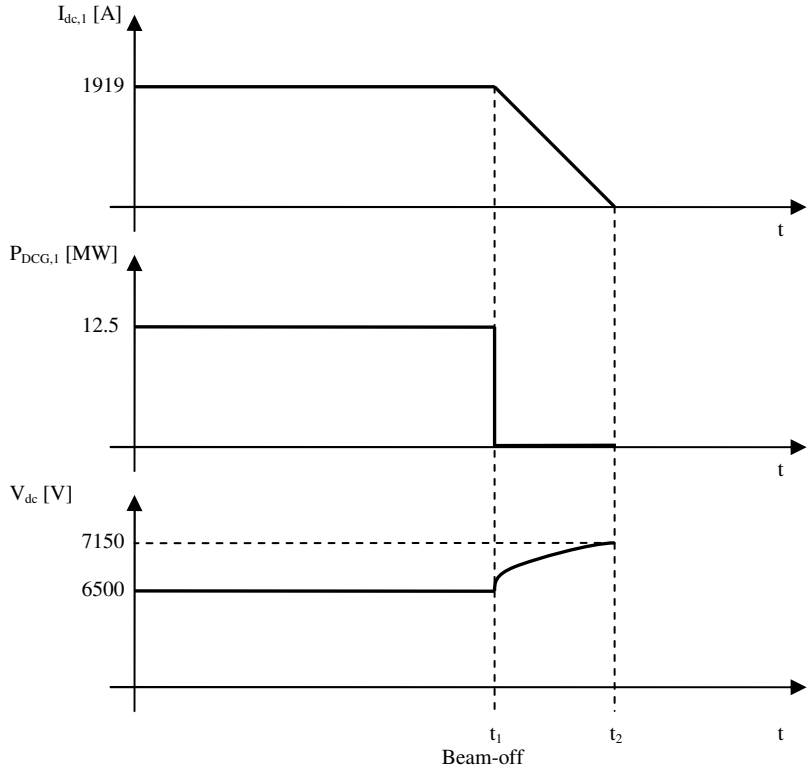

Figure 9-2 NPC VSC output current Idc, beam power and dc link voltage before and after a beam off event.

The maximum dc-link voltage variation ΔV_{dc} is 650 V (10% of 6500 V). The following equations are used to determine the maximum time interval $T_{off}=(t_2-t_1)$ to take at 0 A the current I_{dc}. The electrical charge Q_{off} storied in dc link capacitor C_{dc} during the transient is:

$$Q_{off} = \frac{(t_2 - t_1)\cdot I_{dc,1}}{2} = \frac{T_{off}\cdot I_{dc,1}}{2} \qquad \text{(eq. 9-18)}$$

By considering

$$Q_{off} = C_{dc}\cdot \Delta V_{dc} \qquad \text{(eq. 9-19)}$$

the time T_{off} results:

$$T_{off} = \frac{2\cdot Q_{off}}{I_{dc,1}} = \frac{2\cdot C_{dc}\cdot \Delta V_{dc}}{I_{dc,1}} = \frac{2\cdot 10\cdot 10^{-3}\cdot 650}{1919} = 6.77[ms] \qquad \text{(eq. 9-20)}$$

A rough current control bandwidth f_C may be calculated:

$$f_C = \frac{1}{T_{off}} = \frac{1}{6.77\cdot 10^{-3}} = 148[Hz] \qquad \text{(eq. 9-21)}$$

and the switching frequency f_{SW} results:

$$f_{SW} = 2\cdot f_C = 2\cdot 148 = 296[Hz] \qquad \text{(eq. 9-22)}$$

For this study a switching frequency of 450 Hz is chosen, so the frequency modulation ratio m_f (f_{SW}/f=450/50= 9) is an integer and odd number, hence sub and even harmonics are avoided [30]; moreover there is enough margin to design the current control parameter: the maximum f_C value is f_{SW}/2=225 Hz.

9.3 Description of the model and control parameters optimization for AFE converter

The model used to optimize the control parameters for a single AFE converter is shown in Figure 9-3. It is simulated with PSIM a program capapbe to reproduce the instantaneous waveform of voltage and currents. Only a NPC VSC is present and a current source in the dc-link side describes the first acceleration stage DCG1. More details are illustrated below.

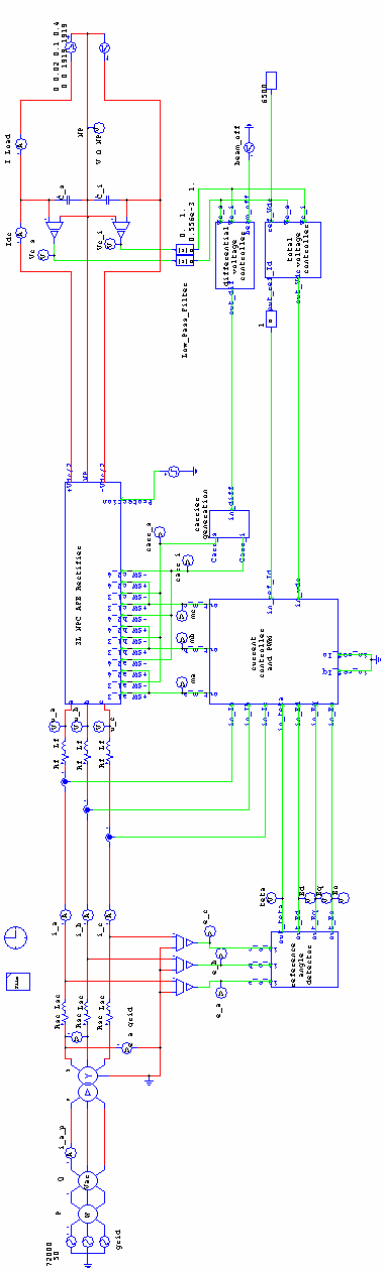

Figure 9-3 Model used to optimize the control parameters

9.3.1 Power circuit model

The grid is represented by three star connected voltage sources, which may supply 62 or 72 kV line voltage at 50 Hz.
The equivalent data for the first acceleration stage found in section 3.1 are used for the transformer and L_f filter models (Figure 9-4):

- Short circuit resistance $R_{SC}= R_{SC,e} = 1.452 \cdot 4.38 = 6.36$ mΩ;
- Short circuit inductance $L_{SC}= L_{SC,e} = 0.0769 \cdot 4.38 = 0.337$ mH;
- Turn ratio n=30;
- With only a NPC VSC the filter L_f is equal to $L_{f,e}= 0.54$ mH (eq. 3-12) and R_f is supposed equal to 1 mΩ.

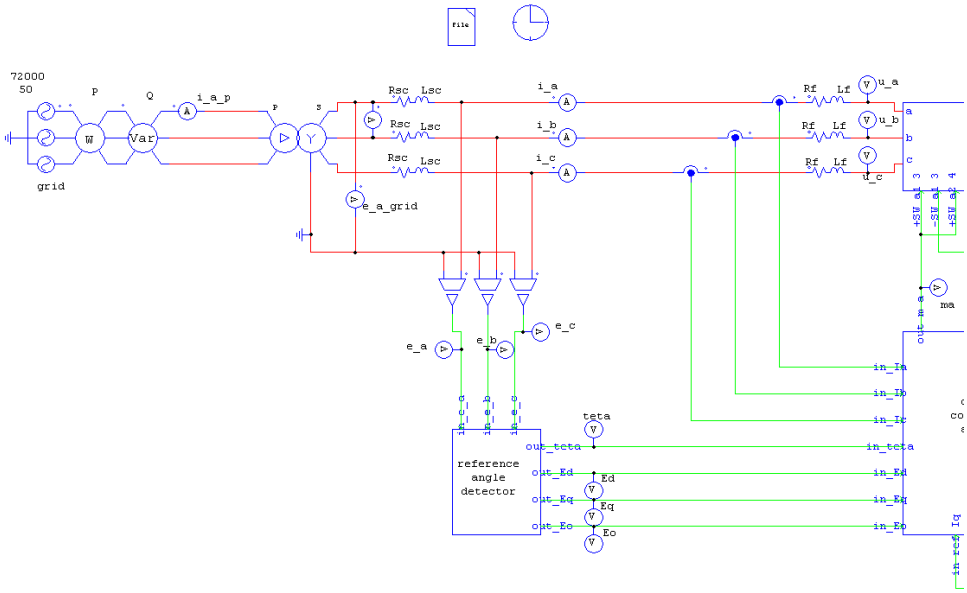

Figure 9-4 Details of grid, transformer and filter models.

The power and control connections and the model of NPC AFE rectifier are shown in Figure 9-5 and Figure 9-6.

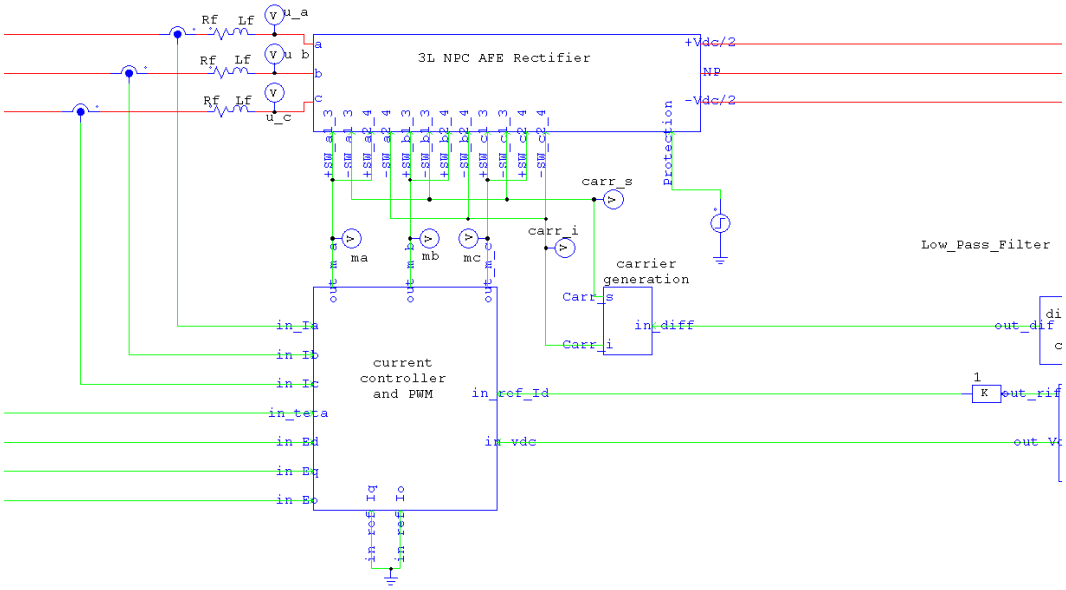

Figure 9-5 NPC AFE rectifier power and control connection.

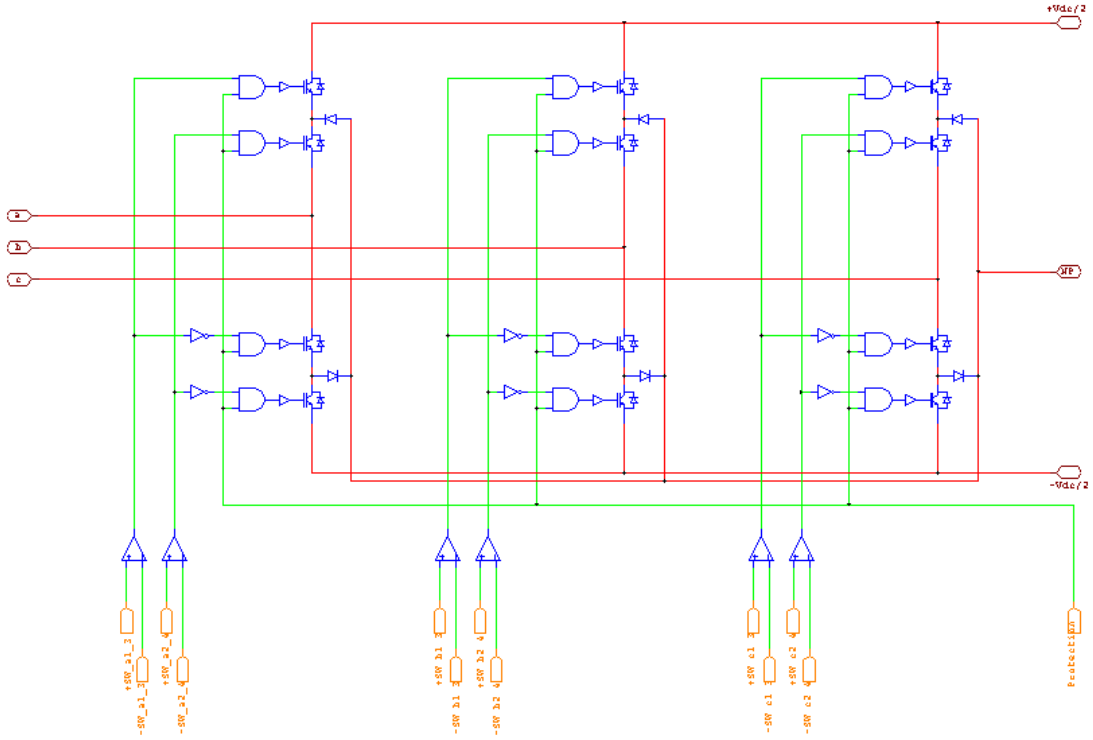

Figure 9-6 NPC AFE rectifier model.

The dc link capacitors of the first stage have a total capacitance of 10 mF, hence the upper Cs and lower Ci capacitors have 20 mF each one. Current source imposes a piecewise linear waveform with a peak current of 1919 A, which corresponds to the rated power of the first stage with a margin of +5% at dc-link voltage of 6500 V, and a frequency of 1.6 Hz. The current rise time is 80 ms; it is chosen equal to the maximum rise time of the acceleration grid voltage [1]. The beam-off event is simulated too (Figure 9-7).

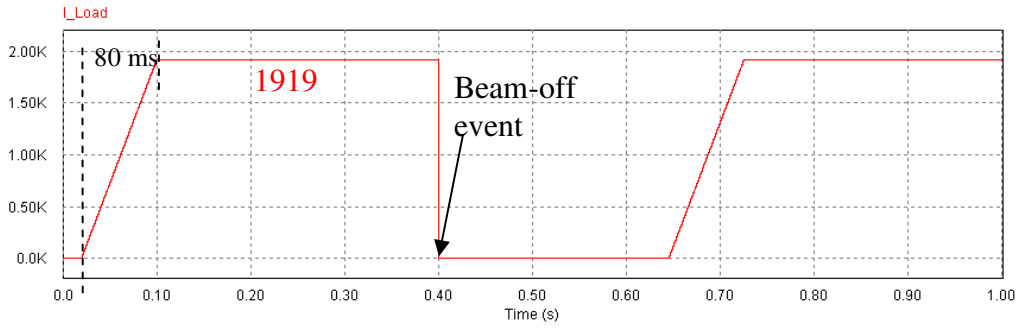

Figure 9-7 Current source waveform used to simulate the acceleration grid load with 1.6 Hz frequency.

The dc link side model is shown in Figure 9-8.

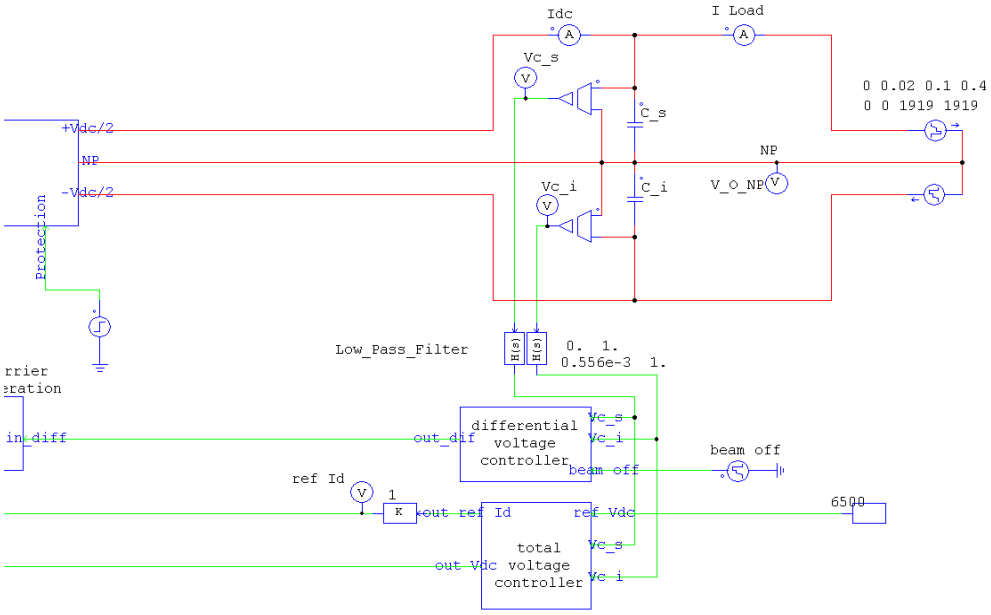

Figure 9-8 The dc link side model.

9.3.2 Current control and CB PWM with 1/6 ZSS strategy model

The maximum dc link voltage variation requested in [1] has been achieved with a current control bandwidth f_C of about 135 Hz (slightly lower than the value calculated in eq. 3-21), and yields:

$$\alpha_C = 2 \cdot \pi \cdot f_C = 2 \cdot \pi \cdot 135 = 850 \left[\frac{rad}{s} \right] \qquad \text{(eq. 9-23)}$$

by considering the equation discussed in the section 8.3, the proportional and integral gain are respectively:

$$K_P = L_f * \alpha_C = 0.54 \cdot 10^{-3} \cdot 850 = 0.459 \qquad \text{(eq. 9-24)}$$

$$K_I = R_f \cdot \alpha_C = 1 \cdot 10^{-3} \cdot 850 = 0.85 \qquad \text{(eq. 9-25)}$$

The low pass filter is used to reduce the high order harmonics in the current measurement; the constant time T_{LPF} has been chosen by considering the control stability (symmetrical optimum criterion):

$$T_{LPF} \le \frac{1}{2 \cdot \alpha_C} = \frac{1}{2 \cdot 850} = 0.588 \cdot 10^{-3} \left[\frac{s}{rad} \right] \qquad \text{(eq. 9-26)}$$

A constant time $T_{LPF}= 0.556 \cdot 10^{-3}$ has been used. The low pass filter may be considered equivalent to the delay introduced by digital sampling process. By using the equation 2-37, the equivalent sampling frequency f_S results:

$$T_{LPF} = 1.5 \cdot T_S \Rightarrow f_S = \frac{1}{T_S} = \frac{1.5}{T_{LPF}} = \frac{1.5}{0.556 \cdot 10^{-3}} = 2700 [Hz] \qquad \text{(eq. 9-27)}$$

The PSIM model of the current control is shown in Figure 9-9.

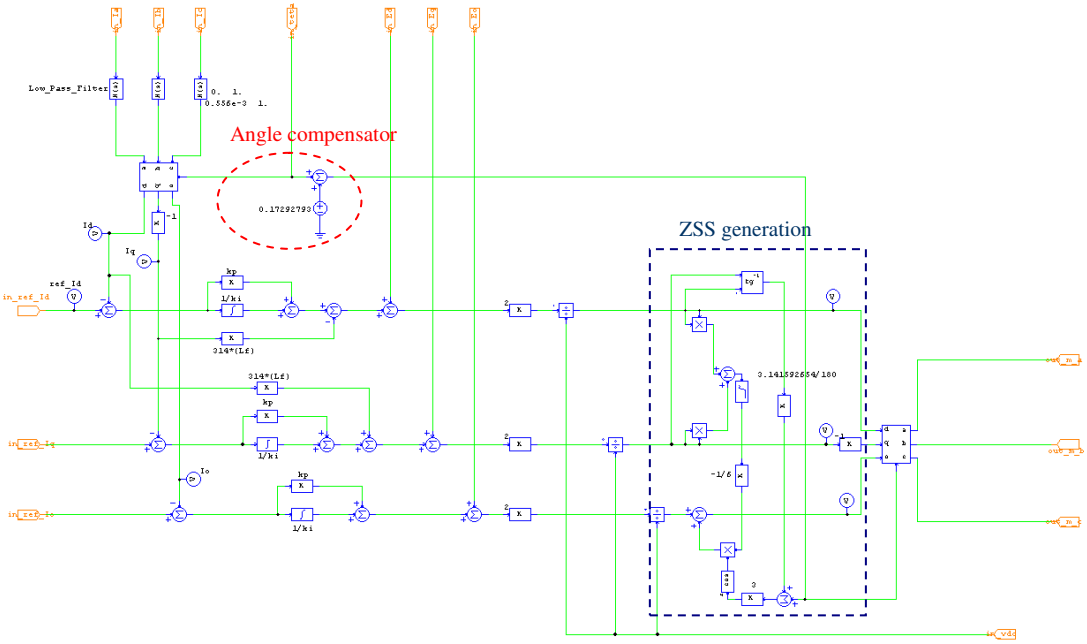

Figure 9-9 The PSIM model of the current control

An angle compensator has been inserted to improve the control, because the Lead-Lag block of the feed-forwarded voltages is not used to avoid harmonics amplification. The angle compensator value is achieved by considering the error phase introduced by the low pass filter at 50 Hz:

$$angle_{comp} = \arctan\left(2 \cdot \pi \cdot 50 \cdot T_{LPF}\right) = \arctan\left(2 \cdot \pi \cdot 50 \cdot 0.556 \cdot 10^{-3}\right) = 0.173[rad] \quad \text{(eq. 9-28)}$$

In the Figure 9-9 it may be noted the circuit model to obtain the zero sequence signal at 1/6 of fundamental amplitude.
The waveforms of the phase current and of the modulation signal, the active and reactive power consumptions in relation with the dc load current are shown in the Figure 9-10.

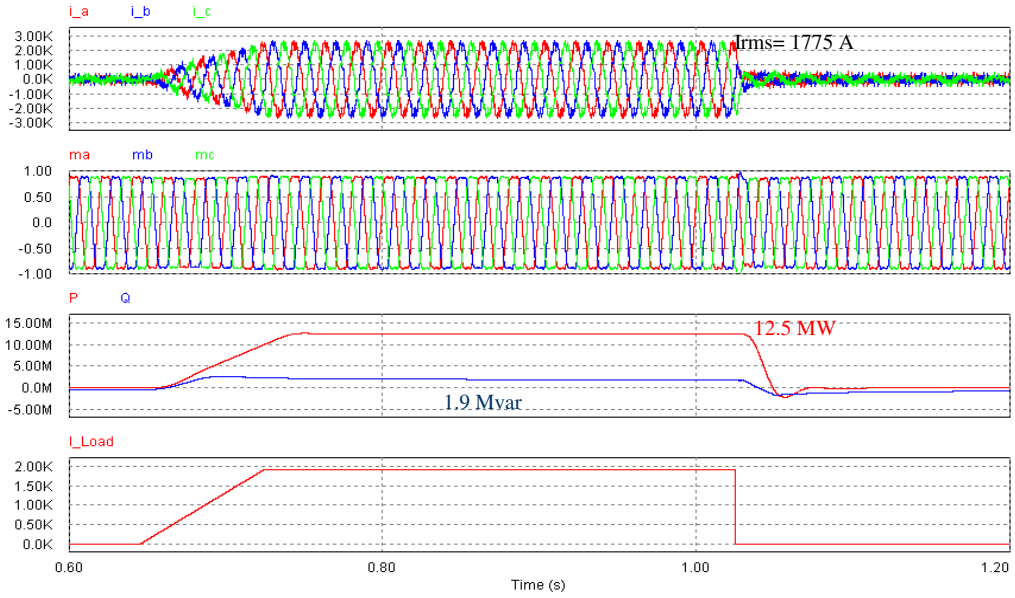

Figure 9-10 The waveforms of the phase current and of the modulation signal, the active and reactive power consumptions in relation with the dc load current with 72 kV grid voltage.

It should be noted that the NPC VSC absorbs a 1.9 Mvar reactive power. It is due principally to the phase voltage measurements, which are taken downstream of the transformer, hence the reactive power of the transformer short circuit inductance L_{SC} is not compensate. For example at 72 kV grid voltage, the secondary phase current rms value is about 1775 A. The reactive power due to the transformer inductance results:

$$Q_{TR} = 3 \cdot \omega \cdot L_{SC,e} \cdot I_{RMS}^2 = 3 \cdot 2 \cdot \pi \cdot 50 \cdot 0.0769 \cdot 4.38 \cdot 10^{-3} \cdot 1775^2 = 1[M \text{ var}] \qquad \text{(eq. 9-29)}$$

The remaining reactive power is due to the low pass filters, which make worse the current control.

9.3.3 The reference angle detector

The model of reference angle detector described in section 8.4 is shown in Figure 9-11.

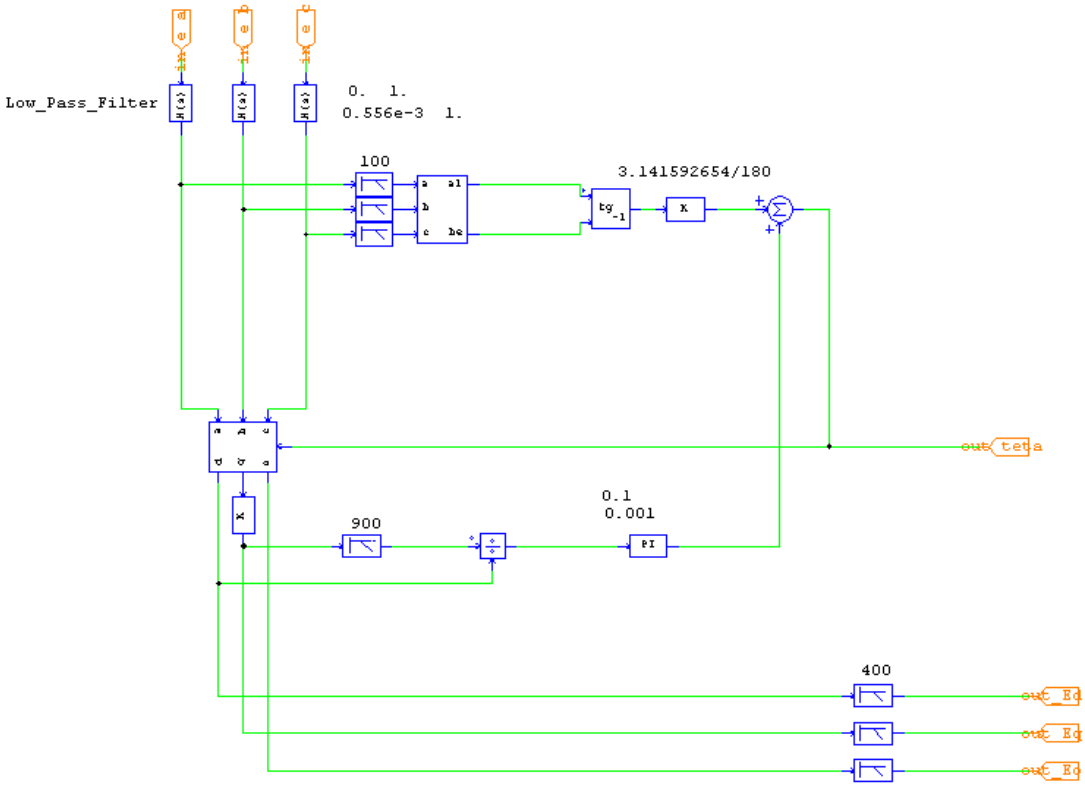

Figure 9-11 The reference angle detector model

The PI transfer function of the reference angle detector is:

$$G_{PI} = K_P \cdot \frac{(1+sT)}{sT} = 0.1 \cdot \frac{(1+s \cdot 0.001)}{s \cdot 0.001} \qquad \text{(eq. 9-30)}$$

The regulator parameters are designed by the simulation in order to achieve a good dynamic response.

A lead lag block is not used, on the contrary second order low pass filters ($f_{cut\text{-}off}$ = 400 Hz) are added in the voltages Ed, Eq and Eo to reduce the harmonics into the modulation signal, even if they make worse the current control. The reference angle θ, Ed, Eq and Eo voltages in relation with the dc load current are shown in Figure 9-12.

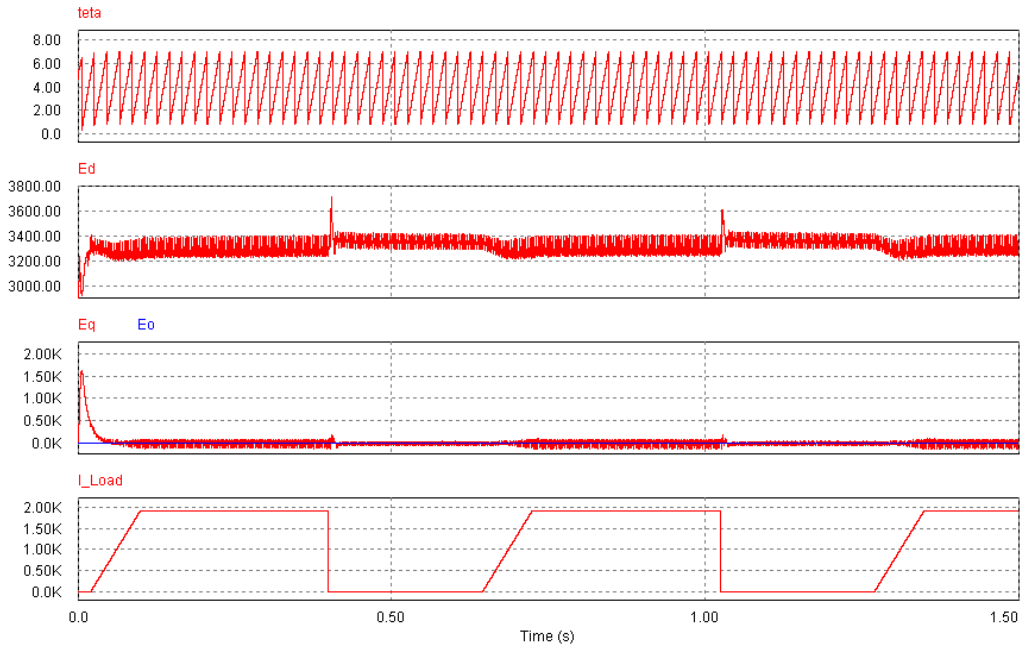

Figure 9-12 The reference angle θ, Ed, Eq and Eo voltages in relation with the dc load current at 72 kV grid voltage.

It should be noted that the Ed voltage changes with the dc load current because of the voltage drop on the transformer short circuit impedance.

9.3.4 The dc-link total voltage controller

The dc link voltage reference is set to 6500 V.
The PI regulator parameters of the dc-link total voltage controller are calculated by considering the equations 8-45 (γ=2.09 has been chosen to achieve good dynamic performance):

$$R_L = \frac{V_{dc}}{I_{dc,1}} = \frac{6500}{1919} = 3.387[\Omega]$$

$$C = 10[mF]$$

$$\gamma = 2.09 \geq 2$$

$$\alpha_{Vdc} = \frac{\alpha_C}{\gamma} = \frac{850}{2.09} = 407\left[\frac{rad}{s}\right] \qquad \text{(eq. 9-31)}$$

$$T_{Vdc} = R_L \cdot C = 3.387 \cdot 10 \cdot 10^{-3} = 3.39 \cdot 10^{-2}\left[\frac{s}{rad}\right]$$

$$K_{Vdc} = \alpha_{Vdc} \cdot \frac{2 \cdot T_{V\,dc}}{\sqrt{3} \cdot R_L} = \alpha_{Vdc} \cdot \frac{2 \cdot C}{\sqrt{3}} = 407 \cdot \frac{2 \cdot 10 \cdot 10^{-3}}{\sqrt{3}} = 4.7$$

The dc link total voltage controller model is shown in Figure 9-13.

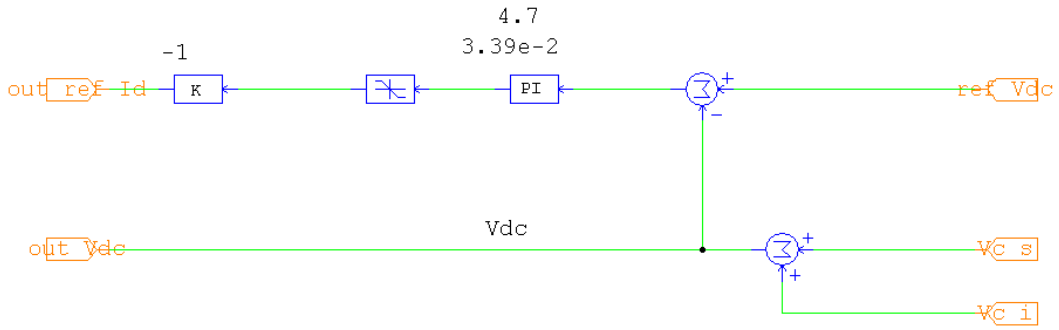

Figure 9-13 The dc link total voltage controller PSIM model.

The constant K -1 is inserted, so the output of the dc link voltage control is coherent with the current reference measurements. The dc link voltages in relation with the dc load current at 72 kV and 62 kV grid voltages are shown in the Figure 9-14.

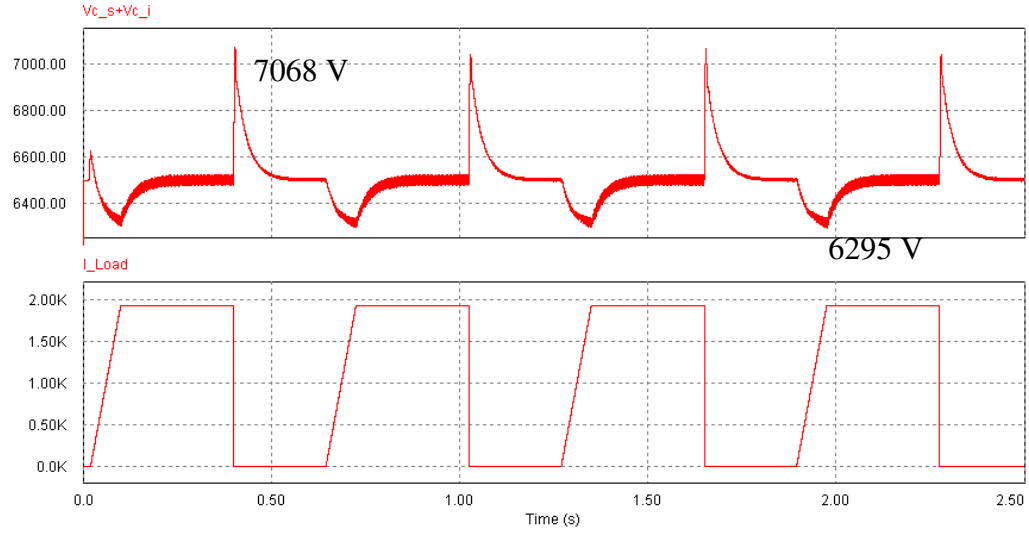

a) 72 kV

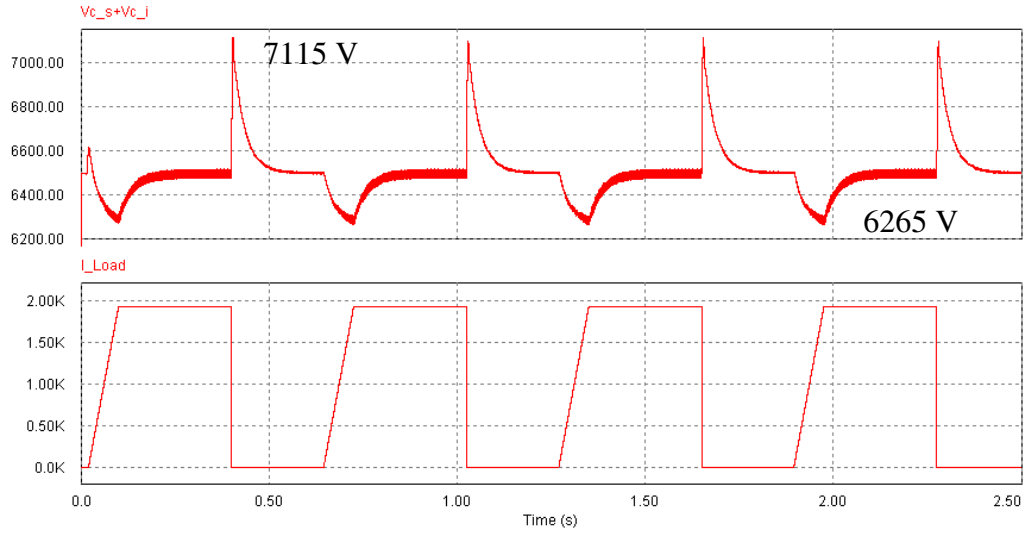

b) 62 kV

Figure 9-14 The dc link voltages in relation with the dc load current at 72 kV (a) and 62 kV (b) grid voltages.

The dynamic response of the dc link control is less efficient with the decrease of the grid voltage; however the dc link total voltage control is able to comply with the limits

±10 % (5850 V ÷ 7150 V) of the dc-link voltage at 6500 V requested in [1] for any grid voltages in the 62 ÷ 72 kV range.

9.3.5 The dc-link differential voltage control

The dc link differential voltage control model is shown in Figure 9-15.

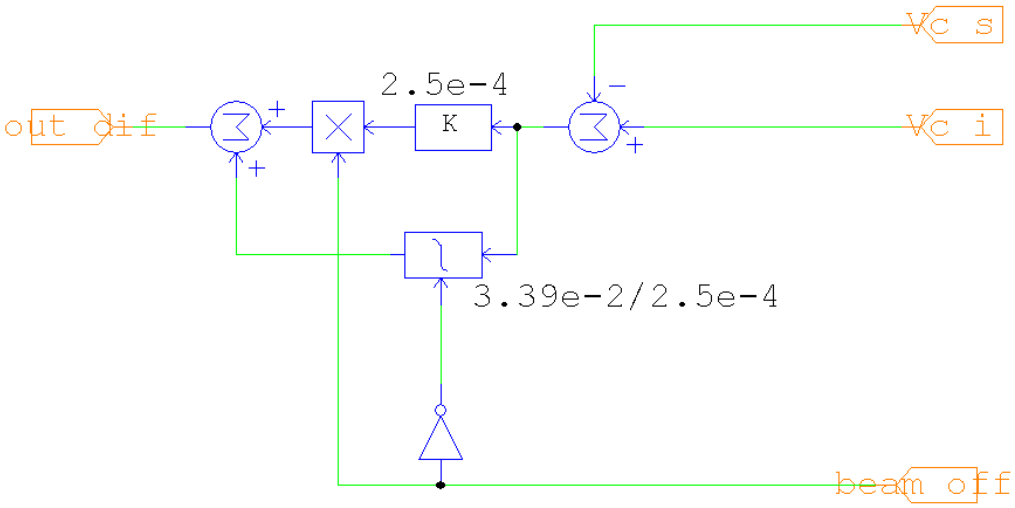

Figure 9-15 The dc link differential voltage control PSIM model.

The transfer function of the PI regulator is:

$$G_{PI} = K_P \cdot \frac{(1+sT)}{sT} = 2.5 \cdot 10^{-4} \cdot \frac{(1+s \cdot 3.39*10^{-2})}{s \cdot 3.39*10^{-2}} \qquad \text{(eq. 9-32)}$$

the constant time T is chosen equal to total voltage control T_{Vdc}.
During the beam-off phase, the output differential voltage control is set to 0 value and the integrator is reset, because this control operates correctly only when an active power is absorbed.
The voltages on the upper Cs and lower Ci capacitors in relation with the dc load at 72 and 62 kV grid voltages are shown in the Figure 9-16.

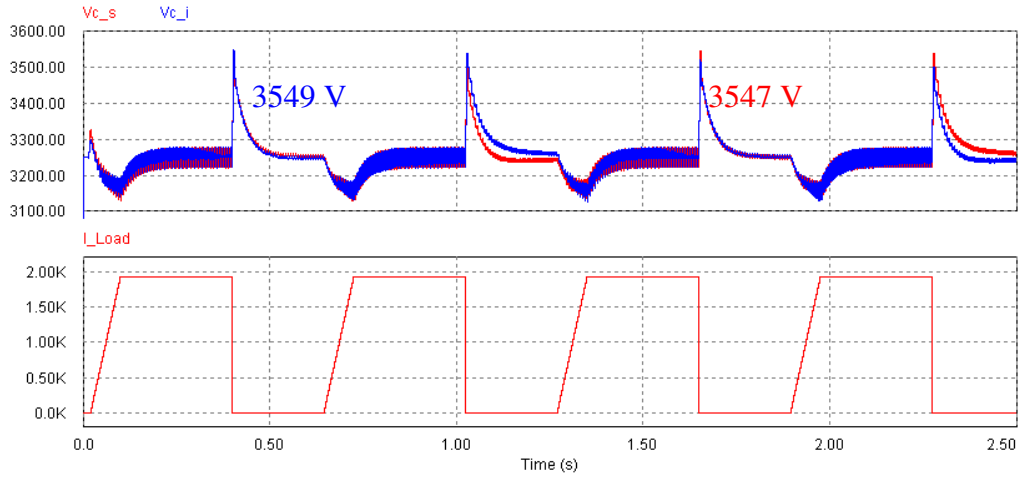

a) 72 kV

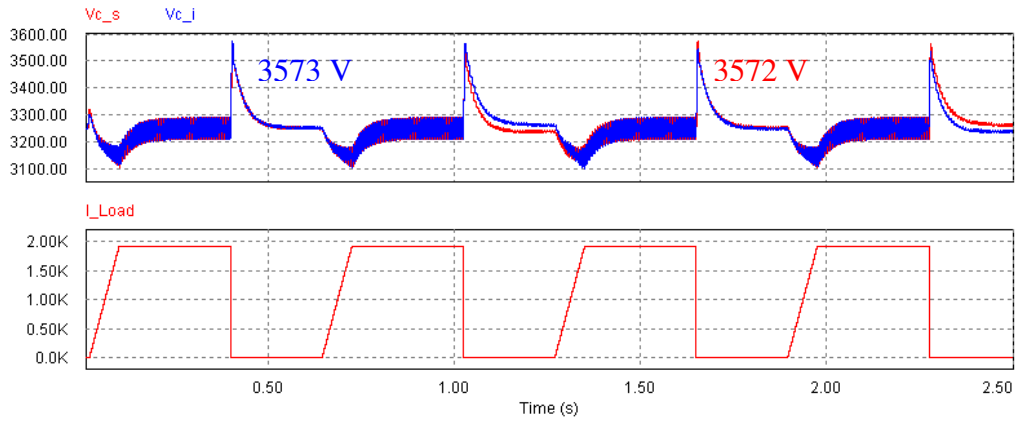

b) 62 kV

Figure 9-16 The voltages on the upper Cs and lower Ci capacitors in relation with the dc load at 72 (a) and 62 kV (b) grid voltages.

The maximum voltage difference between the two capacitors is about 20 V.

9.3.6 The carrier waveforms generation model

The carrier waveforms frequency f_{PWM} is equal to the switching frequency f_{SW} of 450 Hz, chosen in the section 9.2. The PSIM model of the carrier waveforms generation, illustrated in section 8.6, and the respective waveforms are shown respectively in Figure 9-17 and Figure 9-18.

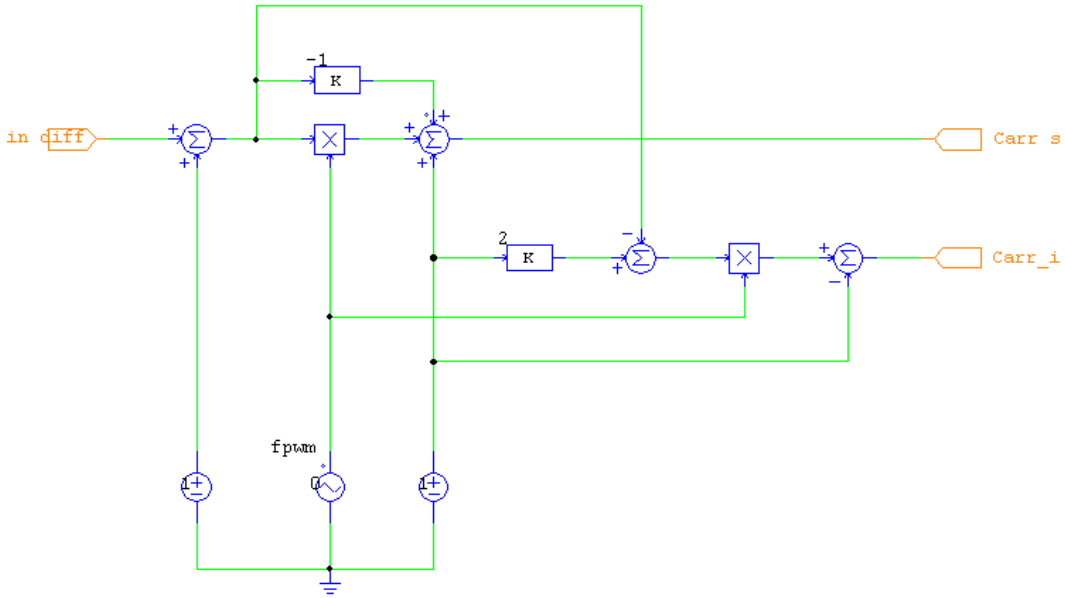

Figure 9-17 The carrier waveforms generation PSIM model.

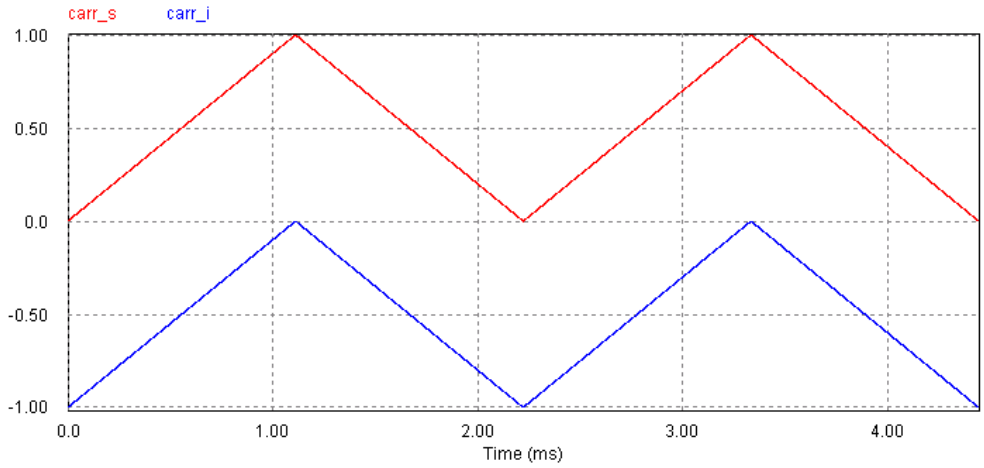

Figure 9-18 The carrier waveforms.

9.4 Thermal analysis on the switches to determine the number of parallel NPC VSC in Synchronous AFE configuration

9.4.1 The PSIM circuit model used to carry out the thermal analysis on the switches

The PSIM model used to calculate the number of NPC VSCs in parallel for every acceleration stage is shown in Figure 9-19. There are five converters, one for each acceleration stage. They are in SAFE configuration, where the respective carrier waveforms have a displacement of phase equal to 360/5 degrees.

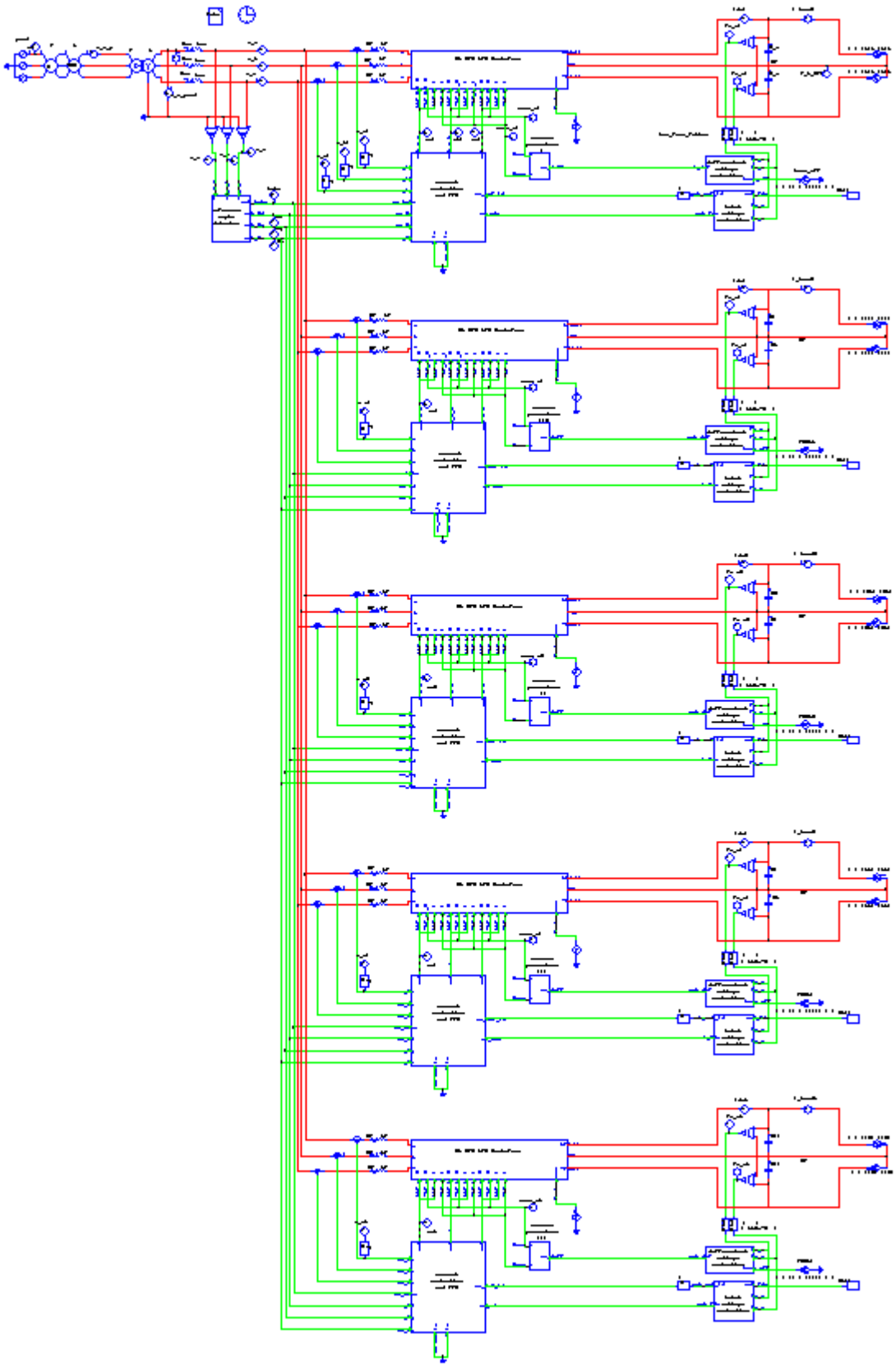

Figure 9-19 The PSIM model of five NPC VSCs in SAFE configuration.

Some modifications have to be done respect to the circuit model seen in the previous section:

- The real transformer resistance and inductance value are used:
  -Short circuit resistance R_{SC}= 1.452 mΩ;
  -Short circuit inductance L_{SC}= 0.0769 mH;
- In the upper NPC VSC 1 model, which supplies the DCG1, some ammeters have been put in series to the switches of each half leg to measure their current (Figure 9-20)

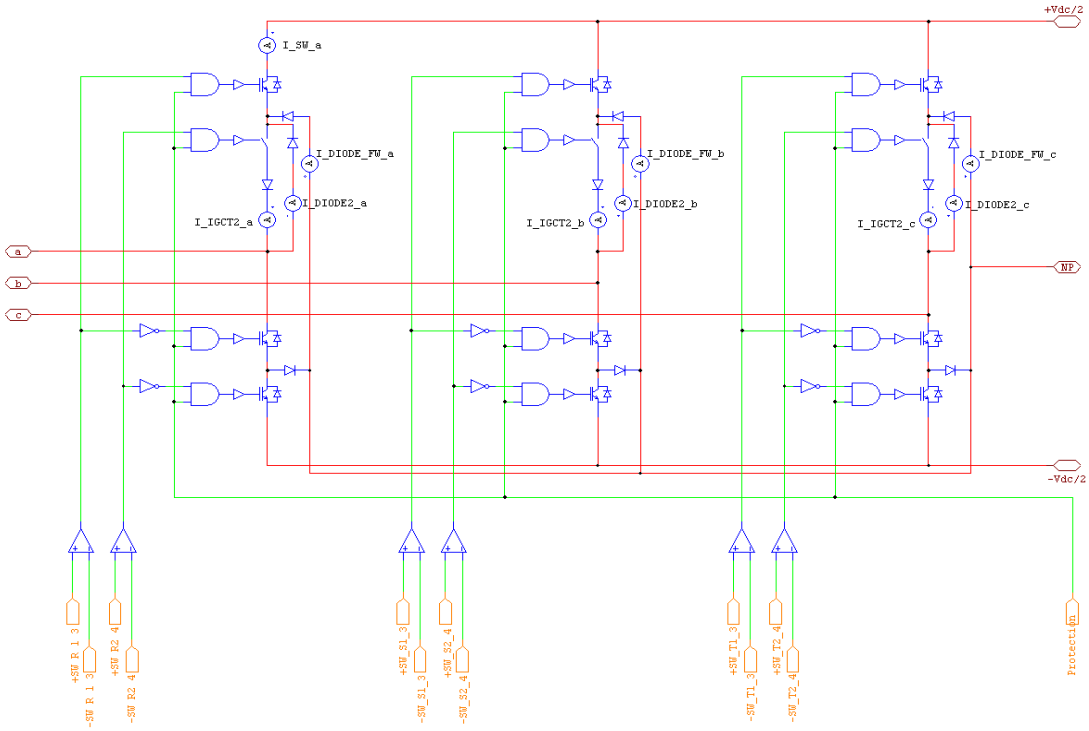

Figure 9-20 The NPC VSC 1 model with current switch measurements.

- In the reference angle detector model the low pass filters on Ed, Eq an Eo components have been removed to improve the control and also because the harmonic content on the voltage measurement point is considerably reduced by using the SAFE configuration with 5 converters (Figure 9-21).

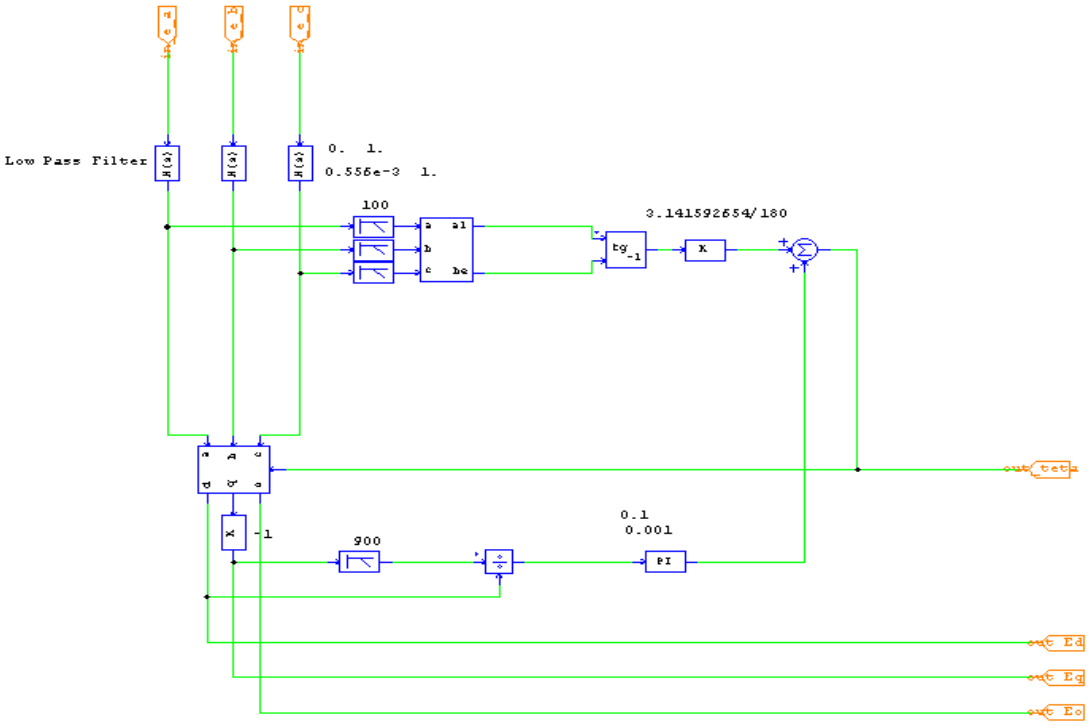

Figure 9-21 The reference angle detector without the low pass filters on Ed, Eq an Eo components.

- The dc loads of every stage have current waveforms shown in the Figure 9-22, where it may be seen the current rises to a peak with a ramp of 80 ms. The flat top current value for every stage has been calculated considering a margin of + 5% on the current of deuterium operation,

$$I_{Load,i} = \frac{E_{AG} \cdot I_{AG,i} \cdot 1.05}{V_{dc}} \qquad \text{(eq. 9-33)}$$

for example the first stage:

$$I_{Load,1} = \frac{200000 \cdot 59.4 \cdot 1.05}{6500} = 1919[A] \qquad \text{(eq. 9-34)}$$

The flat top current values for every acceleration stage are shown Table 9-2.

Table 9-2 Flat top current values for every acceleration stage

Parameter	E_{AG} [kV]	I_{AG} [A]	I_{Load} @ 6500 V
DCG1	1000-800	59.4	1919
DCG2	800-600	56.4	1822
DCG3	600-400	51.1	1651
DCG4	400-200	48	1551
DCG5	200-0	45.3	1464
Total power AGPS	54.7 MW		

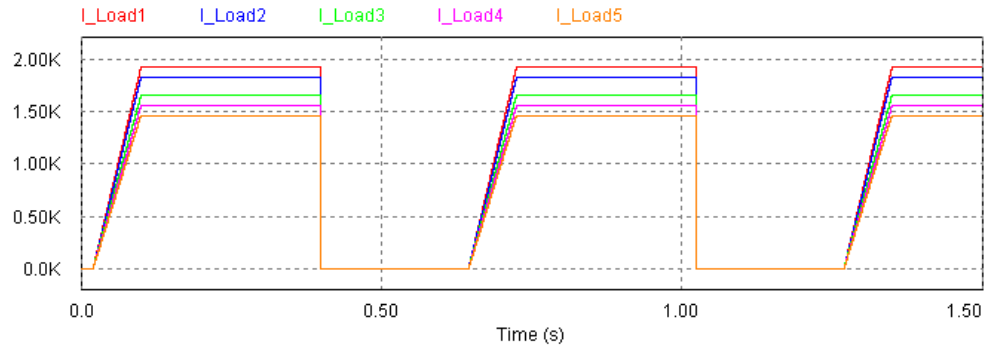

Figure 9-22 The dc load current waveform.

- The carrier waveforms of the 5 acceleration stage are have a phase displacement of 360/5=72 degrees. In particular the first one has 0 degrees, the second one 216, the third one 72, the fourth one 288 and the fifth one 144 (Figure 9-23).

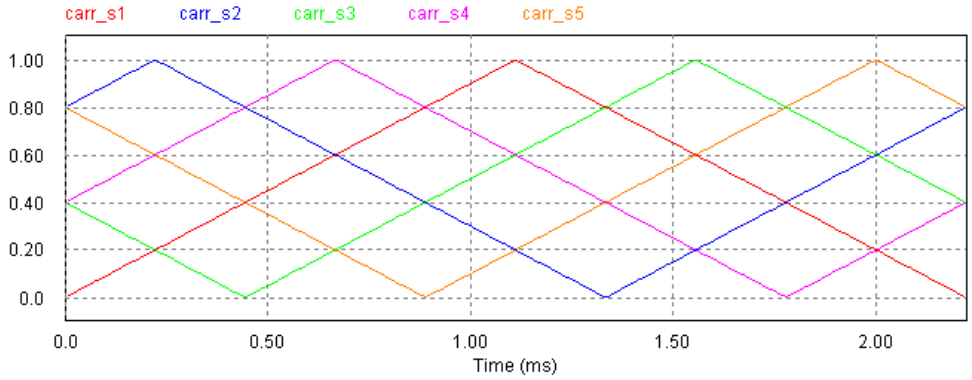

Figure 9-23 The carrier waveforms of the 5 acceleration stage.

9.4.2 Thermal analysis on the switches of the NPC VSCs

The Asymmetric IGCT 5SHY42L6500 and the Fast Recovery Diode 5SDF08H6005 components produced by ABB have been considered for the study of the switches losses.
The ratings of the two components are summarized respectively in Table 9-3 and Table 9-4.

Table 9-3 Main ratings of the Asymmetric IGCT 5SHY42L6500 by ABB semiconductor AG

Parameter	*Description*	*Value*
V_{DC}	Permanent DC voltage	4000 V
I_{TGQM}	Maximum controllable turn-off current	4200 A
V_{DRM}	Repetitive peak off-state voltage	6500 V
r_T	Slope resistance	0.59 mΩ
V_{T0}	Threshold voltage	1.75 V
$R_{th(j-c)}$	Thermal resistance junction-to-case of GCT	8.5 K/kW
$R_{th(c-h)}$	Thermal resistance case-to-heatsink of GCT	3 K/kW
E_{on}	Turn-on energy per pulse @ V_D=4 kV, I_{TGQ}=4 kA	3.1 J
E_{off}	Turn-off energy per pulse @ V_D=4 kV, I_{TGQ}=4 kA	46 J
$t_{d(on)}$	Turn-on delay time @ V_D=4 kV, I_{TGQ}=4 kA	4 µs

t_{ri}	Rise time	1 µs
$t_{d(off)}$	Turn-off delay time @ V_D=4 kV, I_{TGQ}=4 kA	8 µs
T_{vj}	Operating junction temperature range	125°C

Table 9-4 Main ratings of the Fast Recovery Diode 5SDF08H6005 by ABB semiconductor AG

Parameter	*Description*	*Value*
V_{DC}	Permanent DC voltage	3300 V
I_{FSM}	Maximum peak non-repetitive surge current	18 kA
V_{RRM}	Repetitive peak reverse voltage	5500 V
r_T	Slope resistance	1.3 mΩ
V_{T0}	Threshold voltage	4.5 V
$R_{th(j-c)}$	Thermal resistance junction-to-case of diode	12 K/kW
$R_{th(c-h)}$	Thermal resistance case-to-heatsink of diode	3 K/kW
I_{RM}	Reverse recovery current	900 A
E_{off}	Turn-off energy @ V_D=3.3 kV, I_{FM}=1.8 kA	6.5 J
T_{vj}	Operating junction temperature range	115°C

The waveforms of phase currents in the transformer secondary winding and in the input of NPC VSCs in this time interval are shown in Figure 9-24.

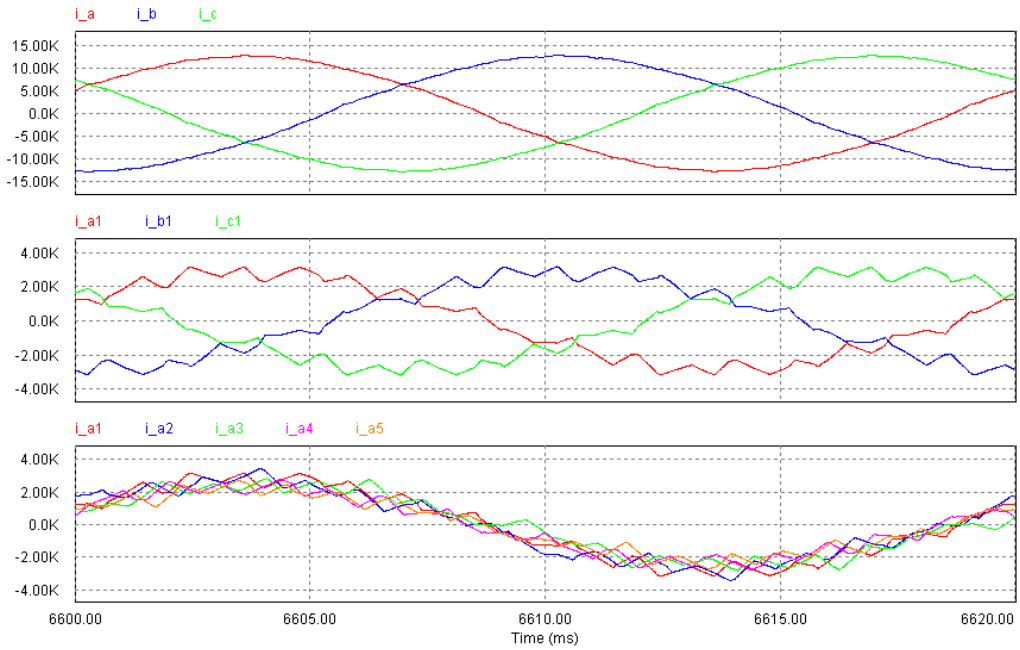

Figure 9-24 Current phase in the time interval 6÷6.02 s. The first row shows the transformer secondary winding phase current. The second row shows the phase currents in the input of the first acceleration stage NPC VSC. The last row shows the phase current i_a of five NPC VSCs.

The r.m.s. values of the phase currents are reported in Table 9-5.

Table 9-5 The effective values of the phase currents.

Side	Phase current rms

	Ia [A]	Ib[A]	Ic[A]
Transformer secondary winding	8921	8930	8933
Acceleration stage 1	2053	2056	2055

Table 9-6 The r.m.s. values of input phase current of the five acceleration stage

Ia1 [A]	Ia2 [A]	Ia3 [A]	Ia4 [A]	Ia5 [A]
2053	1961	1796	1672	1574

The five current have the same phase so they may be added and it results 9056 A, which is bigger than 8921, because in the former the ripple is higher than in the latter one. The total reactive power absorbed from the L filter is about:

$$Q_{L-filter} = 3 \cdot 2\pi \cdot 50 \cdot L_f \cdot \sum_{i=1}^{5} (Ia_i)^2 = \quad \text{(eq. 9-35)}$$

$$= 3 \cdot 2\pi \cdot 50 \cdot 0.54 \cdot 10^{-3} * (2053^2 + 1961^2 + 1796^2 + 1672^2 + 1574^2) = 8.5[M\,\text{var}]$$

The switch losses have been calculated for the first acceleration stage DCG1 (which operates with maximum current) in the worst operative condition for the ac/dc AFE conversion, i.e. at the lowest grid voltage of 62 kV.
The switches losses have been calculated in a cycle at 50 Hz.
The currents on the switches in the phase leg a of first NPC VSC 1 are shown in the Figure 9-25.

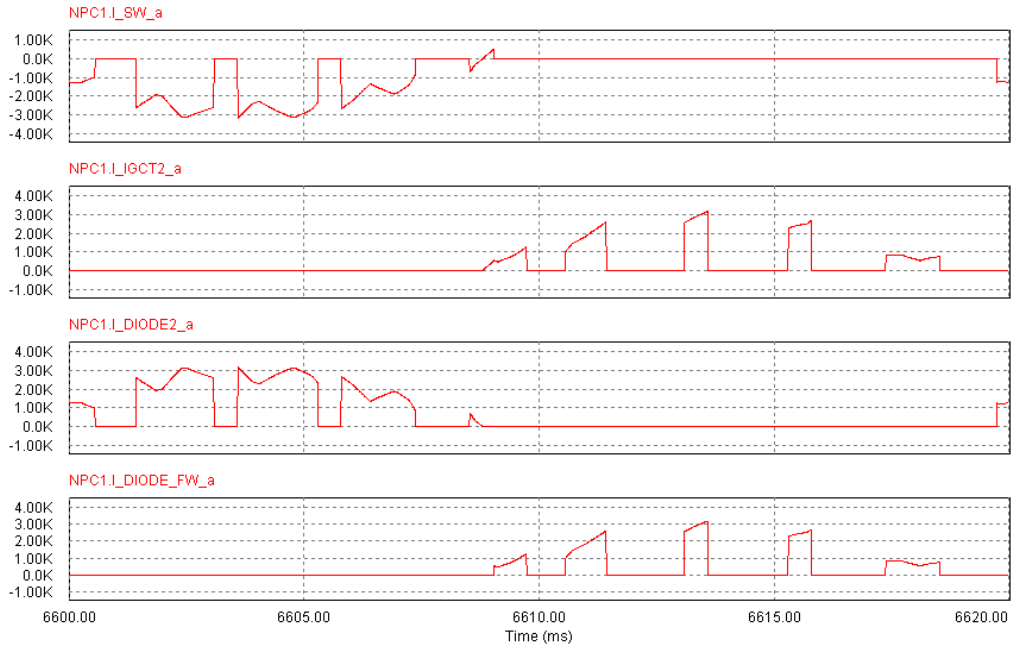

Figure 9-25 Current on the switches: the first row show the current on the external switch (negative current on the diode and the positive one on the IGCT), the second row shows the current on the internal IGCT, the third row shows the current on the internal diode and the last one shows the current on the freewheeling diode.

It should be noted that, when a NPC converter operates as rectifier, the current doesn't flow on the external IGCT.
The switches losses are calculated on internal ones of phase leg b, where the current with the maximum effective value flows. The current waveforms on the IGCT2 b and on the diode2 b are shown in the Figure 9-26, with indicated the values of the commutated current I_{COMM}.

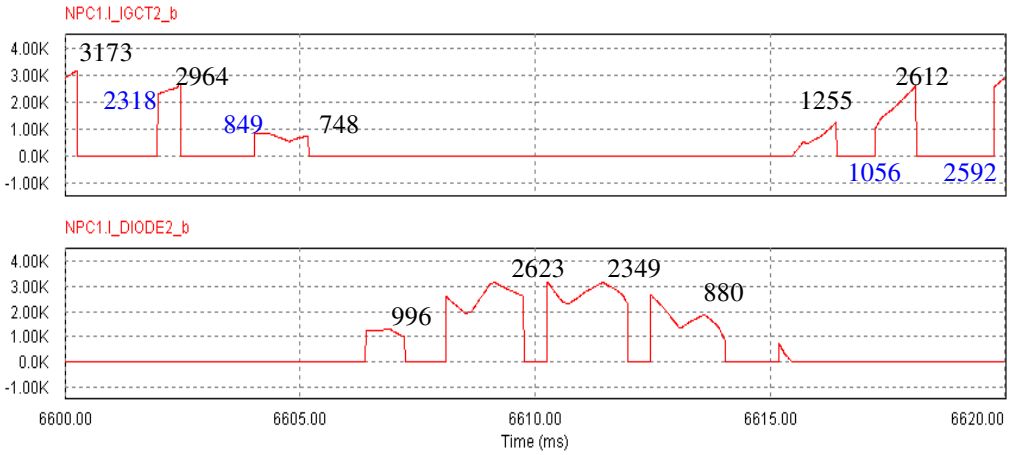

Figure 9-26 Current wave form on the IGCT2 and diode of the phase leg b, with indicated the value in Ampere of the commutated current I_{COMM} (in black the switched off current and in blue the switch on current).

Moreover the r.m.s. I_{RMS} and average I_{AV} value of current on the IGCT are respectively 761 A and 288 A, while on the diode they are 1241 and 643.
If the cooling water temperature is supposed equal to 35°C and a margin of 10°C is taken respect to the maximum junction temperature, the maximum over temperature on the junction of the two components are:

- For IGCT $\Delta T_{MAX}=T_{vj}$-10-35=125-45=80 K;
- For diode $\Delta T_{MAX}=T_{vj}$-10-35=115-45=70 K;

The following equations have been used to calculate the over temperature on the junction in relation with the number N_C of the NPC VSC in parallel.
The conducting, switch on and off losses on the IGCT have been considered, and they result:

$$P_{CON}=V_{T0}\cdot\left(\frac{I_{AV}}{N_C}\right)+r_T\cdot\left(\frac{I_{RMS}}{N_C}\right)^2=1.75\cdot\left(\frac{288}{N_C}\right)+0.59\cdot10^{-3}\cdot\left(\frac{761}{N_C}\right)^2 \qquad \text{(eq. 9-36)}$$

$$P_{SW-ON}=E_{ON}\cdot f\cdot\frac{V_{dc}}{V_D}\cdot\frac{\sum I_{COMM}}{I_T}\cdot\frac{1}{N_C}= \qquad \text{(eq. 9-37)}$$
$$=3.1\cdot50\cdot\frac{3250}{4000}\cdot\frac{2318+849+1056+2592}{4000}\cdot\frac{1}{N_C}$$

$$P_{SW-OFF}=E_{OFF}\cdot f\cdot\frac{V_{dc}}{V_D}\cdot\frac{\sum I_{COMM}}{I_{TGQ}}\cdot\frac{1}{N_C}= \qquad \text{(eq. 9-38)}$$
$$=46\cdot50\cdot\frac{3250}{4000}\cdot\frac{3173+2694+748+1255+2612}{4000}\cdot\frac{1}{N_C}$$

$$P_{TOT}=P_{CON}+P_{SW-ON}+P_{SW-OFF}\ [\mathrm{W}] \qquad \text{(eq. 9-39)}$$

$$\Delta T=\left(R_{th(j-c)}+R_{th(c-h)}+R_{th(h-s)}\right)\cdot P_{TOT}=(8.5+3+5)\cdot P_{TOT}\cdot10^{-3}\quad[\mathrm{K}] \qquad \text{(eq. 9-40)}$$

where the heat sink thermal resistance $R_{th(h-s)}$ is supposed equal to 5 K/kW.

The conducting and switching losses and junction over-temperature on the internal IGCT in relation with the number N_C of the NPC VSC in parallel are shown in Table 9-7.

Table 9-7 The conducting and switching losses and junction over temperature of the internal IGCT

N_C of NPC VSC	P_{COND} [W]	P_{SW-ON} [W]	P_{SW-OFF} [W]	P_{TOT} [W]	ΔT [°C]
1	846	215	4897	5957	98
2	337	107	2449	2893	48

Considering the maximum over-temperature on the IGCT junction of 80 K, a minimum of 2 converters are requested for the first acceleration stage.

For the other stage the maximum over temperature on the junction of the IGCT is calculated as illustrated below, for example in the second acceleration stage:

- The ratio k_R between the current phase rms values has been calculated

$$k_R = \frac{I_{a2}}{I_{a1}} = \frac{1961}{2053} = 0.96 \qquad \text{(eq. 9-41)}$$

- The conducting losses of the second acceleration stage are

$$P_{CON} = V_{T0} \cdot (I_{AV} \cdot k_R) + r_T \cdot (I_{RMS} \cdot k_R)^2 = \\ = 1.75 \cdot (288 \cdot 0.96) + 0.59 \cdot 10^{-3} \cdot (761 \cdot 0.96)^2 = 799[W] \qquad \text{(eq. 9-42)}$$

- The switching losses are:

$$P_{SW} = (P_{SW-ON} + P_{SW-OFF}) \cdot k_R = (215 + 4897) \cdot 0.96 = 4908[W] \qquad \text{(eq. 9-43)}$$

- the maximum over temperature on the junction results:

$$\Delta T = (R_{th(j-c)} + R_{th(c-h)} + R_{th(h-s)}) \cdot P_{SW+CON} = \\ = (8.5 + 3 + 5) \cdot (799 + 4908) \cdot 10^{-3} = 94[K] \qquad \text{(eq. 9-44)}$$

Table 9-8 The maximum over temperature on the junction of the IGCT for every stage

Acceleration stage	Ia rms [A]	k_R	PCOND [W]	PSW-ON [W]	PSW-OFF [W]	PTOT [W]	ΔT [°C]
1000-800 kV	2053	1.00	846	215	4897	5957	98
800-600 kV	1961	0.96	793	205	4678	5676	94
600-400 kV	1796	0.87	702	188	4284	5174	85
400-200 kV	1672	0.81	637	175	3988	4800	79
200-0 kV	1574	0.77	587	165	3754	4506	74

Also the conducting and switch-off losses on the diode have been considered (the switch-on losses are negligible), and they result:

$$P_{CON} = V_{T0} \cdot \left(\frac{I_{AV}}{N_C}\right) + r_T \cdot \left(\frac{I_{RMS}}{N_C}\right)^2 = 4.5 \cdot \left(\frac{643}{N_C}\right) + 1.3 \cdot 10^{-3} \cdot \left(\frac{1241}{N_C}\right)^2 \qquad \text{(eq. 9-45)}$$

$$P_{SW-OFF} = E_{OFF} \cdot f \cdot \frac{V_{dc}}{V_D} \cdot \frac{\sum I_{COMM}}{I_{FM}} \cdot \frac{1}{N_C} = \\ = 6.5 \cdot 50 \cdot \frac{3250}{3300} \cdot \frac{996 + 2623 + 2349 + 877}{1800} \cdot \frac{1}{N_C} \qquad \text{(eq. 9-46)}$$

$$P_{TOT} = P_{CON} + P_{SW-OFF} \ \text{[W]} \qquad \text{(eq. 9-47)}$$

$$\Delta T = \left(R_{th(j-c)} + R_{th(c-h)} + R_{th(h-s)}\right) \cdot P_{TOT} = (12+3+5) \cdot P_{TOT} \cdot 10^{-3}[K] \qquad \text{(eq. 9-48)}$$

where the heat sink thermal resistance $R_{th(h-s)}$ is supposed equal to 5 K/kW.
The conducting and switching losses and junction over-temperature on the internal diode in relation with the number N_C of the NPC VSC in parallel are shown in Table 9-9.

Table 9-9 The conducting and switching losses and junction over temperature of the internal diode

N_C of NPC VSC	P_{COND} [W]	P_{SW-OFF} [W]	P_{TOT} [W]	ΔT [°C]
1	4896	1217	6113	122
2	1947	609	2556	51

Considering the maximum over-temperature on the diode junction of 70 K, a minimum of 2 converters are requested for the first stage.

For the other stage the maximum over temperature on the junction of the diode is calculated as illustrated below, for example in the second acceleration stage:

- The ratio k_R between the current phase rms values has been calculated
$$k_R = \frac{I_{a2}}{I_{a1}} = \frac{1961}{2053} = 0.96 \qquad \text{(eq. 9-49)}$$
- The conducting losses of the second acceleration stage are
$$P_{CON} = V_{T0} \cdot \left(I_{AV} \cdot k_R\right) + r_T \cdot \left(I_{RMS} \cdot k_R\right)^2 = \\ = 4.5 \cdot \left(643 \cdot 0.96\right) + 1.3 \cdot 10^{-3} \cdot \left(1242 \cdot 0.96\right)^2 = 4626\ [W] \qquad \text{(eq. 9-50)}$$
- The switching losses are:
$$P_{SW} = \left(P_{SW-OFF}\right) \cdot k_R = (1217) \cdot 0.96 = 1168[W] \qquad \text{(eq. 9-51)}$$
- the maximum over temperature on the junction results:
$$\Delta T = \left(R_{th(j-c)} + R_{th(c-h)} + R_{th(h-s)}\right) \cdot P_{CON+SW} = \\ = (12+3+5) \cdot (4626 + 1168) \cdot 10^{-3} = 116[K] \qquad \text{(eq. 9-52)}$$

Table 9-10 The maximum over temperature on the junction of the IGCT for every stage

Acceleration stage	Ia rms [A]	k_R	PCOND [W]	PSW-OFF [W]	PTOT [W]	ΔT [°C]
1000-800 kV	2053	1.00	4896	1217	6113	122
800-600 kV	1961	0.96	4591	1163	5753	115
600-400 kV	1796	0.87	4064	1065	5128	103
400-200 kV	1672	0.81	3684	991	4676	94
200-0 kV	1574	0.77	3395	933	4328	87

From the analysis carried out above, the ac/dc conversion of the AGPS needs at least of two NPC VSCs for every acceleration stage; therefore the total number of NPC VSC is 10.

9.5 The harmonic content on the grid phase current

The harmonic content on the grid phase current has to satisfy the requirements of standard IEEE-519-1992 [23]. The maximum power P absorbed from the AGPS is 54.7 MW and the minimum short circuit power S_{SC} of the grid is 1.7 GVA. The ratio S_{SC}/P results:

$$\frac{S_{SC}}{P} = \frac{1.7 \cdot 10^9}{54.7 \cdot 10^6} = 31 \qquad \text{(eq. 9-53)}$$

Considering the standard IEEE-519-1992 [23], the current harmonic limits in percentage of the rated current for the AGPS are:

- $h < 11$ ($f_h < 550$) → $I_{h\%} < 7$ %;
- $11 \leq h < 17$ ($550 \leq f_h < 850$) → $I_{h\%} < 3.5$ %;
- $17 \leq h < 23$ ($850 \leq f_h < 1150$) → $I_{h\%} < 2.5$ %;
- $23 \leq h < 35$ ($1150 \leq f_h < 1750$) → $I_{h\%} < 1$ %;
- $35 \leq h$ ($1750 \leq f_h$) → $I_{h\%} < 0.5$ %.

At 72 kV grid voltage there is the maximum harmonic content on the grid phase current; indeed the current ripple increases with the grid voltage, while the fundamental component of the current decreases.
A simulation has been done using the PSIM model with 8 converters at 72 kV grid voltage. The waveforms of the transformer secondary winding currents are shown in Figure 9-27.

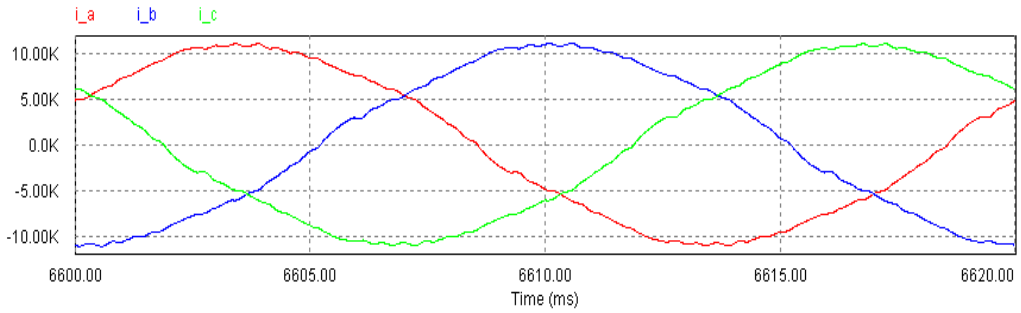

Figure 9-27 The waveforms of the transformer secondary windings currents.

The effective values of these currents are: Ia = 7656 A, Ib = 7674 A and Ic = 7647.
The Fast Fourier Transformers carried out on the current waveforms are shown in Figure 9-28.

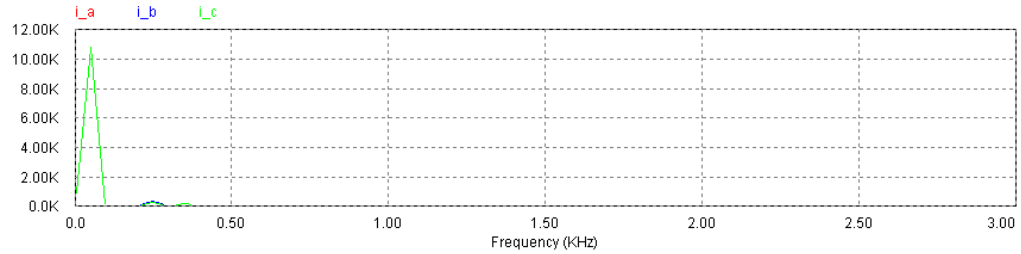

Figure 9-28 The Fast Fourier Transformers carried out on the current waveforms ia, ib and ic.

It may be noted the harmonic content is the same for the three phase currents. The current peak values at fundamental frequency of 50 Hz are: Iap = 10821 A, Ibp = 10842 A and Icp = 10808.

The FFT of the phase current in percentage values of the current peak values at 50 Hz and the limits request in IEEE 519-1992 [23] are shown in Figure 9-29.

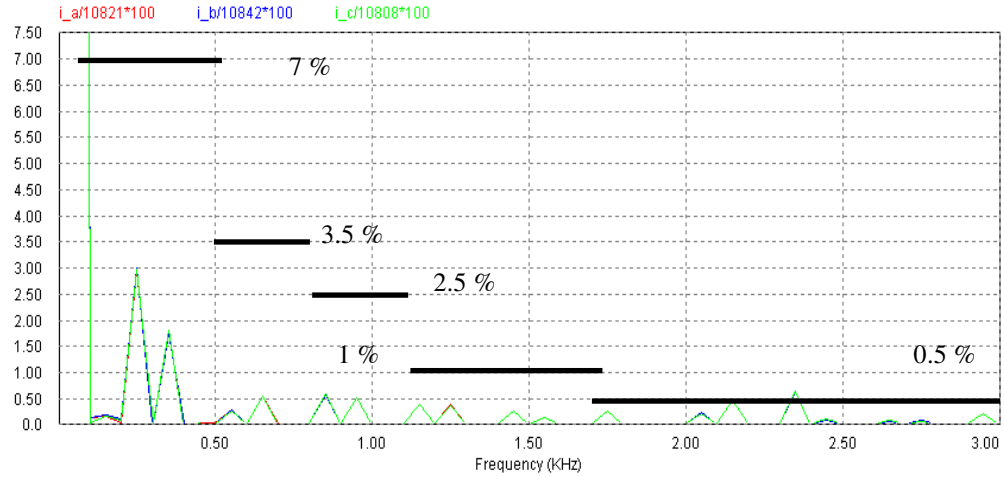

Figure 9-29 The Fast Fourier Transformer carried out on the current waveforms in percentage values of the current peak values at 50 Hz.

It may be noted that the ac/dc conversion system based on 5 NPC VSCs in SAFE configuration complies with the requirements of the IEEE 519-1992 [23] for all the current harmonics except only the one to 2350 Hz, which exceeds the limit value of about 0.1%. It should be noted that this exceeding occurs at the maximum grid voltage of 72 kV, not the nominal voltage; nevertheless the harmonic content could be improved increasing slightly the inductance value of the L filter.
The common mode voltage between the star point of the transformer and the neutral point of the NPC VSC of first acceleration stage and its FFT are shown in the Figure 9-30.

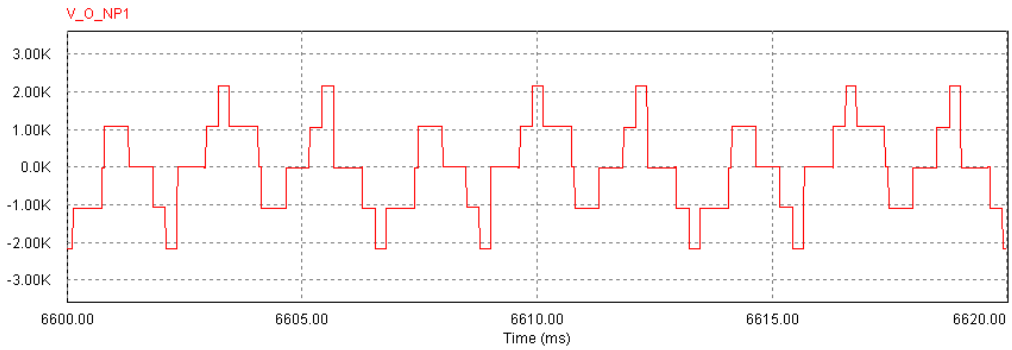

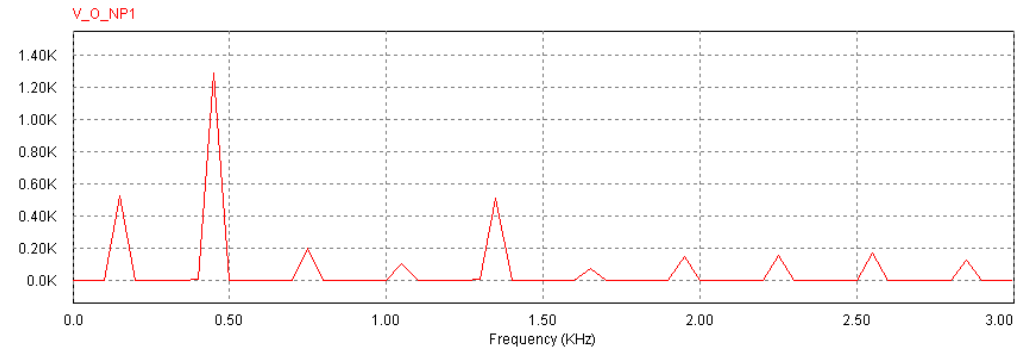

Figure 9-30 The common mode voltage between the star point of the transformer and the neutral point of the ac/dc conversion system of the first acceleration stage in the time (first row) and frequency (second row) domains.

The harmonic components of the voltage between the two neutral points are multiple of the 3rd harmonic, because the switching frequency 450 Hz is a multiple of the 3rd harmonic. A part of the harmonic at 150 Hz is due to the used modulation strategy.

9.6 Fault analysis

Two fault condition of short circuit on the converter dc terminals of an acceleration stage has been analyzed.
The short circuit on the converter dc terminals of an acceleration stage is shown Figure 9-31.

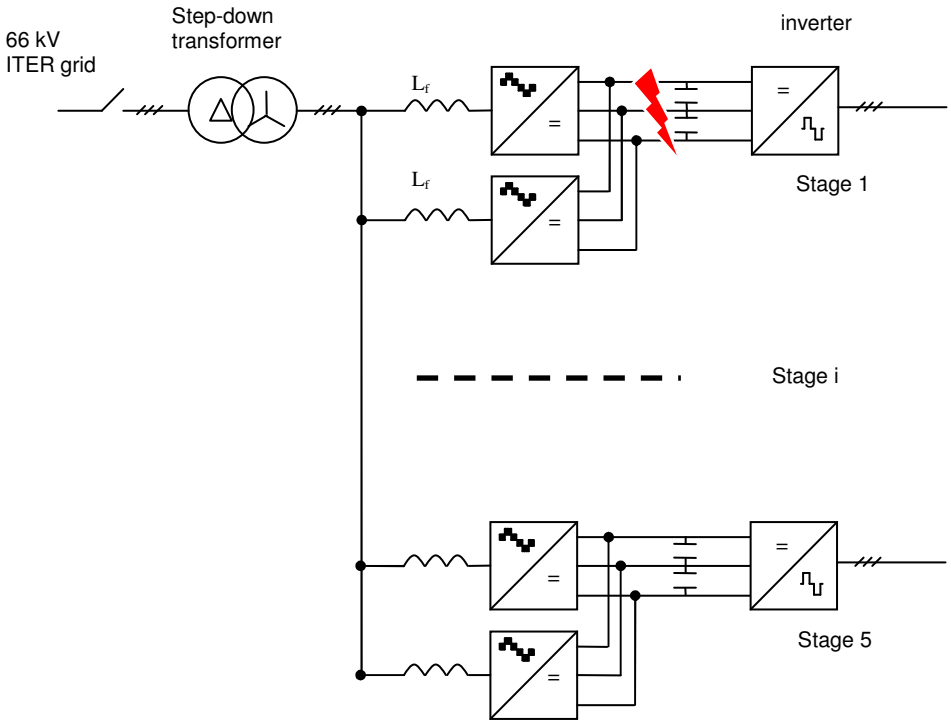

Figure 9-31 The short circuit on the converter dc terminals of an acceleration stage.

The r.m.s value of the fault current in steady state condition, considering that the other acceleration stages don't contribute to the fault, is:

$$I_{fault} = \frac{V_{2,MAX}}{\sqrt{3} * 2 * \pi * 50 * (L_{SC} + L_f / 2)} = \quad \text{(eq. 9-54)}$$

$$= \frac{72000 / 17.32}{\sqrt{3} * 2 * \pi * 50 * (0.0769 + 0.54) * 10^{-3}} = 12384 \ [A]$$

where $V_{2,MAX}$ is the secondary voltage correspondent to maximum grid voltage at 72 kV, L_{SC} is the secondary side short circuit inductance of the transformer and L_f is the inductance of the filter for each converter.

Nevertheless it should be considered that the L filter may have an iron core and during fault condition it may saturated. So the real fault current is calculated neglecting the L filter inductance value:

$$I_{fault} = \frac{V_{2,MAX}}{\sqrt{3} * 2 * \pi * 50 * L_{SC}} = \quad \text{(eq. 9-55)}$$

$$= \frac{72000 / 17.32}{\sqrt{3} * 2 * \pi * 50 * 0.0769 * 10^{-3}} = 99342 \ [A]$$

The maximum peak non repetitive surge current of the diode [33] of the NPC converter used in this study is 18 kA. The fuses are necessary to protect the converters. The rated value of a single converter of the first acceleration stage are (the current r.m.s. values are achieved by PSIM model illustrated in the previous paragraph at 54.7 MW):

- V_{1N} = 66 kV, $V_{2N} = V_{1N}/k$ = 66000/17.32= 3811 V, I_{2N} = 967 A
- V_1 = 62 kV, $V_2 = V_1/k$ = 62000/17.32= 3580 V, I_2 = 1027 A
- V_1 = 72 kV, $V_2 = V_1/k$ = 72000/17.32= 4157 V, I_2 = 891 A

Hence a rated voltage and current of the fuses are respectively 4157 V and 1027 A. The Ferraz Shauwmut makes fuses for large rectifier and the biggest voltage and current rated value are respectively 3800 V and 400 A with breaking capacity I_R = 100 - 200 kA [33].

Some considerations have been done:

- The maximum converter operating voltage (4157 V) is bigger than the rated voltage of the fuse; so it means that the rated breaking capacity should be reduced. If the rated I_R is 100 kA (worst case), the I_R at 4157 V is 100kA*3800/4157= 91 kA.
- The fuse rated current is 400 A while the maximum current r.m.s value of the converter is 1027 A, so three parallel fuses have to been installed. When fuses operate in parallel, the fault is eliminated by the last operating fuse; so the breaking capacity of every fuse should be bigger than the value 99 kA calculated in the eq. 3-54. This value is slightly higher than the breaking capacity at 4157 V.

At this moment no fuses seem available to protect the NPC converter, nevertheless the voltage and current requirements for the fuse are not so far from the state of the art.

A new configuration is proposed to reduce the r.m.s. value of the fault current by using a transformer with two secondary windings.

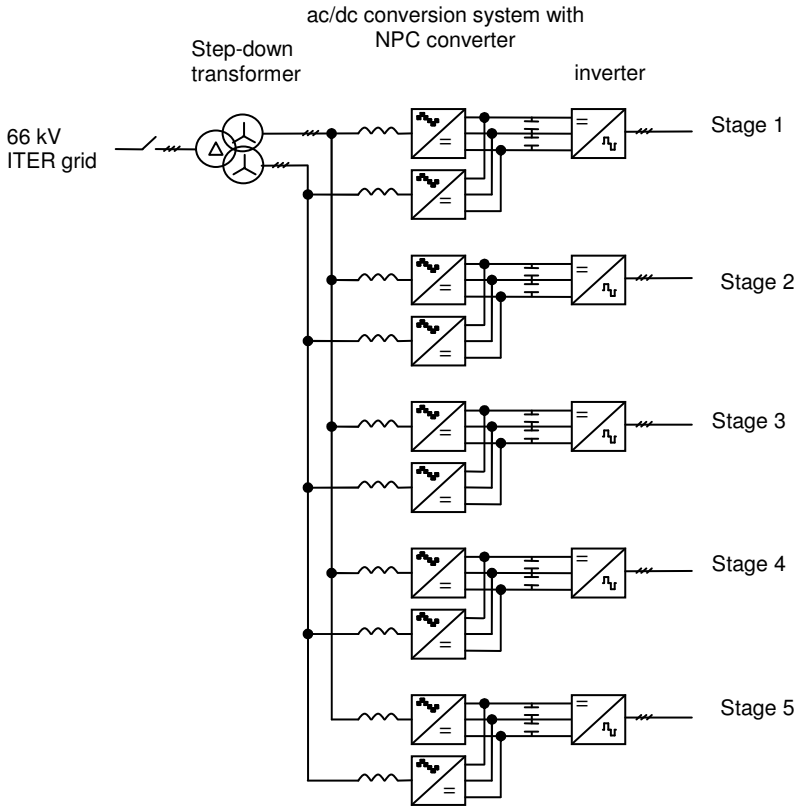

Figure 9-32 AFE ac/dc conversion system with two secondary windings.

If the two secondary windings have the same topology, i.e. Y-Y or D-D, the NPC VSCs can be controlled with CBPWM with injection of ZSS equal to 1/6 amplitude of the fundamental (which has been used in this study). If the two secondary windings have different topology, i.e. Y-D, the NPC cannot controlled with CBPWM with added ZSS, to avoid circulation current between the NPC converters.

10 Thyristor versus Active Front-End ac/dc conversion systems

10.1 Ac/dc conversion models with the acceleration grids load

In this section the AGPS dynamic responses on the dc link voltage with the two different ac/dc conversion topologies, thyrirstor and Active Front-End, are compared in the case of nominal deuterium operation. In the technical note TW6-THHN-NBD1 [2] the analysis with thyristor converters have been done, and it has been repeated here and it is compared with the one carried out with the AFE system.
The AGPS models with the two different ac/dc conversion system and the five acceleration grid stages are shown in Figure 10-1 and Figure 10-2.

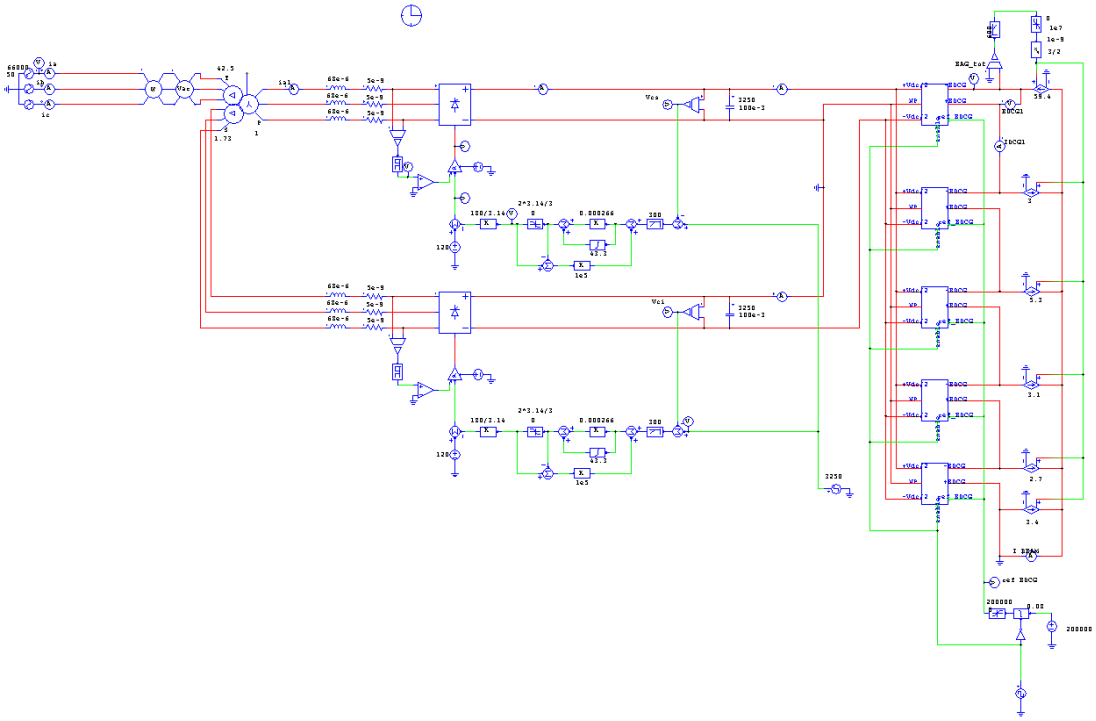

Figure 10-1 The AGPS model with thyristor rectifier.

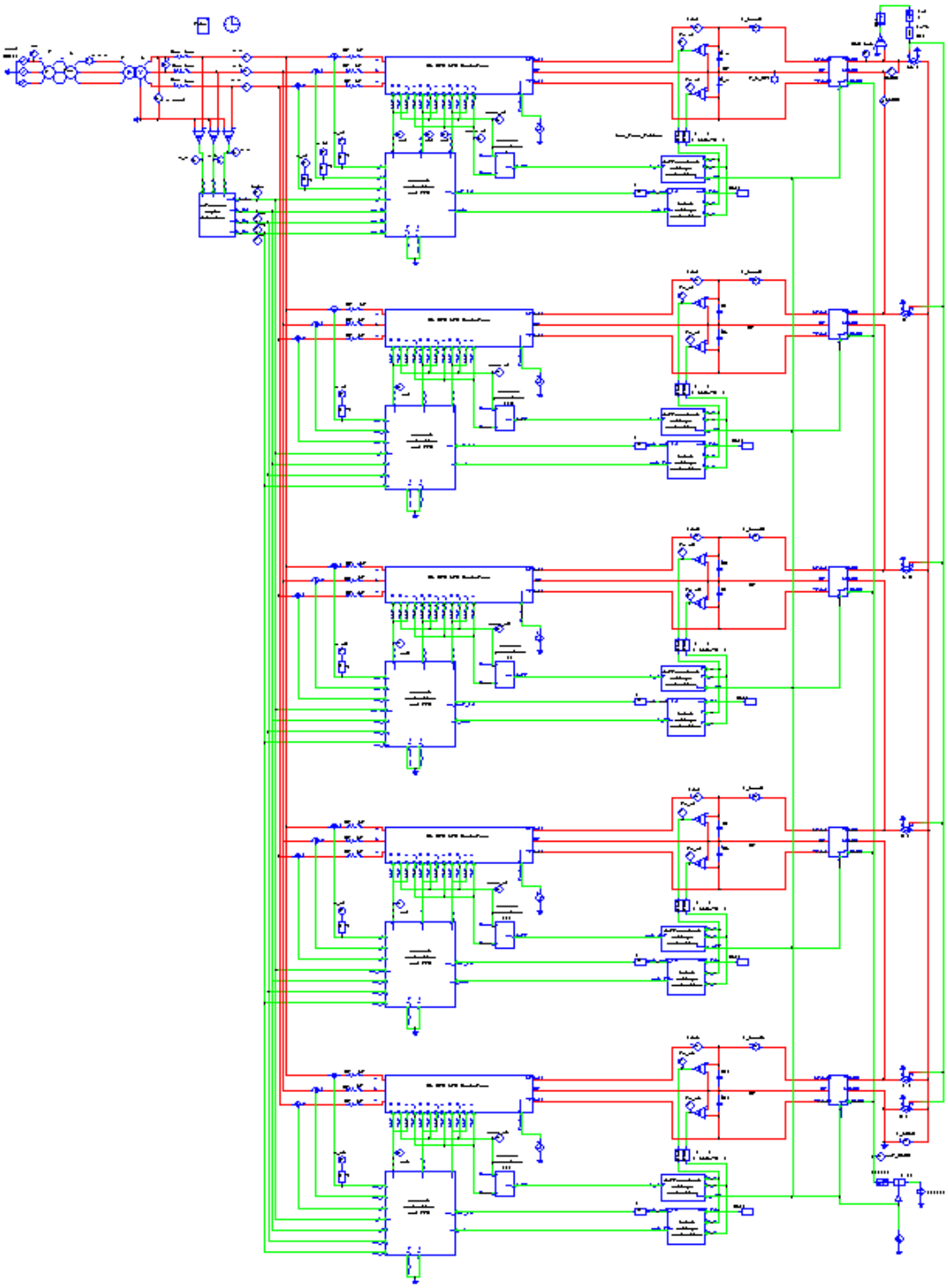

Figure 10-2 The AGPS model with the AFE converters.

In deuterium operation the AGPS has to supply five acceleration stages with the respective parameters shown in the Table 10-1 and Table 10-2 [1].

Table 10-1 - Main electrical parameters of the grids in MAMuG configuration

Parameter	**D^-, 1MeV, 40 A**	
	Voltage	Current
Extraction Grid (EG)	-1000 kV	59.7 A
Grid 1 (AG1)	-800 KV	3.0 A
Grid 2 (AG2)	-600 KV	5.3 A
Grid 3 (AG3)	-400 KV	3.1 A
Grid 4 (AG4)	-200 KV	2.7 A
Grounded Grid (GG)	0 KV	3.4 A

Table 10-2 - AGPS main parameters in MAMuG configuration

Parameter	**D^-, 1MeV, 40 A**	
	Voltage	Current
DCG1	200 KV	59.4 A
DCG2	200 KV	56.4 A
DCG3	200 KV	51.1 A
DCG4	200 KV	48.0 A
DCG5	200 KV	45.3 A

The same acceleration grids model (Figure 10-3) has been used for both the ac/dc conversion topologies with the only difference that with the thyristor conversion system the five acceleration stages are connected to the same dc link, while with the AFE one every acceleration stage has an independent dc link. As done in the THHN-NBD1 [2], the load is represented with an ideal controlled current generator, regulated in order to maintain the perveance matching:

$$I = \frac{k}{\sqrt{m_i}} \cdot V_{acc}^{1.5} \qquad \text{(eq. 10-1)}$$

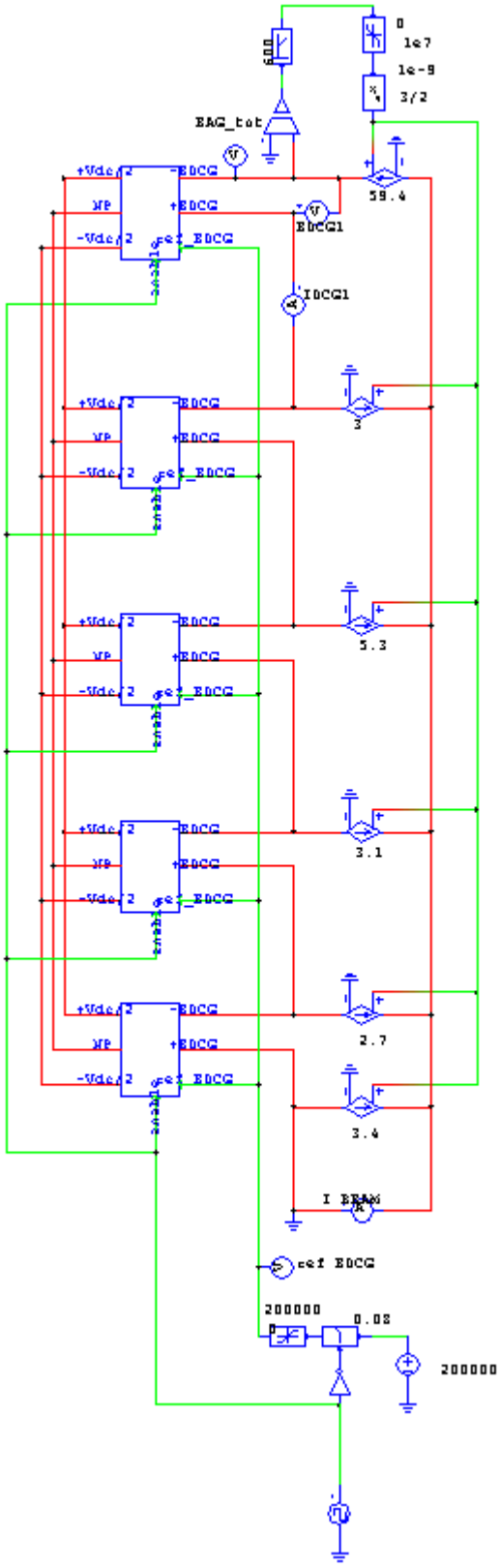

Figure 10-3 The acceleration grids model [2].

The PSIM model of the DCG is shown in Figure 10-4, it is may be seen the NPC inverter, the step up transformer, the diode rectifier and the DCG voltage control. It is the same used in the THHN-NBD1 [2].

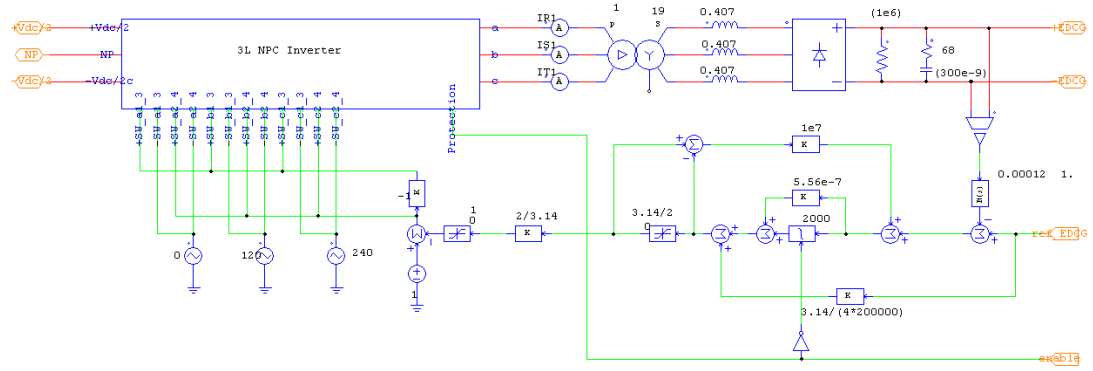

Figure 10-4 The PSIM model of the DCG.

A simplified NPC inverter model has been used to reduce the time simulation; it should be noted that the switches have a unit time delay for the closing. The respective model has been used as rectifier in the AFE model.

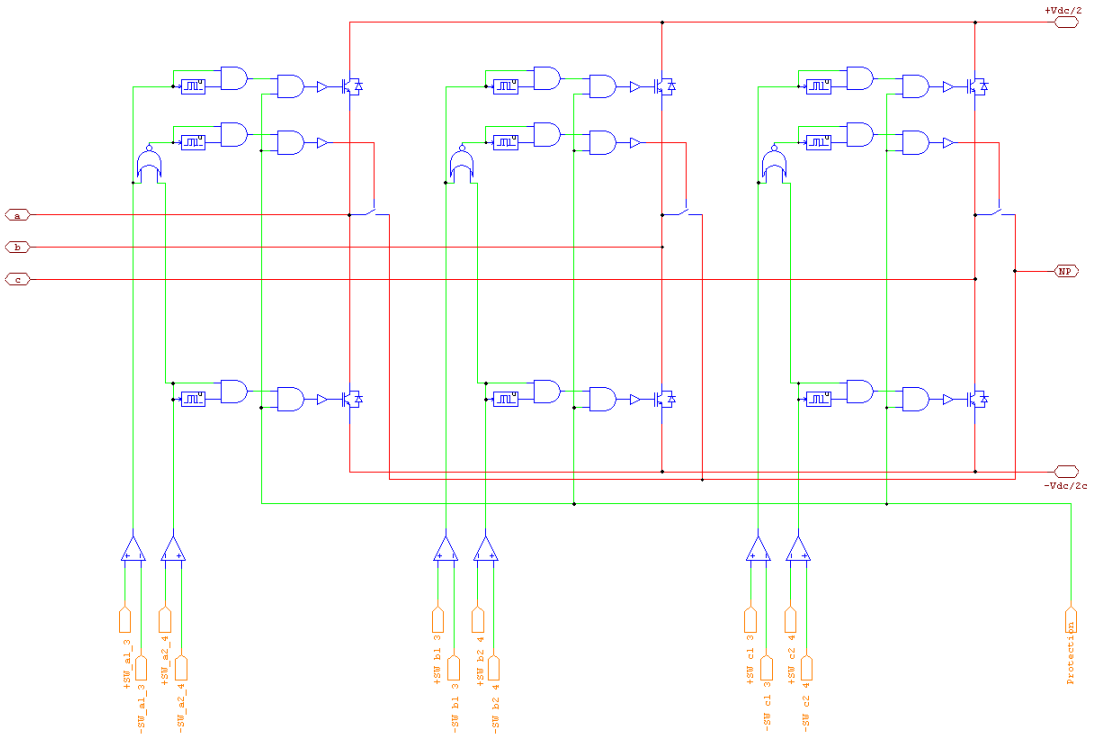

Figure 10-5 The detail of the single equivalent stage of acceleration grid load model.

10.2 Comparison among the dynamic responses between the two ac/dc conversion topologies

In both cases the AGPS system is supplied to the nominal voltage of 66 kV and the reference dc link voltage is 6500 V. The voltage reference on the 200 kV generator is given by a ramp up of 80 ms from 0 to 200 kV, a flat top 300 ms long, after that the semiconductor devices of the NPC inverter are switched off. After 20 ms the system has to be able to restart a new sequence with the same ramp-up as before. The PI controller parameters of 200 kV generator has been chosen as a trade-off between the stability and the dynamic performances when the DCG is supplied by the ac/dc thyristor conversion system [2].

The dynamic response of the thyristor and AFE solutions are shown respectively in Figure 10-6 a and b. The first row show the two halves of the dc link voltage, the second one shows the output voltages of the acceleration grid load with its reference and the third one represents the beam current.

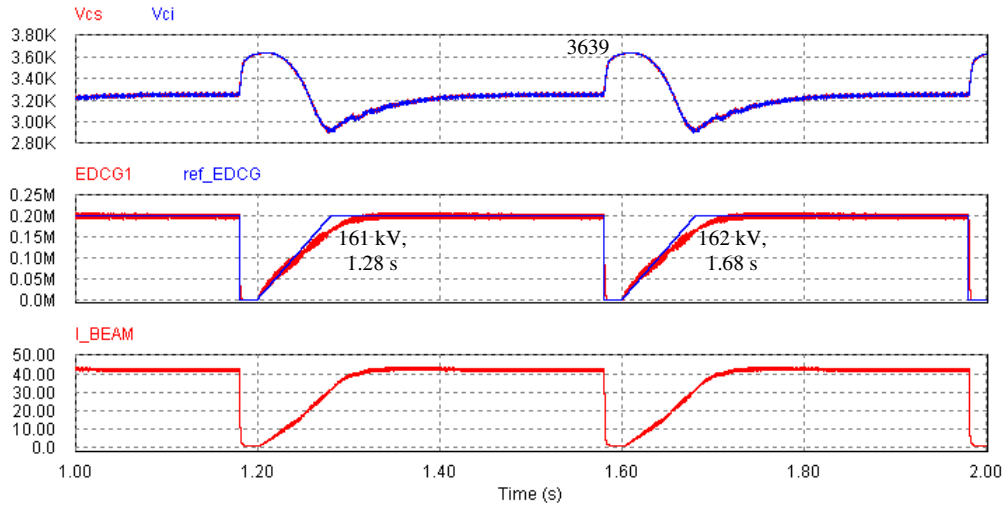

(a)

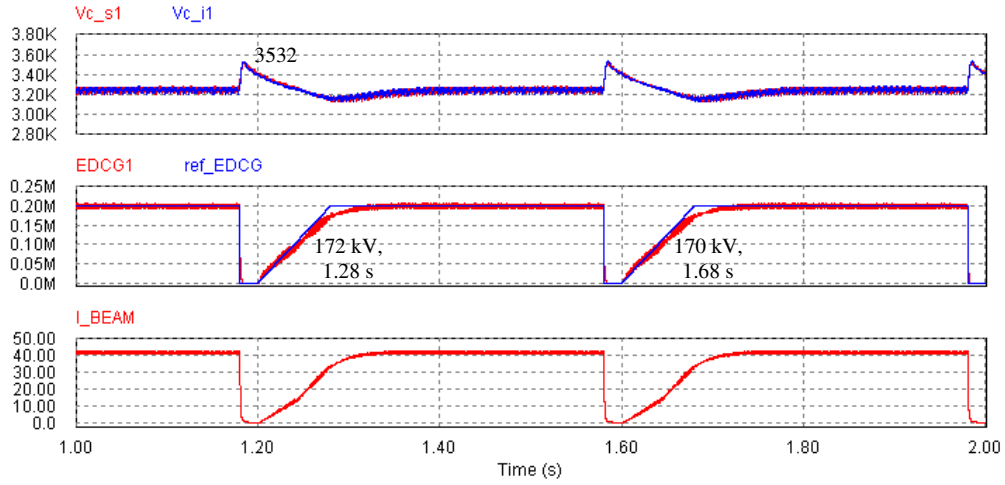

(b)

Figure 10-6 The dynamic response on dc link voltage of the thyristor [2] and AFE solutions are shown respectively in a and b. The first row show the two halves of the dc link voltage, the second one shows the output voltages of the acceleration grid load with its reference and the third one represents the beam current.

At the end of the 80 ms ramp-up the voltage EDCG1 it should be 180 kV (90 %): it results 161 kV with the thyristor solution and 170 kV with the AFE one. With the thyristor solution, the dc link shows an overvoltage 3639·2=7278 kV (+12 %), while with the AFE one the dc link shows an over voltage 3532·2=7064 (+9 %). Hence the AFE conversion system is able to satisfy the technical specifications requested for dc link voltage in the annex B [1] (± 10 %). After the dc link overvoltage, the AFE conversion system discharge the dc link capacitors until 6500 V before of the beginning of following DCG voltage ramp up and so the DCG voltage controller gives better dynamic response.

The voltage between the acceleration grids may be varied in the regulation range 20 % ÷ 100 % of the rated value of 200 kV, without exceed in each case the maximum voltage ripple of ± 5%.

A drawback of AFE implementation in this specific application is that it does not allow reducing the dc link voltage, thus the DCG output voltage may be controlled only by the regulation of the duty cycle of the square wave NPC inverter output voltage, which doesn't comply with DCG ripple requirement at low voltage. For example, the simulations with reference DCG voltage at 150 kV and dc link voltage at 6500 V with AFE ac/dc conversion topology and at 5500 V with thyristor one have been carried out. The DCG voltage ripple waveforms in per cent are shown in Fig. 11 for both cases, and it may be noted that in AFE one the ripple overcomes the requirement of ±5%. Therefore in this case it would be necessary to increase the NPC inverters frequency and/or dc filter capacitors to comply with the ripple requirement also with fix dc link voltage.

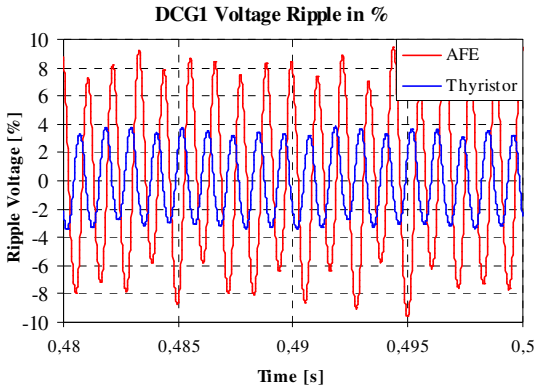

Figure 10-7 DCG1 Voltage Ripple in per cent of reference voltage at 150 kV, in AFE case with dc link voltage at 6500 V and in thyristor case with dc link voltage at 5500 V.

10.3 Reactive Power Consumption and Current Harmonic Content

The AGPS system has to respect the limit of maximum consumption of reactive power, i.e. the power factor PF has to be higher than 0.9 ($\tan\varphi \leq 0.5$). Moreover in this study it has been assumed that the current harmonic current has to comply with the IEEE 519-1992 [23].

10.3.1 Reactive power consumption and current harmonic content with ac/dc thyristor conversion system

The power factor of ac/dc thyristor conversion system is about [30]:

$$PF \cong \cos(\alpha_1) = \frac{V_{dc}/2}{1.35 \cdot V_{20,SD}} \qquad \text{(eq. 10-2)}$$

with $\alpha_1=\alpha+u/2$, where α is the firing angle of the thyristor converter and u is the overlap angle due to the short-circuit impedance of each step-down transformer.
The Active Front-End topology operates as boost converter and dc link voltage cannot be less than a minimum value, which has been chosen equal to 6500 V. Hence in this study the dc link voltage is considered constant to 6500 V to compare the two ac/dc conversion solutions at the same conditions. In the AGPS system with thyristor ac/dc

conversion system the minimum Power Factor is obtain with the maximum grid voltage of 72 kV, which means a secondary winding voltage of

$$V_{20,SD,72} = 2700 \cdot \frac{72}{66} = 2945[V] \qquad \text{(eq. 10-3)}$$

The minimum Power Factor is:

$$PF = \cos(\alpha_1) = \frac{6500/2}{1.35 \cdot 2945} = 0.817 \qquad \text{(eq. 10-4)}$$

The ratio between the reactive Q and active power P in the input of the ac/dc converters is:

$$\frac{Q}{P} = \tan[\arccos(PF)] = \tan[\arccos(0.817)] = 0.705 \qquad \text{(eq. 10-5)}$$

In deuterium operation the power is 52 MW and the reactive power consumption Q is:

$$Q = P \cdot 0.705 = 52 \cdot 0.705 = 36.64[M\ \text{var}] \qquad \text{(eq. 10-6)}$$

The calculation has verified by using the complete AGPS model with the ac/dc thyristor rectifier at 72 kV grid voltage.

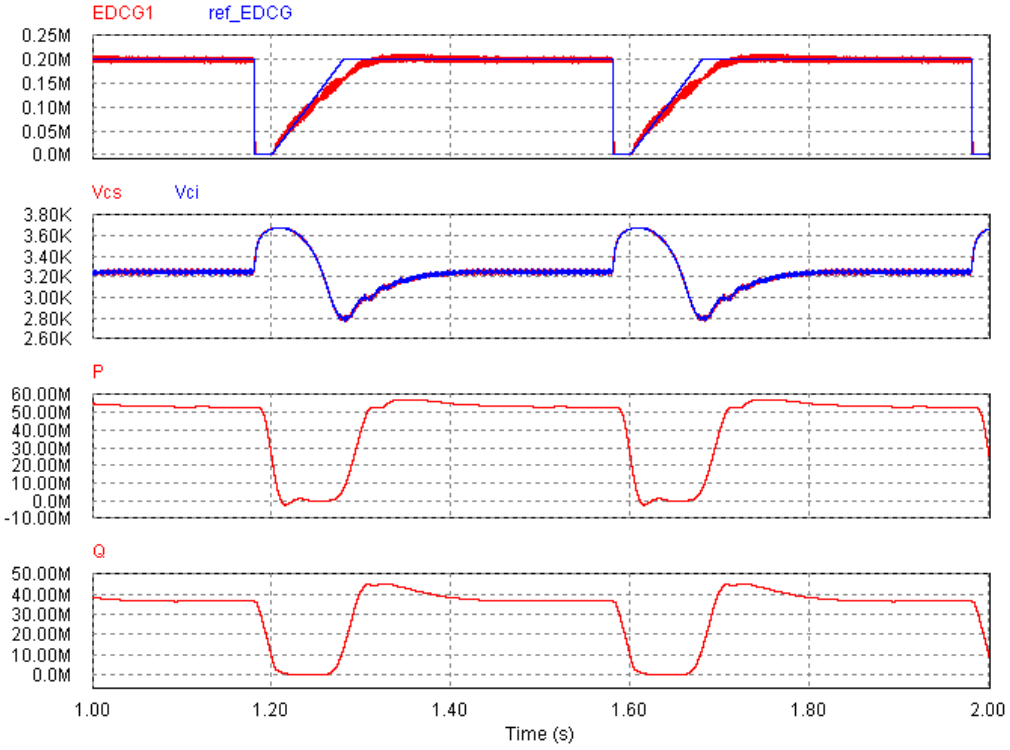

Figure 10-8 The waveforms of voltage on the single acceleration stage (1st row), the voltages on the dc link capacitors (2nd row) and the active P and reactive Q power consumptions (respectively 3rd and 4th row).

The active power is about 53 MW and the reactive one is 36.6 Mvar, as foreseen in the calculation 4-6.

A reactive power compensation system has to been installed to obtain the Power Factor equal to 0.9.

As in ITER power supply, Thyristor Controlled Reactor (TCR) system may be used to reduce the reactive power consumption. A fixed capacitor bank is permanently connected to the 66 kV grid and has to supply a reactive power Q_C of:

$$Q_C = P \cdot (0.705 - 0.5) \cdot 1.05 = 52 \cdot 0.205 \cdot 1.05 = 11.2[M\ \text{var}] \qquad \text{(eq. 10-7)}$$

where a margin of 5% has been taken.

At 72 kV grid voltage there is the maximum harmonic content on the grid phase current. The waveforms of the transformer primary winding currents are shown in Figure 9-27.

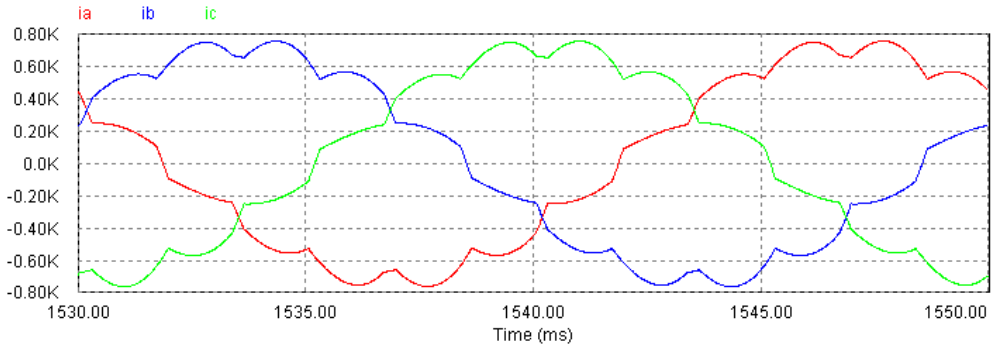

Figure 10-9 The waveforms of the transformer primary windings currents.

The effective values of these currents are: Ia = 519 A, Ib = 519 A and Ic = 519 A. The current peak values at fundamental frequency of 50 Hz are: Iap = 731 A, Ibp = 731 A and Icp = 731 A.
The FFT of the phase current in percentage values of the current peak values at 50 Hz and the limits request in IEEE 519-1992 [23] are shown in Figure 9-29.

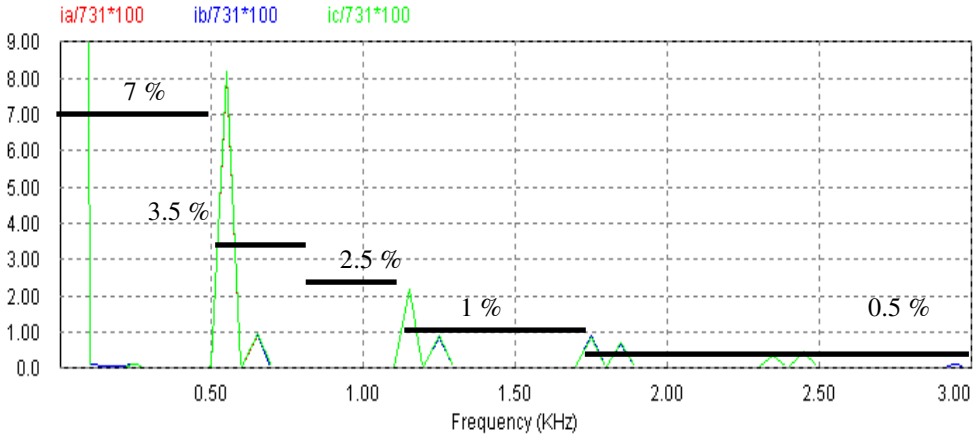

Figure 10-10 The Fast Fourier Transformer carried out on the current waveforms in percentage values of the current peak values at 50 Hz.

The harmonic content is the same for the three phase currents. It may be noted that the ac/dc conversion system based on twelve pulse thysistor doesn't comply with the requirements of the IEEE 519-1992 [23] in particular for 11^{th} and 23^{rd} order harmonics. Moreover it should be considered that the TCR injected into the grid a 3^{rd} order current harmonic, hence a harmonic filtering system is necessary.

10.3.2 Reactive power consumption and current harmonic content with ac/dc AFE conversion system

The reactive power consumption in ac/dc AFE conversion system is due to the transformer short circuit inductance, which is not compensated by the current control. The following equations are used to achieve a rough calculation.

The primary side short circuit reactance X_{SC1} is about:

$$X_{SC1} = v_{SC} \cdot \frac{V_{1N}}{\sqrt{3} \cdot I_{1N}} = v_{SC} \cdot \frac{V_{1N}^2}{S_N} \qquad \text{(eq. 10-8)}$$

where v_{SC}, S_N, V_{1N} and I_{1N} are respectively the short circuit voltage, nominal power and primary winding nominal voltage and current of the transformer.
The reactive power Q may be write:

$$Q = 3 \cdot X_{SC1} \cdot I_1^2 = 3 \cdot X_{SC1} \cdot \frac{P_{AGPS}^2}{3 * V_1^2} = v_{SC} \cdot \frac{V_{1N}^2}{S_N} \cdot \frac{P_{AGPS}^2}{V_1^2} \qquad \text{(eq. 10-9)}$$

where P_{AGPS} is the active power absorb from AGPS, V_1 is the effective voltage supplied to the transformer and I_1 is load current seen at the primary side (V_1 and I_1 may be considered in phase so $P_{AGPS} = \sqrt{3} \cdot V_1 \cdot I_1$)
The tanφ results:

$$\tan \varphi = \frac{Q}{P_{AGPS}} = \frac{v_{SC} \cdot \frac{P_{AGPS}^2}{S_N} \cdot \frac{V_{1N}^2}{V_1^2}}{P_{AGPS}} = v_{SC} \cdot \frac{P_{AGPS}}{S_N} \cdot \frac{V_{1N}^2}{V_1^2} \qquad \text{(eq. 10-10)}$$

The maximum greatest reactive power consumption is achieved with the maximum current, i.e whit the minimum grid voltage at 62 kV. Considering the data transformer the maximum value of tanφ is=

$$\tan \varphi = v_{SC} \cdot \frac{P_{AGPS}}{S_N} \cdot \frac{V_{1N}^2}{V_1^2} = 0.1 \cdot \frac{52}{60} \cdot \frac{66^2}{62^2} = 0.1 \qquad \text{(eq. 10-11)}$$

The calculation has verified by using the complete AGPS model with the ac/dc AFE conversion system at 62 kV grid voltage.

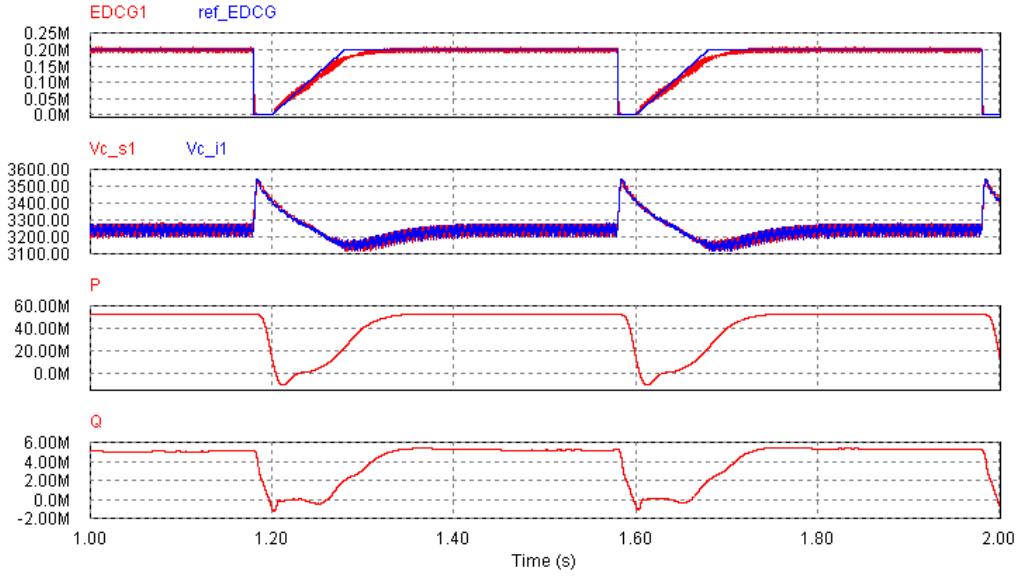

Figure 10-11 The waveforms of voltage on the single acceleration stage (1st row), the voltages on the dc link capacitors (2nd row) and the active P and reactive Q power consumptions (respectively 3rd and 4th row).

The active power is about 53 MW and the reactive one is 5.25 Mvar, the maximum value of tanφ is:

$$\tan \varphi = \frac{Q}{P} = \frac{5.25}{53} = 0.099 \qquad \text{(eq. 10-12)}$$

as foreseen in the calculation 4-11.

It may be noted that the tanφ is much lower than the grid requirement of 0.5. The ac/dc AFE conversion doesn't need of reactive power compensation system.

The current harmonic content has been analyzed in the worst operation condition at 72 kV grid voltage and the current waveforms are shown in Figure 10-12.

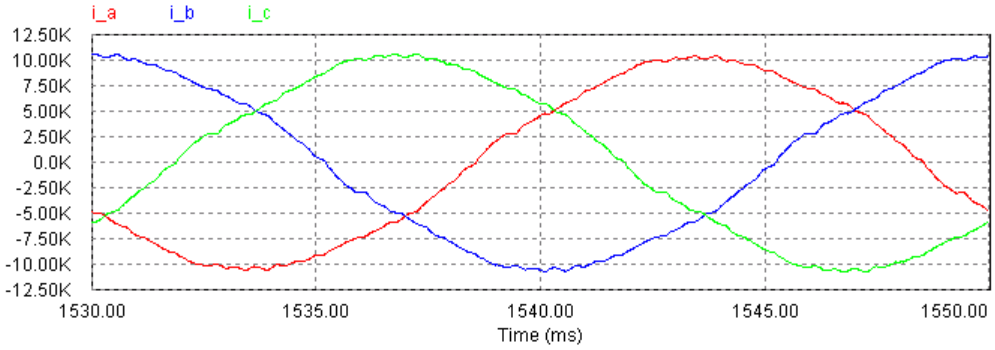

Figure 10-12 The waveforms of the transformer primary windings currents.

The rms values of these currents are: Ia = 7306 A, Ib = 7352 A and Ic = 7345 A. The current peak values at fundamental frequency of 50 Hz are: Iap = 10328 A, Ibp = 10386 A and Icp = 10381 A.
The FFT of the phase current in percentage values of the current peak values at 50 Hz and the limits request in IEEE 519-1992 [23] are shown in Figure 10-13.

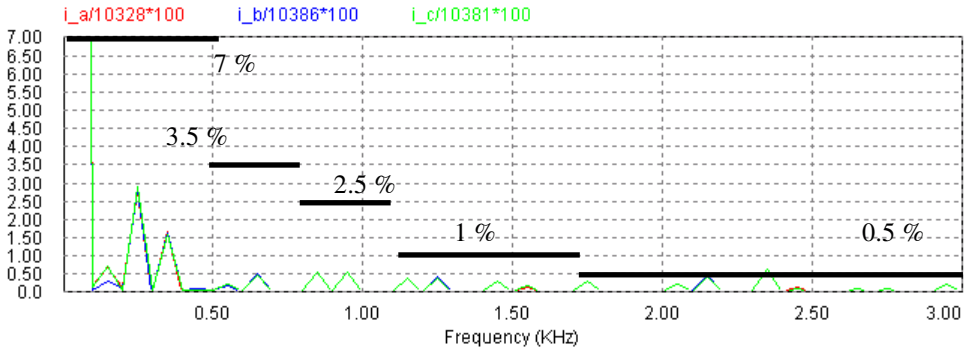

Figure 10-13 The Fast Fourier Transformer carried out on the current waveforms in percentage values of the current peak values at 50 Hz.

The harmonic content is about the same for the three phase currents. It may be noted that the ac/dc conversion system based on AFE solution complies with the requirements of the IEEE 519-1992 [23] for all the current harmonics except only the one to 2350 Hz, which exceeds the limit value of about 0.1%.

It has been highlight that the ac/dc AFE conversion system doesn't need of reactive power compensation and harmonic filtering system on the contrary of thyristor one.

11 Conclusion

In the second part of this PhD thesis the ac/dc conversion system of the Acceleration Grid Power Supply (AGPS) of the Neutral Beam Injector (NBI) based on Active Front-End solution has been illustrated.

Several models have been developed in order to verify the compliance of the AFE solution to the AGPS technical specifications and to design the main components of the ac/dc conversion system. In particular the rating of the transformer and of the AFE ac/dc conversion system (which consist of the converter topology, semiconductor device, switching frequency, L-filter) have been defined.

The analyses show that this solution is feasible and could be effectively implemented with two parallel Neutral Point Clamped Voltage Source Converters (NPC VSCs) for each acceleration stage, such that the junction temperature of the semiconductor devices does not overcome the thermal limit. The selected semiconductor device is based on IGCT technology and operates with a switching frequency of 450 Hz. The maximum power supplied by each NPC VSC is about 6.3 MW.

With respect to the thyristor ac/dc conversion system, the harmonic content of the ac input currents significantly improves with AFE solution due to the adopted SAFE configuration; in this configuration an appropriate displacement of phase has been introduced among the carrier waveforms of the NPC VSCs of the different acceleration stages. Also the reactive power is significantly reduced.

A comparison between the dynamic responses of the control system of the dc link voltage of the thyristor and AFE ac/dc conversion system has been carried out in case of a grid breakdown phenomenon. The AFE ac/dc conversion system is able to minimize the transient dc link voltage oscillation and to comply with the technical requirement of maximum dc link voltage variation of ± 10 % in transient condition.

However, the AFE implementation implies maintaining the dc link voltage fix at 6500 V, therefore the compliance with the ripple specification of the high output voltage would require increasing the NPC inverter frequency and output dc filter capacitance.

The results obtained by the analysis show that the AFE solution is feasible and it significantly improves the impact of the AGPS on the Pulsed Power Electrical Network of ITER with respect to thyristor one; the modifications of the present design parameters to allow the full compliance with the requirements of the technical specifications with the AFE design have been also proposed and discussed.
.

References

[1] Technical Specification ANNEX B [1 to n] to Procurement Arrangement 5.3.P6.EU.01.0 between the ITER International Fusion Energy Organization for the Joint Implementation of the ITER Project and EU-Domestic Agency, June 2009.
[2] A. Ferro, V. Toigo and L. Zanotto, "Supporting Analyses for the Integrated Design of the Acceleration Grid Power Supply", *Technical Note TW6-THHN-NBD1,* Consorzio RFX, 28/02/2008.
[3] J. Rodrìguez, S. Bernet, B. Wu, J. O. Pontt and S. Kouro, "Multilevel Voltage Source-Converter Topologies for Industrial Medium-Voltage Drives", *in IEEE Transaction on Industrial Electronics,* December 2007.
[4] D. Krug, M. Malinowski and S. Bernet, "Design and Comparison of Medium Voltage Multi-Level Converters for Industry Applications", *in IEEE Industry Applications Conference*, 2004.
[5] O. Apeldoorn, B. Odegard, P. Steimer and S. Bernet, "A 16 MVA ANPC-PEBB with 6 kA IGCT", *in IEEE Industry Application Society, Hong Kong, China,* October 2005.
[6] F. Hernàndez, L. Moràn, J. Espinoza and J. Dixon, "A Generalized Control Scheme for Active Front-End Multilevel Converters" *in IEEE Industrial Electronics Conference,* Denver, November 2002.
[7] F. Hernàndez, L. Moràn, J. Espinoza and J. Dixon, " A Multilevel Active Front-End Rectifier With Current Harmonic Compensation Capability" *in IEEE Industrial Electronics Society,* Busan, Korea, November 2004.
[8] M.P. Kamierkowski and L. Malesani, "Current Control Techniques for Three-Phase Voltage-Source Converters: A Survey" *in IEEE Transactions on Industrial Electronics,* October 1998.
[9] M.P. Kamierkowski, R. Krishnan and F. Blaabjerg, "Control in Power Electronics", Academic Press Series in Engineering, 2002.
[10] F. Blaabjerg, R. Teodorescu, M. Liserre and A. V. Timbus, "Overview of Control and Grid Synchronization for Distributed Power generation Systems" *in IEEE Transaction on Industrial Electronics,* October 2006.
[11] M. Milosevic, G. Andersson, "Decoupling Current Control and Maximum Power Point Control in Small Power Network with Photovoltaic Source" *in IEEE Power Systems Conference and Exposition,* 2006.
[12] J. Morren, S.W.H. de Hann, J.A. Ferreira, "Model reduction and control of electronic interfaces of voltage dip proof DG units" *in IEEE Power Engineering Society General Meeting,* June 2004.
[13] V. Blasko and V. Kaura, "A Novel Control to Actively Damp Resonance in Input LC Filter of a Three-Phase Voltage Source Converter", *in IEEE Transaction on Industry Application,* March/April 1997.
[14] K. Jalili and S. Bernet, "Design of LCL-Filters of Active Front End Two Level-Voltage Source Converters" *in IEEE Transaction on Industrial Electronics,* 2009.
[15] M.P. Kazmierkowski, R. Bracha and M. Malinowski, "Web Based Teaching of Pulse Width Modulation Methods for Three-Phase Two-Level Converters", *in Power Electronics and Motion Control Conference,* 2006.
[16] D.R. Alexander and S. M. Williams, "An optimal PWM algorithm implementation in a high performance 125 kVA inverter", *in Applied Power Electronics Conference and Exposition*, 1993.
[17] A.S.A. Luiz and B.J.C. Filho, "Minimum reactive power filter design for high power converters" *in IEEE Industrial Electronics Conference*, 2008.

[18] J.O. Pontt, J.P. Rodriguez, and R.C. Huerta, "Mitigation of noneliminated harmonics of SHEPWM three-level multipulse three-phase active front end converters with low switching frequency for IEEE-519-92" in *IEEE Transactions on Power Electronics*, 2004
[19] H. Zhang; K. Liu; M. Braun, C.C. Chan, "Selective Harmonic Controlling for Three-Level High Power Active Front End Converter with Low Switching Frequency" *in IEEE Power Electronics and Motion Control Conference*, 2006.
[20] L.G. Franquelo, J. Nàpoles, R.C.P. Guisado, J.I. Leon and M.A. Aguirre, "A Flexible Selective Harmonic Mitigation Technique to Meet Grid Codes in Three-Level PWM Converters" *in IEEE Transactions on Industrial Electronics*, 2007.
[21] C. Klumpner, M. Liserre, F. Blaabjerg, "Improved Control of an Active-Front-End Adjustable Speed Drive with a Small dc-link Capacitor under Real Grid Conditions" *in IEEE Power Electronics Specialists Conference,* Aachen, Germany, 2004.
[22] J.R. Espinoza, G. Joòs, M. Pérez, T.L.A. Moràn, "Stability Issues in Three-Phase PWM Current/Voltage Source Rectifiers in the Regeneration Mode" *in IEEE International Symposium on Industrial Electronics, Cholula, Puebla, Mexico 2000.*
[23] IEEE Std 519-1992, *IEEE Recommended Practices and Requirements for Harmonic Control in Electrical Power Systems.*
[24] M. Liserre. F. Blaabjerg and S. Hansen, "Design and Control of an LCL-Filter Based Three-Phase Active Rectifier", *in IEEE Transaction on Industry Applications,* October 2005.
[25] S. Ponnaluri, V. Krishnamurthy and V. Kanetkar, "Generalized system design and analysis of PWM based power electronic converters", *in IEEE Industry Applications Conference,* 2000.
[26] M. Triggianese, P. Marino, J. Morren and S.W.H de Haan, "Reduction of Harmonics from MW-class Wind Turbines by Interlaced Active Front-Ends", *in IEEE International Symposium on Industrial Electronics*, 2007.
[27] F. Liccardo, P. Marino and M. Triggianese, "High Power Three phase four wires Synchronous Active Front-End", *in IEEE International Symposium on Industrial Electronics*, 2006.
[28] F. Liccardo, P. Marino and M. Triggianese, "Design criteria for a synchronous active front-end in high power applications", *in International Symposium on Power Electronics, Electrical Drives, Automation and Motion*, 2006.
[29] K. Xing, F.C. Lee, D. Borojevic, Z. Ye and S. Mazumder, "Interleaved PWM with Discontinuos Space-Vector Modulation", *in IEEE Transaction on Power Electronics,* 1999.
[30] N.Mohan, T.M. Undeland and W.P. Robbins, "Power Electronics, 3rd Edition", John Wiley & Sons, Inc, 2003.
[31] Asymmetric IGCT 5SHY42L6500 by ABB, 02 May 2008.
[32] Fast Recovery Diode 5SDF08H6005 by ABB, 01 Oct 2006.
[33] Semiconductor (AC) Fuses for Power Electronics: Protistor http://www.ferrazshawmut.com/en/act-e-advisor.php
[34] Applying IGCTs by ABB, Oct 2007.

12 Acknoledgements

The author wishes to thank the power supply group of Consorzio RFX for the scientific support on the issues of ITER neutral beam power supplies and the power supply group of ITER for scientific support on the issues on ITER power supply system.
Special thanks also to the tutor Elena Gaio, for his contribution and support given throughout all the studies and the drawing up of this thesis and for the complete revision of the work.